Meenakshi Suku, B.Tech., M.Sc.

Engineering Innate Immunology in a Humanised, Functional, *In Vitro* Model of Healthy Myocardium

Trinity College Dublin, April 2024

A thesis submitted to the University of Dublin in partial fulfilment of the requirements for the degree of

Doctor in Philosophy

Primary Supervisor: Prof. Michael G. Monaghan

Internal Examiner: Prof. Maeve Caldwell

External Examiner: Prof. Christine Mummery

Declaration

I declare that this thesis has not been submitted as an exercise for a degree at this or any other university and it is entirely my own work.

I agree to deposit this thesis in the University's open access institutional repository or allow the library to do so on my behalf, subject to Irish Copyright Legislation and Trinity College Library conditions of use and acknowledgment.

Meenakshi Suku

April, 2024

Summary

Cardiovascular diseases are the leading cause of death worldwide, claiming millions of lives annually. Myocardial infarction - the most common cause of acute damage to the heart, results from compromised blood flow to the heart, leading to tissue damage and eventual heart failure. The limited regenerative capacity of the myocardium exacerbates post-MI complications, including remodeling, fibrosis, and impaired cardiac function. With sparse treatment options, alternative therapies are constantly getting screened. Due to the highly limited availability of human hearts to test novel therapeutics on, there is also a need for a reliable platform to study certain cardiac pathophysiology, as well as to test new drugs. One interesting avenue of investigation is tissue engineering, which aims to create physiologically relevant models of cardiac tissue for therapeutic development and disease modelling. Previous efforts have focused on incorporating various cell types, such as cardiomyocytes, fibroblasts and endothelial cells into engineered heart tissue (EHT) models. However, these models often lack complexity and fail to fully replicate the native myocardium, particularly because it lacks an innate immune cell population.

In vitro models of the myocardium have evolved over the years, with researchers exploring various cell compositions and scaffold materials to mimic native cardiac tissue. While cardiomyocytes are a central component of these models, incorporating supporting cell types such as fibroblasts and endothelial cells has shown promise in enhancing tissue functionality. A critical cell type in the myocardium that has gained attention in recent years is cardiac resident macrophages (CRMs). These immune cells

play diverse roles in the heart, including maintaining homeostasis, facilitating electrical conduction, and responding to tissue injury. While the functions of CRMs are still being elucidated, the inclusion of macrophages in EHT models represents a novel approach to improve physiological relevance and better understand the role of immune cells in cardiac function and disease.

The main objective of this thesis is to develop a physiologically relevant 3D *in vitro* model of the human myocardium using induced pluripotent stem cell (iPSC)-derived cardiomyocytes, macrophages, and cardiac fibroblasts. The first step involves differentiating these cell types from iPSCs, followed by thoroughly characterising the interactions between macrophages and cardiomyocytes (derived from iPSCs) *in vitro* in a 2D culture setting. Subsequently, the impact of electrical stimulation to enhance cardiomyocyte maturation when in co-culture with macrophages, is explored. Finally, EHTs are fabricated using iPSC-derived cardiomyocytes, macrophages, and cardiac fibroblasts to assess their structural and functional responses.

Overall, this work underscores the importance of developing a humanised model of the myocardium, leveraging an innate immune response, for therapeutic development and disease modelling. By incorporating macrophages into EHT models, this work aims to enhance the complexity and functionality of these systems, ultimately advancing our understanding of cardiac physiology and pathology.

Acknowledgements

A grand total of 1641 days, over 4 years, with a global pandemic in the middle of it, has not been easy at the slightest. However, I can look back with IMMENSE gratitude and joy, because of some key individuals who made this journey a very memorable one. Huge thanks to my supervisor, Prof. Michael Monaghan, for being an incredible PI, mentor and friend – I consider myself extremely lucky to have chosen this project and your group. We were both new to iPSCs, macrophages and engineered heart tissues, but like a true mentor, you always made sure I had expert advice at every point when I needed help. Thanks to my internal examiner Prof. Maeve Caldwell, thesis committee chair Prof. David Hoey and external examiner Prof. Christine Mummery, for all the input on how to improve the quality of my work and for taking the time to read through this thesis. Thanks also to the funding bodies of this work - CURAM, SFI, LifETIME CDT and Naughton Fellowship.

As any good scientific work goes, this project was highly collaborative, with plenty of input from leaders in the field from around the world. Thanks to Prof. Lesley Forrester and her team from University of Edinburgh for sharing iPSC lines and SOPs with me. Thanks to Prof. Kevin Costa and Dr. Irene Turnbull from Icahn School of Medicine at Mount Sinai, New York for sharing the EHT model and also for all the help to get the model set up. Thanks to Prof. Giancarlo Forte and the Mechanos from Kings College London/FNUSA for welcoming me with open arms, introducing me to Brno's green beer and also for all the help with human heart tissues! Thanks to Prof. Pinar Zorlutuna and team from University of Notre Dame for the scientific input that has significantly improved the quality of my work. Huge thanks to Prof. Matt Dalby from University of

Glasgow for being a great mentor over the years and prioritising my mental health over everything else.

My most sincere gratitude to the members of Monaghan Lab, starting with the OGs, in particular Sinead, for taking me under your wing, for your immense patience and for training me on techniques that have now become my bread and butter! Thanks to Dinorath, Matteo and Nuno for making me feel at home in Monaghan Lab and TCBE. Thanks to Jack and Daniel for all the help in the lab – couldn't be happier to have such young and talented scientists involved in this work! Thanks to Peppe for showing me that mentoring is enjoyable and for very quickly turning into one of my closest friends in the lab – I'm so happy for you and proud of all your achievements! Thanks to the best manager/life coach Teresa, for always being so positive and motivating – your girl is forever indebted! Finally, the biggest thanks to my two little superstars Sara and Annalisa – you're both going to do incredible things and I can't wait to witness them and cheer you on!

Although the individuals involved in the big picture are critical, the true heroes are always the ones who have seen, supported and pulled me back up every day. Heartfelt gratitude to my very dear spice b!tches, survival group, lab girls, serious work chat crew, cuticles, nothing else to think about, secret society, DAM and mates. The many pints, coffees and rants did not go wasted! For over 4 years, I've walked in to TBSI every morning to be greeted with "good morning Princess!" – big big thanks to TBSI reception and housekeeping staff for making all the 7 Am starts pleasant! Thanks also to the staff at TCD sports centre.

Collaborators, mentors, friends and supporters all aside, some real troopers who I have never met also need to be acknowledged here. Thanks to Dr. Harvey Motulsky for

GraphPad Prism, Wayne Rasband for ImageJ, Richard Niles for EndNote and all the many hands that put together Microsoft Office. You all walked, so we could run.

Words fall short to express my gratitude towards my biggest cheerleader, Will. I admire your patience and appreciate you for giving me a family and a home in Dublin – I shall try to make up for it with many many apple crumbles. Last but very much not the least, thanks to my family – I have only spent 20 days with you in the last 4+ years, but you are why I am here, and this thesis is dedicated to you.

List of publications, conference proceedings and prizes

Publications

Nuno Neto, **Meenakshi Suku**, David Hoey, Michael G Monaghan, 2P-FLIM unveils time-dependent metabolic shifts during osteogenic differentiation with a key role of lactate to fuel osteogenesis via glutaminolysis identified, Stem Cell Res Ther 14, 364 (2023)

Giuseppe A Asaro, Matteo Solazzo, **Meenakshi Suku**, Dahnan Spurling, Katelyn Genoud, Javier Gutierrez Gonzalez, Fergal J O' Brien, Valeria Nicolosi, Michael G Monaghan. MXene functionalized collagen biomaterials for cardiac tissue engineering driving iPSC-derived cardiomyocyte maturation. npj 2D Mater Appl 7, 44 (2023)

Conor Darroch, Giuseppe A Asaro, Coralie Gréant, **Meenakshi Suku**, Nele Pien, Sandra Van Vlierberghe, Michael G Monaghan. Melt electrowriting of a biocompatible photo-crosslinkable poly(D,L-lactic acid)/poly(ε-caprolactone)-based material with tunable mechanical and functionalization properties. J Biomed Mater Res. 2023; 111(6): 851-862.

Meenakshi Suku, Lesley Forrester, Manus Biggs, and Michael G Monaghan, "Resident macrophages and their potential in cardiac tissue engineering", Tissue Eng Part B Rev, vol. 28, no. 3, pp. 579-591, Jun 2022

Conference proceedings

Oral presentations (* presenting author):

Suku. M*, Forrester. L, Biggs. M, Monaghan. MG, "Development of humanized, functional, tissue engineered in vitro model of healthy myocardium", Gordon Research Conference in Immunoengineering, Feb 13th 2024, Tuscany, Italy

Suku. M*, Forrester. L, Biggs. M, Monaghan. MG, "Development of humanized, functional, tissue engineered in vitro model of healthy myocardium", Gordon Research Seminar in Immunoengineering, Feb 10th 2024, Tuscany, Italy

Suku. M*, Forrester. L, Biggs. M, Monaghan. MG, "Engineering innate immunology in a humanized, functional, in vitro model of healthy myocardium", Gordon Research Seminar in Biomaterials and Tissue Engineering, July 15th 2023, New Hampshire, USA

Suku. M*, Forrester. L, Biggs. M, Monaghan. MG, "Development of humanized, functional, tissue engineered in vitro model of healthy myocardium", CÚRAM "Organ-on-a-Chip/Organoids" Meeting, June 23rd 2023, Virtual

Suku. M*, Forrester. L, Biggs. M, Monaghan. MG, "Functional cardiac organoids modeling the inflammatory environment of myocardial infarction", TERMIS-EU 2023, March 29th 2023, Manchester, UK

Suku. M*, Forrester. L, Biggs. M, Monaghan. MG, "Development of humanized, functional, tissue engineered in vitro model of healthy myocardium", Bioengineering In Ireland 2023, January 27th 2023, Enfield, Ireland

Suku. M.*, Forrester. L., Biggs. M, Monaghan, M. G., "Tuning of Macrophage Polarization in the generation of functional cardiac organoids", TERMIS-EU 2022, June 28th 2022, Krakow, Poland

Suku. M.*, Forrester. L., Biggs. M, Monaghan, M. G., "Tuning of Macrophage Polarization in the generation of functional cardiac organoids", Bioengineering In Ireland 2022, May 20th 2022, Galway, Ireland

Suku. M.*, Forrester. L., Biggs. M, Monaghan, M. G., "Tuning of Macrophage Polarization in the generation of functional cardiac organoids", EPSRC-SFI Joint Student Day, September 7th 2021, Virtual

Suku. M.*, Forrester. L., Biggs. M, Monaghan, M. G., "Tuning of Macrophage Polarization in the generation of functional cardiac organoids", lifETIME CDT Webinar, March 31st 2021, Virtual

Poster presentations (* presenting author):

Suku. M*, Forrester. L, Biggs. M, Monaghan. MG, "Development of humanized, functional, tissue engineered in vitro model of healthy myocardium", Gordon Research Conference in Immunoengineering, February 13th 2024, Tuscany, Italy

Suku. M*, Forrester. L, Biggs. M, Monaghan. MG, “Development of humanized, functional, tissue engineered in vitro model of healthy myocardium”, BioBrillouin 2023, December 6th 2023, Dublin, Ireland

Suku. M*, Forrester. L, Biggs. M, Monaghan. MG, “Development of humanized, functional, tissue engineered in vitro model of healthy myocardium”, Gordon Research Conference in Biomaterials and Tissue Engineering, July 19th 2023, New Hampshire, USA

Asaro. GA, Solazzo. M, Suku. M*, Spurling. D, Genoud. K, Gonzalez. JG, O'Brien. FJ, Nicolosi. V, Monaghan. MG, “Crosslinked extracellular matrix biomaterials functionalized with 2D-nanomaterial MXenes for cardiac tissue engineering drive iPSC-derived cardiomyocyte maturation”, TERMIS-EU 2023, March 30th 2023, Manchester, UK

Suku. M.*, Forrester. L., Biggs. M, Monaghan, M. G., “Tuning of Macrophage Polarization in the generation of functional cardiac organoids”, British Society for Cardiovascular Research, 6th September 2021, Virtual

Suku. M.*, Forrester. L., Biggs. M, Monaghan, M. G., “Tuning of Macrophage Polarization in the generation of functional cardiac organoids”, European Congress of Immunology, 1st September 2021, Virtual

Suku. M.*, Forrester. L., Biggs. M, Monaghan, M. G., “Tuning of Macrophage Polarization in the generation of functional cardiac organoids”, Future Leaders in Regenerative Medicine - Joint CDT UKSB conference, 15th June 2021, Virtual

Suku. M.*, Forrester. L., Biggs. M, Monaghan, M. G. “Tuning of Macrophage Polarization in the generation of functional cardiac organoids”, TERMIS workshop, 11th June 2021, Virtual

Prizes

1. 1st prize, lifETIME CDT 3-minute thesis competition, virtual, May 2023, UK and Ireland
2. Best oral presentation in the Regenerative Medicine track, Bioengineering In Ireland 2023, January 27th 2023, Enfield, Ireland
3. EMBO Scientific Exchange Grant to carry out internship in Prof. Giancarlo Forte's lab at Centre for Translational Medicine, Brno, Czechia (Grant code 9960), November 2022
4. 1st prize, Thesis in three competition, TCBE Research Day, March 11th, 2022, Dublin, Ireland

Table of Contents

Declaration i
Summary ii
Acknowledgements iv
List of publications, conference proceedings and prizes vii
Table of Contents xii
List of Figures xviii
List of Tables xxxii
Abbreviations xxxiii
Chapter 1 Introduction 36
1.1. Cardiovascular health and disease 36
1.2. Macrophages in the heart 37
1.3. *In vitro* models of the myocardium 38
1.4. Thesis objectives 39
Chapter 2 Literature Review 40
2.1. Anatomy of human heart and the conduction system 41
2.2. Cardiac diseases and its global impact 42
2.3. Cells of the heart 44
2.4. Inflammatory cardiac events 46
2.5. Immune cells in the heart 47
2.5.1. Macrophages: origin and types 49
2.5.2. Cardiac macrophages in homeostasis 52
2.5.3. Cardiac macrophages in disease 55

2.6. iPSCs in cardiac tissue engineering 59
2.6.1. iPSC-derived cardiomyocytes and cardiac fibroblasts 59
2.6.2. iPSC-derived macrophages 65
2.7. Macrophages in Tissue Engineering 67
2.8. Macrophages in cardiac tissue engineering 69
2.9. Engineered heart tissue models 72
2.9.1. EHT based disease models 75
2.10. Conclusion 77
Chapter 3 General Materials and Methods 78
3.1. iPSC expansion and culture 78
3.2. Isolation of PBMCs from buffy coats 78
3.3. Processing and handling of human heart samples 80
3.4. Flow cytometry 80
3.5. RT-qPCR 83
3.6. ELISA 87
3.7. Immunofluorescence Imaging 88
3.8. Calcium Imaging 89
Chapter 4 Thesis Objectives 90
Chapter 5 Generation and characterisation of iPSC-derived macrophages 91
5.1. Abstract 91
5.2. Introduction 91

5.3. Materials and Methods 93

5.3.1. Experimental design 93

5.3.2. Differentiation of iPSCs to macrophages 94

5.3.3. Characterisation of iMacs using flow cytometry 95

5.3.4. Polarisation of iMacs 95

5.3.5. Phagocytic potential of iMacs 95

5.4. Results and Discussion 96

5.4.1. Aggrewell™, agarose and ULA plates successfully facilitated EB formation and consequent iMac differentiation 96

5.4.2. The EB-based differentiation protocol is robust and generates iMacs for up to 100 days 101

5.4.3. iMacs are functionally active, with the ability to polarise to pro- and anti-inflammatory states 104

5.5. Conclusion 108

Chapter 6 Generation and characterisation of iPSC-derived cardiomyocytes and cardiac fibroblasts 109

6.1. Abstract 109

6.2. Introduction 109

6.3. Materials and Methods 113

6.3.1. Experimental design 113

6.3.2. Differentiation of iPSCs to cardiomyocytes 114

6.3.3. Differentiation of iPSCs to cardiac fibroblasts 115

6.4. Results and discussion 116

6.4.1. iCMs can be successfully obtained from iPSCs using GiWi protocol..... 116

6.4.2. iCFs can be successfully obtained from SFCi55 iPSCs 118

6.4.3. iCMs and iCFs express cardiac developmental markers 121

6.5. Conclusion..... 123

Chapter 7 Conditioning a cardiac resident macrophage phenotype in iMacs by performing co-cultures with iCMs.....125

7.1. Abstract..... 125

7.2. Introduction 126

7.3. Materials and Methods..... 129

7.3.1. Experimental design 129

7.3.2. iMacs treated with iCM conditioned media 131

7.3.3. Co-culture of iMacs and iCMs..... 132

7.4. Results and discussion 133

7.4.1. iMacs are functionally active, with a differential protein expression profile upon culture with iCM conditioned media 133

7.4.2. iMacs integrate well with iCM cultures and exhibit functional improvement . 138

7.4.3. iMacs express CRM-specific as well as cardiac developmental genes when in co-culture with iCMs 144

7.4.4. iCMs demonstrate phenotypic changes and express cardiac maturation genes when in co-culture with iMacs 145

7.4.5. iCMs in co-culture with iMacs display improved calcium handling 149

7.5. Conclusion 153

Chapter 8 Electrical Stimulation to improve the maturation of iCMs, iMacs and co-cultures 157

8.1. Abstract 157

8.2. Introduction 158

8.3. Materials and Methods 162

8.3.1. Experimental design 162

8.3.2. Electrical Stimulation bioreactor setup 164

8.3.3. Electrical stimulation on iCMs, iMacs and iCM/iMac co-cultures 164

8.4. Results and discussion 166

8.4.1. The gene expression profile of iCMs indicate maturation when subjected to 5 days of electrical stimulation 166

8.4.2. iMacs are highly pro-regenerative and functionally active when subjected to 5 days of electrical stimulation 169

8.4.3. iMacs separated from electrically stimulated iCM/iMac co-cultures remain highly quiescent, with notable functional activation. 171

8.4.4. iCMs FACS sorted from electrically stimulated iCM/iMac co-cultures show an elongated morphology and functional maturity with improved beat rate and calcium handling. 175

8.5. Conclusion 179

Chapter 9 Fabrication of engineered heart tissues to model healthy and diseased myocardium 181

9.1. Abstract 181

9.2. Introduction 182

9.3. Materials and Methods 186

9.3.1. Experimental design 186

9.3.2. Collagen/Matrigel® hydrogel fabrication 188

9.3.3. Engineered heart tissue bioreactor fabrication 189

9.3.4. Engineered heart tissue fabrication 191

9.4. Results and discussion 192

9.4.1. Collagen-Matrigel® hydrogel does not trigger pro-inflammatory response in iMacs 192

9.4.2. EHTs fabricated using the custom-built bioreactor shows improved alignment and beat rate 193

9.4.3. EHTs containing iMacs display improved iCM elongation, beat rate and tissue compaction 196

9.4.4. Addition of iCFs into EHTs containing iMacs indicate increased myofibroblast activation 201

9.5. Conclusion 207

Chapter 10 Discussion and future perspectives 210

References 217

Appendices 246

List of Figures

Figure 2.1: Anatomy of human heart, highlighting the layers of the heart wall. Image modified from a Biorender® template. 42

Figure 2.2: Schematic representation of the conducting system of human heart. Image modified from a Biorender® template. 44

Figure 2.3: The cellular landscape of adult human heart [42]. The main cell types of the myocardium include cardiomyocytes, fibroblasts, mural cells (pericytes and smooth muscle cells), endothelial cells and immune cells. However, the number of these cell types vary across the atria and the ventricles. Image created using Biorender® 45

Figure 2.4: Schematic representation of the origin of macrophages in the heart. Resident macrophages originate prenatally and populate the heart, whereas circulating macrophages originate in the adult bone marrow. According to most recent reports [64], the macrophage populations present in the heart include TLF^{+} (cardiac resident macrophages), $CCR2^{+}$ (bone marrow-derived macrophages) and MHC-II^{hi} (derived postnatally from cardiac macrophages). Image created using Biorender®. 48

Figure 2.5: Functions of cardiac resident macrophages in healthy myocardium. In steady state, cardiac resident macrophages perform several important functions in the myocardium. One of their major functions is to facilitate electrical conduction by coupling with cardiomyocytes through connexin-43 gap junctions. They help in sustaining normal cardiac autophagy by capturing and eliminating exophers (containing defective mitochondria) released by cardiomyocytes, through Mertk. They also perform immunosurveillance and clear dead cells and debris in the myocardium, to maintain

homeostasis. The presence of cardiac resident macrophages is found to be essential in promoting cardiac regeneration. Created with BioRender.com 54

Figure 2.6: Macrophage origin and function in infarcted heart. After MI, the monocytes that infiltrate the heart originate from bone marrow (~60%) and spleen (~40%). The recruitment of bone marrow-derived monocytes is CCR2 dependent and that of spleen-derived monocytes is angiotensin II-dependent. Resident macrophages reside, self-renew and carry out a number of functions in the myocardium. However, at the infarct site and remote myocardium, infiltrating macrophages differentiate to M1 and M2 macrophages in response to different cues and secrete pro-inflammatory and pro-healing factors based on their macrophage phenotype. The number of M1 and M2 macrophages peak in the infarct site and remote myocardium at different pace. Created with BioRender.com 58

Figure 2.7: Strategies to improve iPSC-derived cardiomyocyte maturation i*n vitro*. iCMs are known to be immature in phenotype, resembling foetal cardiomyocytes. Multiple strategies have been employed to improve iCM maturity, including long term culture, using metabolic maturation media, modifying the culture surface to have microgrooves and micropatterns, mechanical stimulation, using biomaterials of stiffness resembling the native myocardium as well as using electroconductive materials, co-culturing with support cells, electrical stimulation and fabricating 3D engineered heart tissues. Image created using Biorender.com. 64

Figure 2.8: Resident macrophage derivation from iPSCs and applications. iPSCs can be derived from humans and other vertebrates by reprogramming somatic cells (fibroblasts, blood cells etc.). On specifying the ontogenic lineage, they can be differentiated into macrophages. Resident macrophages can potentially be obtained by

giving iPSC-derived macrophages tissue specific cues or activating specific transcriptional factors. These resident macrophages can be used for a number of applications such as disease modelling, cell therapy, genomics (to identify new genes) and drug testing. *Created with BioRender.com* 66

Figure 2.9: Brief overview of the evolution of Engineered Heart Tissues. The very first EHT was generated in 1997 by using chick embryonic cardiomyocytes on Velcro-coated glass tubes [13]. This model and the geometry of EHTs evolved over the years, from ring-shaped EHTs [251] to mini-EHTs adapted to a 24-well plate format [252], to EHTs with fluorescent cantilevers that can track contractile motions [248], followed by Biowire [14], cardiobundles [257], and Biowire II [191], to finally reach a human-scale EHT patch [15]. EHT, engineered heart tissue. Image created using *Biorender.com*. 75

Figure 5.1: Graphical Abstract. In this chapter, a reproducible protocol for the generation of iPSC-derived macrophages (iMacs) is screened from a number of existing protocols. iMacs obtained from the optimised protocol is compared with blood-derived macrophages (BDMs) to establish the difference between them in terms of basic macrophage characteristics, such as phagocytic and polarisation potential, as well as their expression of a number of different resident macrophage genes..... 93

Figure 5.2: Schematic diagram of the three different approaches used to differentiate iPSCs to iMacs. The differentiation was performed by modifying a previously established protocol [288], wherein, iPSCs were expanded to form embryoid bodies using Aggrewell™, agarose well and ULA plates. Embryoid bodies were then replated and kept in culture for up to a 100 days and monitored for successful iMac differentiation. 98

Figure 5.3: Differentiation of iPSCs to macrophages. (a) Representative images of iPSCs (11b cell line) and ZGiPSCs (zombie green tagged SFCi55 iPSC line) during expansion. (b) Representative images of iPSCs and ZGiPSCs undergoing mesodermal induction in Aggrewell™ , agarose and ultra-low attachment plates. (c) Representative images of terminally differentiated iMacs obtained from embryoid bodies formed using Aggrewell™ , agarose and ultra-low attachment plates. Scale bar: 200µm. 99

Figure 5.4: Characterization of iMacs using flow cytometry. (a) Gating strategy used to characterize iMacs. (b) Quantification of CD14 and CD11b positive populations of iMacs on day 7 and day 10 of differentiation (using gating strategy a.1). (c) Quantification of the population of iMacs positive for CX3CR1, within the CD14+ population (using gating strategy a.2). (d) Quantification of the population of iMacs negative for CCR2, within the CD14+ population (using gating strategy a.2). Statistical analysis - Ordinary One way and Two way ANOVA. ** represents P<0.01, *** represents P<0.001 and **** represents P<0.0001..... 100

Figure 5.5: Comparison of iMacs to BDMs. (a) Yield of iMacs over 100 days using three different plates for differentiation, with two iPSC lines. (b) Comparison of CD14 expression between BDMs and iMacs, 7 days after MCSF treatment. (c) Comparison of CCR2 expression between BDMs and iMacs, 7 days after MCSF treatment. (d) Quantification of CD14+CCR2- population in BDMs and iMacs. (e) Quantification of CD14+CCR2-HLADR+ population in BDMs and iMacs. (g) Comparison of phagocytic potential of BDMs and iMacs. (h) Quantification of phagocytic potential of BDMs and iMacs. Statistical analysis - Student T test with Welch's correction. * represents P<0.05, ** represents P<0.01, *** represents P<0.001 and **** represents P<0.0001..... 103

Figure 5.6: Assessment of polarisation potential of iMacs, using LPS, IFNγ and IL4. (a) Quantification of release of pro-inflammatory cytokines TNFα and IL6, using ELISA. (b) Quantification of release of anti-inflammatory cytokine IL10, using ELISA. (c) Quantification of mean fluorescence intensity of pro-inflammatory markers CD80 and CD86, using flow cytometry. (d) Quantification of mean fluorescence intensity of anti-inflammatory markers CD206 and CD163, using flow cytometry. Statistical analysis - Ordinary One way ANOVA. * represents P<0.05, ** represents P<0.01, *** represents P<0.001 and **** represents P<0.0001. 105

Figure 5.7: Comparison of the expression of a set of genes between iMacs and BDMs. (a) Expression of a set of pro-regenerative genes (b) Expression of a set of pro-inflammatory genes (c) Expression of a set of functional genes. Statistical analysis - Student T Test with Welch's correction. * represents P<0.05, ** represents P<0.01 and **** represents P<0.0001. 107

Figure 6.1: Graphical abstract. iPSCs were expanded and differentiated to obtain iCMs and iCFs. The efficacy of the differentiation was assessed using gene and protein expressions, using techniques such as RT-qPCR, flow cytometry and immunofluorescence imaging. 114

Figure 6.2: Characterisation of iCMs. (a) Schematic representation of the iCM differentiation protocol. (b) Representative image of iCMs obtained from SFCi55 iPSCs. Scale bar – 200 µm. (c) Representative image of iCMs derived using zombie green tagged SFCi55 iPSCs. Scale bar – 200 µm. (d) Representative image of iCMs stained with cTnT and connexin43 (Cx43). Scale bar – 10 µm, magnified image scale bar – 5 µm. (e) Representative image of iCMs stained with connexin43 (Cx43). Scale bar – 100 µm. (f) Representative image of iCMs stained with sarcomeric actinin. Scale bar – 100 µm. (g)

Representative flow cytometry plot showing the percentage of iCM population positive for cTnT. (h) Flow cytometry plot showing the percentage of iCM population positive for cTnT and MLC2a. Flow cytometry analysis performed using FlowJo. 117

Figure 6.3: Characterisation of iCFs. (a) Schematic representation of the iCF differentiation protocol. (b) Expression of a set of cardiac developmental genes. (c) Expression of a set of cardiac fibroblast-specific genes. (d) Mean fluorescence intensity of CD90 expression, quantified using flow cytometry. (e) Representative image of iCFs stained with DAPI and phalloidin. Scale bar – 200 µm, magnified image scale bar – 100 µm. Statistical analysis - One Way ANOVA. * represents P<0.05, ** represents P<0.01, *** represents P<0.001 and **** represents P<0.0001. 120

Figure 6.4: Comparison between iCMs and iCFs. (a) Expression of a set of cardiac developmental genes. (b) Expression of a set of cardiac fibroblast-specific genes. (c) Representative images of iCMs and iCFs using phase contrast microscopy (scale bar – 100 µm), stained with cTnT (iCM scale bar – 100 µm, iCF scale bar – 200 µm) and stained with sarcomeric actinin (iCM scale bar – 100 µm, iCF scale bar – 200 µm). Statistical analysis - Student T test with Welch's correction. * represents P<0.05, ** represents P<0.01 and *** represents P<0.001. 122

Figure 7.1: Graphical abstract. iPSCs were expanded and differentiated to obtain iCMs and iMacs. In order to provide iMacs with cardiac cues, two approaches were used. In approach (1), iMacs were cultured for 7 days in conditioned media and in approach (2), a co-culture of iCMs and iMacs were performed. The gene and protein expressions of both iMacs and iCMs were individually characterised, using techniques such as RT-qPCR, flow cytometry, immunofluorescence imaging and calcium imaging. 133

Figure 7.2: Characterisation of iCM conditioned media treated iMacs (iMacs_CM). (a) Schematic representation of the experimental set up. (b) Representative flow cytometry plots showing CD14 expression in BDMs, iMacs and iMacs_CM. (c) Representative flow cytometry plots showing CCR2 expression in $CD14^{high}$ BDMs, iMacs and iMacs_CM. (d) Quantification of $CD14^{high}CCR2^{low}$ populations of BDMs, iMacs and iMacs_CM. (e) Quantification of $CD14^{high}CCR2^{low}CX3CR1^{high}$ populations of BDMs, iMacs and iMacs_CM. (f) Quantification of $CD14^{high}CCR2^{low}$HLA-DR^{high} populations of BDMs, iMacs and iMacs_CM. (g) Quantification of phagocytic cell populations in iMacs and iMacs_CM. (h) Quantification of IL6 release by iMacs and iMacs_CM, post-LPS stimulation. (i) Quantification of TNFα release by iMacs and iMacs_CM, post-LPS stimulation. (j) Quantification of IL10 release by iMacs and iMacs_CM, post-LPS stimulation. Flow cytometry analysis performed using FlowJo. Statistical analysis used: one-way ANOVA with Tukey's comparison test for d, e, f, h, i and j; Student T test with Welch's correction for g. * represents P<0.05, ** represents P<0.01, *** represents P<0.001 and **** represents P<0.0001. 136

Figure 7.3: Characterisation of iCM conditioned media treated iMacs (iMacs_CM) using immunofluorescence imaging. (a) Schematic representation of the experimental set up. (b) Representative images of iMacs and iMacs_CM stained with DAPI and connexin43. Scale bar – 20 µm, magnified image scale bar – 10 µm. (c) Mean fluorescence intensity (normalised to cell number) of connexin43 expression, quantified using ImageJ. (d) Representative images of BDMs, iMacs and iMacs_CM stained with DAPI and CCR2. Scale bar – 100 µm (e) Mean fluorescence intensity (normalised to cell number) of CCR2 expression, quantified using ImageJ. Statistical analysis - one-way ANOVA with Tukey's

comparison test for e; Student T test with Welch's correction for c. ** represents P<0.01 and **** represents P<0.0001. 137

Figure 7.4: Characterisation of iMacs in co-culture with iCMs (iMacs_co-culture). (a) Schematic representation of the experimental set up. (b) Representative 3D reconstructed image of iCMs stained with Sarcomeric actinin, highlighting the integration of iMacs into iCM cultures. Scale bar – 50 µm (c) Representative images of iCMs and co-cultures of iMacs and iCMs stained with DAPI and connexin43. Scale bar – 100 µm. (d) Quantification of TNFα, IL6 and IL10 release by iMacs, iMacs_CM, iMacs_co-culture and iMacs cultured in RPMI with B27™. Statistical analysis - one-way ANOVA with Tukey's comparison test. **** represents P<0.0001. 139

Figure 7.5: Gene expression analysis of iCM conditioned media treated iMacs (iMacs_CM) and iMacs in co-culture with iCMs (iMacs_co-culture). (a) Schematic representation of the experimental set up. (b) Representative images of iCMs and iCM/iMac co-cultures, highlighting the reduction in dead cells and debris. Scale bar – 100 µm (c) Expression of a set of pro-regenerative genes. (d) Expression of a set of pro-inflammatory genes. (e) Expression of a set of functional genes. (f) Expression of a set of cardiac resident macrophage-specific genes. (g) Expression of a set of cardiac developmental genes. Statistical analysis - one-way ANOVA with Tukey's comparison test. * represents P<0.05, ** represents P<0.01, *** represents P<0.001 and **** represents P<0.0001. 143

Figure 7.6: Characterisation of iCMs in co-culture with iMacs. (a) Schematic representation of the experimental set up. (b) Representative images of iCMs and iCM/iMac co-cultures stained with cardiac troponin T (cTnT). Scale bar – 100 µm (c) Representative images of iCMs and iCM/iMac co-cultures stained with Sarcomeric

actinin. Scale bar – 100 µm (d) Expression of a set of cardiomyocyte-specific genes. (e) Ratio of the expression of MYH7/MHY6. (f) Expression of SERCA2. (g) Representative images of primary human atrial and ventricular tissue samples, stained with Sarcomeric actinin. Scale bar – 10 µm. (h) Quantification of sarcomere lengths obtained from analysis using ImageJ. Statistical analysis - Student T test with Welch's correction for (d, e and f)l; one-way ANOVA with Tukey's comparison test for (h). * represents P<0.05, *** represents P<0.001 and **** represents P<0.0001. 148

Figure 7.7: Characterisation of calcium handling and beat rate in iCMs and iCMs in co-culture with iMacs. (a) Schematic representation of the experimental set up. (b) Representative plots of the calcium transients in iCMs and iCMs in co-culture with iMacs. Nine regions of interest are assessed and the peaks denote individual spontaneous beat of the cells. Red lines highlight the synchronous beating of iCMs in co-culture with iMacs. (c) Quantified beat rate of iCMs and iCMs in co-culture with iMacs at day 25. (d) Quantified beat rate of iCMs and iCMs in co-culture with iMacs in response to treatment with carbachol, isoproterenol and caffeine. (e) Quantified beat rate of iCMs and iCMs in co-culture with iMacs at day 65. Statistical analysis - Student T test with Welch's correction for (c and e), Two-way ANOVA with Tukey's multiple comparison for (d). ** represents P<0.01, *** represents P<0.001 and **** represents P<0.0001. 152

Figure 8.1: Graphical abstract. iPSCs were expanded and differentiated to obtain iCMs and iMacs. iCMs, iMacs and co-cultures of iCMs and iMacs were subjected to electrical stimulation. The cells were characterised using gene and protein expressions, using techniques such as RT-qPCR, ELISA, immunofluorescence imaging and calcium imaging. 163

Figure 8.2: Representation of the electrical stimulation set up, modified from Solazzo *et al*. [439]. (a) Schematic representation of the carbon electrode, attached to platinum wires, kept in place using PDMS Sylgard^{TM} 184. (a i to vi) Schematic representation of the fabrication of the attached carbon electrode and platinum wire system (b i) Schematic representation of the lid of a 6-well plate, the 3D printed lid adaptor and the electrodes. The 3D printed lid adaptor also facilitates live imaging, by virtue of the empty spaces built into the adaptor. (b ii, iii) Schematic representation of the entire ES set up, with the plate stand and the digital microscope. (c) Image of the 6-well plate with the ES bioreactor lid. (d) Image of the oscilloscope (left) and waveform generator (right). 165

Figure 8.3: Characterisation of electrically stimulated iCMs. (a) Schematic representation of the experimental set up. (b) Expression of the genes TNNT2, MYH6 and MYH7, normalised to unstimulated iCMs. (c) Expression of the genes SERCA2, GJA1 and ratio between MYH7/MHY6, normalised to unstimulated iCMs. Statistical analysis – One-way ANOVA with Tukey's multiple comparison test. * represents P<0.05, ** represents P<0.01, *** represents P<0.001 and **** represents P<0.0001..... 168

Figure 8.4: Characterisation of electrically stimulated iMacs. (a) Expression of a set of pro-regenerative genes. (b) Schematic representation of the experimental set up. (c) Expression of a set of macrophage functional genes. (d) Expression of a set of pro-inflammatory genes. Statistical analysis - Student T test with Welch's correction. ** represents P<0.01, *** represents P<0.001 and **** represents P<0.0001..... 171

Figure 8.5: Characterisation of electrically stimulated iMacs in co-culture with iCMs, compared to of electrically stimulated iMacs and unstimulated iMacs as well as unstimulated iMacs in co-culture with iCMs. (a) Schematic representation of the

experimental set up. (b) Expression of a set of pro-regenerative genes. (c) Expression of a set of pro-inflammatory genes. (d) Expression of a set of macrophage functional genes. (e) Representative images of iCMs and iCM/iMac co-culture stained with sarcomeric actinin. Scale bar – 200 µm. iCMs generated using SFCi55 iPSCs and iMacs generated using Zombie green tagged SFCi55 iPSCs. Statistical analysis - Student T test with Welch's correction. * represents P<0.05, ** represents P<0.01 and *** represents P<0.001 and **** represents P<0.0001. 174

Figure 8.6: Characterisation of electrically stimulated iCMs in co-culture with iMacs, compared to of electrically stimulated iCMs and unstimulated iCMs as well as unstimulated iCMs in co-culture with iMacs. (a) Schematic representation of the experimental set up. (b) Quantified beat rate of iCMs and co-cultures after 5 days of ES. (c) Expression of a set of cardiomyocyte maturation genes. (d) Aspect ratio of iCMs and co-cultures, with and without 5 days of ES. (e) Quantified beat rate of iCMs and co-cultures after 2 days of ES. (f) Quantified beat rate of iCMs and co-cultures at day 25, day 65 and after 2 days of ES. (g) Intensity (F/F0) of calcium signalling by iCMs and co-cultures at day 25, day 65 and after 2 days of ES. (h) Quantified beat rate of iCMs and co-cultures in response to treatment with carbachol, isoproterenol and caffeine, after 2 days of ES. Statistical analysis - Students T test with Welch's correction for (b and e); One-Way ANOVA with Tukey's multiple comparison for (c and d); Two-way ANOVA with Tukey's multiple comparison for (f, g and h). * represents P<0.05, ** represents P<0.01 and *** represents P<0.001 and **** represents P<0.0001. 178

Figure 9.1: Graphical abstract. iPSCs were expanded and differentiated to obtain iCMs, iCFs and iMacs. Initially, engineered heart tissues (EHTs) were developed either using only iCMs, or a combination of iCMs and iMacs, to perform preliminary evaluation of

the performance of the tissues. Subsequently, EHTs were fabricated using iCMs and iCFs, as well as iCMs, iCFs and iMacs. These tissues were also subjected to electrical stimulation Techniques such as ELISA and immunofluorescence imaging was performed to assess tissue maturation and performance. 188

Figure 9.2: Engineered heart tissue bioreactor fabrication. (a) The four components required for the fabrication of EHTs. 1 and 2 are made with aluminium and are attached with each other; 3 is the frame and 4 is the baseplate. (b) Parts 1 and 2 attached to each other. (c) EHT bioreactor with posts, obtained by casting PDMS on to the aluminium moulds in (b). (d) EHT bioreactor attached to the frame. (e) Final EHT bioreactor set up with the baseplate. (f) Sample image of hydrogels made with the EHT bioreactor (without cells). Scale bar – 1mm. (g) Sample image of a tissue made with 1.5 million mouse embryonic fibroblasts, attached to the EHT bioreactor posts. Scale bar – 1mm. 190

Figure 9.3: Characterisation of the hydrogel. (a) Collagen-Matrigel® hydrogels with iMacs were casted on PDMS mould of 2.56 mm x 3 mm dimension. (b) Representative images of hydrogels after 2 hours of incubation at 37°C. Scale bar – 3 mm. (c) Quantification of the mean fluorescence intensity (MFI) of CD80, CD86, CD163 and CD206 stains on iMacs cultured in Collagen-Matrigel® hydrogels for 7 days. Flow cytometry analysis performed using FlowJo. Statistical analysis - One Way ANOVA. 193

Figure 9.4: Comparison between free and anchored EHTs. (a) Representative images of EHTs that are free and EHTs that are fabricated using the bioreactor (anchored). Scale bar – 1 mm (b) Representative images of free and anchored EHTs stained with cardiac troponin T (cTnT). Scale bar – 100 µm. (c) Quantification of the alignment of free and anchored EHTs. Yellow area with dotted lines indicate the alignment of free EHTs; green

area with solid line indicates the alignment of anchored EHTs. (d) Quantification of beat rate of free and anchored EHTs. Statistical analysis - Student T test with Welch's correction. 195

Figure 9.5: Structural comparison between iCM EHTs and iCM/iMac EHTs. (a) Schematic representation of the experimental set up (b) Quantification of the alignment of iCM and iCM/iMac EHTs. Green area with indicates the alignment of iCM EHTs; orange area indicates the alignment of iCM/iMac EHTs. (c) Representative images of human atrial and ventricular tissue samples stained with cardiac troponin T (staining iCMs) and CD68 (staining macrophages). Scale bar – 100 µm (d) Representative images of iCM and iCM/iMac EHTs stained with cardiac troponin T. Scale bar – 100 µm. 198

Figure 9.6: Functional comparison between iCM EHTs and iCM/iMac EHTs. (a) Schematic representation of the experimental set up (b) Representative images of iCM/iMac EHTs in culture. Scale bar – 1 mm (c) Quantified aspect ratio of iCMs in iCM EHTs and in iCM/iMac EHTs. (d) Quantified beat rate (in bpm) of iCM and iCM/iMac EHTs. Light green area highlights range of human heart beat rate. (e) Compaction of EHTs over a period of 7 days. Statistical analysis - Student T test with Welch's correction for c and d; Two-way ANOVA with Tukey's multiple comparison for e. ** represents P<0.01 and **** represents P<0.0001..... 201

Figure 9.7: Comparison between iCM/iCF and iCM/iCF/iMac EHTs (a) Schematic representation of the experimental set up. (b) Compaction of EHTs over a period of 14 days (c) Representative images of iCM/iCF and iCM/iCF/iMac EHTs in culture, undergoing compaction. Scale bar – 1 mm (d) Quantified beat rate (in bpm) of iCM/iCF and iCM/iCF/iMac EHTs. Light green area highlights range of human heart beat rate. (e) Representative image of iCM/iCF/iMac EHT with macrophages coming out of the

tissues. Scale bar – 0.5 mm. Statistical analysis - Two-way ANOVA with Tukey's multiple comparison for b; Student T test with Welch's correction for d. **** represents P<0.0001. 203

Figure 9.8: Comparison between iCM/iCF and iCM/iCF/iMac EHTs with and without electrical stimulation (a) Schematic representation of the experimental set up. (b) Representative images of iCM/iCF and iCM/iCF/iMac EHTs stained with alpha SMA, highlighting fibrosis. Scale bar – 100 μm (c) Mean fluorescence intensity of alpha SMA staining (normalised to cell number). Statistical analysis - One-way ANOVA with Tukey's multiple comparison. * represents P<0.05 and ** represents P<0.01. 206

Figure 9.9: ELISAs assessing iMac and iCF activation. Quantification of endogenous (a) IL6, (b) TNFα and (c) IL10 in electrically stimulated and non-stimulated iCM/iCF/iMac EHTs. (d) Endogenous TGFβ-1 in iCM/iCF and iCM/iCF/iMac EHTs. (e) Endogenous TGFβ-1 in electrically stimulated iCM/iCF and iCM/iCF/iMac EHTs. Statistical analysis - Student T test with Welch's correction. * represents P<0.05, ** represents P<0.01 and **** represents P<0.0001. 206

List of Tables

Table 1: Examples of iPSC-derived macrophage subsets and their respective phenotypic markers 67

Table 2: Examples of macrophage use in tissue engineering 68

Table 3: Details of iPSC lines used 78

Table 4: Macrophage-specific antibodies with fluorochromes and dilution information for flow cytometry 81

Table 5: Cardiomyocyte-specific antibodies with fluorochromes and dilution information for flow cytometry 82

Table 6: Volumes for sample preparation for reverse transcription 84

Table 7: Volumes for sample preparation for RT-qPCR 84

Table 8: Gene primer sequences 85

Table 9: Primary and secondary antibodies with dilution information for immunofluorescence imaging 88

Table 10: Collagen-Matrigel® hydrogel composition 189

Abbreviations

2D	2 dimensional
3D	3 dimensional
ANOVA	analysis of variance
AV	atrioventricular
BDMs	blood-derived macrophages
BMP	bone morphogenetic protein
BSA	bovine serum albumin
CAD	coronary artery disease
CANTOS	Canakinumab Anti-Inflammatory Thrombosis Outcomes Study
CCR2	C-C chemokine receptor type 2
COLCOT	colchicine cardiovascular outcomes trial
CRM	cardiac resident macrophages
cTnT	cardiac troponin T
CVD	cardiovascular diseases
CX43	connexin 43
DAPI	4’,6-Diamidine-2’-phenylindoledihydrochloride
DNA	deoxyribonucleic acid
EB	embryoid body
ECM	extracellular matrix
EHT	engineered heart tissue
ELISA	enzyme linked immunosorbent assay
EMPs	Erythromyeloid progenitors
ES	electrical stimulation
ESC	embryonic stem cells
FACS	fluorescence activated cell sorting
FBS	foetal bovine serum
FGF	fibroblast growth factor
HSCs	haematopoietic stem cells
iCF	iPSC-derived cardiac fibroblasts

iCM	iPSC-derived cardiomyocytes
IHDs	inflammatory heart diseases
IL	interleukins
iMac	iPSC-derived macrophages
iPSC	induced pluripotent stem cells
LoDoCO2	low dose colchicine after myocardial infarction
LQT	long QT
LV	left ventricular
LYVE1	lymphatic vessel endothelial hyaluronan receptor 1
M-CSF	macrophage-colony stimulating factor
M1	pro-inflammatory macrophage phenotype
M2	anti-inflammatory macrophage phenotype
MACS	magnetic activated cell sorting
MAPK	mitogen activated protein kinase
MEMS	microelectromechanical systems
MERTK	myeloid epithelial reproductive tyrosine kinase
MHC	major histocompatibility complex
MI	myocardial infarction
MMP	matrix metalloproteinases
MPS	mononuclear phagocyte system
MSC	mesenchymal stromal cells
MYB	myeloblastosis
PAD	peripheral artery disease
PBMCs	peripheral blood mononuclear cells
PBS	phosphate buffered saline
PCR	polymerase chain reaction
PDMS	polydimethylsiloxane
PFA	paraformaldehyde
RAAS	renin-angiotensin-aldosterone system
RNA	ribonucleic acid
SA	sinoatrial
TGF-β	transforming growth factor-β

TIMD4	T-cell immunoglobulin and mucin domain containing 4
TNFα	tumour necrosis factor alpha
TRM	tissue resident macrophages
VEGF	vascular endothelial growth factor
YS	yolk sac
ZGiPSC	zombie green tagged induced pluripotent stem cells

Chapter 1 Introduction

1.1. Cardiovascular health and disease

Cardiovascular disease stands as the leading cause of death globally, claiming approximately 19.05 million lives in 2020 [1]. Myocardial infarction (MI) is a common cardiovascular disease, caused by decreased or complete cessation of blood flow to a portion of the myocardium [2]. Given the limited regenerative capacity of the myocardium, the infarcted region undergoes remodeling and fibrosis, marked by dilation, segmental hypertrophy of the remaining viable tissue, and the onset of cardiac dysfunction [3]. Over time, a dense collagenous scar replaces the contractile tissue, hindering both the heart's pumping function and long-term efficacy [4]. To compensate, the remaining viable myocardium hypertrophies, the infarct wall thins, scar tissue replaces the viable myocardium, and the left ventricle dilates, culminating in heart failure [5]. Current state-of-the-art treatments for end-stage heart failure predominantly involve LV assist devices and total heart transplantation [6], both requiring invasive surgeries, some form of immunomodulation and variable success. Hence, there is a critical clinical demand for novel therapies addressing the adverse post-MI responses leading to HF, including negative LV remodeling, arrhythmias, and diastolic dysfunction [7].

While numerous classes of pharmacologic drugs are routinely employed to address heart failure, and an increasing array of new molecules and signalling pathways are under investigation [8, 9], a subset of patients with heart failure do not achieve satisfactory responses to optimal pharmacologic therapy [8]. However, the scarcity of donor organs [10] and complications arising from the continuous immunosuppression required for these patients considerably limit this therapeutic avenue, prompting the exploration of alternative treatments. In order to develop effective therapeutic drugs, the pre-clinical evaluation stages are long and most commonly performed in animals. Although animal models are an accepted tool to understand the mechanism of action

of therapeutics and to understand the response of a whole living organism to the drug [11], there still remains challenges in terms of transferring disease-related knowledge from animal models into human pharmaceutical testing, stemming from specie variations [12]. Through tissue engineering strategies, a number of cardiac tissue models have been developed *in vitro* (healthy and diseased) [13-17]. However, these models lack complexities of the native myocardium, in terms of structure and cellular composition. Human myocardium hosts five major cell types – cardiomyocytes, cardiac fibroblasts, endothelial cells, smooth muscle cells and immune cells. The last decade revealed some critical functions of immune cells, in particular, macrophages, in the myocardium, making them a key cell type to include in engineered heart tissue models, to improve the functional capacity of engineered heart tissues and to make them more physiologically relevant.

1.2. Macrophages in the heart

Macrophages are present in almost every vertebrate tissue. They contribute to the maintenance of immunity by phagocyting microbes, clearing senescent cells and promoting homeostasis by repairing and regulating the functions of organs. Initially perceived as a cell population only present in, and originating from the blood, recent studies have brought to light the stark heterogeneity in blood-derived and a pre-natal embryologically derived macrophage populations. Most tissues in the body contain a resident macrophage population exhibiting diverse phenotypes, specific to that tissue and niche [18]. This phenotypic heterogeneity is potentially due to the impact of the resident tissue environment as well as differences in the macrophage origin [19]. Although multiple macrophage subsets exist within the heart, the macrophage population that is resident to the heart - cardiac resident macrophages (CRMs) - originate during embryogenesis and populate the heart prenatally [20]. Only within the past 3-4 years, seminal studies unravelling the functions and the physiological importance of cardiac macrophages have emerged (in mice), identifying these cells as a potential candidate, to incorporate into *in vitro* models. In addition to performing

critical functions in healthy myocardium, cardiac resident macrophages respond uniquely to subtle changes in the homeostatic equilibrium. Under healthy conditions, CRMs perform critical functions in the heart, such as facilitating electrical conduction [21], capture and eliminate particles released by cardiomyocytes (exophers) [22], perform phagocytosis and efferocytosis [23], and promote regeneration [24-26]. Furthermore, when the homeostasis is disturbed, such as during MI, CRMs exert cardioprotective functions to help alleviate intense inflammatory responses [27]. Although there has been a limited number of studies focusing on the role of CRMs in the heart, there exists enough groundwork to explore the possibilities of achieving more humanised cardiac tissue models using resident macrophages.

1.3. *In vitro* models of the myocardium

Human myocardium is a complex and contractile tissue, and numerous attempts have been made to recapitulate the complexities of the myocardium *in vitro*. Tissue engineered 3D cardiac models provide a unique platform to understand cell-cell interactions in addition to cell-extracellular matrix (ECM) interactions. Since the pioneering effort reported by Eschenhagen *et al.* in 1997, multiple architectures, materials and cell types have been tried and tested to generate engineered heart tissue (EHT) models [13-17]. While all reported EHT models include cardiomyocytes, some studies have also looked at the potential of improving the functional response of the EHTs by incorporation of supporting cells such as fibroblasts [16], endothelial cells [28] and mesenchymal stromal cells [29]. However, there is no EHT model in existence, that has harnessed an innate immune response by adding CRMs. Hence, by incorporating resident macrophages within EHTs, models can be more physiologically relevant, with applications in regenerative medicine, disease modelling and drug screening. However, there remain a lot of questions to be answered – what is the optimal way to derive CRMs *in vitro*; how do cardiomyocytes and embryonic-like macrophages interact with each other *in vitro*, how do macrophages affect the function of EHTs, to name but a few.

1.4. Thesis objectives

The main aim of this thesis is to develop a physiologically relevant model of the human myocardium, using induced pluripotent stem cell (iPSC)-derived cardiomyocytes, macrophages and cardiac fibroblasts. To achieve this, first, the 3 cell types are differentiated from iPSCs. Next, the interaction between iPSC-derived cardiomyocytes and macrophages are characterised in detail. Subsequently, the potential of electrical stimulation to facilitate maturation of cardiomyocytes is explored. Finally, EHTs are fabricated using iPSC-derived cardiomyocytes, macrophages and cardiac fibroblasts and their structural and functional responses are assessed.

Chapter 2 Literature Review

The majority of the work in this chapter has been peer reviewed and published in the journal Tissue Engineering. Part B, Reviews:

Suku M, Forrester L, Biggs M, Monaghan MG. Resident Macrophages and Their Potential in Cardiac Tissue Engineering. Tissue Eng Part B Rev. 2022 Jun;28(3):579-591. doi: 10.1089/ten.TEB.2021.0036. Epub 2021 Aug 18. PMID: 34088222; PMCID: PMC9242717.

2.1. Anatomy of human heart and the conduction system

The heart plays a crucial role in pumping blood and nutrients to all organs, supporting their normal function. The synchronised contraction of the heart generates pressure, propelling the blood flow in arteries to distal organs. The constant, repetitive pumping action ensures the continuous circulation to all organs. The human heart wall has three distinct layers – endocardium, myocardium and epicardium [30] (Figure.2.1). the myocardium is a thick, contractile muscle layer, which lies between the single-celled endocardium layer, and the outer epicardium [30]. While the endocardial layer lines the inner chambers, the epicardium makes up part of the pericardium that surrounds and protects the heart. Additionally, a highly dense structure known as the fibrous or cardiac skeleton resides at the base of the heart, providing strong framework for cardiac muscle cells, acting as an anchor for valvular leaflets and facilitating electrical insulation between the atria and ventricles [31]. The initiation of electrical impulses occurs at the sinoatrial (SA) node, positioned at the junction of the superior vena cava and right atrium [32] (Figure.2.2). These impulses propagate through the atria until reaching the atrioventricular (AV) node, which is situated between the interatrial and interventricular septum. Continuing towards the base, the fibres penetrate the central fibrous body of the cardiac skeleton, giving rise to the bundle of His. Following division within the interventricular septum, these fibres become the Purkinje fibres, branching into the ventricles [32]. On a cellular level, the contraction of the heart is facilitated by the cardiac muscle cells residing in the myocardium, called cardiomyocytes.

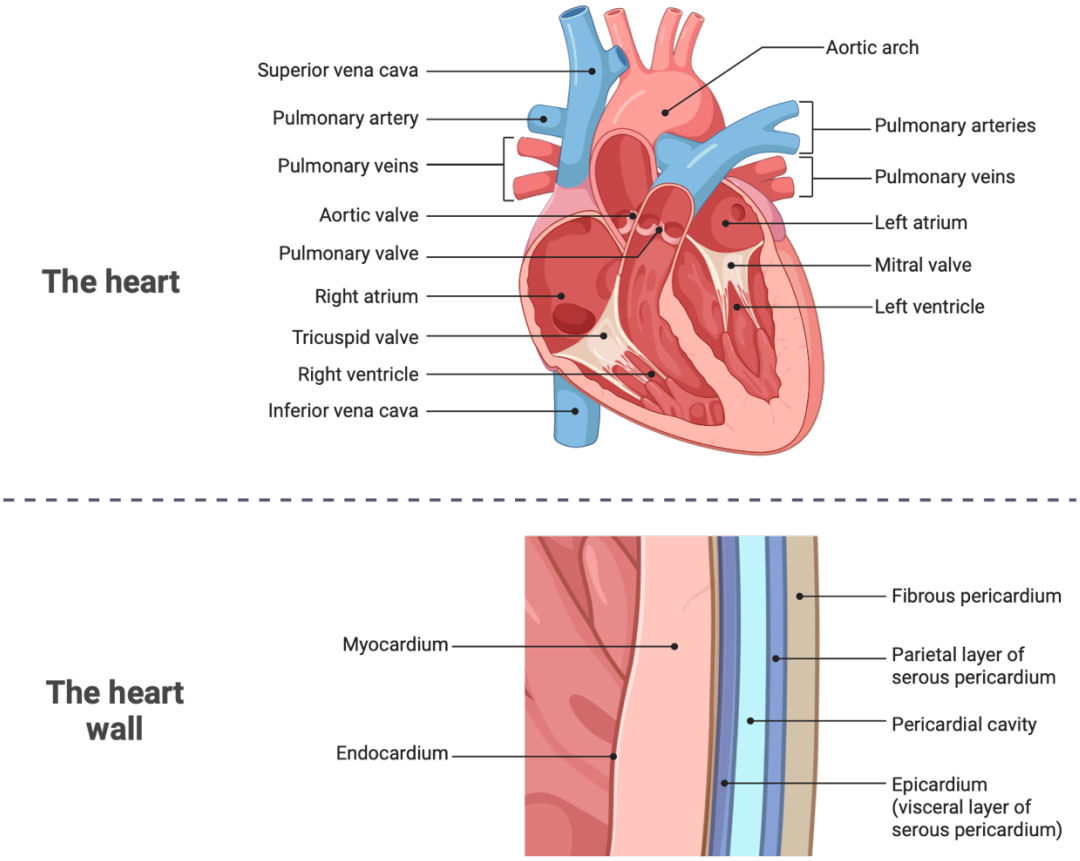

Figure 2.1: Anatomy of human heart, highlighting the layers of the heart wall. Image modified from a Biorender® template.

2.2. Cardiac diseases and its global impact

Cardiovascular disease (CVD) remains a leading cause of mortality and morbidity worldwide [33, 34]. According to the Global Burden Disease, Injuries and Risk Factors Study (GBD) 2019, the total number of CVD cases have reportedly increased from 272 million in 1990 to 523 million in 2019 [35] Additionally, the number of deaths due to CVDs also saw an increase, from 12.1 million in 1990, to 18.6 million in 2019 [35]. CVDs broadly refer to four diseases, namely, coronary artery disease (CAD), cerebrovascular disease, peripheral artery disease (PAD) and aortic atherosclerosis [36]. The most common cause of CAD is decreased myocardial perfusion due to ischemia, which can result in myocardial infarction (MI) [34, 37]. Despite therapeutic advances, a limited regeneration potential of the heart impedes appropriate functional tissue repair.

Instead, a scar is formed due to ongoing adverse compensatory mechanisms that are not only focused on the site of injury, but also exert their effects in remote areas [37]. This scar tissue impairs the ability of electrical signals to travel across the heart wall and in doing so, cardiomyocytes in that region become electrically isolated and the heart's ability to beat becomes compromised [38]. Our understanding of MI has progressed considerably in the recent years, with immune cell-driven inflammation being recognised as a key driver in the remodeling of cardiac tissue post-MI, resulting in heart failure. While the age-adjusted rate and acute mortality from MI have been on a decline over time, indicative of advancements in diagnosis and treatment in recent decades, the risk of heart disease persists at a notable level [39]. Calculations suggest a substantial 50% risk by the age of 45 in the general population [39, 40]. The incidence exhibits a significant rise with age, displaying some gender-related variations. Notably, the incidence is higher in men at younger ages, although for women, this difference gradually diminishes in the post-menopausal state [41]. Although current pharmacological interventions can attenuate adverse remodeling, the prognosis for these patients is poor, with increased risk of death and reduced quality of life. There requires a deeper understanding of the interaction of immune cells in the cardiac environment to delineate the process of tissue remodeling, as well as recognise therapeutic targets for the treatment of MI.

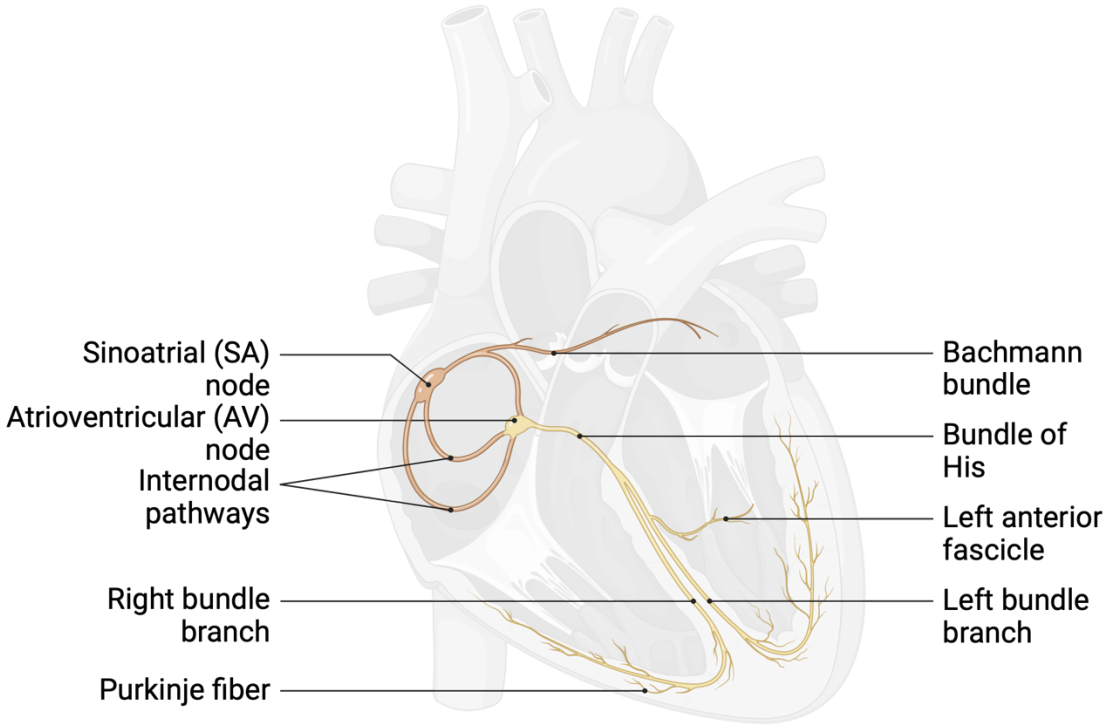

Figure 2.2: Schematic representation of the conducting system of human heart. Image modified from a Biorender® template.

2.3. Cells of the heart

The human heart is a highly complex tissue, populated by a number of different cell types, of distinct lineages. The cellular content of human myocardium (by number) predominantly consists of cardiomyocytes, fibroblasts, pericytes and smooth muscle cells, endothelial cells and immune cells [42] (Figure.2.3). Cardiomyocytes dominate the human myocardial volume at 70-80%, which constitutes 30-40% of cells by number [43]. While cardiomyocytes conduit electrical conduction and maintain the contractile functions inherent to the heart, the non-myocytes (fibroblasts, pericytes and smooth muscle cells, endothelial cells and immune cells) facilitate matrix deposition, vascularisation, immunosurveillance etc. [44]. Cardiomyocytes and non-myocytes constantly interact with each other through cytokine and growth factor secretion. For

instance, the release of vascular endothelial growth factor (VEGF) promotes angiogenesis in the myocardium, which is mediated by cardiac endothelial cells [45, 46]. Similarly, inflammatory cytokines such as tumour necrosis factor alpha (TNFα) and various interleukins (IL) such as IL4, IL6, IL8 etc. that are produced in response to an injury, facilitate extracellular matrix (ECM) remodeling [47, 48]. Cardiac fibroblasts express markers that are crucial for the construction of ECM such as collagen I, platelet-derived growth factor receptor alpha, vimentin etc., as a result of which they are vital for both normal cardiac function and remodeling in response to injury [49, 50]. Furthermore, non-myocyte interactions such as the crosstalk between cardiac fibroblasts and cardiac macrophages are key to maintaining of structural integrity of the heart [49].

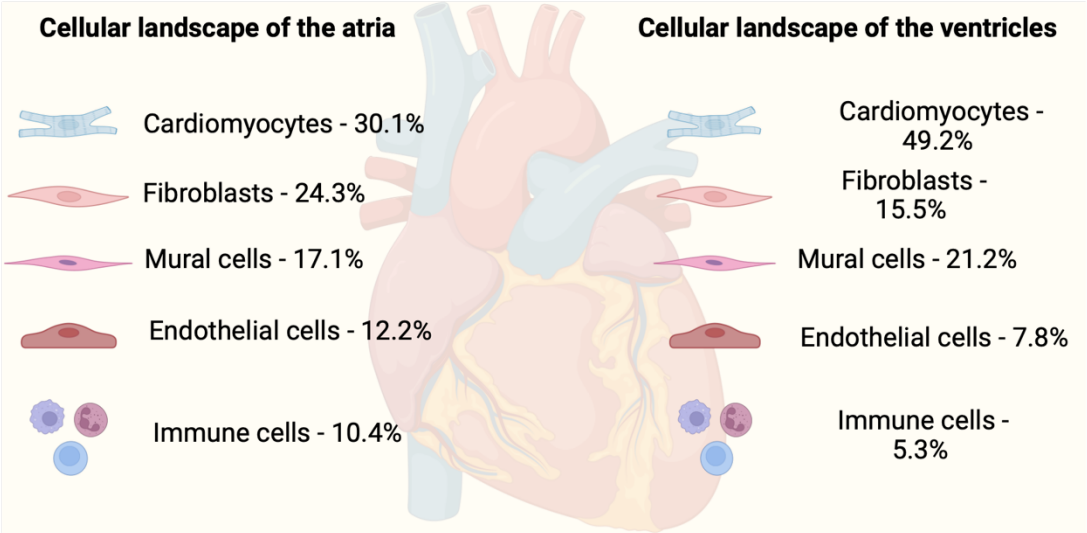

Figure 2.3: The cellular landscape of adult human heart [42]. The main cell types of the myocardium include cardiomyocytes, fibroblasts, mural cells (pericytes and smooth muscle cells), endothelial cells and immune cells. However, the number of these cell types vary across the atria and the ventricles. Image created using Biorender.com.

2.4. Inflammatory cardiac events

In addition to MI, a number of other cardiac diseases are mediated by inflammatory pathways. Atherosclerosis is a pathological progression occurring in arteries and the aorta, with the potential to induce diseases stemming from reduced or obstructed blood flow due to the narrowing (stenosis) of blood vessels [51]. During the onset of atherosclerosis, antigen-presenting cells play a crucial role by providing major histocompatibility complex (MHC) molecules, cytokines and costimulatory molecules. This process drives polarisation of the adaptive immune response [52]. Macrophages and dendritic cells, present in the arterial adventitia and neointima, become activated by Toll-like receptor ligands and scavenger receptors [53]. The presence of inflammatory cytokines further intensifies atherosclerosis, while attracting additional immune cells. In mature atherosclerotic plaques, T cells specific to atherosclerotic antigens secrete cytokines, perpetuating inflammation and influencing the composition of the immune cell infiltrate [54]. Furthermore, inflammatory heart diseases (IHDs) are a group of diseases that affect different layers of the heart. Inflammation of pericardium, myocardium and endocardium are known as Pericarditis, Myocarditis and Endocarditis, respectively [55]. Although IHDs are commonly caused by autoimmune disorders, they can sometimes be caused due to microbial infections [56], making these diseases highly complicated.

The pivotal role of innate immunity in CVDs was illuminated by the CANTOS (Canakinumab Anti-Inflammatory Thrombosis Outcomes Study) trial [57]. This clinical trial revealed that the targeting of IL1β using a specific monoclonal antibody (Canakinumab) resulted in a reduction in the rate of recurrent cardiovascular events among patients with a history of MI and elevated levels of C-reactive protein. Furthermore, these effects were correlated with a decrease in IL6 levels [57]. Although Canakinumab was not ultimately approved for cardiovascular treatment, this ground-breaking study highlights the potential therapeutic impact of modulating innate immune responses in the context of cardiovascular health. Interestingly, most of the common drugs employed in clinical practice for treating CVDs, exhibit notable anti-inflammatory effects [58]. Beta-blockers, agents affecting the renin-angiotensin-

aldosterone system (RAAS), and neprilysin inhibitors, while primarily impacting cardiomyocytes, also contribute to a reduction in the release of inflammatory cytokines [58]. These observations highlight the prevalence of inflammatory events associated with numerous cardiac events, while also suggesting the possibility that a targeted immunomodulatory therapy could emerge as a viable strategy in the treatment of heart failure.

2.5. Immune cells in the heart

A healthy myocardium hosts almost all major immune cell types, such as T cells, B cells, dendritic cells, innate lymphoid cells (such as natural killer cells) and myeloid cells (granulocytes and macrophages) [42]. Using state-of-the-art techniques such as single-cell and single-nucleus RNA sequencing, and multiplex single-molecule fluorescence in situ hybridisation single cell RNA sequencing, Litviňuková *et al.* demonstrated the existence of a total of 21 immune cell states, in adult human heart [42]. Notably, the most abundant cardiac immune cell type, are the embryonically derived cardiac resident macrophages (CRMs) [59]. While CRMs are critical in maintaining homeostasis in the myocardium (detailed in subsection 2.5.1), adaptive immune cell types such as T cell and B cells are also important in the normal functioning of the myocardium [27]. Maladaptive T cell aging has been associated with the promotion of chronic inflammatory disorders, with a drop in the function of protective T cells and enrichment in pro-inflammatory effector T cells [60, 61], indicating that maladaptive T cell responses could make the heart susceptible to chronic inflammation, leading to tissue damage. Similarly, using murine hearts, the potential role of B cells in maintaining cardiac homeostasis has also been suggested. In this study, Adamo *et al.* revealed that a subset of B cells transiently arrested on the cardiac microvascular endothelium during their transit through the heart [62]. The majority of myocardial B cells remained intravascular, with less than 5% extravasating into the myocardial tissue. However, mice deficient in B cells exhibited reduced myocardial mass, increased left ventricular ejection fraction, faster relaxation, and an augmented cardiac T cell composition [62]. However, the specific mechanisms by which B cells might influence cardiac growth and contractility

require further investigation. In a more recent study, Grune *et al.* optimised a mouse model in which hypokalaemia combined with MI initiated ventricular tachycardia in mice [63]. Using this model, it was revealed that neutrophils aggravated ventricular tachycardia, while macrophages protected against arrhythmia. Grune *et al.* also reported that depleting recruited and resident macrophage populations increased ventricular tachycardia and fibrillation [63]. These findings signify the cardioprotective role played by macrophages in the myocardium, making them a cell population of interest in cardiac tissue engineering.

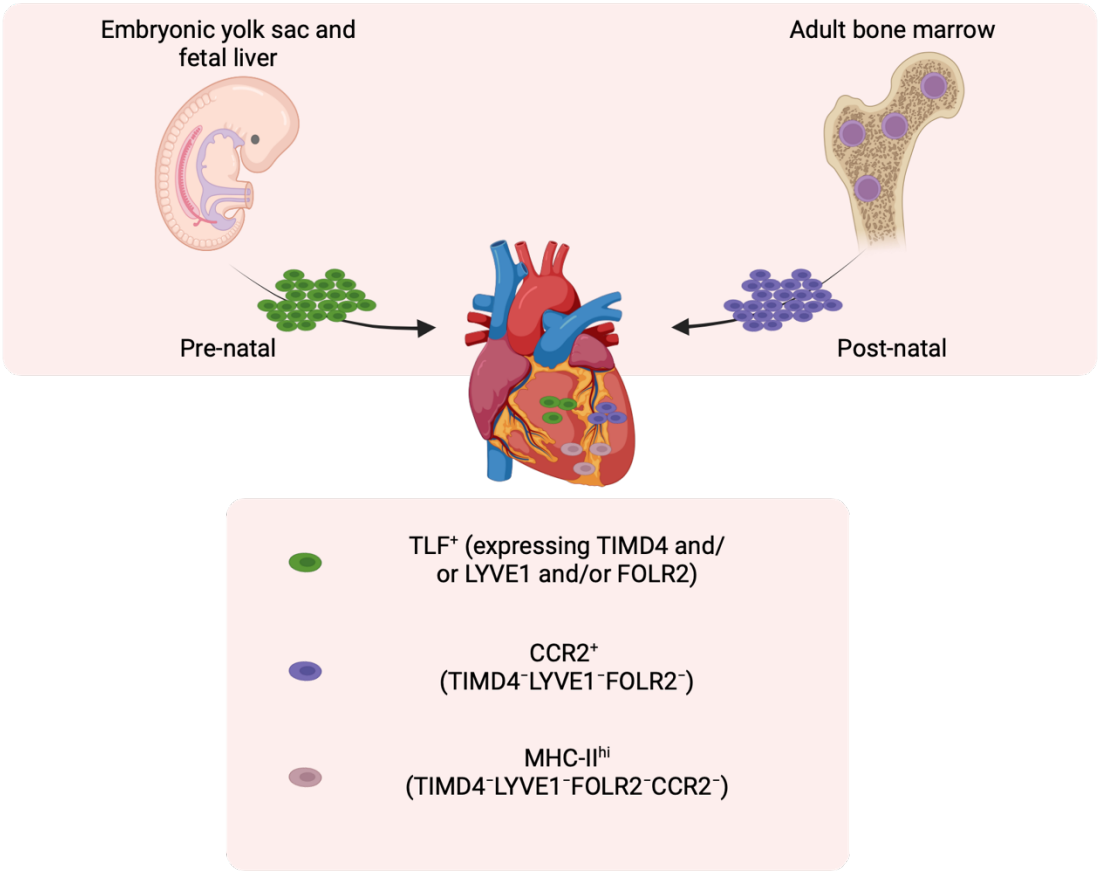

Figure 2.4: Schematic representation of the origin of macrophages in the heart. Resident macrophages originate prenatally and populate the heart, whereas circulating macrophages originate in the adult bone marrow. According to most recent reports [64], the macrophage populations present in the heart include TLF^+ (cardiac resident macrophages), $CCR2^+$ (bone marrow-derived macrophages) and MHC-II^{hi} (derived postnatally from cardiac macrophages). Image created using Biorender.com.

2.5.1. Macrophages: origin and types

Macrophages exist throughout almost every tissue within vertebrates. They contribute to the maintenance of immunity by phagocytosing microbes, clearing senescent cells and promoting homeostasis by repairing and regulating the functions of organs. Initially perceived as a cell population only present and originating in the blood, recent studies have brought to light the stark heterogeneity in the hematopoietic and the pre-natal embryo-derived macrophage populations. Most tissues in the body contain a resident macrophage population exhibiting diverse phenotypes, specific to tissue and niche [65]. This heterogeneity in their phenotypes is potentially due to the impact of their resident tissue environment as well as the differences in their origin. However, despite being best known as the key mediators in tissue defence, the exact role of these subsets of macrophages in protecting the body from pathogens or environmental change, are still unclear.

Ilya Metchnikoff first identified macrophages in the late 19th century, where he described them as phagocytic cells that help in host defence [66]. He was one of the first people to highlight the importance of phagocytosis in unicellular organisms for feeding, in embryogenesis (when the egg phagocytoses the sperm) and finally in host defence [67]. Successors of Metchnikoff worked around this theory and by early 20th century, coined the term "reticuloendothelial cells" for the mononuclear and polymorphonuclear cells present in the blood - "reticulo" for their ability to form networks and "endothelial" because they were located adjacent to the vascular endothelium [68]. By 1969, this term was deemed insufficient to describe resident phagocytes and their precursors, resulting in the conception of a new term – mononuclear phagocyte system (MPS) [69]. MPS initially comprised of only monocytes and macrophages and dendritic cells were later added to this group [70, 71]. According to this system, macrophages were considered terminally differentiated with no proliferation potential and constantly replenished by circulating monocytes originating from the bone marrow [72]. Having evolved more than 500 million years ago, phagocytic cells have been present in animals, as motile cells executing a range of defence and housekeeping functions [73, 74]. But it was only by early 20th century, that macrophage heterogeneity started gaining more appreciation.

With the emergence of modern detection techniques such as fate mapping and lineage tracing, scientists started understanding that some macrophages do indeed proliferate [75] and are present in the embryo before definitive haematopoiesis [76]. Interestingly, these macrophages of distinct ontogeny are found to coexist with each other in the body, performing tissue-specific functions. Haematopoiesis is reported to occur in multiple waves [77]. During gestation in mice, around embryonic day (E) 6.5 and 8.5, primitive haematopoiesis occurs in the Yolk Sac (YS) [78], where Erythromyeloid progenitors (EMPs) develop independent of cellular myeloblastosis (c-Myb) – a master transcriptional regulator of haematopoiesis [79]. As circulation is established (E8.5-E10.5), these EMPs migrate to the foetal liver. Instead of passing through a monocytic stage, the c-Myb-independent EMPs directly become macrophage precursors, acquiring a core macrophage transcriptional program. Simultaneously, the aorta-gonad-mesonephros produces the hematopoietic precursors which also migrate to the foetal liver around E10 leading to the development of definitive Hematopoietic Stem Cells (HSCs). From E11, foetal liver acts as the primary site of embryonic haematopoiesis which is later taken over by HSCs in the bone marrow (E16.5) [80]. Tissue-resident macrophages (TRMs) arise at different waves of haematopoiesis and the origin of some are still unknown. However, there have been indications that the expression of tissue-specific transcriptional regulators arises from around E10.25, leading to niche-specific heterogeneity of the YS-derived macrophages [81].

Initial fate mapping studies that focused on microglia and Langerhans cells showed that microglia originated from the primitive YS [82], while Langerhans cells originated from both foetal liver and primitive YS [83]. Langerhans cells were initially perceived to be dendritic cells, but later were classified as TRMs owing to its dependence on Macrophage-Colony Stimulating Factor (M-CSF) receptor during development [84], prenatal origin and transcriptional evidences [85]. The discovery that Langerhans cells and microglia originate prenatally, was a major deviation from the MPS model, which steered more researchers to explore the origin of different macrophage subtypes. During embryonic development, the surface markers and the transcriptional factors expressed by HSC-derived and YS-derived macrophages contrast each other. The

presence of transcriptional factor MYB is essential for definitive HSC development whereas YS-derived progenitors develop independent of MYB [86].

Murine monocytes are usually categorised based on their Ly6C expression as two populations – Ly6C^{high} and Ly6C^{low}. Under healthy physiological conditions Ly6C^{low} monocytes patrol along vessel walls and clear damaged endothelial cells of the vasculature [87], whereas Ly6C^{high} monocytes infiltrate sites of inflammation, where they differentiate into macrophages. Ly6C^{high} monocytes also infiltrate tissues in homeostasis to transport antigens to lymph nodes [88]. Characteristically, YS derived macrophages in mice are CX3CR1^{high}F4/80^{high} [89, 90], but sometimes, the surface markers alter as the organism matures, making it impossible to trace them using just these markers. CX3CR1^{high} macrophages of embryonic origin in mice tend to lose CX3CR1 expression post-birth, serving as a perfect example for this limitation [91].

With reference to recent studies, the effect of the local biochemical environment on the specialisation of TRMs is becoming more evident. For example, the presence of heme has been shown to induce *Spi-c*, which is required for the development of the red pulp macrophages in spleen [92, 93] and *Nr1h3* helps in the splenic marginal zone macrophage development [94]. Similarly, TGF-β1 through the transcription factor SMAD has been shown to regulate microglia expression [95, 96]. Peritoneal macrophage expression has been shown to be regulated through the stimulation of GATA6 by retinoic acid [97]. The transcription factor ID3 has been identified to play a role in maintaining Kupffer cell expression [81], RUNX3 and ID2 help in the development of Langerhans cells [98, 99] and PPAR-γ regulates alveolar macrophage expression [100]. It has also been found that transplanting TRMs to a new tissue microenvironment can alter their genomic profile [101]. Nonetheless, the transcriptional regulators of a wide number of TRMs are yet to be discovered, however there are reports that provide evidence on the role of the tissue environment in governing the tissue-specific macrophage expression.

2.5.2. Cardiac macrophages in homeostasis

In the murine heart, macrophage populations can be discerned based on their differential expressions of C-C chemokine receptor type 2 (CCR2), major histocompatibility complex-II (MHC-II), T-cell immunoglobulin and mucin domain containing 4 (TIMD4) and Lymphatic Vessel Endothelial Hyaluronan Receptor 1 (LYVE1). Four populations of macrophages have been identified in the murine heart [102]. The minority are two subsets of $CCR2^{+}MHC\text{-}II^{high}$ macrophage populations derived from hematopoietic stem cells (HSCs), whereas the most dominant subset, cardiac resident macrophages derived from the yolk sac, are $CCR2^{-}MHC\text{-}II^{low}TIMD4^{+}LYVE1^{-}$. There also exists a fourth subset that consists of $CCR2^{-}MHC\text{-}II^{high}TIMD4^{+}LYVE1^{+}$ macrophages which are likely derived from $CCR2\text{-}MHC\text{-}II^{low}$ macrophages during postnatal development [102, 103] and partially maintained by $CCR2^{+}MHC\text{-}II^{high}$ macrophages. $CCR2^{+}MHC\text{-}II^{high}$ macrophages populate the heart soon after birth and are maintained through monocyte recruitment and proliferation[104]. Also, under homeostasis, cardiac macrophages continually self-renew with a turnover period of almost five weeks [105]. Recently this same $CCR2^{+}$ and $CCR2^{-}$ macrophage distinction has been identified in humans [106], with the yolk sac-derived $CCR2^{-}$ human counterpart showing $CD14^{+}CD45^{+}CD64^{+}CCR2^{-}$ $HLA\text{-}DR^{high}$ expression [102, 106]. In a more recent study, Tucker *et al.* reported two cardiac macrophage subsets within the human heart which were positive for CD163, COLEC12, mannose receptor MRC1, E3 ubiquitin ligase MARCH1 and natural resistance–associated macrophage protein 1 (NRAMP1). While both of the identified subsets express anti-inflammatory (M2) polarisation–associated genes, one subset particularly expressed RBPJ, F13A1 and the other expressed transmembrane collagen COL23A1 [107]. However, according to most recent findings, the macrophage populations of the heart include TLF^{+} macrophages that are maintained through self-renewal with minimal monocyte input (expressing TIMD4 and/or LYVE1 and/or FOLR2), $CCR2^{+}$ macrophages that are almost entirely replaced by monocytes ($TIMD4^{-}LYVE1^{-}FOLR2^{-}$), and $MHC\text{-}II^{hi}$ macrophages that are partially replaced by circulating monocytes ($TIMD4^{-}LYVE1^{-}FOLR2^{-}CCR2^{-}$) [64] (Figure 2.4).

$CCR2^{+}$ and $CCR2^{-}$ macrophage populations are present in specific locations within the heart, performing distinct functions. $CCR2^{+}$ macrophages are usually found in the

trabecular projections of the heart and their role in cardiac development has not been fully delineated. However, they are activated when homeostatic balance is interrupted-such as during a disease [108]. In contrast, $CCR2^-$ macrophages, herein referred to as cardiac resident macrophages (CRMs), occupy the myocardial wall and play a principal role in normal coronary development and maturation [109]. However, such studies are mostly limited to murine models. In addition to demonstrating robust phagocytic behaviour [23], CRMs have demonstrated a role in neonatal cardiac regeneration in mice, salamanders and zebrafish [24-26], potentially through the stimulation of angiogenesis [110].

Furthermore, CRMs interact very closely with cardiomyocytes and form signalling complexes through connexin-43 allowing synchronous depolarisation [21] (Figure 2.5). Hulsmans *et al.* showed that depletion of either CRMs or connexin-43 effects a delay in conduction and blockage in the atrioventricular node in mice. This study highlighted a critical role of CRMs in coupling with cardiomyocytes to facilitate electrical conduction within the heart. Undoubtedly, the coupling of cardiomyocytes and CRMs holds a lot of possibilities in regenerative medicine, to be explored in the future.

In addition to their involvement in the conduction system of the heart, cardiac macrophages also play a role in phagocytosis and efferocytosis [111]. Cardiac macrophages express high levels of myeloid epithelial reproductive tyrosine kinase (Mertk), which plays a role in macrophage-mediated efferocytosis. In the absence of this protein, cell debris removal during cardiac repair is severely affected, resulting in increased infarct size and reduced cardiac function [112]. Removal of debris and other materials ejected by cardiomyocytes is crucial in maintaining adequate cardiac function even in non-pathological settings. Similar to how the central nervous system disposes of dysfunctional organelles [113], cardiomyocytes remove dysfunctional subcellular particles with the help of CMRs [22]. Nicolas-Avila *et al.* documented that cardiomyocytes, which are continuously contracting and metabolically active cells, release subcellular particles termed “exophers” containing defective mitochondria [22]. These exophers are taken up by CRMs through Mertk to maintain cardiac homeostasis. This maintenance role of CRMs is further demonstrated when they are depleted in the myocardium (by intraperitoneal injection of 10 μg/kg diphtheria toxin in mice) [22],

which in turn reduces the presence of these exophers, delineating the role of CRMs in maintaining normal cardiac autophagy. In addition to unveiling this unique role of CRMs, this is the first study to show that myocardial tissue releases exophers (in mice).

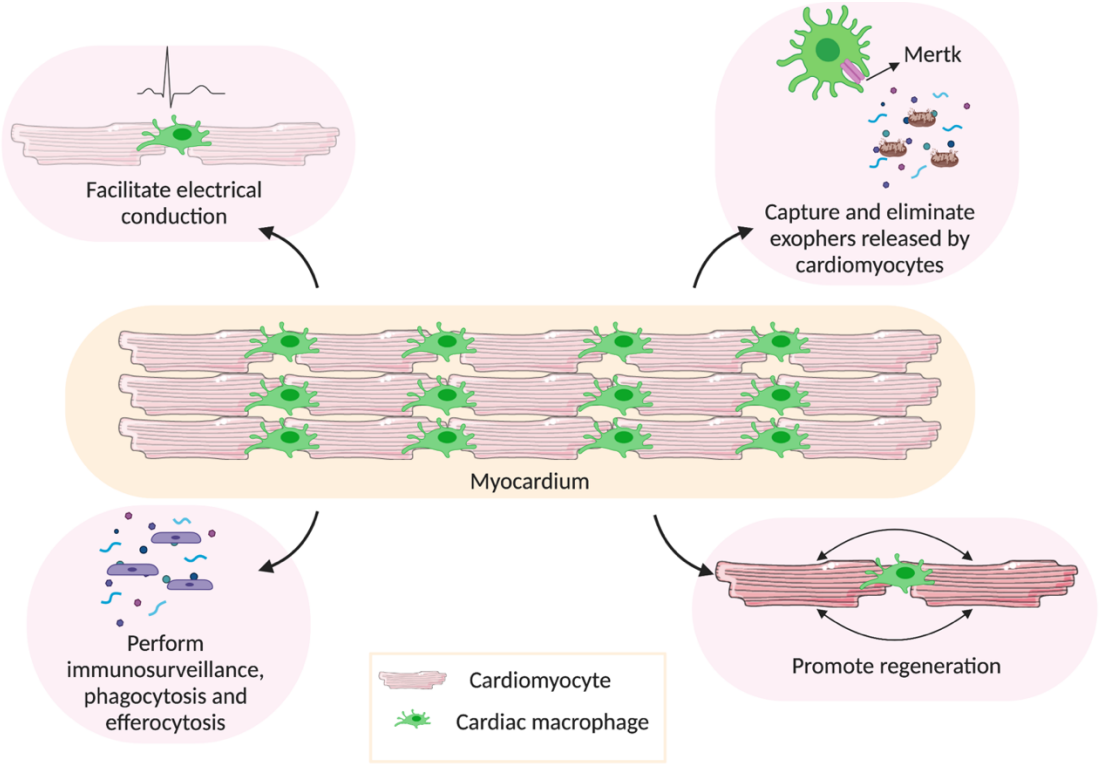

Figure 2.5: Functions of cardiac resident macrophages in healthy myocardium. In steady state, cardiac resident macrophages perform several important functions in the myocardium. One of their major functions is to facilitate electrical conduction by coupling with cardiomyocytes through connexin-43 gap junctions. They help in sustaining normal cardiac autophagy by capturing and eliminating exophers (containing defective mitochondria) released by cardiomyocytes, through Mertk. They also perform immunosurveillance and clear dead cells and debris in the myocardium, to maintain homeostasis. The presence of cardiac resident macrophages is found to be essential in promoting cardiac regeneration. Created with BioRender.com.

2.5.3. Cardiac macrophages in disease

Moreover, CRMs have also been found to be pivotal contributors in the mitigation and progression of several cardiac impairments [114]. MI is a common cardiac disease, resulting from a decreased or complete cessation of blood flow to a portion of the myocardium [2]. The area of the myocardium impacted by MI is severely deprived of oxygen, which in turn leads to tissue necrosis and in severe cases, chronic heart failure and death [115]. In the murine heart, the macrophage and monocyte populations in the myocardium following an infarct is dramatically different from that in steady state (Figure 2.6). The temporal dynamics of leukocyte infiltration following surgically induced MI has been assessed using flow cytometry and determines that neutrophils are among the first leukocytes to reach ischemic heart tissue[116]. This migration of leukocytes to the ischemic site is mediated by C-X-C motif chemokine ligand 2 (CXCL2) and CXCL5 production by $CCR2^{+}$ macrophages [117]. Monocyte recruitment to the infarct site begins as early as 30 minutes depending on CCR2 signalling, from both the bone marrow and the spleen, via MCP-1/CCR2 signalling [111]. This infiltration of monocytes and macrophages to the infarcted tissue occurs in two phases [116]. The Ly-$6C^{high}$ monocytes exhibiting a pro-inflammatory phenotype predominate the early days (marking the first phase), peaking on day 3 [116] (Figure 2.6). Around 40% of the infiltrating Ly-$6C^{high}$ monocytes in the first 24 hours post-MI are from the splenic monocyte reservoir [118]. During this period, also known as the inflammatory phase, macrophages and neutrophils clear dead cells and debris. After proper resolution of the inflammatory phase, there occurs a phenotypic transition from Ly-$6C^{high}$ monocytes to Ly-$6C^{low}$ monocytes and M2 macrophages which exert reparative functions and renew locally [118]. Ly-$6C^{low}$ macrophages predominate the later stages as inflammation resolves (marking the second phase), peaking between days 5 to 7 post-infarct [119] (Figure 2.6). Similarly, the remote myocardium also undergoes a sequential Ly-$6C^{high}$ to Ly-$6C^{low}$ differentiation pattern, with the Ly-$6C^{low}$ cells peaking 5 days later than at the infarct [120]. CRMs in the infarct area die shortly after MI [103]. However, more recent studies show that in the post-MI phase, the majority of the CRMs proliferate locally with a minor contribution from blood-derived monocytes [103].

During the inflammatory phase, classically activated (M1) macrophages secrete cytokines such as tumour necrosis factor α (TNFα), IL1β, IL6 and matrix metalloproteinases (MMPs) to facilitate extracellular matrix (ECM) breakdown [121]. Phagocytosis mediated by M1 macrophages is crucial for the initiation of the wound healing process. However, prolonged and chronic production of these inflammatory cytokines could lead to a number of pathological consequences including cardiomyocyte death, cardiac rupture, fibrosis, dilated cardiomyopathy due to matrix degradation etc. [122]. For example, TNFα (produced by macrophages, cardiomyocytes and endothelial cells) induces cardiomyocyte hypertrophy which can lead to post-MI heart failure [123]. Over the following days, macrophages promote fibroblast differentiation into myofibroblasts which express smooth muscle actin and lay down collagen, contributing to scar formation [124]. Additionally, vascular endothelial growth factor (VEGF) and transforming growth factor-β (TGF-β) produced by the macrophages facilitate revascularisation of tissues [116, 125]. Finally, macrophages also produce MMPs that help in breaking down the ECM and promote tissue remodeling.

Any abnormalities in either of the phases can be detrimental to the cardiovascular system. In particular, macrophage depletion is deleterious to infarct healing and worsens the remodeling process [126, 127]. Despite being merely 2-5% of the total macrophage population in the heart in the initial weeks post-MI, the depletion of cardiac resident macrophages can impair normal infarct healing and adversely affect the remodeling process [102]. Shirishi *et al.* demonstrated the effect of inactivation of alternatively activated (M2) macrophages post-MI by using a mouse model with Trib1 gene deletion [128]. The impaired wound remodeling was rescued by the introduction of M2 macrophages exogenously. Additionally, limiting the number of infiltrating monocytes via CCR2 blockage has shown to decrease the infarct size in MI recovery animal models [129-131], demonstrating the relevance of therapeutic approaches to limit infiltrating monocyte numbers is patients with increased systemic inflammatory activity to improve post-MI recovery.

As mentioned previously, initial fibrosis following MI is necessary to facilitate scar formation and initiate tissue remodeling. However, extensive fibrosis can result in morbid cardiac remodeling and heart failure [132]. The macrophage number in the

heart progressively increases from the onset of MI to heart failure, with local proliferation as well as recruitment responsible [133]. While macrophages in the remote myocardium increase, their number depletes at the site of infarct [103]. This local expansion of cardiac macrophages in the remote myocardium aggravates the progression of heart failure by producing factors that promote fibrosis in areas not initially impacted by the MI event, such as TGF-β, platelet derived growth factor and angiotensin-II [134]. Myofibroblasts and cardiomyocytes further prompt TGF-β production causing adverse remodeling that leads to heart failure. The detrimental effects of recruited monocytes/macrophages are further recognised as splenectomy reduces infiltrating macrophages and improves cardiac function [135]. A recent report also suggested that mechanical strain can trigger macrophage proliferation by activating mitogen activated protein kinase (MAPK) pathway, demonstrating that increased higher mechanical strain in failing heart could stimulate macrophage expansion [103]. These evidences further highlight the ill impacts of infiltrating macrophages in the infarcted heart. It is also of importance to note that latest studies suggest opportunity for successful regeneration of the heart after MI is restricted to 3 days post-MI and is potentially mediated by CRMs and fibroblasts [136].

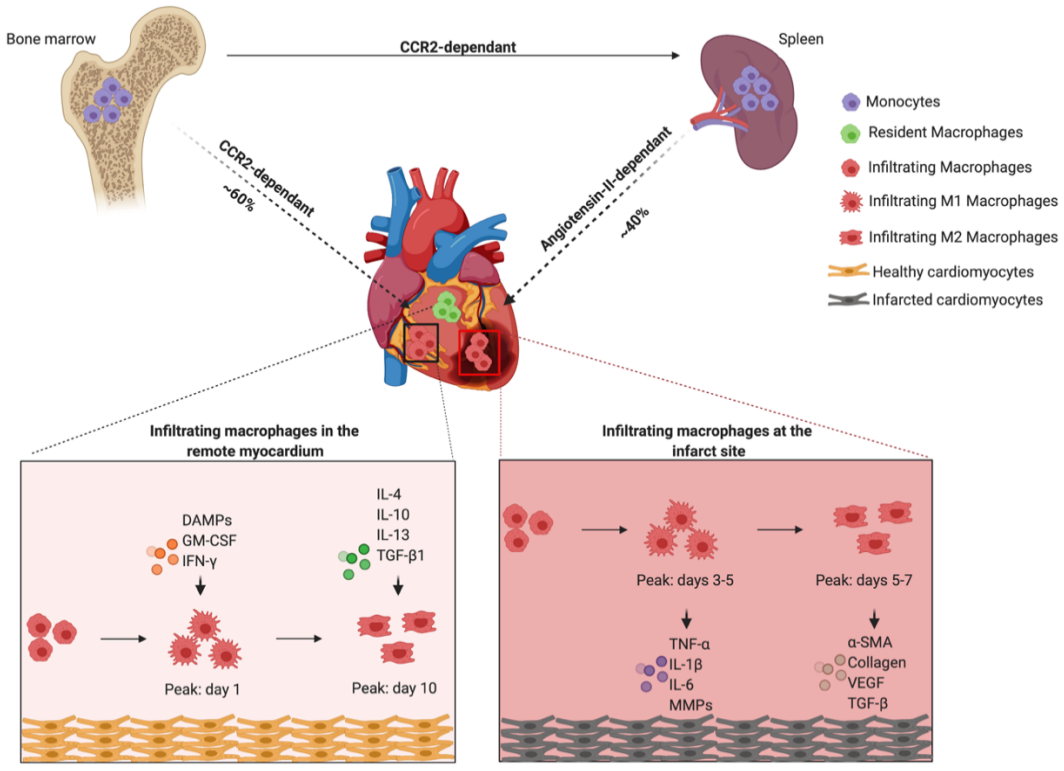

Figure 2.6: Macrophage origin and function in infarcted heart. After MI, the monocytes that infiltrate the heart originate from bone marrow (~60%) and spleen (~40%). The recruitment of bone marrow-derived monocytes is CCR2 dependent and that of spleen-derived monocytes is angiotensin II-dependent. Resident macrophages reside, self-renew and carry out a number of functions in the myocardium. However, at the infarct site and remote myocardium, infiltrating macrophages differentiate to M1 and M2 macrophages in response to different cues and secrete pro-inflammatory and pro-healing factors based on their macrophage phenotype. The number of M1 and M2 macrophages peak in the infarct site and remote myocardium at different pace. Created with BioRender.com

Myocarditis is another cardiac impairment, which causes inflammation in the cardiac muscle and can occur due to viral infections, autoimmunity, drug toxicity, or even sudden emotional/physiological stress [137]. Post-myocarditis, the number of macrophages derived from circulating monocytes increase dramatically in the heart, aggravating the inflammatory response by recruiting lymphocytes [138]. A similar response is also seen in isoproterenol-induced cardiomyopathy [139]. CRMs are numerically reduced in both viral and doxorubicin-induced cardiomyopathy, with poor population recovery in the long term [140]. However, the residual CRMs in doxorubicin-induced cardiomyopathy undergo proliferation to mitigate myocarditis; nevertheless, the specific mechanism facilitating this process remains to be fully comprehended [140]. More recent studies also illustrate the role of a specialised TREM2^{high} CRM population that can prevent sepsis-induced cardiomyopathy [141]. Furthermore, Revelo *et al.* recently reported the impressive ability of CRMs to prevent fibrosis and facilitate angiogenesis in response to cardiac pressure overload induced by transverse aortic constriction [142]. Taken together, these studies further highlight the cardioprotective role played by CRMs in various injury models, emphasising their importance in the myocardium.

2.6. iPSCs in cardiac tissue engineering

Obtaining healthy human cardiac cells for *in vitro* studies is challenging. Conventional research practices heavily rely on animal models, whose physiological nuances did not faithfully translate to the complexities of the human cardiovascular system. However, the advent of iPSC technology has ushered in a revolutionary era in cardiac tissue engineering [143]. iPSCs, reprogrammed from adult somatic cells, possess the remarkable ability to differentiate into any cell type within the human body [144]. This versatility has allowed scientists to obtain various cell types present in the heart, including cardiomyocytes [145], cardiac endothelial cells [146] and cardiac fibroblasts [147], directly from iPSCs, paving the way for a deeper understanding of cardiac physiology and pathology.

Before the era of iPSCs, researchers faced considerable challenges in mimicking human cardiac conditions. Animal cells, while valuable for certain studies, often fail to capture the intricacies of human cardiac physiology [8]. Using a detailed and quantitatively accurate mathematical model of ventricular action potentials across human, guinea pig and dog hearts, O'Hara et al. reported large differences in the cell electrophysiology mechanisms and response to drugs [9]. Together with many similar studies, this highlights the translational gap between animal models and human biology, and how this hinders the progress in developing effective treatments for cardiac diseases. iPSCs, by offering a platform for studying human-specific cells, have revolutionised this landscape.

2.6.1. iPSC-derived cardiomyocytes and cardiac fibroblasts

Efficient differentiation of iPSC-derived cardiomyocytes (iCMs) has come into existence only in the last decade, and it has not only advanced our understanding of cardiac diseases but also provided a promising avenue for discovering novel therapeutic interventions. Initial efforts of cardiomyocyte differentiations used embryonic stem cells (ESCs), and employed an EB-based differentiation protocol [148]. Although this protocol only yielded less than 1% cardiomyocytes [145], with steady advancement over

the years [149-151], updated protocols have shown to be effective in iPSCs [152]. Further improvements led to one of the most reproducible protocol for iCM differentiation that has been established, which relies on a monolayer differentiation approach and small molecule treatments to inhibit GSK3 pathway (to induce mesodermal lineage) followed by the inhibition of Wnt pathway (GiWi protocol) [145]. Owing to the reproducibility of such protocols, as well as the ease of deriving human cardiomyocytes with no ethical considerations, has resulted in a surge in efforts to significantly improve our understanding of cardiomyocyte function and potential therapeutics in a human-specific context.

In mammals, although cardiomyocytes are the most dominant cell type of the heart by volume (over two-third) [153], non-myocytes such as fibroblasts and endothelial cells outnumber cardiomyocytes by double the cardiomyocyte amount [154]. Studies focusing on interactions between cardiomyocytes and non-myocytes have resulted in improving our understanding of their functional coupling [155]. Vasquez *et al.* pioneered this investigation and showed an upregulation in connexin43 expression in addition to functional coupling between cardiomyocytes and cardiac fibroblasts isolated from infarcted rat ventricles [155]. To that end, the synergy between iCMs and iPSC-derived cardiac fibroblasts (iCFs) has proven to be invaluable in the realm of cardiac tissue engineering [156]. The interplay between these cell types *in vitro*, mirrors the intricate dynamics of the native heart, allowing researchers to explore the complexities of cardiac diseases such as fibrosis and hypertrophy. Although fibroblasts have been identified as the low abundance cell type present in iCM cultures [157, 158], more directed differentiation strategies targeting epicardial cells have given rise to iCF differentiation protocols [159-161]. In 2019, Zhang *et al.* developed a protocol for iCF differentiation wherein iPSCs were first differentiated to epicardial cells [160], followed by the use of a commercially available fibroblast growth medium in the presence of fibroblast growth factor (FGF2) and TGF-β inhibitor SB431542 [162]. In the same year, Zhang *et al.* used an approach of iCF derivation via second heart field progenitors, by GSK3 inhibition followed by FGF2 stimulation [147]. The derivatisation of iCFs, together with the nuanced understanding of iCM-iCF interaction is pivotal for the development

of targeted therapies that address the specific cellular and molecular intricacies of cardiac pathologies.

2.6.1.1. Maturation strategies for iPSC-derived cardiomyocytes

iCMs have been increasingly used in tissue engineering, regenerative medicine, and the development of organ-on-a-chip systems. Yet, iCMs display a highly immature phenotype, functionally closer to foetal cardiomyocytes rather than adult [163]. While adult human cardiomyocytes are large, binucleated cells, iCMs are often small, rounded and mononucleated [164]. Additionally, adult cardiomyocytes exhibit a more positive maximum diastolic potential and a slower upstroke velocity, in comparison to iCMs [163]. Moreover, iCMs display spontaneous beating, unlike mature ventricular cardiomyocytes that only beat upon excitation [152, 165]. Some reports suggest that the immature phenotype observed in iCMs could potentially be intensified by the common practice of selecting cells for analysis based on their spontaneous contractions, causing a bias in the analysis, by selecting the most immature subset of cells [165]. In order to address these dissimilarities, one of the first approaches tested, was long term culture of iCMs [164] (Figure 2.7). In early experiments using embryoid body (EB) based differentiation to obtain iCMs, the EBs were kept in culture for up to 60 days [166]. During this period, the cells exhibited several structural alterations, such as changes in sarcomere organisation, increase in cell size, and a notable reduction in proliferation [166]. Similarly, monolayer differentiation approaches with long term cultures (3 to 4 months) also yielded additional maturation features such as increased cell size, myofibril alignment, elongation and improved contractile performance, calcium handling and action potential amplitudes [167]. Furthermore, longer term studies (1 year) with iCMs have reported gradual increases in the ratio of MLC2V (ventricular cardiomyocyte marker) to MLV2A (atrial cardiomyocyte marker), in addition to increased sarcomere organisation [168]. However, the time required for iCMs to reach maturation comparable to adult cardiomyocytes is too long, with often only a small subset of cells expressing the maturation [169]. To truly improve the maturation of iCMs, there is a need for *in vitro* conditioning techniques that address this limitation.

Some commonly used strategies of improving iCM maturation also include the use of metabolic and hormonal cues. After birth, the levels of thyroid hormone tri-iodothyronine (T_3) is known to rise sharply, and this hormonal axis is essential for the normal functioning of the heart [170]. Yang *et al.* demonstrated strongly improvement in iCM maturation on treatment with T_3, with an increase in cell size, sarcomere length, contractile force, calcium-transient kinetics, mitochondrial biogenesis and mitochondrial respiration capacity [171]. Additionally, glucocorticoids [172], a combination of glucocorticoids and T_3 [173], as well as angiotensin II [174] have been used by several studies to demonstrate improved structural and functional maturation in iCMs. Furthermore, in terms of metabolic maturation, fatty-acid rich media [175, 176] and glucose deprivation [177] have shown notable improvement in metabolic and structural properties of iCMs. Another exciting approach to improve iCM maturation is the addition of supporting cells, such as fibroblasts or endothelial cells [178].

Efforts to enhance iCM maturation and function *in vitro*, have also explored the roles of mechanical stimulation. Previous studies show improvement in iCM elongation and Cx43 polarisation with cyclic uniaxial mechanical stretching [179]. Additionally, the use of micro gradient or micro grooved patterned surfaces [180, 181], have also shown promising results in terms of morphological improvement and contractile function of iCMs. Another interesting avenue within the realm of mechanical maturation of iCMs include the use of biomaterials with stiffness properties comparable to native human myocardium (~10 kPa) [182]. Using substrates of over 1 GPa and 1 MPa stiffness, Herron *et al.* showed that the softer substrates induced an upregulation in the expression of ion-channel genes (SCN5A and KCNJ2) and in the levels of associated sodium currents and cellular hypertrophy [183]. However, while mechanical stimulation contributes to increased iCM maturation and contraction through hypertrophic pathways, achievement of cell-cell coupling and improved calcium handling requires electrical stimulation (ES).

In recent years, ES has emerged as one of the most effective techniques for inducing maturation of cardiomyocytes *in vitro*. Typically, ES setups are straightforward in design,

employing two electrodes to deliver bulk electric field stimulation to the culture container, with electrical impulses directed through the culture media [184]. Electrodes commonly consist of either carbon rods or platinum wires, and optimising parameters such as stimulation duration, voltage, and frequency has been shown to enhance cell response within a specific biomaterial system [184]. In pioneering work, over two decades ago, Radisic *et al.* demonstrated that ES significantly improved cell alignment and enhanced sarcomere structure in 2D culture of rat neonatal cardiomyocytes [185]. Radisic *et al.* employed pulsatile rectangular 5 V/cm waves, at 2 ms pulse width and 1 Hz frequency, which are characteristic to the native myocardium [185, 186]. This work opened up multiple avenues, increasing more focused research into various waveforms, pulse widths, durations and frequencies to be tested on cardiomyocytes. Since, numerous 2D studies have employed ES on cardiomyocytes, to show improved expression of cardiac transcriptional factors such as GATA4, NFAT3 and NRF-1 [187], robust calcium handling [187, 188] and increased Cx43 expression [189]. Translating early studies performed using rat cardiomyocytes into iCMs, Nunes *et al.* reported that progressively increasing the ES from 1 Hz to 6 Hz over 1 week using the 'Biowire' device (iCMs seeded with endothelial and stromal cells on top of a surgical suture) improved multiple aspects of maturation, including sarcomere organisation, calcium handling, conduction velocity, reduction of proliferation rates and induction of a more negative resting membrane potential and increased action potential amplitude [190]. Another similar ramped ES regime reported by Ronaldson-Bouchard *et al.* (referred to as 'intensity training') also showed remarkable structural maturity in iCMs [16]. This involved a gradual increase in frequency from 2 Hz to 6 Hz over a span of 2 weeks, followed by an additional week at 2 Hz [16]. More recent studies using the ramped ES scheme have also achieved chamber-specific (atrial and ventricular) differentiation of iCMs [191]. For ventricular differentiation, the frequency was increased by 1 Hz every week and for atrial differentiation, the frequency was increased by 0.4 Hz daily (from 2 Hz to 6 Hz) [191]. To that end, ES remains at the forefront of efficient techniques to facilitate iCM maturation, showing great potential towards disease modelling, drug testing, and critically sized construct formation.

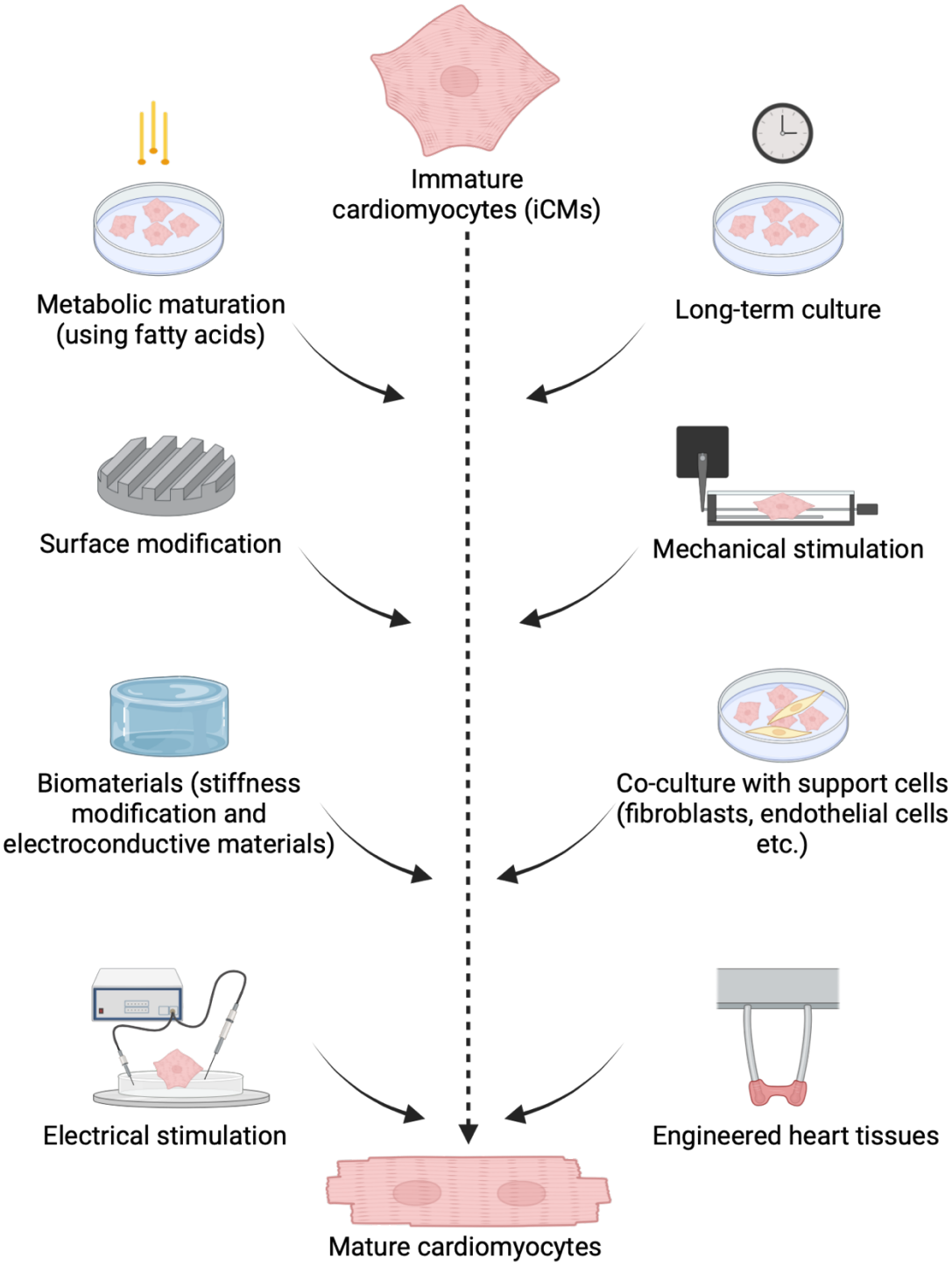

Figure 2.7: Strategies to improve iPSC-derived cardiomyocyte maturation i*n vitro*. iCMs are known to be immature in phenotype, resembling foetal cardiomyocytes. Multiple strategies have been employed to improve iCM maturity, including long term culture, using metabolic maturation media, modifying the culture surface to have microgrooves and micropatterns, mechanical stimulation, using biomaterials of stiffness resembling the native myocardium as

well as using electroconductive materials, co-culturing with support cells, electrical stimulation and fabricating 3D engineered heart tissues. Image created using Biorender.com.

2.6.2. iPSC-derived macrophages

To date, macrophage studies have heavily relied on murine or human blood-derived monocytes but these cells are not ideal for appropriating tissue resident phenotypes due to their vast transcriptomic and epigenetic variations, as well as difference in origin between blood-derived and resident macrophages [192]. Obtaining primary resident macrophages from vital organs (cardiac macrophages, Kupffer cells, microglia etc.) is not feasible, as acquiring tissue samples from healthy donors is often associated with donor site morbidity, in addition to ethical considerations. To circumvent these limitations, the use of iPSCs and hESCs as macrophage progenitor sources has come to the forefront (Figure 2.8) (Table 1). Over the last decade, a number of different protocols have been established for stem cell culture and differentiation, to obtain $CD14^{high}CD16^{low}CD163^{+}CD11b^{+}$ macrophages, morphologically similar to blood-derived macrophages[193-197]. Critically, iPSC and hESC-derived macrophage sources have shown therapeutic benefits in ameliorating liver fibrosis [198], acute lung injury [199] and are also under clinical trial for liver cirrhosis [200].

Furthermore, recent studies have shown that iMacs share ontogeny with TRMs and are independent of MYB [199, 201, 202], suggesting that iMacs in isogenic co-cultures may offer a facile and effective approach to obtaining physiologically relevant resident macrophages[203]. For example, iMacs in co-culture with neural cells were found to become microglia-like cells [204, 205]. Haenseler *et al.* showed that iMacs in co-culture with iPSC-derived neurons, expressed markers relevant to microglia as well as major neurodegenerative disorders [193]. Similarly, iMacs in co-culture with hepatocytes were found to show Kupffer cell-like characteristics [202].

In addition to co-culture models, the effect of the local biochemical environment on the specialisation of TRMs is becoming more evident in regenerative medicine. Certain

transcriptional factors regulate the expression of TRMs [206], such as Spi-c for the development of the red pulp macrophages in spleen [92], Sall1 for microglia [207], and Id3 for Kupffer cells [81]. In a more recent study, activation of iMacs with transcriptional factor KLF1 was found to drive them towards an erythroblastic island-like phenotype [208]. These studies demonstrate that physiologically relevant TMRs could be obtained *in vitro* by providing tissue specific cues or by activating specific transcriptional factors. Although, CRMs have not yet been derived from iPSCs, research is proceeding in the right direction, paving way to understanding optimal methods of CRM acquisition *in vitro*, such as using primary cardiomyocyte conditioned media on iMacs, establishing co-culture models of cardiomyocytes and iMacs or using bioinformatics tools to determine transcriptional factors for their induction. Taken together, iMacs offer great potential in understanding and modelling TRMs.

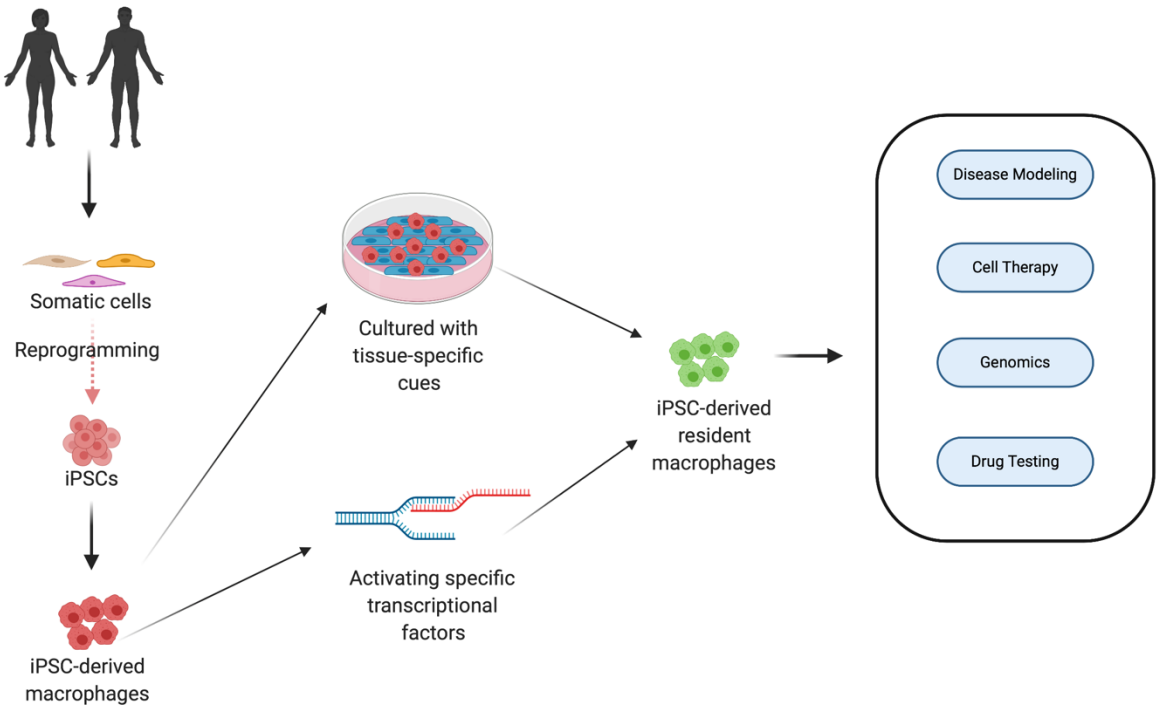

Figure 2.8: Resident macrophage derivation from iPSCs and applications. iPSCs can be derived from humans and other vertebrates by reprogramming somatic cells (fibroblasts, blood cells etc.). On specifying the ontogenic lineage, they can be differentiated into macrophages. Resident macrophages can potentially be obtained by giving iPSC-derived macrophages tissue specific cues or activating specific transcriptional factors. These resident macrophages can be

used for a number of applications such as disease modelling, cell therapy, genomics (to identify new genes) and drug testing. Created with BioRender.com.

Table 1: Examples of iPSC-derived macrophage subsets and their respective phenotypic markers

Tissue	Cell-type	Phenotypic markers
Blood	Blood-derived macrophages	CD18+, CD11b+, CD11c+, CD14+, CD16+, CD115+, CD1a-, CD83-, CD3-, CD19-[209] CD14+, CD16+, CD163+, CD86+[210] CD45+, CD11b+, CD14+, CD163+, CD68+[211]
Lungs	Alveolar macrophages	CD80+, SIRPa+, MHCII-, Langerin-[199]
Liver	Kupffer cells	CLEC-4F+, ID1+ and ID3+ [202]
Brain	Microglia	IBA1+, CD11c+, TMEM119+, P2RY12+, CD11b+, and CX3CR1+[212] CD11b+, ITGB2+, CSF1R+, CD45+, IBA1+ and ADORA3+[213]

2.7. Macrophages in Tissue Engineering

Over the past decades, the critical importance of incorporating macrophages into engineered constructs is being recognised [214, 215] and aside from the immunological responses of host macrophages, their role has been harnessed in a number of tissue engineering approaches to improve tissue maturation, repair and regeneration [216]. Understanding macrophage responses during biomaterial design [217, 218], as well as exploring the effects of mechanical cues on macrophage polarisation are other areas within tissue engineering that have gained attention [219, 220]. Over the last decade,

researchers have studied the potential of immune assisted tissue engineering, by incorporating macrophages into tissue engineered constructs (Table 2). In particular, macrophages have been used to vascularise biomaterials [221], by promoting angiogenesis [222] and vessel formation [223]. Although immune assisted tissue engineering has not been largely investigated, these data show the significance of macrophages in various tissue engineered constructs.

Table 2: Examples of macrophage use in tissue engineering

Tissue	Macrophage	Application
Bone	Blood-derived macrophages	Vascularisation of scaffold[221]
	Blood-derived macrophages	Osteogenesis[224, 225]
Skeletal muscle	Blood-derived macrophages	Regeneration[215]
Blood vessel	Blood-derived macrophages	Vascularisation of scaffold[223]
Liver	Kupffer cells	Hepatotoxicity[226]
	Kupffer cells	Disease-drug interaction[227]
Nerve	Microglia	Regeneration[228]
Brain/spinal cord	Microglia	Understand cellular crosstalk during neuroinflammation[229]
Lungs	Alveolar macrophages	Understanding response to atmospheric particles[230]
	Alveolar macrophages	*In vitro* lung inflammation platform[231]

	Alveolar macrophages	*In vitro* model for air-blood barrier[232]

2.8. Macrophages in cardiac tissue engineering

Within cardiac tissue engineering, the specific functional requirement includes contraction, which is inherent to cardiac function [233]. As macrophages have been shown to be integral during signal propagation, their inclusion in engineered tissue could facilitate robust and more physiologically accurate contraction mechanics. Engineered constructs are typically generated using primary cardiomyocytes (adult, neonatal, foetal), as well as cardiomyocytes obtained through iPSCs or ESCs [234]. Since the critical role played by macrophages in cardiac regeneration, maintenance of homeostasis and disease progression has been recognised (in mice), cardiac tissue engineering has begun to focus on incorporating macrophages into engineered heart tissues to recapitulate native tissue functions. A pioneering *in vitro* study in which human peripheral blood-derived macrophages and iPSC-derived cardiomyocyte interaction was assessed, attempted to recapitulate critical cellular events during myocardial injury, using a 3D inversion assay. They proposed a bone morphogenetic protein (BMP) mediated crosstalk between these two cell types [235]. Cardiomyocyte-derived BMP promoted pro-inflammatory (M1) macrophage recruitment and M1 macrophage-derived BMP improved cardiomyocyte proliferation and differentiation potential. This proposed paracrine mechanism of BMPs was new and provided a new insight into the mechanism of interaction between cardiomyocytes and peripheral blood-derived macrophages. Interestingly, a recent study has shown that the presence of macrophages in engineered cardiac tissue facilitates cardiomyocyte de-differentiation and remodeling [236]. In this study, it was observed that during the initial days (up to 3 days), the macrophages in the engineered cardiac tissue were polarised to an M1 state (CD86 positive), followed by a predominance of M2 macrophages (CD206 positive) as the cardiomyocytes de-differentiated. The effects of macrophage activity on the engineered cardiac tissue model could not be explained in this study however, as a

heterogenous population of whole cells from rat heart was used to make the engineered cardiac tissue. Nonetheless, future studies into the influence of macrophage populations of different ontological origin on cardiac function will shed light on their potential role in cardiac tissue engineering.

Interestingly, Wrona et al. explored the response of human ESC-derived cardiomyocytes to peripheral blood derived monocytes, with a focus on investigating the effects of polarised macrophages and their activation inducing cytokine profiles on cardiomyocyte function [237]. In this study, the gene expression profile of macrophages remained unaffected upon exposure to ESC-derived cardiomyocytes while cardiac-specific genes were downregulated on exposure to M1 and M2 polarised macrophages [237]. Tying in with the findings of this work, a study by Hitscherich et al. using murine ESC-derived cardiomyocytes also showed a decrease in the expression of cardiac-specific genes such as cardiac troponin T and sarcoplasmic/endoplasmic reticulum calcium ATPase when cultured with conditioned media from M1 polarised blood-derived murine macrophages [238]. Here, a co-culture system was employed, to demonstrate that M1 macrophages promoted a higher Ca^{2+} fractional release and both macrophage subtypes downregulated the store-operated Ca^{2+} entry in murine ESC-derived cardiomyocytes. Engineered heart tissues (EHTs) and other scaffold-based tissue engineered models for the myocardium heavily rely on cardiomyocytes, cardiac fibroblasts and endothelial cells to represent the myocardium. Although literature shows the potential of EHTs in guiding us towards obtaining robust *in vitro* models of human myocardium that has the ability to mature, beat in synchrony and respond to drugs, the addition of macrophages into these models could benefit our understanding on the *in vitro* behaviour of macrophages in a complex, multicellular humanised setting. For example, from the available *in vivo* studies (in mice), it is hypothesised that the incorporation of CRMs within an EHT (containing cardiomyocytes) will facilitate improved contractility and electrical conduction of the tissue. Additionally, the tissue could be hypothesised to exhibit improved maturity as there could be constant exophers elimination and maintenance of homeostasis.

Another interesting avenue that can be pursued using an EHT model that incorporates CRMs is screening anti-inflammatory drugs for post-MI treatment. Although clinical

studies on drug treatment in MI patients is limited, there are a number of drugs that have been developed for regulating immune response post-MI [239]. This includes non-steroidal anti-inflammatory drugs, glucocorticoids, cyclosporine etc. [240]. Despite showing an improvement in mortality, these broad anti-inflammatory drugs often fail to provide a cardio-protective effect [240]. To circumvent this limitation, targeted anti-inflammatory drugs can be used. An example for such drugs is demonstrated by the CANTOS trial [241]. Although canakinumab (the drug tested in the CANTOS trial) was not ultimately approved for cardiovascular treatment, CANTOS trial demonstrated that targeting the inflammatory pathway involving IL1β and hsCRP reduces adverse cardiovascular events. CANTOS was followed by CIRT (Cardiovascular Inflammation Reduction Trial) in which 4786 patients with stable atherosclerosis with diabetes mellitus or metabolic syndrome were subjected to low-dose methotrexate [242]. Low-dose methotrexate failed to reduce major adverse cardiovascular events, and also failed to reduced plasma levels of IL1β and hsCRP, further demonstrating the importance of adequate inhibition of IL1β to IL6 pathway for long-term cardiovascular benefits [243]. Further large cardiovascular outcome trials targeting the inflammatory pathways that followed includes COLCOT (Colchicine Cardiovascular Outcomes Trial) [244] and LoDoCO2 (Low Dose Colchicine after Myocardial Infarction) [245]. Both of these trials used low doses of colchicine (0.5mg/day), which is a repurposed anti-inflammatory agent. While COLCOT had 4745 patients with recent MI (less than 30 days), LoDOCO2 had 5522 patients with chronic coronary artery disease and both the studies showed reduction in the incidence of adverse cardiac events such as MI, stroke, cardiovascular death etc. [244, 245]. However, colchicine being associated with increase in pneumonia, nausea and flatulence poses risk [243]. To that end, the lack of success for most of these drugs could also stem from the fact that they are not thoroughly validated *in vitro* prior to human trials. The trajectory of recent and ongoing cardiovascular outcome trials show an increased interest towards novel anti-inflammatory and anti-cytokine drugs [243]. This further demonstrates the benefit of an *in vitro* model of the myocardium that has innate immune cells (especially macrophages) as they serve as the primary target for these drugs and can potentially fill the gap between the patient and the pharmaceutical industry.

2.9. Engineered heart tissue models

With an increasing prevalence of CVDs, there is a strong demand for platforms to study these disorders. A common strategy in healthcare industries to study CVDs and to develop new therapeutics is to use two-dimensional (2D) *in vitro* models, such as monolayer cell culture assays. The advent of cardiomyocyte differentiation using iPSCs and ESCs further increased the use of 2D assays as this provided with a potentially unlimited source of cardiomyocytes which not only could be patient specific, but also genetically manipulated to mimic certain diseases. However, this strategy is limited since 2D studies fail to recapitulate the structural and functional complexity of human myocardium. Specifically, monolayer cultures are unable to mimic the interaction between cells as well as between cells and ECM. This limitation is overcome by using animal models (e.g. mice). Although animal models have improved our understanding of CVDs and provide important preclinical findings that can be translated to humans [11], there still remains challenges in terms of transferring disease-related knowledge from animal models into human pharmaceutical testing stemming from specie variations [12]. An approach to tackle this is by producing 3D cardiac tissues *in vitro*, that can recapitulate the mechanistic intricacies as well as cellular complexity of native myocardium [246-249]. Engineered constructs are typically generated using primary cardiomyocytes (adult, neonatal, foetal), as well as cardiomyocytes obtained through iPSCs or ESCs [234]. Although EHTs can be fabricated purely using cardiomyocytes, the contractile function and the complexity of native myocardium is better recapitulated with the addition of non-myocytes such as fibroblasts and endothelial cells [250]. Other non-myocytes that have been explored include cardiac stem cells [29]. Not only can these EHTs provide better control over cell-cell and cell-ECM interactions, they can also incorporate complex details of the myocardium such as anisotropic structure and electrical and mechanical stimulations, by virtue of which they are now being used to understand disease progression and improve the efficacy of drug testing.

Over two decades ago, the first EHT model (Figure 2.9) was fabricated with chick embryonic cardiomyocytes mixed with Matrigel™ which anchored on to opposite ends of two Velcro coated glass tubes [13]. This culture provided mechanical strain to the

engineered tissue and hence was utilised as a platform for understanding the effects of uniaxial and multiaxial stretching, growth factors, cardiomyocyte maturation etc. This same principle was used to modify the geometry of the EHT to obtain a ring-shaped model which supported mammalian (rat) cardiomyocytes and also facilitated long-term force measurements [17, 251]. Although a number of different scaffold-based cardiac tissue engineered models were developed around this period, the next major modification to the EHT design was miniaturised EHTs made with fibrin, that were adapted to 24-well format, to facilitate drug screening [252]. This study demonstrated the use of video-optical recording for the measurement of contractility of the tissues, which is a commonly used method of contractility measurement at the moment [252]. Shortly after, Boudou *et al.* generated collagen/fibrin matrix-based cardiac microtissues using microfabricated tissue gauges that incorporate microelectromechanical systems (MEMS) cantilevers [253]. This facilitated in simultaneously constraining and reporting forces generated by the tissues in real time [253]. Similar approaches with cantilevers/posts to allow tissue anchorage has also been used by Turnbull *et al.* [254]. Another interesting modification to the EHT came with the use of a surgical suture within PDMS moulds to obtain aligned cardiac tissues with striations called 'Biowire' [255]. Following this study, Bian *et al.* demonstrated that fabricating cardiac tissues with longer elliptical pores within the patch networks improve ECM alignment within the patch [256]. In the past 5 years, the field of EHTs further underwent drastic advances where fibrin based EHTs under dynamic culture (using platform rockers) showed improvement in tissue maturation [257]. These EHTs, called 'cardiobundles' were designed to be cylindrically shaped and anchored within porous flexible nylon frames that supported chronic auxotonic loading and free-floating culture of the tissues [257]. More recently, the advanced successor of Biowire, named 'Biowire II', a heteropolar cardiac tissues containing distinct atrial and ventricular ends was generated [191]. This heteropolar tissue formation was achieved using directed cell differentiation and electrical field conditioning [191]. With over two decades of input, one of the most remarkable advancement in EHTs is a mesh structured EHT patch of dimension 5 x 7 cm, that closely resemble human ventricular tissue [258].

One of the key features of EHTs is their ability of respond to drugs. Most of the different types of EHTs fabricated over the years aim to feature their drug response. For example, over a decade ago, Hansen *et al.* showed that EHTs display a concentration-dependent increase in relaxation time on treatment with chromanol, quinidine, and erythromycin, while doxorubicin treatment resulted in decreased contractile force [252]. Similarly, Boudou *et al.* tested isoproterenol and digoxin on their EHTs to understand the functional consequences of pharmacologic agents [253]. They showed that small doses (10 and 100nM) of isoproterenol increased the contractility of the EHTs while 1 and 10mM decreased the contractility [253]. On the other hand, digoxin improved the contractility at 1 nM and 1 mM but was found to be cardiotoxic at 10 mM concentration [253]. Hence, the varied and dose dependent sensitivity of EHTs towards different drugs make them an exciting alternative to animal models in addition to being a useful tool in understanding the effect of various drugs on the myocardium [259]. Despite the proven efficacies of these EHTs, there still remain challenges in making them more humanised, including the addition of right cell types to mimic the complexity of the myocardium. One of the potential additions to improve the response of EHTs would be CRMs, as they are critical in the normal functioning of the heart. Notably, Bailey *et al.* studied the effects of SARS-CoV-2 on EHTs fabricated with iCMs, iCFs and cardiac macrophages derived from human patient samples [260]. Although, this served as a model to study myocarditis due to SARS-CoV-2 infection [260], the intricacies of cardiomyocyte-macrophage interactions or the structural and functional abilities of the EHTs without SARS-CoV-2 were not assessed.

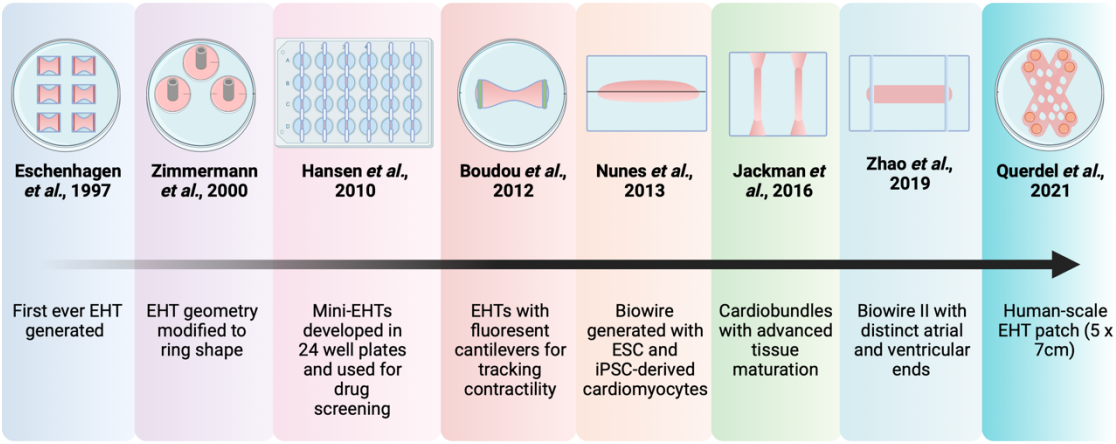

Figure 2.9: Brief overview of the evolution of Engineered Heart Tissues. The very first EHT was generated in 1997 by using chick embryonic cardiomyocytes on Velcro-coated glass tubes [13]. This model and the geometry of EHTs evolved over the years, from ring-shaped EHTs [251] to mini-EHTs adapted to a 24-well plate format [252], to EHTs with fluorescent cantilevers that can track contractile motions [248], followed by Biowire [14], cardiobundles [257], and Biowire II [191], to finally reach a human-scale EHT patch [15]. EHT, engineered heart tissue. Image created using Biorender.com.

2.9.1. EHT based disease models

Successful modelling of any cardiac disease using iPSCs relies on understanding the cellular pathology relevant to the disease, alongside the development of robust phenotypic assays. Most of the *in vitro* cardiac disease models in existence aim towards using patient-derived iPSCs to model genetic conditions [261]. Patient-derived iPSC lines have been generated for conditions such as long QT syndrome (LQT) 1 [262], LQT2 [263], LQT3/Burgada syndrome [264], Timothy syndrome [265], dilated cardiomyopathy [266], hypertrophic cardiomyopathy [267] etc. Moreover, in terms of 3D disease modelling, numerous innovative approaches have been made. Using 'cardioids' which recapitulate the myocardial and endocardial lineages of the heart, Hofbauer *et al.* modelled foetal heart injury by performing a cryoinjury on the cardioids [268]. The cryoinjury initiated a high accumulation of fibrin and collagen, similar to the response seen *in vivo* [268]. In a more recent study, cardioids were also used to model genetic and teratogen-induced heart defects *in vitro* [269]. Similar organoid-based models have also been used to study

the effects of maternal diabetes on congenital heart defects [270, 271], myocardial defects post NKX2.5 deletion [272] and genetic cardiomyopathies [273].

Although EHTs facilitate iCM maturation and alignment, disease modelling using EHTs is yet to be fully explored. Zhao *et al.* using the 'Biowire' platform measured spatially confined responses of serotonin and the sodium channel blocker ranolazine on atrial and ventricular cardiomyocytes [191]. Both of the compounds tested showed preferential effects on the atrial end of the Biowire and not the ventricular. Additionally, Biowires have also been used to model aspects of left ventricular hypertrophy, using patient-derived cells [191]. Kensah et al. reported fabrication of bioartificial cardiac tissues (similar to EHTs) with iCMs and human foreskin fibroblasts [274]. Interestingly, replacement of fibroblasts with iPSC-derived pericytes resulted in tissues with fibrosis-like phenotype, which was found to be even more pronounced when iPSC-derived endothelial cells were added to the tissues [275]. In another interesting study, Voges *et al.* showed that engineered cardiac tissues resemble immature human heart tissues and have the endogenous regenerative capacity to achieve full functional recovery, 2 weeks after a cryoinjury [276]. More recent work from this same group highlights using EHTs infected with SARS-CoV-2 to study compounds that can block inflammation associated with SARS-CoV-2 in the heart [277]. Similarly, EHTs have been fabricated with SARS-CoV-2 and PBMCs to model SARS-CoV-2 associated myocarditis [278]. Furthermore, EHTs have also been used to study desmosome-linked arrhythmogenic cardiomyopathy with patient-derived iCMs [279]. Novel attempts have also been made to model myocardial fibrosis using EHTs. Using high cardiac fibroblast numbers (75%) in EHTs, Wang *et al.* demonstrated that a successful model of fibrosis-on-a-chip can be fabricated [280]. Fibrotic EHTs displayed inferior contractile properties, abnormal calcium handling and electrophysiological properties [280]. To that end, the use of EHTs stand at the forefront of *in vitro* cardiac disease modelling, to understand human cardiac pathological conditions and for novel therapeutic interventions.

2.10. Conclusion

From regarding macrophages as a system of clearing dead cells, to appreciating their role in tissue defence, homeostasis, regeneration and organ development, our understanding of macrophages has advanced significantly in recent years. Lineage tracing and fate mapping studies demonstrated that most vital organs are largely populated by resident macrophages at the onset of embryological development and play critical roles in health and disease. Within the heart, resident macrophages ensure homeostatic cardiac function by performing a number of vital functions including phagocytosis, efferocytosis, eliminating exophers, facilitation of electrical conduction etc. Our understanding of cardiac immunology has progressed well enough to regard cardiac resident macrophages a potential candidate to include in engineered heart tissues, to further our understanding of cell interactions in addition to making the engineered tissues more physiologically relevant. But much more still remains to be understood, such as what degree of these cells are lost during myocardial disease/ischemia; how do they function in response to injury and disease, their paracrine effects in tissue engineered models etc. The next step in cardiac tissue engineering is to unravel the crosstalk between cardiac macrophages and cardiomyocytes *in vitro* and further our understanding the molecular processing involved in their interaction and their potential in regenerative medicine, therapeutics, disease modelling and drug screening. With engineered heart tissues gaining great research interest, it is highly pertinent to include a resident macrophage population to make the tissue more physiologically relevant. By building on our strong foundational knowledge on different macrophage populations and with the assistance of new technologies, we will hopefully see rapid progress in finding new therapeutics using cardiac tissue engineering.

Chapter 3 General Materials and Methods

3.1. iPSC expansion and culture

All experiments were performed using three iPSC lines (Table 3). Matrigel™ stocks were stored at -80°C and plates were coated by diluting the stock (1:4 dilution) in ice cold DMEM/F-12 (Stemcell™ Technologies) media. A total of 2 ml per well (for 6-well plates) or 0.5 ml per well (for 24-well plates) of Matrigel™ working solution was added and coated plates were kept in a 37°C incubator for as little as 2 hours or as long as 1 week. To begin iPSC culture, one vial of iPSCs was thawed and plated on to one well of a Matrigel™ coated 6-well plate. Upon reaching ~95% confluency, iPSCs were incubated with 1 ml (for 6-well plate) or 0.5 ml (for 24-well plate) of Versene (Gibco™) for 6 minutes at room temperature, and lifted as clumps. Suspended iPSCs were plated at a 1:5 split ratio. On the day of plating/splitting, the culture media (mTESR, Stemcell™ Technologies) was supplemented with ROCK inhibitor Y-27632 (Stemcell™ Technologies) for 24 hours. iPSCs were expanded at least 4 times before initiating differentiations.

Table 3: Details of iPSC lines used

Cell line	Sex of donor	Accession
11b	Male	CVCL_8988
SFCi55	Female	CVCL_UL47
SFCi55-ZsGr	Female	CVCL_UL48

3.2. Isolation of PBMCs from buffy coats

The plasma depleted fraction of anti-coagulated blood (also known as buffy coats), from healthy human donors were obtained through Irish Blood Transfusion Board (IBTS), St. James's Hospital, Dublin. The procurement of buffy coats was supported by a Level 2

Ethics approval from Trinity College Dublin, whereby, when required, the age and sex of the blood donors can be disclosed by IBTS.

Buffy coats were diluted at a 1:1 ratio using PBS and centrifuged at 1250 G for 10 minutes at room temperature, with the centrifuge de-acceleration occurring with brake off. The leukocyte containing layer of the buffy coat was extracted using a Pasteur pipette and diluted by half in sterile PBS. The diluted leukocytes were split across multiple 50 ml conical falcon tubes and layered over Lymphoprep™ such that every falcon tube held 20 ml Lymphoprep™ and 25 ml diluted leukocytes. Next, leukopcyte-Lymphoprep™ mix was centrifuged at 800 G for 20 minutes with the brake off and the PBMC layer was carefully removed using a Pasteur pipette. The PBMC layer was washed in sterile PBS and further centrifuged for 10 minutes at 650 G. The supernatant was discarded and the PBMC pellet was washed again in sterile PBS and centrifuged at 300 G for 10 minutes, followed by a final suspension in 50 ml of complete Roswell Park Memorial Institute (RPMI) media (supplemented with 10% Foetal Bovine Serum (FBS) and 2% Penicillin/Streptomycin (P/S)) before counting.

After counting, $CD14^+$ monocytes were isolated from the suspension using the MagniSort™ Human CD14 Positive Selection Kit (Invitrogen) according to the manufacturer's protocol. Briefly, cells were washed in MACS buffer (PBS with 2% FBS and 0.4% EDTA) and centrifuged at 300 G for 5 minutes. The resultant pellet was resuspended in MACS buffer at 1×10^8 cells/ml in a FACS tube and incubated with anti-CD14 biotin (10 µl per 100 µl cells) for 10 minutes at room temperature. Cells were then washed in 4 ml MACS buffer and centrifuged at 300 G for 5 minutes. Cells were then re-suspended in MACS buffer and incubated with MagniSort™ positive selection beads (15 µl per 100 µl cells) for 10 minutes at room temperature. The volume in the FACS tube was adjusted to 2.5 ml and the tube was placed inside the magnetic field of a EasySep™ cell sorter magnet (STEMCELL Technologies) for 5 minutes. The negative fraction was discarded by inverting the tube while held inside EasySep™ magnet, and the remaining cells were resuspended in 2.5 ml MACS buffer. The wash step was repeated twice and the positive fraction containing the $CD14^+$ monocytes was re-suspended in complete RPMI media and counted.

The magnetically sorted $CD14^+$ monocytes were plated at a concentration of 500,000 cells per well of a 24 well plate (1 million cells/ml concentration) in complete RPMI containing macrophage colony stimulating factor (M-CSF) at a final concentration of 50 ng/ml. Cells were kept in culture in a 37°C incubator, with 5% CO_2 and 19% O_2 concentrations. $CD14^+/CD11b^+$ blood derived macrophages (BDMs) were obtained after 7 days of culture, with media change every 3 days.

3.3. Processing and handling of human heart samples

Human atrial and ventricular tissue samples were obtained from St. Anne's University Hospital (FNUSA), Brno, Czech Republic. Briefly, the tissues were perfused with PBS (calcium free) 4 times, after which one half of the tissue samples were finely minced to small pieces and the other half was cut to roughly 3-4 thick mm pieces. The tissues that were cut to 3-4 mm chunks were fixed in 4% paraformaldehyde and snap frozen in liquid nitrogen before embedding in OCT solution for histology. The minced tissues were incubated in a digestion reaction media containing Collagenase II (450 U/ml), DNAse I (60 U/ml) and Hyaluronidase (60 U/ml) for 1 hour in 37°C with agitation at low speed. After 1 hour of incubation, the digested tissue samples were passed through a 40 µm cell strainer and diluted with DMEM before distributing the total volume between four 15 ml conical tubes. The samples were centrifuged at 400 G for 5 minutes. After discarding the supernatant, the samples were resuspended in 1 ml of ammonium-chloride-potassium (ACK) buffer (for red blood cell lysis) for 5 minutes. 9 mls of DMEM was added to each tube followed by a final round of filtration through a 40 µm cell strainer. The cells were centrifuged at 400 G for 5minutes and resuspended in Leibowitz's L-15 medium and plated in a T175 flask for 2 hours to allow fibroblast attachment. After 2 hours, the media was changed to fresh L-15 media and the cells were kept in culture until confluent before lysing them to perform RT-qPCR.

3.4. Flow cytometry

On reaching the end of the experiment, cells were suspended in PBS using a cell scraper and collected into FACS tubes at a concentration of 500,000 cells per tube.

3.2.1 For cell-surface markers

Cells were centrifuged at 300 G for 5 minutes followed by incubation in Fc-γ blocker (in FACS buffer: PBS with 2% FBS) for 10 minutes at 4°C to reduce non-specific binding and background fluorescence. Next, cells were centrifuged at 300 G for 5 minutes followed by incubation in the antibodies of interest (detailed in table 4) made up in FACS buffer at a concentration of 10 µl/ml. Each tube was treated with 100 µl of the antibody cocktail for 30 minutes, in the dark at room temperature. The cells were then washed using FACS buffer and centrifuged at 300 G for 5 minutes and used directly for flow cytometry. If being used the next day, the cells were fixed using 1% paraformaldehyde (PFA). Compensation beads (Invitrogen™) were also prepared for each channel by adding 1 µl of the conjugated antibody to a drop of compensation beads. Unstained zombie green tagged iMacs (ZGiMacs) were used for compensating for zombie green.
Flow cytometry was performed using LD Fortessa (BD). The flow cytometry plots were first gated for the events of interest, followed by single cells. The single cells were then gated for cells positive for CD14 and CD11b. The populations that were positive for CD14 and CD11b were also assessed for their CX3CR1, CCR2 and HLA-DR expressions.

Table 4: Macrophage-specific antibodies with fluorochromes and dilution information for flow cytometry

Marker	**Fluorochrome**	**Dilution**	**Host Specie**	**Supplier**	**Cat no.**
CD14	eFlour 506	1:100	Rat	ThermoFisher Scientific	69-0149-41
CD11b	APC-eFlour 780	1:100	Mouse	ThermoFisher Scientific	47-0118-41
CCR2	Dylight 650	1:100	Rabbit	ThermoFisher Scientific	PA523039

CX3CR1	PE	1:100	Rat	ThermoFisher Scientific	12-6099-41
HLA-DR	Alexa Flour 700	1:100	Mouse	ThermoFisher Scientific	56-9956-41
CD80	PerCP-eFluor 710	1:100	Mouse	ThermoFisher Scientific	46-0809-41
CD163	PE-Cyanine7	1:100	Mouse	ThermoFisher Scientific	25-1639-41
CD206	eFluor 450	1:100	Mouse	ThermoFisher Scientific	48-2069-41
CD86	PE-Cyanine5	1:100	Mouse	ThermoFisher Scientific	46-0809-41

3.2.2 For intracellular markers

Cells were centrifuged at 300 G for 5 minutes and resuspend in 500 µl of 1% PFA. The resuspended cells were incubated in room temperature for 20 minutes. Cells were then centrifuged at 300 x g for 5 minutes and resuspended in 1 ml of Flow Buffer 1 (PBS with 0.5% BSA) followed by centrifugation at 300 G for 5 minutes to remove PFA. Cells were then resuspended in 100 µl of Flow Buffer 2 (PBS with 0.5% BSA and 1% Triton-X), with the appropriate stains of interest for 30 minutes at room temperature in the dark. Cells were resuspended in 1 ml of Flow Buffer 2 and centrifuged at 300 G for 5 minutes before finally resuspending in 300 µl of Flow Buffer 2 to perform flow cytometric analysis. Compensation beads (Miltenyi) were prepared and stained the same way as cells.

Table 5: Cardiomyocyte-specific antibodies with fluorochromes and dilution information for flow cytometry

Marker	**Fluorochrome**	**Dilution**	**Host Specie**	**Supplier**	**Cat no.**

Cardiac troponin T	VioBlue	1:50	Human	Miltenyi Biotec	130-120-542
MLC2a	APC	1:50	Human	Miltenyi Biotec	130-118-546
MLC2v	PE	1:50	Human	Miltenyi Biotec	130-119-581
CD90	PE	1:50	Human	Miltenyi Biotec	130-128-255

3.5. RT-qPCR

Samples were stored in (-80°C) Trizol™ until ready for RNA isolation. To carry out RNA isolation, samples in Trizol™ were thawed on ice before adding chloroform (600 µl for 1 ml of Trizol™). The samples were then vortexed and rested for 15 minutes to allow phase separation. The samples were centrifuged at 12,000 G for 15 minutes at 4°C. The upper aqueous phase containing the RNA was removed and placed on to fresh RNAse-free tubes. GlycoBlue™ was added to the samples, followed by isopropanol and incubated overnight in -20°C to improve the purity of the RNA. The following day, samples were thawed and centrifuged at 14,000 G for 10 minutes at 4°C. The pellet obtained was washed with 70% ethanol followed by centrifugation at 12,000 G for 10 minutes (4°C). The wash step with ethanol was repeated twice and the pellets were allowed to dry entirely before adding 20 µl of RNAse-free water.

The yield and purity of the RNA was assessed using a NanoDrop™. After calculating the total RNA yield, the amount of RNA to be reverse transcribed was decided (500-1000 ng) and was reverse transcribed using a kit from Applied Biosystems (high capacity cDNA reverse transcription kit). The components of the kit were added to 13.2 µl of RNA sample at the volumes mentioned in Table 6 and reverse transcribed using a Thermocycler (BioRad^{TM}), to obtain cDNA.

Table 6: Volumes for sample preparation for reverse transcription

Components from the kit	**Quantity (per sample, µl)**
10X RT Buffer	2
25X dNTP Mix (100 mM)	0.8
10x RT Random Primers	2
RNase Inhibitor	1
MultiScribe Reverse Transcriptase	1
Total amount per reaction	6.8

The cDNA was reconstituted at 10 ng/µl concentration in nuclease-free water. PCR plates were prepared using SYBR Green Mastermix (Universal iTaq Syber Green, Biorad^{TM}), primers of interest and 10 ng of cDNA per well (Table 7). Plates were run in an Applied Biosystems Fast 7500 PCR machine and the Ct values were used to make calculations for fold change of mRNA expression, using $2^{-\Delta\Delta CT}$ method [281].

Table 7: Volumes for sample preparation for RT-qPCR

	Per well (µl)
Sybr Green Mastermix	6
RNase Free H2O	2
Forward Primer	.5
Reverse Primer	.5
cDNA	1
Total	10

The primer sequences used are detailed in Table 8.

Table 8: Gene primer sequences

Gene	Forward primer sequence	Reverse primer sequence
TGFB	AACCCACAACGAAATCTATG	CTTTTAACTTGAGCCTCAGC
MRC1	AGCCAACACCAGCTCCTCAAGA	CAAAACGCTCGCGCATTGTCCA
IL10	GAAGAGAAGGCAACCAAGACAG	GATCTTCCAGTGACAAGCTTCC
NOS2	GCTCTACACCTCCAATGTGACC	CTGCCGAGATTTGAGCCTCATG
HIF1A	GAAACTTCTGGATGCTGGTGATTT	GCAATTCATCTGTGCTTTCATGTCA
TNF	ACCTCCGAGATGACACCATCAC	ACAGGCTGGTAGGAGTCCTTCT
CCR2	CAGGTGACAGAGACTCTTGGGA	GGCAATCCTACAGCCAAGAGCT
TRPV4	AAGATTGAGAACCGCCACGA	GGTAGTAGGCGGTGAGAGTGAAG
VEGFA	AGGGCAGAATCATCACGAAGT	AGGGTCTCGATTGGATGGCA
AREG	GCACCTGGAAGCAGTAACATGC	GGCAGCTATGGCTGCTAATGCA
MMP9	GTACTCGACCTGTACCAGCG	TCAGGGCGAGGACCATAGAG
IFNG	AGTGCTTAGCCTGGTATTCATCTG	GGCTGGTATGACGTGATGAGTG
GJA1	GGGTTAAGGGAAAGAGCGACC	CCCCATTCGATTTTGTTCTGC
TNNT2	AAGAGGCAGACTGAGCGGGAAA	AGATGCTCTGCCACAGCTCCTT
MYH6	CGGCCCAGATTCTTCAGGATT	CTGACTTGCGGAGGTACTGG

MYH7	ACCAACCTGTCCAAGTTCCG	TTCAAGCCCTTCGTGCCAAT
SERCA2	GCAATTGTGGGTGTATGGCA	ATCCGCTGCACACTCTTTCT
SOX17	ACGCTTTCATGGTGTGGGCTAAG	GTCAGCGCCTTCCACGACTTG
GATA4	GCGGTGCTTCCAGCAACTCCA	GACATCGCACTGACTGAGAACG
TBX18	TGTAAAACGACGGCCAGT	CAGGAAACAGCTATGACC
TBX5	ACAACCACCTGGACCCATTTGG	GGAAAGACGTGAGTGCAGAACG
TCF21	CAGATCCTGGCTAACGACAAA	CCACTTCTTTCAGGTCACTCTC
POSTN	GGAGACTGAATGCCTTTTGGGATA	AATGTAGAAGTGGGATTCCATGGAAC
DDR2	ACGAAACTGTTTAGTGGGTAAGAACT	ACAGGGCTTTAAAATGCTGAGAACTTA
ACTA2	GCAGTAGTGTGGTGTTCTGTATCA	GGCTTGGCTGTAATTGATTCACAAG
TIMD4	TGTAAAACGACGGCCAGT	CAGGAAACAGCTATGACC
LYVE1	GCCGACAGTTTGCAGCCTATTG	CCGAGTAGGTACTGTCACTGAC
FOLR2	CTTTCCCCTCAGGACTTGGTTT	CCTGACTTTCTCCTCCCTGTTAGA
MERTK	GAACATAAAGGTGTCAAATTTAATTGCTCAATCA	GGCTACAGAATGATACTCTGTCTCAATAAG
CCL24	TGAGAACCGAGTGGTCAGCTAC	TTCTGCTTGGCGTCCAGGTTCT
ACTB	GGACTTCGAGCAAGAGATGG	AGCACTGTGTTGGCGTACAG

3.6. ELISA

Supernatants were collected from samples and stored in -80°C for long term storage. ELISA kits (Invitrogen) for TNFα, IL6 and IL10 were used and manufacturer's instructions were followed. Briefly, high binding plates (Greiner one) were treated with capture antibody diluted in 1x coating buffer and incubated overnight at 4°C. The following day, the unbound capture antibody was removed and the plates were blocked using 1x assay diluent. The plates were incubated in room temperature for 1 hour, after which the samples and standards were added to the plates and incubated overnight at 4°C. The following day, the plates were washed four times followed by an incubation with detection antibody diluted in 1x assay diluent for 2 hours in room temperature. The plates were washed for four times and incubated for 30 minutes with Streptavidin-HRP in the dark. The plates were then washed four times and treated with TMB. The development of the colour was stopped by the addition of 1 M sulphuric acid. The absorbance was read at 450 nm using a plate reader.

For measuring exogenous TGF-β1 (Invitrogen), a slightly modified approach was used. After overnight incubation of the plates with the coating buffer, the plates were incubated with the blocking buffer. Samples were prepared by performing a 1:10 dilution in 1x assay buffer, followed by incubation in room temperature for 1 hour with 1 N HCl (20 µl HCl in 200 µl prediluted sample). The samples were then neutralised using 1 N NaOH and added to the wells together with standards and incubated overnight at 4°C. The following day, the plates were washed and incubated with detection antibody diluted in 1x assay diluent for 2 hours in room temperature. The plates were washed for four times and incubated for 30 minutes with Streptavidin-HRP in the dark followed by four more washes before treatment with TMB. The development of the colour was stopped by the addition of 1 M sulphuric acid. The absorbance was read at 450 nm using a plate reader.

3.7. Immunofluorescence Imaging

Once the time point was reached, samples were washed with PBS followed by fixation in 4% paraformaldehyde (PFA) (15 minutes for monolayer cells; 30 minutes for hydrogels; 1 hour for human tissues).

Sample preparation for 3D samples:

Post fixation, samples were incubated in 10% sucrose solution for 2 hours, followed by overnight incubation in 30% sucrose at 4°C. Once the samples settle down at the bottom of the tubes, they were then snap frozen in OCT solution using liquid nitrogen and left at -80°C overnight. Frozen samples were sliced using a cryotome at a thickness of 10 µm and stored at -20°C until ready for staining.

Fixed/sliced samples were blocked using a buffer containing PBS with 10% triton-X, 5% Tween-20 and 4% bovine serum albumin (BSA) at room temperature for 30 minutes. The samples were then incubated in the primary antibody of interest, in a buffer containing PBS with 10% triton-X, 5% Tween20 and 1% BSA overnight, at 4°C. The following day, samples were washed 3 times in a wash buffer containing PBS and 0.05% Tween20, followed by incubation in the secondary antibody of choice, for 30 minutes at room temperature. Following one wash with the wash buffer, the samples were incubated with DAPI (1 in 1000 dilution) for 15 minutes at room temperature. Finally, the samples were washed with PBS for 3 times and optionally, incubated overnight in the dark with a drop of prolong gold anti-fade solution. The antibodies used and their respective dilutions as detailed in Table 9.

Table 9: Primary and secondary antibodies with dilution information for immunofluorescence imaging

Antibody	**Host**	**Dilution**
Anti-Cardiac troponin T	Mouse	1:300
Anti-Sarcomeric actinin	Mouse	1:300
Anti-connexin 43	Rabbit	1:300
Anti-CD68	Rabbit	1:300
Anti-alpha smooth muscle actin	Mouse	1:300

Rhodamine Phalloidin Red		1:40
Anti-Rabbit Alexa Flour 594	Donkey	1:300
Anti-Mouse Alexa Flour 488	Goat	1:300
Anti-Mouse Alexa Flour 647	Goat	1:300

3.8. Calcium Imaging

iCMs and co-cultures of iCMs and iMacs were cultured in 6 or 24 well plates. On the day of the experiment, 5 mM stock of Cal-520® AM dye was made up to a 3 µM solution, in RPMI media with B-27™ supplement (RPMI+i). Samples were incubated in the media with Cal-520®AM dye for 90 minutes, followed by a media wash and further incubation in RPMI+i. Samples were imaged using a CellSense epi-florescent microscope with heated and motorised stage. Excitation/emission of 490/525 nm was used and videos were recorded at a fixed exposure time of 100 ms. Videos were analysed using FIJI (ImageJ), where 5 to 9 regions of interest were picked and the intensity variations were tracked. The plots of the intensity variation were used to determine the intensity of calcium signalling (F/F0), beating rate (in beats per minute; bpm), time to peak and time to decay.

3.9. Statistical analysis

Results are represented as mean ± standard deviation. Normalisation tests were performed prior to statistical analysis and comparisons were made based on the experiments and groups being analysed, using GraphPad Prism 10. Kindly refer to figure legends for the exact statistical test performed. * $P<0.05$, ** $P<0.01$, *** $P<0.001$ and **** $P<0.0001$ were considered significant differences.

Chapter 4 Thesis Objectives

There exists a large translational gap between animal models employed for studying CVDs and the actual events occurring in humans. While animal models provide valuable insights into disease mechanisms, responses to therapies, and potential interventions, their translation to human physiology is not always straightforward. Animals, even genetically modified or disease-induced models, often do not fully recapitulate the complexity and nuances of human cardiovascular physiology and pathology. However, using tissue engineering strategies, fabricating human cardiac tissues *in vitro* offers an exciting prospect to understand and mimic the myocardium. Although over two decades of research has culminated in highly complex EHT models, our recent appreciation of the intricate functions of CRMs are yet to be explored *in vitro*. To that end, the aim of this work is to **harness an innate immune response in engineered heart tissues, using iPSC-derived macrophages, to serve as a platform to model healthy and diseased myocardium.** The individual objectives to achieve this aim include:

Objective 1. Generation and characterisation of iPSC-derived macrophages (iMacs) (Chapter 5).

Objective 2. Generation and characterisation of iPSC-derived cardiomyocytes (iCMs) and iPSC-derived cardiac fibroblasts (iCFs) from the same iPSC line as iMacs (Chapter 6).

Objective 3. Exposing iMacs to different cardiac cues, such as treatment with iCM conditioned media and co-cultures with iCMs, to fully delineate the *in vitro* interactions between iMacs and iCMs (Chapter 7).

Objective 4. Improving the maturation of iCMs and co-cultures of iCMs and iMacs using electrical stimulation (Chapter 8)

Objective 5. Fabrication of engineered heart tissues to model the myocardium using iCMs, iMacs and iCFs, together with electrical stimulation (Chapter 9)

Chapter 5 Generation and characterisation of iPSC-derived macrophages

5.1. Abstract

Macrophages are highly versatile immune cells, crucial for tissue homeostasis, immune responses, and disease pathogenesis. In general, macrophages are classified into two categories: blood-derived circulating macrophages (BDMs) and embryonically derived tissue-resident macrophages (TRMs). While both types share fundamental immune functions, they differ in origin, distribution, and specialisation. Obtaining TRMs for research has been challenging due to limited accessibility and invasive procedures, leading to the exploration of induced pluripotent stem cells (iPSCs) as a tool for generating resident-like macrophages *in vitro*. With numerous papers supporting the similarities between iPSC-derived macrophages (iMacs) and TRMs in terms of their origin, in this chapter, an optimal differentiation protocol to obtain iMacs, is explored. Despite existing protocols for iMac differentiation, variations exist depending on iPSC lines. Hence, in this chapter, three different varieties of iMac differentiation protocols were compared, using two different iPSC lines, to establish an optimal protocol. Optimally derived iMacs were $CD14^{high}CD11b^{high}CCR2^{low}CX3CR1^{high}$. Additionally, iMacs were found to successfully perform phagocytosis and polarise to classically and alternatively activated states. Finally, in comparison to BDMs, iMacs were found to be highly quiescent, further underlining their similarities to TRMs.

5.2. Introduction

Macrophages are highly versatile immune cells, that are integral components of the body's defence system; playing key roles in tissue homeostasis, immune responses, and disease pathogenesis [114, 282-284]. Macrophages can be broadly classified into two categories: monocyte-derived circulating macrophages (or blood-derived macrophages (BDMs)) and embryonically derived tissue-resident macrophages (TRMs) [90]. While

these categories share similarities in their fundamental immune functions, they exhibit key differences in terms of origin, distribution, and specialisation. BDMs are derived from bone marrow precursors, circulate in the bloodstream, and migrate to various tissues in response to inflammatory signals [285]. They exhibit remarkable plasticity, adapting their function to the microenvironment they encounter. In contrast, TRMs are established during foetal development and reside in specific tissues, such as the brain, liver, lungs, heart etc [286]. These resident macrophages are often responsible for maintaining tissue integrity and performing specialized functions unique to their respective niches [65]. There has been increasing interest in developing methods for obtaining TRMs *in vitro* as the use of BDMs and macrophage cell lines to study human TRM biology is redundant.

The biology and functions of human BDMs have been extensively researched as they are easily obtained from blood samples. However, obtaining TRMs has proven challenging due to their limited accessibility and the need for invasive procedures. As a result, induced pluripotent stem cells (iPSCs) have emerged as a valuable tool for generating resident-like macrophages *in vitro* [201, 204]. By reprogramming somatic cells into iPSCs and subsequently differentiating them into macrophages (iMacs), researchers can create models that closely mimic TRMs [201]. A number of previous studies highlight how iMacs are similar to highly specialised TRMs, making them a particularly interesting addition to *in vitro* models for disease modelling, drug screening and personalised medicine.

Although established protocols exist for obtaining iMacs, most differentiations vary depending on the iPSC line [143]. Therefore, in this chapter, we screen and establish an efficient protocol for obtaining iMacs. We chose a particularly robust protocol which was first developed by Karlsson et al. [287] for differentiating human embryonic stem cells (ESCs) to macrophages, later modified by van Wilgenburg et al. [210] to differentiate iPSCs to iMacs. Here, we screen three different varieties of this protocol and demonstrate its reproducibility across two different iPSC lines.

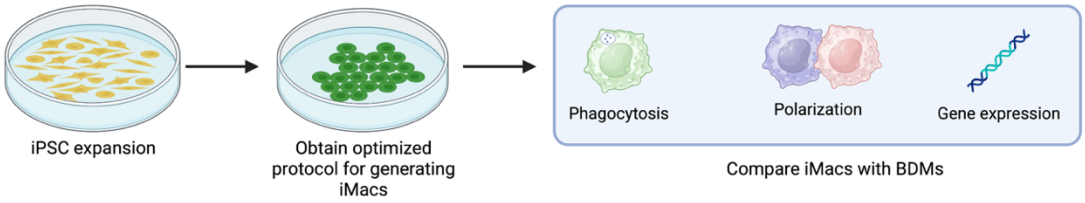

Figure 5.1: Graphical Abstract. In this chapter, a reproducible protocol for the generation of iPSC-derived macrophages (iMacs) is screened from a number of existing protocols. iMacs obtained from the optimised protocol is compared with blood-derived macrophages (BDMs) to establish the difference between them in terms of basic macrophage characteristics, such as phagocytic and polarisation potential, as well as their expression of a number of different resident macrophage genes.

5.3. Materials and Methods

5.3.1. Experimental design

In order to generate macrophages from iPSCs, three different approaches for the same differentiation protocol available from the literature were tested. The most common methods used in previous studies involve the induction of mesoderm through embryoid body (EB) formation, followed by the induction of haematopoiesis [210, 288]. The formation of EBs can be performed either using low adherence microwell plates with defined cell numbers, or using ultra-low attachment (ULA) plates where cells clump together naturally to form EBs . Hence, EBs were developed using the following three approaches: (a) Aggrewell^{TM} plates, which are commercially available, (b) agarose well plates, which were custom-made and (c) 6-well ULA plates. In addition to the yield, the robustness of the differentiation process was assessed using flow cytometry, by analysing the expression of some common macrophage markers such as CD14, CD11b and HLA-DR, as well as some resident macrophage markers such as upregulation of CX3CR1 and downregulation of CCR2. The reproducibility of the protocol was demonstrated by using two iPSC lines (11b and SFCi55); and based on the yield and macrophage marker expression, an optimised differentiation method was selected.

After obtaining an optimised protocol, the functional capability of iMacs were characterised by assessing their polarisation and phagocytic potential, using BDMs as a

control. RT-qPCR, ELISA and flow cytometry techniques were used to fully characterise iMacs (methods described in Chapter 3).

5.3.2. Differentiation of iPSCs to macrophages

A well-established iPSC line from University of Edinburgh (SFCi55) tagged with zombie green (ZGiPSCs) [288] was expanded using mTESR media (Stemcell Technologies) in Matrigel™ (Corning) coated plates, with the addition of 10 µM ROCK inhibitor (Stemcell Technologies) on days of passaging. Two different methods were used for EB formation. For EB formation using 6 well ULA plates, one well of 80-90% confluent ZGiPSCs (at P18 to P22) were lifted using Versene (Gibco) and split to two wells of a ULA plate (Greiner Bio-One), where EB formation occurred by virtue of cell clumping. On the other hand, for EB formation using microwell plates (Aggrewell™ and agarose well plates), one well of 80-90% confluent ZGiPSCs were lifted using Accutase (Stemcell Technologies) and broken down into single cell suspension. ZGiPSCs were spun down and counted, following which they were seeded on Aggrewell™ (Stemcell Technologies) plates as well as custom made Agarose-well plates, at a concentration of 10,000 cells per microwell, to obtain uniformly formed EBs. On day 0, cells were cultured in mTESR media supplemented with BMP-4 (50 ng/ml), VEGF (50 ng/ml) and SCF (20 ng/ml) in both ULA plate and the microwell plates, with an addition of 10 µM/ml ROCK inhibitor for cells in the Aggrewell and Agarose-well plates. On day 2 of differentiation, an additional 0.5 ml media was added per well, with concentrations of BMP-4 (Biotechne), VEGF (Biotechne) and SCF (Biotechne) adjusted to make up for the entire media volume. On day 4 of differentiation, the EBs were collected and plated on 0.1 % Gelatine (Stemcell Technologies) coated 6-well plates at a concentration of 12-15 EBs per well, to initiate haematopoiesis induction. The plated EBs were cultured in X-VIVO media (Lonza) supplemented with M-CSF (100 ng/ml; Miltenyi), IL3 (25 ng/ml; Biotechne), Glutamax (2 mM; Gibco), 2% penicillin/streptomycin (Gibco) and beta mercaptoethanol (55 mM; Gibco). At about 14 days after the initiation of haematopoiesis, the non-adherent cells or pre-macrophages (pre-macs) present in the wells were collected and plated at a density of 500,000 cells per well of a 6-well plate and cultured in X-VIVO media,

supplemented with 100 ng/ml M-CSF, 1% Glutamax and 2% penicillin/streptomycin for 7 days, to obtain macrophages. Non-adherent cells were collected, replated and cultured for a period of 100 days to compare the yield of iMacs being generated using the two different EB formation methods.

To further prove the reproducibility of this protocol, the differentiation was repeated with iPSC lines 11b as well as SFCi55 without zombie green.

5.3.3. Characterisation of iMacs using flow cytometry

Flow cytometry was carried out as described in Chapter 3. The flow cytometry plots were first gated for the events of interest, followed by single cells. The single cells were then gated for cells positive for CD14 and CD11b. The populations that were positive for CD14 and CD11b were also assessed for their CX3CR1, CCR2 and HLA-DR expressions. CX3CR1 and HLA-DR expressions were quantified based on mean fluorescence intensity (MFI).

5.3.4. Polarisation of iMacs

Polarisation was induced in iMacs by treating them with certain factors that trigger a pro-inflammatory and anti-inflammatory response. To drive a pro-inflammatory response, iMacs were treated with 100 ng/ml lipopolysaccharide (LPS) and 50 ng/ml of interferon gamma (IFNγ) (Biotechne) for 24 hours. Similarly, to drive an anti-inflammatory response, iMacs were treated with 20 ng/ml IL4 (Biotechne) for 24 hours, with untreated iMacs used as control. The polarisation potential of iMacs were evaluated through ELISA and flow cytometry. ELISA was performed to quantify the presence of cytokines such as TNFα, IL6 and IL10 in the secretome, and flow cytometry was performed to quantify the expression of CD80, CD86, CD163 and CD206.

5.3.5. Phagocytic potential of iMacs

Pre-macs were plated on 24 well plates at a density of 300,000 cells/well and cultured for 7 days in the presence of 100 ng/ml M-SCF. Red zymosan particles (Phagocytosis

Assay Kit, (Red Zymosan) Abcam) were added to the culture and incubated for 3 hours to facilitate phagocytosis. After incubation, the cells were washed with ice cold phagocytosis assay buffer and retrieved from the plates using a cell scraper. Flow cytometry was used to quantify the population of cells positive for the red zymosan particles (550 nm). BDMs were used as control.

5.4. Results and Discussion

5.4.1. Aggrewell™, agarose and ULA plates successfully facilitated EB formation and consequent iMac differentiation

As discussed in Chapter 2, ESCs and iPSCs have been used in the past to derive CD14+ macrophages, and a number of different protocols exist for this differentiation [90]. Buchrieser et al. have reported that iMacs sharing ontogeny with MYB-independent tissue resident macrophages can be successfully derived, using a protocol previously published by Van Wilgenburg et al [90, 201]. The efficacy and reproducibility of this differentiation protocol were assessed by using 2 different iPSC lines as well as 3 different approaches for EB formation (Aggrewell™, agarose well and ULA plates) (Figure 5.2). Both iPSC lines - 11b and SFCi55 – (Figure 5.3(a)) successfully formed EBs and iMacs (Figure 5.3(b,c)). Morphologically, iMacs were found to be large cells (15-20 µm diameter), with plenty of vacuoles, unlike BDMs. This phenotype has been previously reported [196] and could be due to prolonged culture or due to differences in developmental origin of iMacs to BDMs [210]. Flow cytometry was used to assess the purity of the macrophage populations obtained. Single cells were first gated based on their expression of common macrophage markers such as CD14 and CD11b to determine the purity of the population on day 7 and 14 (Figure 5.4 (a,b)). iMacs generated from iPSCs and ZGiPSCs using Aggrewell™ plates showed significant differences in the percentage of population that was positive for CD14 and CD11b, between day 7 and day 10 of culture (Figure.5.4(b)). iMacs on day 7 were found to express a two-fold greater population percentage positive for CD14 and CD11b, as compared to iMacs on day 10 (Figure 5.4(b)). Interestingly, iMacs generated using agarose well plates showed differences between cell lines, with three-fold higher

percentage of iPSCs being positive for CD14 and CD11b on day 7 as opposed to day 10 (Figure 5.4(b)). iMacs generated using ULA plates were found to be the most stable across time points and cell lines, with no significant differences (Figure 5.4(b)).

As discussed in Chapter 2, a key function of macrophages in the body is to perform efferocytosis. Although cell apoptosis can happen routinely, efferocytosis is critical for the cessation of apoptosis, whereby an accumulation of dead cells, prolonged inflammation and further necrosis of cells are prevented [195]. Macrophages and other phagocytes respond to the “find me” and ”eat me” signals released by apoptotic cells, to perform efferocytosis. This response is mediated by a number of receptors such as CX3CR1, S1PR1, MERTK etc. [289]. Upon examining the population percentage of iMacs positive for both CD14 and CX3CR1, almost 99% of iMacs generated using ZGiPSCs (using Aggrewell^{TM}, agarose well and ULA plates) were found to be $CD14^{high}CX3CR1^{high}$ (Figure 5.4(c)), demonstrating high efferocytosis potential. It was also interesting to note that, iMacs generated using ULA plates were $CD14^{high}CX3CR1^{high}$ across both iPSC lines assessed (Figure 5.4(c)). In addition to being linked to efferocytosis, in the myocardium, the expression of CX3CR1 is often used to distinguish between BDMs and TRMs, with TRMs being highly positive for CX3CR1 [102, 104, 106]. A major similarity amongst macrophages present in the heart, liver, lungs, kidney etc. is an abundance in the population of $CCR2^{-}$ or $CCR2^{low}$ macrophages. [64, 102, 104, 290]. Interestingly, iMacs obtained from ZGiPSCs on agarose and ULA plates were $CD14^{high}CCR2^{low}$, with ULA plates generally yielding more resident macrophage-like iMacs (Figure 5.4(d)), in agreement to results reported in literature [291].

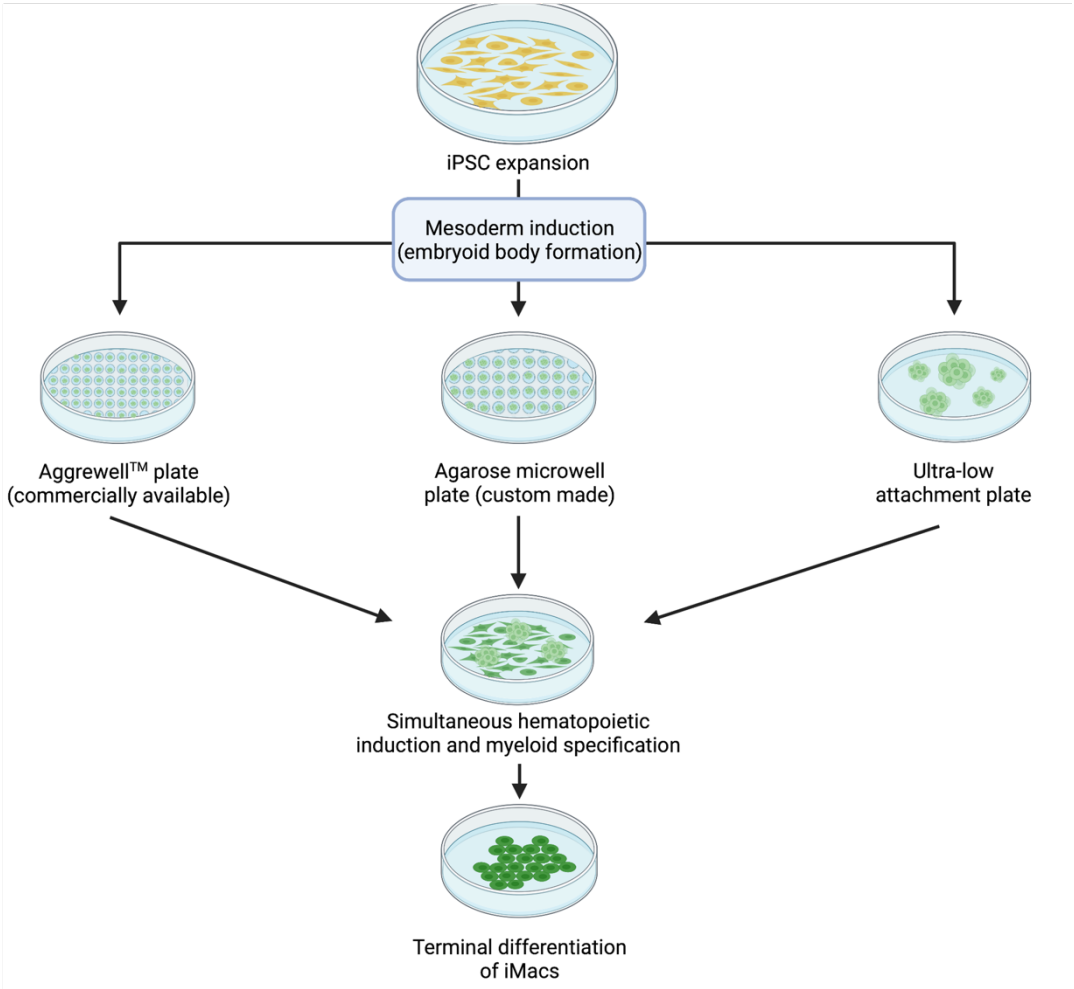

Figure 5.2: Schematic diagram of the three different approaches used to differentiate iPSCs to iMacs. The differentiation was performed by modifying a previously established protocol [288], wherein, iPSCs were expanded to form embryoid bodies using Aggrewell™, agarose well and ULA plates. Embryoid bodies were then replated and kept in culture for up to a 100 days and monitored for successful iMac differentiation.

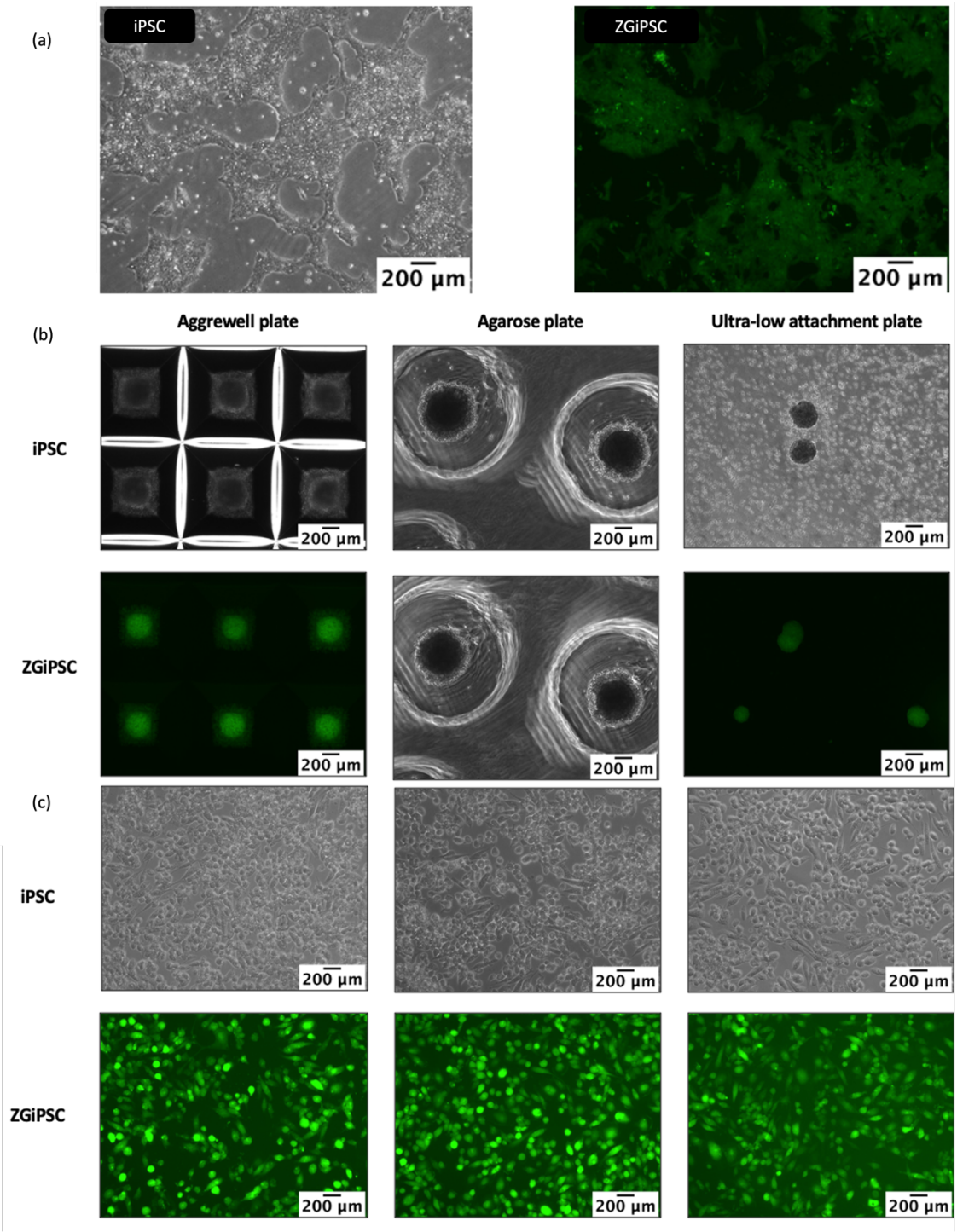

Figure 5.3: Differentiation of iPSCs to macrophages. (a) Representative images of iPSCs (11b cell line) and ZGiPSCs (zombie green tagged SFCi55 iPSC line) during expansion. (b) Representative images of iPSCs and ZGiPSCs undergoing mesodermal induction in Aggrewell™ , agarose and ultra-low attachment plates. (c) Representative images of terminally differentiated iMacs obtained from embryoid bodies formed using Aggrewell™ , agarose and ultra-low attachment plates. Scale bar: 200µm.

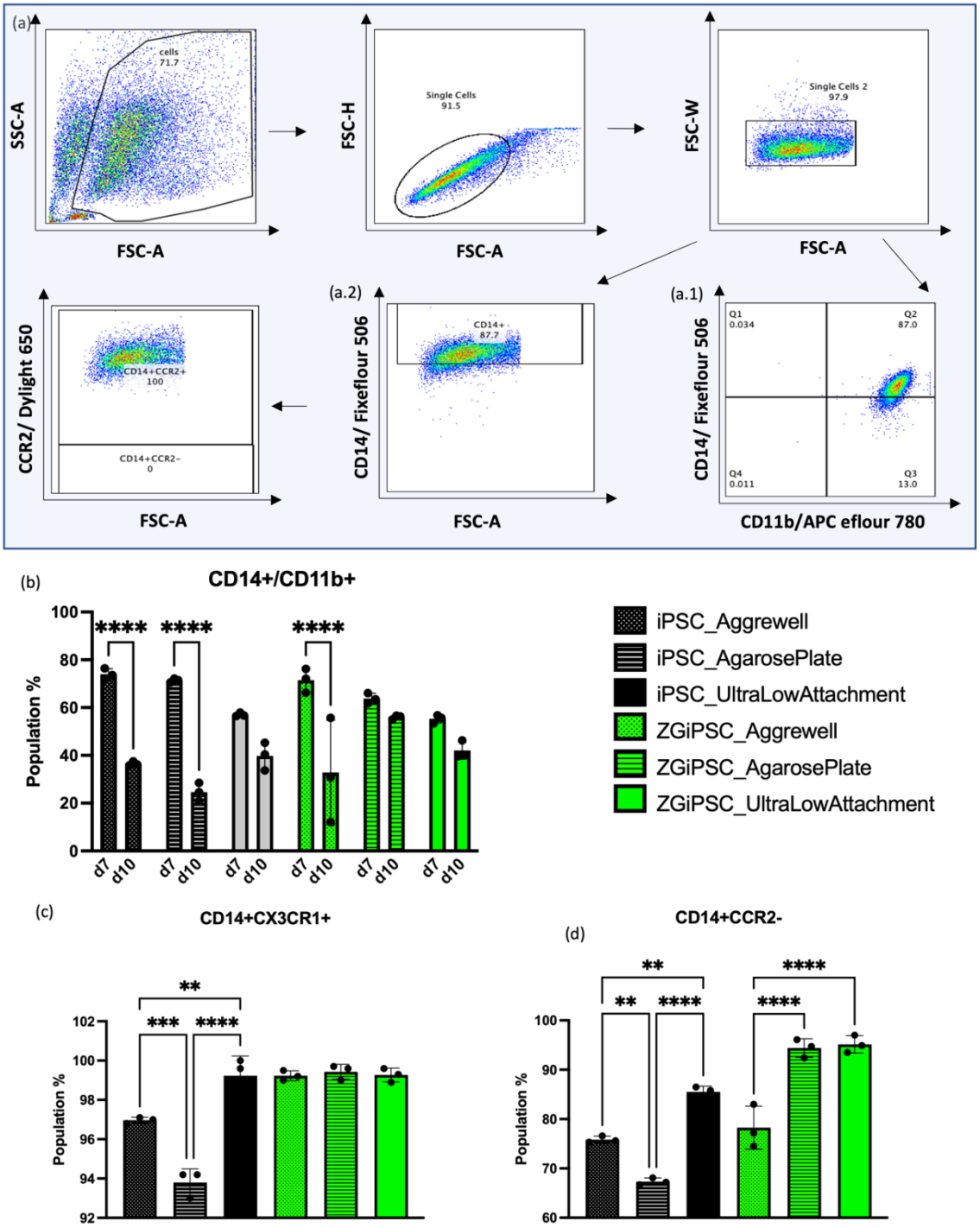

Figure 5.4: Characterization of iMacs using flow cytometry. (a) Gating strategy used to characterize iMacs. (b) Quantification of CD14 and CD11b positive populations of iMacs on day 7 and day 10 of differentiation (using gating strategy a.1). (c) Quantification of the population of iMacs positive for CX3CR1, within the CD14+ population (using gating strategy a.2). (d) Quantification of the population of iMacs negative for CCR2, within the CD14+ population (using gating strategy a.2). Statistical analysis - Ordinary One way and Two way ANOVA. ** represents

P<0.01, *** represents P<0.001 and **** represents P<0.0001. N = 3 (biological replicates), with each point signifying the average of 3 technical replicates.

5.4.2. The EB-based differentiation protocol is robust and generates iMacs for up to 100 days

The differentiation protocol used was found to be highly robust with excellent yield of iMacs for up to 100 days, with iMacs obtained from ZGiPSCs on ULA plates exhibiting the highest yield of 1.5 to 6 million cells per harvest up to day 50 and a steady 0.5 million cells per harvest up to day 100 (Figure 5.5(a)). Using monolayer differentiation approaches (without forming EBs), Cui *et al.* has previously reported a yield of about 240,000 $CD14^+$ cells/cm^2 on day 15 of harvest [292], which is 400-fold more than the yield reported by Cao *et al* [195]. In comparison to these reports, iMacs obtained using ZGiPSCs on ULA was found to be 187,500 $CD14^+$ cells/cm^2 on day 15. Based on CD14, CD11b, CX3CR1 and CCR2 expressions, together with the yield over a period of 100 days, generation of iMacs using ZGiPSCs on ULA plates and cultured for 7 days, was chosen as the optimised method for deriving iMacs for the rest of the experiments. Optimally derived iMacs were found to be $CD14^{high}CCR2^{low}CX3CR1^{high}$HLA-$DR^{high}$ in comparison to BDMs (Figure 5.5(b-f)). Impressively, this protocol has also been adapted in large scale bioreactor based cultures with high yields of iMac production [194].

The differentiation protocol yielded variations between the two iPSC lines assessed (11b and SFCi55). Since the inception of iPSC technology, large variations across iPSC lines has remained an important topic of discussion [293]. The variations in the responses seen with different iPSC lines have been linked to a number of potential reasons such as donor age, donor sex, incomplete reprogramming and existing genetic dispositions in donors [293, 294]. Variability has also been reported in iPSC lines reprogrammed from the same donor [293]. In a very detailed study, Boulting *et al.* reprogrammed 16 iPSC lines from 7 individuals of different age, sex and health conditions, and characterised their pluripotency and their ability to terminally differentiate into functional motor neurons, in two different laboratories [293]. Although reprogramming was reported to be successful in all the iPSC lines, not every iPSC line performed well when terminally

differentiated. Out of the 16 iPSC lines assessed, 3 reportedly failed to differentiate to motor neurons, one of which is the 11b iPSC line, which has also been used in our iMac differentiation studies. The same study also reports genomic instabilities in the 11b iPSC line, when kept in culture for longer passages (P42) [293]. The variabilities between the performance of iPSCs (11b) and ZGiPSCs (SFCi55) reported in this chapter could potentially be attributed to the genomic profile of the 11b iPSC line. Similarly, gene expression variations have also been reported across 4 iPSC lines undergoing iMac differentiation, addressing variability across iPSC lines and demonstrating such variations in iMac differentiation protocols as well [195, 291].

Having successfully optimised a differentiation protocol for the generation of iMacs, the next focus was to assess their functionality. Phagocytosis is a key macrophage function by virtue of which pathogens, cell debris, dead cells etc. are engulfed by macrophages, from their vicinity [295]. A number of methods exist to assess the phagocytic potential of macrophages; on treating iMacs and BDMs with pHrodo-labelled zymosan particles, iMacs were found to perform phagocytosis, although 19% less than BDMs (Figure 5.5(g,h)), similar to other reports from literature [201, 210, 295]. Using a bacterial phagocytosis assay, Cao *et al.* reported similar phagocytic potential between iMacs and BDMs, but higher phagocytic potential in iMacs when treated with DiI-acetylated low-density lipoprotein (AcLDL) [195]. Similarly, Cui *et al.* also reported comparable phagocytic capacity between iMacs and BDMs, on performing a bacterial phagocytosis assay [292]. However, there is no reported study comparing the zymosan uptake between iMacs and BDMs.

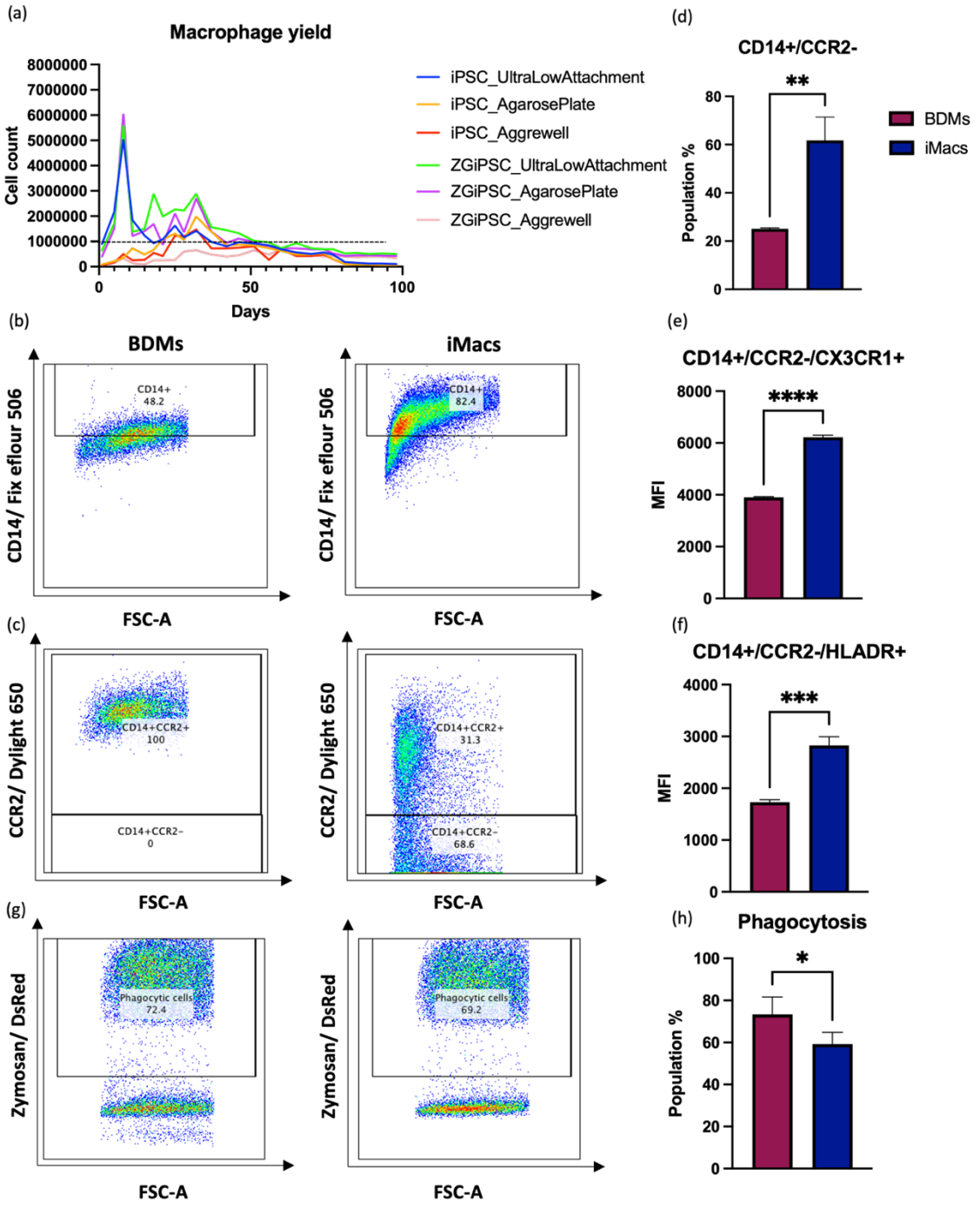

Figure 5.5: Comparison of iMacs to BDMs. (a) Yield of iMacs over 100 days using three different plates for differentiation, with two iPSC lines. (b) Comparison of CD14 expression between BDMs and iMacs, 7 days after MCSF treatment. (c) Comparison of CCR2 expression between BDMs and iMacs, 7 days after MCSF treatment. (d) Quantification of CD14+CCR2- population in BDMs and iMacs. (e) Quantification of CD14+CCR2-HLADR+ population in BDMs and iMacs. (g) Comparison of phagocytic potential of BDMs and iMacs. (h) Quantification of phagocytic potential of BDMs and

iMacs. Statistical analysis - Student T test with Welch's correction. * represents P<0.05, ** represents P<0.01, *** represents P<0.001 and **** represents P<0.0001. N = 3 (biological replicates), with each point signifying the average of 3 technical replicates.

5.4.3. iMacs are functionally active, with the ability to polarise to pro- and anti-inflammatory states

In addition to efferocytosis and phagocytosis, the capacity of macrophages to switch to pro- and anti-inflammatory states is a highly distinguishing feature that plays a critical role in macrophage function *in vivo* [296]. On treating iMacs with known stimulants such as LPS, IFNγ and IL4, robust responses were noted. ELISA studies showed high expression of cytokines such as TNFα, IL6 and IL10 on treatment with LPS (Figure 5.6(a,b)). Although LPS is known to trigger a pro-inflammatory response in macrophages, the production of anti-inflammatory cytokine IL10 in response to LPS treatment, has been reported in the past [297, 298]. Similarly, on examining the expression of cell surface markers through flow cytometry, iMacs showed an upregulation of CD80 expression with LPS treatment (Figure 5.6 (c)), upregulation of CD86 expression with IFNγ treatment (Figure 5.6 (c)) and upregulation of CD206 expression with IL4 treatment (Figure 5.6 (d)), further demonstrating the functional ability of iMacs. Similar upregulation of TNFα and IL6 production with LPS stimulation has been previously reported with iMacs, by Alasoo *et al.* [291]. Additionally, similar trends in CD80 expression has also been reported in literature, with a combined stimulation using LPS and IFNγ [195]. Cao *et al.* also reports no significant difference in CD163 expression (marker for anti-inflammatory response) for both classically and alternatively activated iMacs [195].

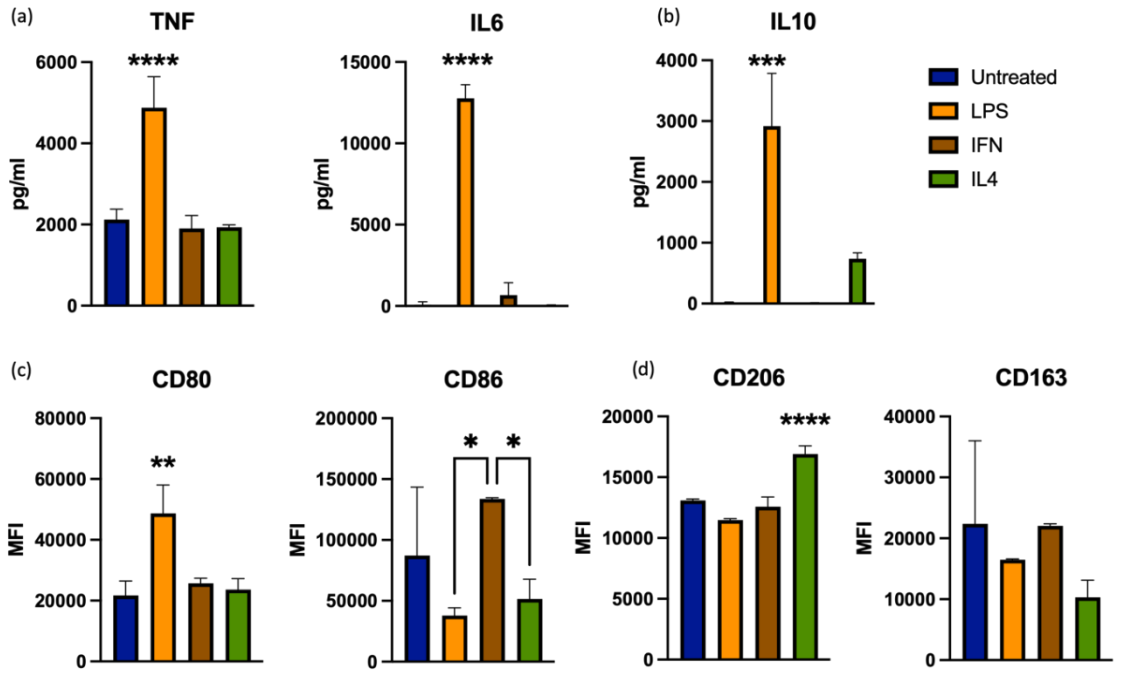

Figure 5.6: Assessment of polarisation potential of iMacs, using LPS, IFNγ and IL4. (a) Quantification of release of pro-inflammatory cytokines TNFα and IL6, using ELISA. (b) Quantification of release of anti-inflammatory cytokine IL10, using ELISA. (c) Quantification of mean fluorescence intensity of pro-inflammatory markers CD80 and CD86, using flow cytometry. (d) Quantification of mean fluorescence intensity of anti-inflammatory markers CD206 and CD163, using flow cytometry. Statistical analysis - Ordinary One way ANOVA. * represents P<0.05, ** represents P<0.01, *** represents P<0.001 and **** represents P<0.0001. N = 3 (biological replicates), with each point signifying the average of 3 technical replicates.

3.4 iMacs are highly quiescent and show strong phenotypic and functional differences in comparison to BDMs

It is critical for TRMs to maintain quiescence until triggered by an external stimulus, such as infection and pathogens [299, 300]. In order to assess the resting state of iMacs, BDMs were used as a control and the expression of a set of genes was used to distinguish their phenotypic and functional states. As reported in literature, iMacs were found to exhibit highly quiescent characteristics [90], with a downregulation in the expression of

both pro-regenerative and pro-inflammatory genes (Figure 5.7 (a,b)). Similarly, the quiescent state was also reflected in the expression of genes highlighting functional activation of macrophages, such as CCR2, TRPV4 and VEGFA (Figure 5.7 (c)). Interestingly, the downregulation of CCR2 expression in iMacs, in comparison to BDMs has been previously reported [201]. However, Spiller *et al.* reports similar expression levels for genes such as TNF, MRC1, and TGFB1 between iMacs and BDMs [301]. These disparities could be because of a multitude of factors such as different iPSC lines, differences in the iMac differentiation protocol and health conditions of the blood donor used to isolate BDMs. The comparison between untreated iMacs and BDMs performed in this chapter to evaluate the quiescence of iMacs is first of its kind, and strongly highlights a TRM-like genomic profile in iMacs.

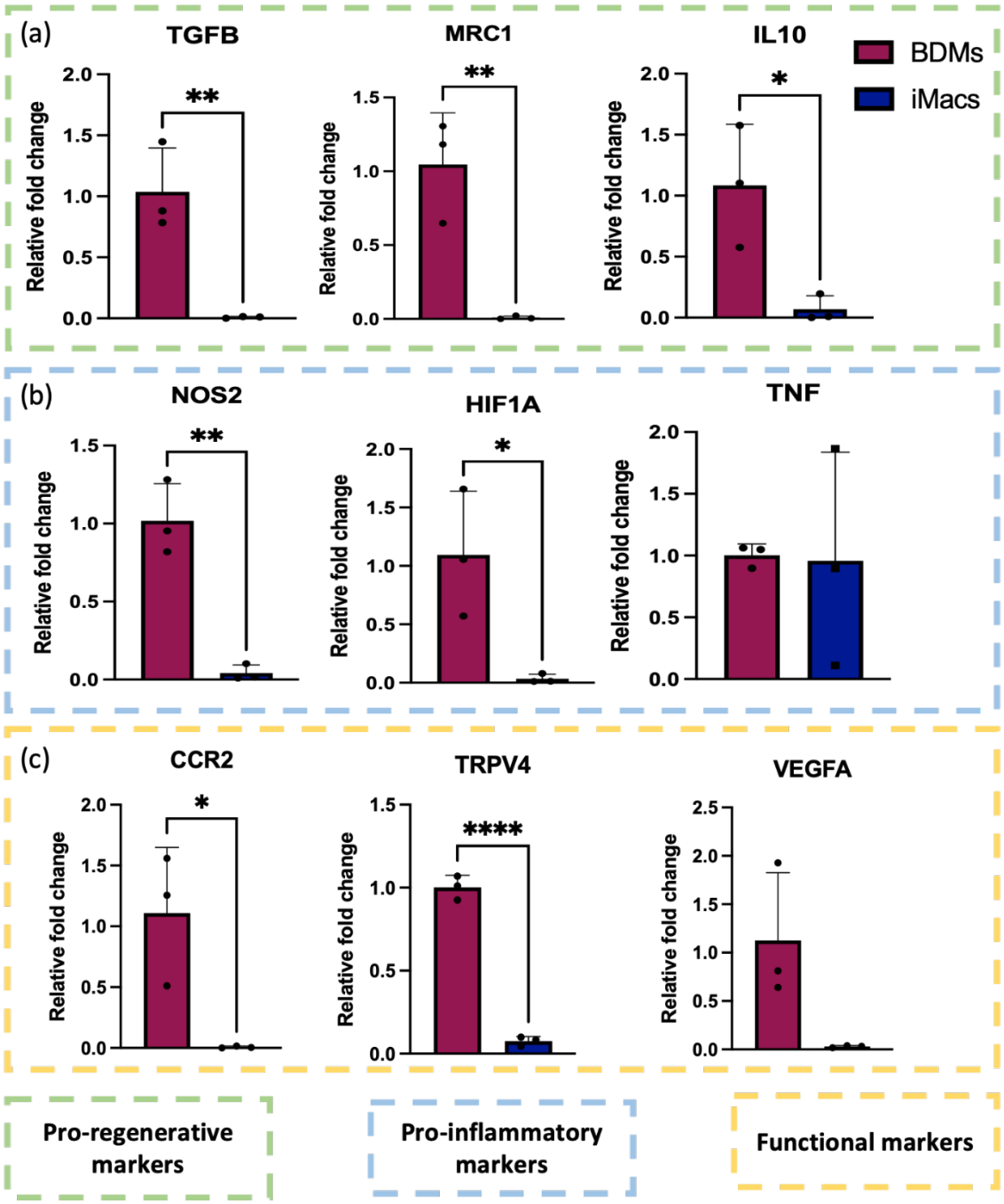

Figure 5.7: Comparison of the expression of a set of genes between iMacs and BDMs. (a) Expression of a set of pro-regenerative genes (b) Expression of a set of pro-inflammatory genes (c) Expression of a set of functional genes. Statistical analysis - Student T Test with Welch's correction. * represents P<0.05, ** represents P<0.01 and **** represents P<0.0001. N = 3 (biological replicates), with each point signifying the average of 3 technical replicates. Fold change of mRNA relative to blood-derived macrophages (BDMs).

5.5. Conclusion

The use of iPSC-derived macrophages stands at the forefront of medical research, promising a deeper understanding of tissue-specific immune responses and novel strategies for improving personalised medicine and disease modelling. In this chapter, three existing methods for iMac generation were systematically screened, in order to optimise the most efficient method to derive iMacs *in vitro*.

The iMacs obtained through the optimised protocol exhibited distinct features compared to conventionally used BDMs. Protein expression patterns of iMacs showed abundance of key macrophage markers (CD14 and CD11b), leaning more towards a resident macrophage phenotype ($CCR2^{low}CX3CR1^{high}$). Similarly, gene expression analysis of iMacs revealed a unique transcriptional profile, highlighting their quiescent state, with downregulation in the expressions of all genes assessed. Taken together, these results underline the phenotypic and genotypic differences between iMacs and BDMs, not only accentuating the potential of using iMacs as a reliable source for generating resident-like macrophages, but also validating the reproducibility of the optimised differentiation protocol. In addition to the gene and protein expression profiles, the functional capacity of iMacs were assessed by conducting polarisation studies. In response to specific stimuli (LPS and IFNγ treatment for pro-inflammatory stimulation; IL4 for anti-inflammatory stimulation), iMacs demonstrated ability to exhibit both classically and alternatively activated phenotypes. Moreover, their phagocytic activity was comparable to that of BDMs, confirming their efficacy in executing essential immune functions.

The ability to generate functional macrophages with unique molecular profiles opens new avenues for exploring the diversity within the macrophage lineage and understanding various tissue-specific immune responses and disease pathogenesis. Hence, the findings of this study underscore the potential of using iMacs as a source to model resident macrophage response *in vitro*, for disease modelling, personalised medicine and therapeutic applications.

Chapter 6 Generation and characterisation of iPSC-derived cardiomyocytes and cardiac fibroblasts

6.1. Abstract

Although iPSC technology has revolutionised the field of cardiac tissue engineering, there exists large variations in successful differentiation of iPSCs into different cardiac cell types, such as cardiomyocytes (iCMs) and cardiac fibroblasts (iCFs), depending on the iPSC line used. In this chapter, the SFCi55 iPSC line was used to optimally derive iCMs and iCFs, following a well-established differentiation protocol that involves sequential GSK3 and Wnt inhibition to obtain iCMs, and GSK3 inhibition followed by FGF2 treatment to obtain iCFs. iCMs obtained using this protocol showed spontaneous beating by day 8 of the differentiation, and expressed proteins such as cardiac troponin T, sarcomeric actinin, MLC2a and connexin 43. Similarly, iCFs, in comparison to primary human cardiac fibroblasts, expressed comparable levels of genes such as DDR2 and ACTA2, as well as CD90 protein. Comparative analysis not only revealed shared cardiac lineage markers between iCMs and iCFs, but also highlighted key differences in gene expression profiles, emphasising the need for refining purification methods to obtain enriched populations of cardiomyocytes. The established protocols for generating iCMs and iCFs serve as foundational knowledge for further optimisation and refinement, offering potential for producing other functional cardiac cell types involved in cardiovascular diseases, such as cardiac resident macrophages and cardiac endothelial cells.

6.2. Introduction

The human heart is an intricate organ responsible for the steady supply of oxygen and nutrients to all the parts of the body. However, the heart is susceptible to debilitating diseases that pose a significant challenge to medical science, making cardiac diseases one of the most leading causes of death worldwide [302]. Cardiac diseases, ranging from

arrhythmias to heart failure, represent a formidable global health burden [303]. Until recently, our endeavours to comprehend and address these conditions were hindered by the limitations of conventional research practices, often reliant on animal models whose physiological nuances did not faithfully translate to the complexities of the human cardiovascular system. However, the advent of iPSC technology has ushered in a revolutionary era in cardiac tissue engineering [143]. iPSCs, reprogrammed from adult somatic cells, possess the remarkable ability to differentiate into any cell type within the human body [144]. This newfound versatility has allowed scientists to obtain various cell types present in the heart, including cardiomyocytes [145], cardiac endothelial cells [146] and cardiac fibroblasts [147], directly from iPSCs, paving the way for a deeper understanding of cardiac physiology and pathology.

Before the era of iPSCs, researchers faced considerable challenges in mimicking human cardiac conditions. Animal cells, while valuable for certain studies, often fail to capture the intricacies of human cardiac physiology [304]. Using a detailed and quantitatively accurate mathematical model of ventricular action potentials across human, guinea pig and dog hearts, O'Hara *et al.* reported large differences in the cell electrophysiology mechanisms and response to drugs [305]. Together with many similar studies, this highlights the translational gap between animal models and human biology, and how this hinders the progress in developing effective treatments for cardiac diseases. iPSCs, by offering a platform for studying human-specific cells, have revolutionised this landscape.

Efficient differentiation of iPSC-derived cardiomyocytes (iCMs) has come into existence only in the last decade, and it has not only advanced our understanding of cardiac diseases but also provided a promising avenue for discovering novel therapeutic interventions. Initial efforts of cardiomyocyte differentiations used embryonic stem cells (ESCs), which are allogeneic, with a potential for immunogenicity [306]. Additionally, the use of human embryos as a cell source posed serious ethical dilemma, resulting in a push towards more advanced attempts to find alternatives to ESCs [306]. Early cardiomyocyte differentiation protocols using ESCs employed an EB-based

approach [148]. However, this protocol only yielded less than 1% cardiomyocytes [145]. Regardless, the EB-based protocol was improved over the years [149-151] and was also shown to be effective in iPSCs [152]. Further improvements led to one of the most reproducible protocol for iCM differentiation that has been established, which relies on a monolayer differentiation approach and small molecule treatments to inhibit GSK3 pathway (to induce mesodermal lineage) followed by the inhibition of Wnt pathway (GiWi protocol) [145]. With such advancements, iCMs serve as a powerful tool for drug screening and toxicity testing, enabling researchers to assess the efficacy and safety of potential pharmaceuticals in a human-specific context. Additionally, iCMs hold immense potential in regenerative medicine, offering a promising prospect for repairing damaged cardiac tissue.

In mammals, although cardiomyocytes are the most dominant cell type of the heart by volume (over two-third) [153], non-myocytes such as fibroblasts and endothelial cells outnumber cardiomyocytes by double the cardiomyocyte amount [154]. During homeostatic conditions, cardiac fibroblasts are known to remain quiescent, with minimal cell proliferation and matrix turnover [307]. However, the primary function of cardiac fibroblasts is to synthesise extracellular matrix (ECM), which envelops cardiomyocytes and serves as a structural scaffold [308]. Beyond its mechanical support, cardiac fibroblasts engage in intricate cell signalling pathways through interactions with growth factors and integrins, regulating essential biological processes like proliferation, apoptosis, migration, and differentiation of cardiac cells [309, 310]. Consequently, during cardiac development and injury repair, cardiac fibroblasts orchestrate critical functions, highlighting its significance in cardiac embryogenesis and healing processes [311]. Studies focusing on interactions between cardiomyocytes and non-myocytes have resulted in improving our understanding of their functional coupling [155]. Vasquez *et al.* pioneered this investigation and showed an upregulation in connexin43 expression in addition to functional coupling between cardiomyocytes and cardiac fibroblasts isolated from infarcted rat ventricles [155]. In a study attempting to understand the stage-specific role of cardiac fibroblasts in cardiomyocyte maturation, Ieda *et al.* performed co-cultures of embryonic and adult cardiac fibroblasts, with

cardiomyocytes [312]. Interestingly, while embryonic cardiac fibroblasts promoted the proliferation of cardiomyocytes, adult cardiac fibroblasts induced cardiomyocyte hypertrophy [312]. Similarly, the addition of cardiac fibroblasts have shown to be beneficial in improving iCM maturation and engineered heart tissue formation [16, 147, 255, 313]. To that end, the synergy between iCMs and iPSC-derived cardiac fibroblasts (iCFs) has proven to be invaluable in the realm of cardiac tissue engineering [156]. The interplay between these cell types *in vitro*, mirrors the intricate dynamics of the native heart, allowing researchers to explore the complexities of cardiac diseases such as fibrosis and hypertrophy. In addition to acting as a support cell type, *in vitro* cardiac fibroblast-derived matrix has shown potential to improve cardiomyocyte maturation and metabolism [314]. On the contrary, using *in vitro* activated iCF-derived matrix to culture cardiomyocytes, is reported to trigger fibrotic responses in cardiomyocytes, with changes in sarcomere length, phenotype and calcium handling [315]. Although fibroblasts have been identified as the low abundance cell type present in iCM cultures [157, 158], more directed differentiation strategies targeting epicardial cells have given rise to iCF differentiation protocols [159-161]. In 2019, Zhang *et al.* developed a protocol for iCF differentiation wherein iPSCs were first differentiated to epicardial cells [160], followed by the use of a commercially available fibroblast growth medium in the presence of fibroblast growth factor (FGF2) and transforming growth factor-beta (TGF-β) inhibitor SB431542 [162]. In the same year, Zhang *et al.* used an approach of iCF derivation via second heart field progenitors, by GSK3 inhibition followed by FGF2 stimulation [147]. The derivatisation of iCFs, together with the nuanced understanding of iCM-iCF interaction is pivotal for the development of targeted therapies that address the specific cellular and molecular intricacies of cardiac pathologies.

In this chapter, derivatisation of cardiomyocytes and cardiac fibroblasts from SFCi55 (iPSCs) and zombie green tagged SFCi55 iPSC (ZGiPSCs) lines was established and the efficacy and reliability of the differentiation protocols was assessed. iCMs and iCFs were characterised based on their gene and protein expressions; and iCFs were compared to primary human cardiac fibroblasts (hCFs) to establish successful differentiation. Finally,

iCMs and iCFs were also compared with each other, to highlight their phenotypic and genotypic differences.

6.3. Materials and Methods

6.3.1. Experimental design

The generation of iCMs and iCFs was achieved by using previously established protocols (Figure 6.1). As with most iPSC-based protocols, differentiations can be cell line dependant and hence, for iCM differentiation, the most commonly reported GiWi protocol was used [145]. One of the most intricate step in iCM differentiation is the induction of mesoderm using CHIR99021 (GSK3 inhibitor). The concentration of CHIR99021 to be used for the differentiation was decided by screening concentrations from 4 to 12 μM. The optimal concentration was chosen based on whether the cells achieved spontaneous beating by day 10 of differentiation (detailed description of protocol in section 6.2.2). Similarly, iCFs were generated using a previously established protocol [147], with minor changes (detailed description of protocol in 6.2.3).

The efficiency of iCM differentiation was assessed using flow cytometry, to quantify the percentage of population positive for cardiac troponin T (cTnT) and MLC2a (myosin light chain marker for atrial cardiomyocytes). Similarly, efficiency of iCF differentiation was confirmed by comparing the cells to primary human cardiac fibroblasts (hCFs). Detailed protocol of hCF isolation described in Chapter 3 (subsection 3.3). Since the differentiation of iCMs and iCFs follow similar pathways, they were also assessed for their expression of a number of cardiac developmental genes (GATA4, SOX17, TBX5, TBX18, POSTN), cardiac fibroblast specific genes (TCF21, DDR2, ACTA2) and cardiomyocyte specific proteins such as cardiac troponin T (cTnT) and Sarcomeric actinin, to establish changes in their transcriptional profile as well as to confirm successful differentiation.

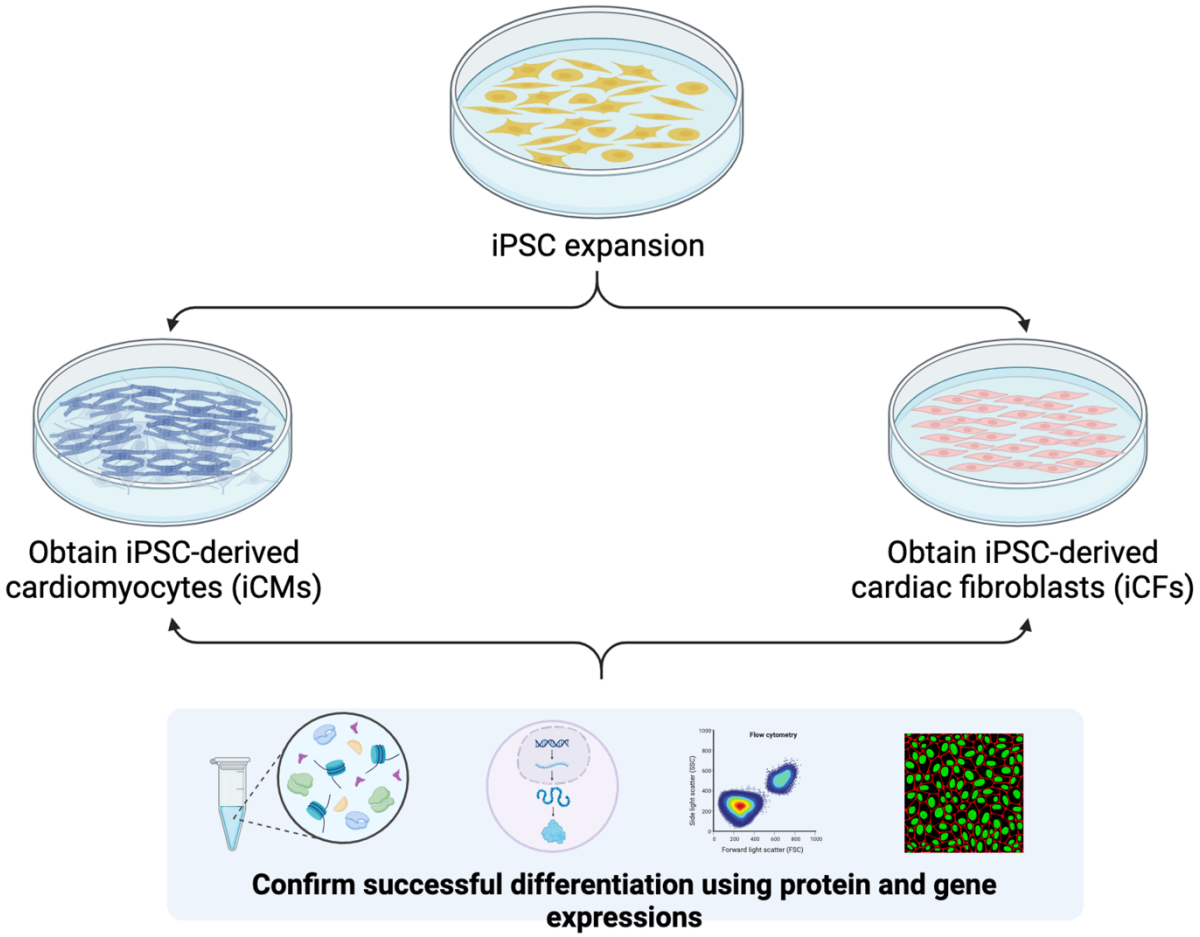

Figure 6.1: Graphical abstract. iPSCs were expanded and differentiated to obtain iCMs and iCFs. The efficacy of the differentiation was assessed using gene and protein expressions, using techniques such as RT-qPCR, flow cytometry and immunofluorescence imaging.

6.3.2. Differentiation of iPSCs to cardiomyocytes

SFCi55 iPSCs and ZGiPSCs were used to derive iCMs, using the GiWi protocol [145]. Briefly, iPSCs were expanded until 95-100% confluency. After screening typically used CHIR99021 concentrations ranging from 4 µM to 12 µM, 10 µM was optimised as the ideal concentration to induce mesodermal specification for SFCi55 iPSCs. Despite this concentration being higher than what is typically reported in literature, 10 µM CHIR99021 yielded the best differentiation. On day 0 of differentiation, RPMI 1640 (Gibco) media containing 2% B-27 minus insulin (Gibco) (RPMI-i) and 10 µM CHIR99021 (Stem Cell Technologies) was added to the iPSCs (Figure 6.2(a)). CHIR99021 containing

media was removed from the cultures after 24 hours and replaced with RPMI-i. On day 3 of the differentiation, RPMI-i was supplemented with 5 mM IWP2 and was added to the cultures, to initiate cardiac mesoderm induction. Another media change was performed on day 5, with RPMI-i and finally, on day 7, cells were treated with RPMI media with complete B-27 (RPMI+i) (Figure 6.2(a)). Media was changed every 3 days and the cells were used for experiments between days 21-30 of differentiation. Success of the differentiation protocol was assessed using flow cytometry (expression of cTnT and MLC2a), RT-qPCR (for expression of cardiac developmental genes such as GATA4, SOX17, TBX5, TBX18 and POSTN) and immunofluorescence imaging (for expression of cTnT, Sarcomeric actinin and connexin43 (Cx43)).

6.3.3. Differentiation of iPSCs to cardiac fibroblasts

SFCi55 iPSCs were used to derive iCFs, using a previously established protocol [147]. The initiation of the differentiation followed similar pathways as iCM differentiation, with mesoderm induction on day 0 using 10 µM CHIR99021. Before 72 hours of mesoderm induction, cells were treated with complete FibroGRO^{TM} media (Sigma-Aldrich) with 75 ng/ml FGF2 (Biotechne). Cells were kept in culture for 20 days and passaged to cell culture treated flasks (T75) or well plates (6 well plates). At 20 days of differentiation, the cells were referred to as iCF progenitors and passaged cells were considered iCFs. iCFs were fed every other day using FibroGRO + 75 ng/ml FGF2 (iCF media). Success of the differentiation was assessed by comparing the genotypic profiles of iCFs with hCFs (expression of cardiac fibroblast specific genes such as TCF21, DDR2 and ACTA2). Since both iCM and iCF differentiations require cardiac mesoderm induction, comparisons were also made between iCFs and iCMs to demonstrate differences in gene and protein expressions.

6.4. Results and discussion

6.4.1. iCMs can be successfully obtained from iPSCs using GiWi protocol

The GiWi protocol was used to differentiate iPSCs to cardiomyocytes (Figure 6.2 (a)). The efficacy and robustness of the differentiation protocol was demonstrated by using both SFCi55 iPSCs and ZGiPSCs (Figure 6.2 (b,c)). Both iPSC lines developed spontaneous beating as early as day 8 of differentiation and stained positive for known cardiomyocyte markers such as cTnT, Cx43 and sarcomeric actinin (Figure 6.2 (d, e and f)). The differentiations were found to be roughly over 75% positive for cTnT (Figure 6.2 (g)) and out of the $cTnT^{+}$ cells, over 90% were positive for MLC2a (Figure 6.2 (h)). In agreement with our findings, Lian *et al.* reports over 85% cells differentiated using GiWi protocol to be positive for cTnT, with about 88% of this population being positive for MLC2a [145]. Additionally, they also report iCMs being positive for cTnT and Sarcomeric actinin with immunofluorescence imaging [145]. Using a similar GSK3/Wnt inhibition approach (using Wnt-C59 instead of IWP2 and a chemically defined media instead of RPMI±i), Burridge *et al.* also reports successful generation of iCMs with over 80% of the cells being cTnT positive and about 80-90% of the cells being positive for MLC2a up to day 30 [316]. Interestingly, multiple methods involving modulation of the GSK3 and Wnt pathways using small-molecule inhibitors unanimously show iCM populations with high cTnT and MLC2a expression [145, 316, 317]. The purity of iCM populations have been shown to further improve with lactate treatment, with over 99% cells expressing cTnT (TNNT2) [318]. It is important to note here that the expression of commonly assessed cardiomyocyte-specific genes such as NKX2.5 have not been evaluated in this study. However, robust spontaneous beating of the cells, together with high cTnT protein expression indicates successful differentiation of iPSCs to cardiomyocytes.

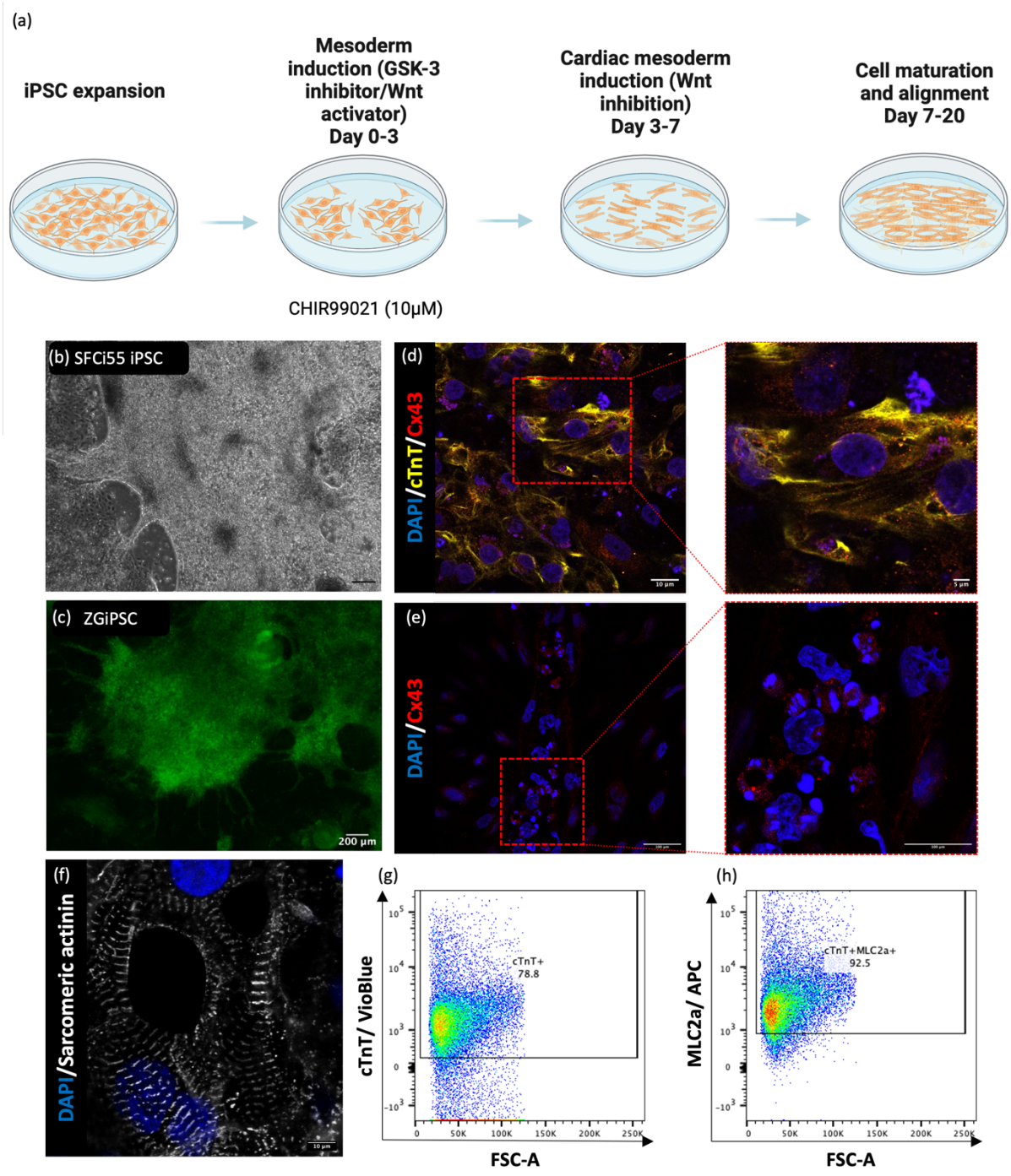

Figure 6.2: Characterisation of iCMs. (a) Schematic representation of the iCM differentiation protocol. (b) Representative image of iCMs obtained from SFCi55 iPSCs. Scale bar – 200 µm. (c) Representative image of iCMs derived using zombie green tagged SFCi55 iPSCs. Scale bar – 200 µm. (d) Representative image of iCMs stained with cTnT and connexin43 (Cx43). Scale bar – 10 µm, magnified image scale bar – 5 µm. (e) Representative image of iCMs stained with connexin43 (Cx43). Scale bar – 100 µm. (f) Representative image of iCMs stained with sarcomeric actinin. Scale bar – 100 µm. (g) Representative flow cytometry plot showing the

percentage of iCM population positive for cTnT. (h) Flow cytometry plot showing the percentage of iCM population positive for cTnT and MLC2a. Flow cytometry analysis performed using FlowJo.

6.4.2. iCFs can be successfully obtained from SFCi55 iPSCs

In murine hearts, approximately 15% of the non-myocyte population has been identified as cardiac fibroblasts [319]. Given their abundance in the myocardium and their role in production and remodelling of extracellular matrix (ECM) [320], we next sought to differentiate iPSCs to cardiac fibroblasts. The differentiation protocol used, followed generation of iCFs via second heart field progenitors, by sequential GSK3 inhibition, followed by FGF2 treatment [147] (Figure 6.3 (a)). In order to confirm cardiac lineage within iCFs and iCF progenitors, a set of cardiac developmental genes were assessed and hCFs were used as positive control. GATA4 and its downstream marker SOX17, which are known markers for cardiac endodermal signalling [321, 322] were found to be highly upregulated in hCFs, unlike iCFs and iCF progenitors (Figure 6.3 (b)). This downregulation in iCFs could be associated with their differentiation being initiated through mesodermal induction, as opposed to endocardial. Similarly, hCFs were found to express 70% more TBX18 than iCFs (Figure 6.3 (b)). In mammalian hearts, cardiac fibroblasts arise from three distinct locations – epicardium, endocardium and from neural crest progenitors [323]. iPSC-derived epicardial cells show a strong expression of TBX18 as demonstrated by previous work from Witty *et al.* [159]. Additionally, upregulation of TBX18 in hCFs has also been previously reported [162]. In this study, although iCFs express TBX18, we report a downregulation in the expression in comparison to hCFs (Figure 6.3 (b)), as the iCF differentiation protocol in this study does not involve the induction of epicardial progenitors, and in turn uses a second heart field progenitor based approach. Furthermore POSTN, a gene highly expressed in adult hCFs [324], was also found to be expressed in iCFs, although 80% less than hCFs, exactly in agreement with the results reported by Zhang *et al*. [147] highlighting similarities

between foetal cardiac fibroblasts and iCFs. Finally, iCFs and hCFs were found to express comparable levels of TBX5, a key marker for early cardiac lineage [325].

On assessing a set of cardiac fibroblast-specific genes, iCFs were found to express 90% less TCF21 than hCFs (Figure 6.3 (c)). Similar to TBX18, TCF21 is another key gene for epicardial cells [326] and the downregulation in this gene expression might also be due to the pathway through which iCFs are induced in this work (using second heart field progenitors). Previous studies suggests that endocardial cells are generated in part from the second heart field progenitors [327], supporting the downregulation in epicardial lineage markers. Additionally, it is worth noting that POSTN upregulation has been associated with myocardial infarction, myocarditis, calcification and pro-fibrotic TGFβ signalling [324]. Similarly, upregulation of TBX18 and TCF21 have been associated with cardiac fibroblast activation and disease progression [328, 329]. Given that the human tissue samples used to derive hCFs were obtained from patients undergoing heart transplants, the upregulation of these genes in hCFs could be linked to underlying health conditions within the patients.

Other markers notably highly expressed in hCFs include DDR2 and ACTA2, which were both found to be expressed in comparable levels between iCFs and hCFs (Figure 6.3 (c)), demonstrating the similarities of iCFs to their primary counterparts. Finally, CD90, a common marker used to identify cardiac fibroblasts (although not specific to fibroblasts in the heart) [330] was found to be highly upregulated in iCFs, in comparison to iCF progenitors (Figure 6.3 (d)). Zhang *et al.* reports high CD90 expression in iCFs at early passages (80-90%) and a steady drop in the expression at later passages [147]. We report a similar trend, with the iCFs analysed in this study being of early passages (P1 and P2). Phenotypically, iCFs were found to be large and elongated as demonstrated by phalloidin staining (Figure 6.3 (e)), consistent with previous findings [147].

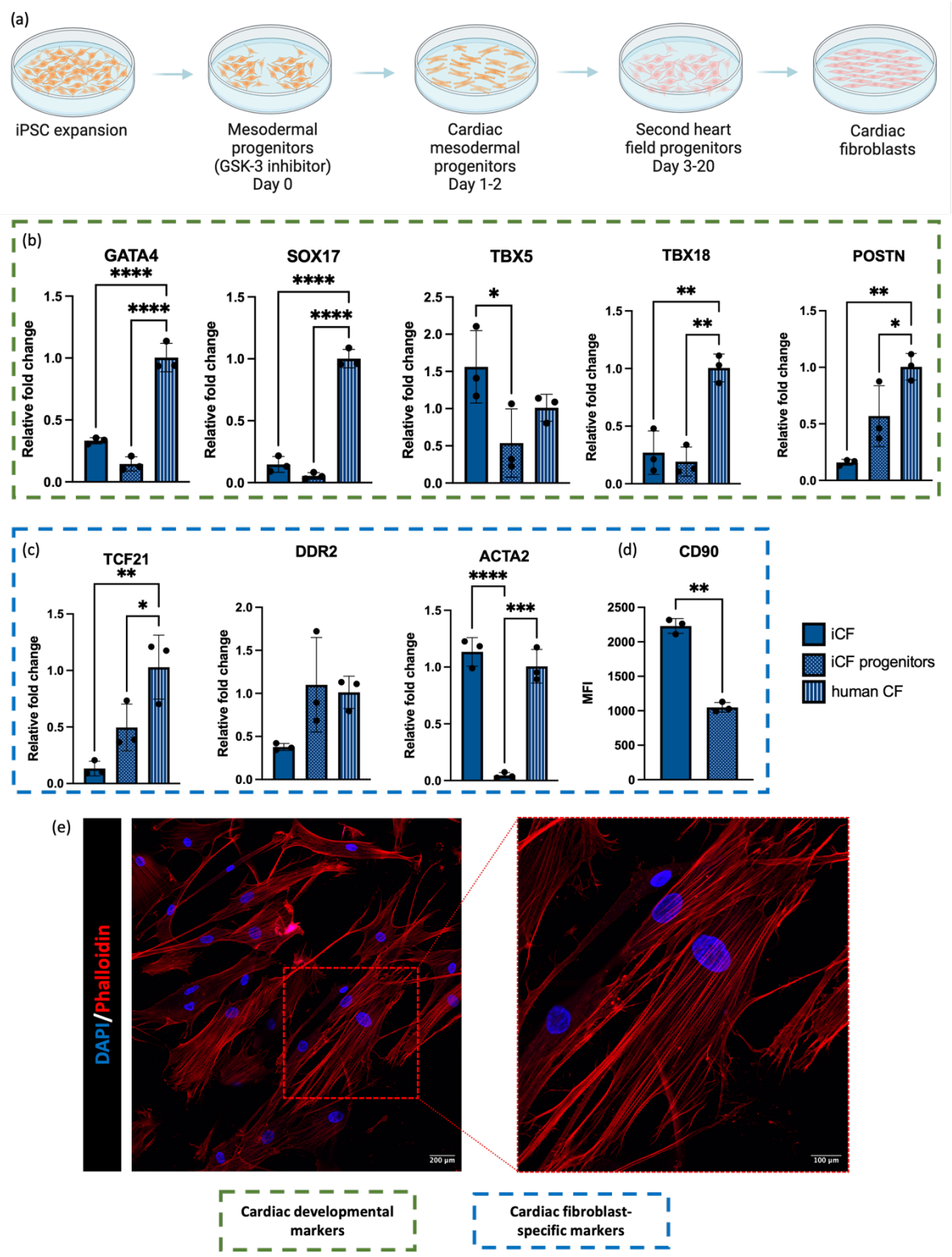

Figure 6.3: Characterisation of iCFs. (a) Schematic representation of the iCF differentiation protocol. (b) Expression of a set of cardiac developmental genes. (c) Expression of a set of cardiac fibroblast-specific genes. (d) Mean fluorescence intensity of CD90 expression, quantified

using flow cytometry. (e) Representative image of iCFs stained with DAPI and phalloidin. Scale bar – 200 µm, magnified image scale bar – 100 µm. Statistical analysis - One Way ANOVA. * represents P<0.05, ** represents P<0.01, *** represents P<0.001 and **** represents P<0.0001. N = 3 (biological replicates), with each point signifying the average of 3 technical replicates. Fold change of mRNA relative to primary human cardiac fibroblasts.

6.4.3. iCMs and iCFs express cardiac developmental markers

The protocols used for generating iCMs and iCFs follow the exact same mesodermal induction step, after which the iCM differentiation specialises on to cardiac progenitor development [145] while the iCF differentiation moves towards second heart field progenitor development [147]. In order to highlight the differences between iCMs and iCFs, we first sought to compare the expression of a set of cardiac developmental genes. iCMs and iCFs expressed comparable levels of SOX17, TBX18 and POSTN (Figure 6.4 (a)), highlighting a shared cardiac lineage. The expression of TBX5 was found to be upregulated in iCMs in comparison to iCFs (Figure 6.4 (a)), consistent with previous findings [147], owing to the fact that the iCM differentiation protocol (GiWi protocol) promotes the expression of transcription factors associated with first heart field progenitors [331]. We also report an upregulation of GATA4 expression in iCFs in comparison to iCMs (Figure 6.4 (a)), contrary to what is documented in literature [147, 162]. The iCMs used in this study were not purified or FACS sorted to obtain pure iCM populations. Hence, the downregulation of GATA4 could be associated with the presence of 10-20% undifferentiated and non-beating cells in the iCM population. Previous studies show that the non-beating cells in iCM cultures are fibroblasts or smooth muscle cells [157]. Due to the likely presence of fibroblasts in the culture, in addition to a stronger epicardial lineage [328], we report iCMs expressing almost three-fold greater expression of TCF21 (Figure 6.4 (b)). However, on examining the expression of other genes specific to cardiac fibroblasts, such as DDR2 and ACTA2, iCFs were found to show a high upregulation (Figure.6.4 (b)).

Under a phase contrast microscope, iCM and iCF cultures, prior to replating, look very similar (Figure 6.4 (c)) with large patches of cells. However, the differences in the protein

expression of iCMs and iCFs was highlighted with immunofluorescence imaging, showing iCMs staining positive for cTnT and Sarcomeric actinin, unlike iCFs (Figure 6.4 (c)). Taken together, these results demonstrate that iCMs and iCFs express cardiac developmental markers, while being functionally different.

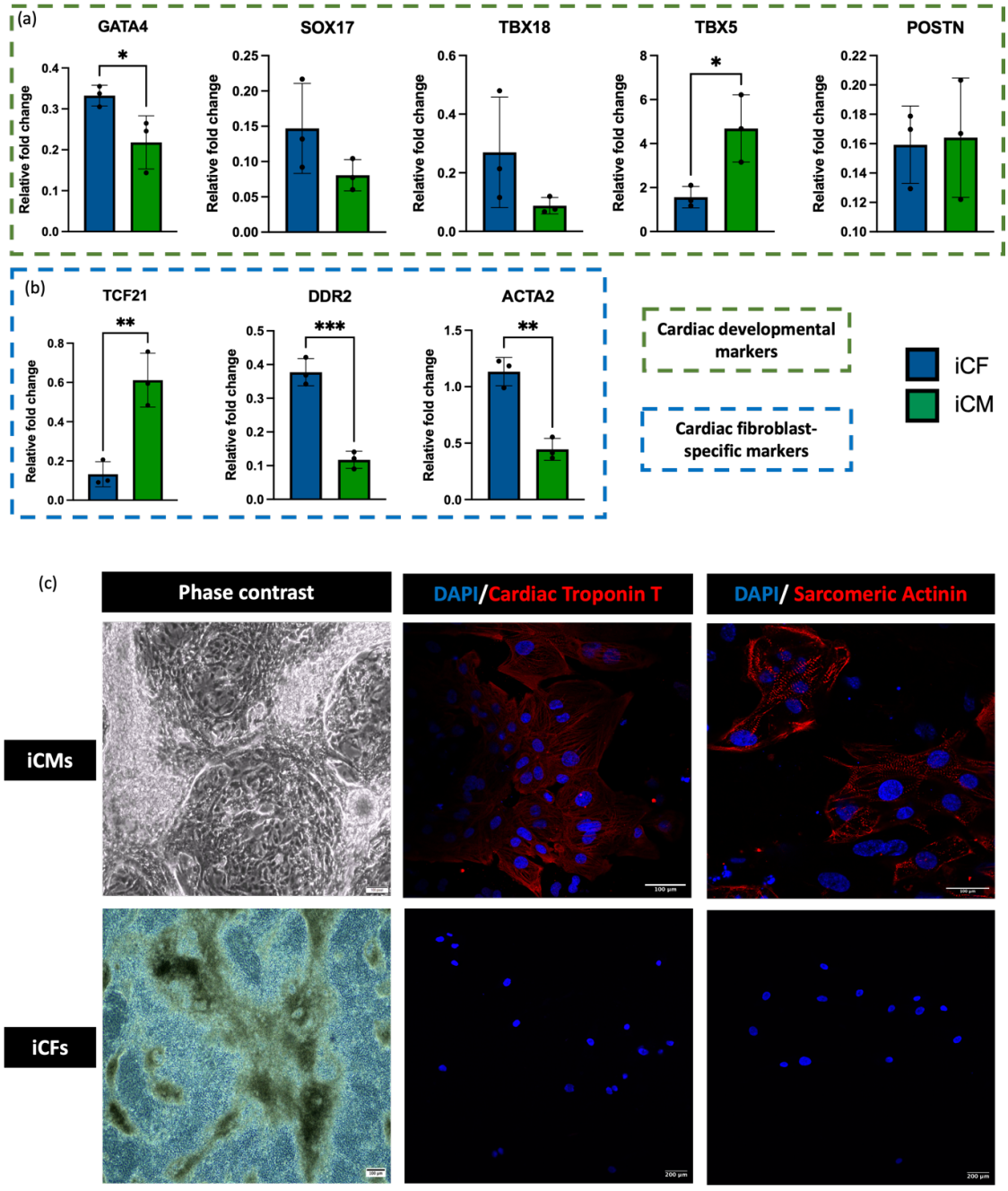

Figure 6.4: Comparison between iCMs and iCFs. (a) Expression of a set of cardiac developmental genes. (b) Expression of a set of cardiac fibroblast-specific genes. (c) Representative images of iCMs and iCFs using phase contrast microscopy (scale bar – 100 µm), stained with cTnT (iCM scale bar – 100 µm, iCF scale bar – 200 µm) and stained with sarcomeric actinin (iCM scale bar

– 100 µm, iCF scale bar – 200 µm). Statistical analysis - Student T test with Welch's correction. * represents P<0.05, ** represents P<0.01 and *** represents P<0.001. N = 3 (biological replicates), with each point signifying the average of 3 technical replicates. Fold change of mRNA relative to primary human cardiac fibroblasts.

6.5. Conclusion

The findings presented in this study hold significant promise for advancing the field of regenerative medicine and cardiac tissue engineering, highlighting the reproducibility of two differentiation protocols – one to derive cardiomyocytes and the other to derive cardiac fibroblasts from iPSCs. The successful differentiation of iPSCs into cardiomyocytes (iCMs) using the GiWi protocol underscores its potential as a reliable and robust method for generating cardiac cells for *in vitro* drug screening and potentially therapeutic applications. The early onset (day 8) of spontaneous beating observed in both SFCi55 iPSCs and ZGiPSCs, coupled with positive staining for well-established cardiomyocyte markers such as cTnT, Sarcomeric actinin, connexin43 and MLC2a holds great promise in using iPSCs as an efficient tool for generating functional cardiac cells.

The successful derivation of cardiac fibroblasts (iCFs) from iPSCs using a sequential GSK3 inhibition and FGF2 treatment approach is equally significant. The identified markers, such as DDR2, ACTA2 and CD90, in iCFs point towards their phenotypic similarity to primary hCFs. The demonstrated similarities between iCFs and hCFs, particularly in the expression of genes associated with cardiac fibrosis and remodeling, provide a valuable tool for studying the underlying mechanisms of these processes. This knowledge has the potential to lead to the identification of novel therapeutic targets for conditions such as myocardial infarction and heart failure.

The comparative analysis between iCMs and iCFs, although revealing shared cardiac lineage markers, also highlighted key differences in gene expression profiles. The upregulation of GATA4 in iCFs and TCF21 in iCMs serve as indicators of the presence of non-cardiomyocyte cells in the cultures. This underscores the importance of refining

purification methods such as lactate selection [318] for obtaining highly enriched populations of cardiomyocytes.

Looking ahead, the established protocols for generating iCMs and iCFs will serve as foundational knowledge for further refining and optimising differentiation methods. This, in turn, could serve as a platform for facilitating the production of other functional cardiac cells, such as cardiac resident macrophages and cardiac endothelial cells, addressing a critical bottleneck in the development of key cell types involved in cardiovascular diseases. In the broader context of tissue engineering and regenerative medicine, this also opens avenues for the development of more complex, multi-cellular tissue constructs, potentially mimicking the native cardiac microenvironment more closely. Such tissue engineered constructs could be utilised as *in vitro* models for drug screening and disease modelling, ultimately advancing our understanding of cardiac biology and pathology. By validating robust protocols and providing insights into the gene expression profiles of differentiated cells, this work lays a solid foundation for further advancements in generating multi-cellular *in vitro* cardiac models, which is the focus of the next chapters.

Chapter 7 Conditioning a cardiac resident macrophage phenotype in iMacs by performing co-cultures with iCMs

7.1. Abstract

The field of cardiac immunology has witnessed increased attention due to the discovery of pivotal interactions between cardiomyocytes and macrophages, particularly cardiac resident macrophages (CRMs), in maintaining myocardial homeostasis. However, most insights into CRM biology originate from murine models, leaving gaps in our understanding of human CRMs. To address this, *in vitro* cultures offer a valuable approach. This chapter aims to elucidate the interactions between cardiomyocytes (iCMs) and macrophages (iMacs) derived from the same iPSC parent line (SFCi55) to simulate a cardiac microenvironment *in vitro*. In order to simulate a cardiac microenvironment *in vitro*, iMacs were either cultured for 7 days in iCM-conditioned media (iMacs_CM) or co-cultured with iCMs (iMacs_co-culture). Interestingly, while both iMacs_CM and iMacs_co-culture revealed TRM-like phenotype in terms of gene expression, iMacs in co-culture with iCMs demonstrated remarkable quiescence, suppressed inflammatory responses and high upregulation in genes such as GJA1 and AREG, more akin to CRMs. Additionally, iMacs in co-culture with iCMs also expressed CRM (TIMD4, LYVE1 and FLOR2) and cardiac developmental (GATA4, TBX18 and TBX5) genes. Furthermore, investigation of phenotypic and functional changes in iCMs in co-culture with iMacs revealed enhanced maturation, improved calcium handling, and synchronised beating patterns. Drug response assays further validated the maturity and functionality of iCMs in the presence of iMacs, achieving physiologically relevant beat rates. Overall, this study underscores the potential of iMacs in co-culture with iCMs, to enhance the maturation and functionality of both iMacs and iCMs. These findings contribute valuable insights into the complex interplay between these cell types, laying the groundwork for further investigations in cardiac regenerative medicine and tissue engineering.

7.2. Introduction

Phagocytes were identified in the late nineteenth century by Élie Metchnikoff (1892) where he described two populations, macrophages (large eaters) and microphages (small eaters, later known as polymorphonuclear leukocytes) [332]. The understanding of phagocytes and their functions evolved further in the early twentieth century with studies carried out by Ludwig Aschoff, leading to further appreciation of the role of macrophages even in the absence of inflammation [333]. However, for a large period of this scientific field, macrophages were predominantly viewed as immune cells specialising in phagocytosis, and assigned a limited role in the broader landscape of physiological functions [334]. The past few decades have witnessed a transformative shift in our understanding of these immune cells, revealing their remarkable versatility and multifaceted functions within the human body [335]. The functional repertoire of macrophages not only includes engulfing pathogens and removing damaged, senescent, or apoptotic cells, but also include their ability to respond to various stimuli in order to polarise to a “classically activated” (or pro-inflammatory) and “alternatively activated” (or anti-inflammatory) state [336].

Although various macrophage populations had been recognised in different tissues (Kupffer cells in the liver [337, 338], microglia in the brain [339] etc.), for almost half a century the prevailing view in the literature has been that tissue macrophages in health and disease originate from circulating monocytes [340]. However, evidence from lineage tracing, cell tracking and parabiosis studies in mice and, to a lesser extent in humans, challenges this long held view [82, 341-343]. This paradigm shift has been accentuated by the realisation that macrophages have distinct origins and can be classified into embryo-derived resident macrophages (TRMs) and recruited monocyte-derived macrophages (BDMs) [344]. TRMs populate diverse tissues where they execute tissue-specific functions crucial for maintaining homeostasis [345]. For example, microglia are critical for synaptic pruning in the brain [346], Kupffer cells perform iron recycling in the liver, helping adapt to fluctuations in erythrocyte integrity [347] and alveolar macrophages clear surfactants in the lungs [348]. Unlike the brain that exclusively hosts yolk-sac derived microglia, the heart contains distinct macrophage populations with mixed ontological origins [90]. Initial characterisations describe two

key macrophage populations in the heart; CCR2^{-}HLA-DR^{high} macrophages which are largely derived from embryonic progenitors with minimal contributions from circulating monocytes, and CCR2^{+}HLA-DR^{high} macrophages that are derived and replenished entirely from circulating monocytes [106]. CCR2^{-}HLA-DR^{high} macrophages are the resident macrophages of the heart (cardiac resident macrophages; CRMs). However, according to most recent findings, CRMs in mice are TLF^{+}, expressing TIMD4 and/or LYVE1 and/or FOLR2, and are maintained through self-renewal with minimal monocyte input [64].

Despite constituting a relatively small fraction of the total cell population, CRMs are the most abundant immune cell type in the myocardium [59], involved in governing a myriad of cellular processes. Aurora *et al.*, using a macrophage/monocyte depleted mouse model showed that CRMs are critical for neonatal heart regeneration and efficient neo-angiogenesis [349]. Furthermore, Hulsmans *et al.* showed that CRMs play a crucial role in facilitating electrical conduction, by coupling with cardiomyocytes through connexin43 gap junctions, in both humans and mice [21]. Helping deepen our insight into the functions of CRMs, Nicolás-Ávila *et al.* reported that CRMs capture and eliminate vesicles released by cardiomyocytes under stress, termed “exophers”, through Mertk receptors, maintaining homeostasis within the myocardium [22]. These critical functions, in addition to routine immunosurveillance, underline CRMs as a key cell type in the healthy myocardium.

Moreover, CRMs have also been found to be pivotal contributors in the mitigation and progression of several cardiac impairments [114]. Myocardial infarction (MI) is a common cardiac disease, resulting from a decreased or complete cessation of blood flow to a portion of the myocardium [2]. The area of the myocardium that is affected by MI is severely deprived of oxygen, which in turn leads to tissue necrosis and in severe cases, chronic heart failure and death [115]. During the onset of MI, an acute emergency myelopoiesis is triggered in the bone marrow, which in turn causes sequential recruitment of neutrophils and monocytes to the myocardium, initiating a sequence of inflammatory responses and clearance of necrotic debris [350, 351]. Following the resolution of acute inflammation, a fibrotic scar tissue replaces the necrotic area, serving as a protective measure against wall rupture [116]. Some of the recruited

monocytes undergo differentiation into macrophages, thereby modifying the composition of the cardiac myeloid population [116]. Interestingly, multiple previous studies (performed in mice) show that both an excessive numerical expansion as well as non-selective depletion of macrophages intensifies tissue injury post-MI, underscoring the distinct and non-overlapping functions of macrophage subsets in the myocardium [125, 352, 353]. CRMs within the infarcted zone experience acute loss post-MI, while those in the remote zone, situated away from the infarct, undergo a proliferative burst [102]. Additionally, studies performing selective elimination of CRMs report restricted cardiac repair, adverse remodelling and dysfunction, highlighting the cardioprotective role of CRMs in ischemic injury primarily localised to peri-infarcted and remote zones [102, 104, 105]. Myocarditis is another cardiac impairment, which causes inflammation in the cardiac muscle and can occur due to viral infections, autoimmunity, drug toxicity, or even sudden emotional/physiological stress [137]. Post-myocarditis, the number of macrophages derived from circulating monocytes increase dramatically in the heart, aggravating the inflammatory response by recruiting lymphocytes [138]. A similar response is seen in isoproterenol-induced cardiomyopathy as well [139]. CRMs are numerically reduced in both viral and doxorubicin-induced cardiomyopathy, with poor numerical recovery in the long term [140]. However, the residual CRMs in doxorubicin-induced cardiomyopathy undergo proliferation to mitigate myocarditis; nevertheless, the specific mechanism facilitating this process remains to be fully comprehended [140]. More recent studies also illustrate the role of a specialised TREM2^{high} CRM population that can prevent sepsis-induced cardiomyopathy [141]. Furthermore, Revelo *et al.* recently reported the impressive ability of CRMs to prevent fibrosis and facilitate angiogenesis in response to cardiac pressure overload induced by transverse aortic constriction [142]. Taken together, these studies highlight the cardioprotective role played by CRMs in various injury models, emphasising their importance in the myocardium.

In the past decade, although we have significantly improved our understanding of CRM biology and function, further refinement of our knowledge requires efficient and reliable *in vitro* culture set up to study CRMs. In an attempt to explore TRM function *in vitro*, a number of cell culture protocols have been developed in the past. Thus far, many

studies have relied on BDMs, which do not reflect TRM heterogeneity [354, 355]. Additional strategies include immortalised cell lines [356, 357], which are also a poor representation of TRMs, in addition to commonly exhibiting an activated phenotype [358]. With most TRMs being rare and difficult to isolate, iPSC-derived macrophages (iMacs) offer an exciting prospect [203], with demonstrated potential to be able to differentiate into TRMs such as microglia [213, 359]. Although the induction of CRMs through the activation of a transcriptional factor has not been successfully achieved yet, some promising previous studies show derivation of microglia by performing a co-culture of iMacs with neural cells [193], as well as derivation of Kupffer cells by treating iMacs with hepatocyte conditioned media and also by performing co-cultures of iMacs and hepatocytes [202]. Using a similar approach, the potential of obtaining CRMs *in vitro* using cardiac cues, is yet to be explored.

Having demonstrated the quiescent nature of iMacs and their expression of TRM-related markers in Chapter 5, in this chapter the response of iMacs to a cardiac-mimicking environment was assessed. In order to understand the *in vitro* interactions between cardiomyocytes and embryonic-like macrophages, iCMs and iMacs from the same iPSC parent line were used. The response of iMacs to an *in vitro* cardiac environment was determined, by exposing iMacs to iCM conditioned media and by performing co-cultures of iCMs and iMacs. The phenotypic and genotypic profiles of iMacs in the *in vitro* cardiac environment was assessed to evaluate potential reconfiguration of iMacs to a CRM-like phenotype. Finally, the response of iCMs to the presence of iMacs was analysed, to determine improvement in iCM maturity and function.

7.3. Materials and Methods

7.3.1. Experimental design

SFCi55 iPSCs were used to generate iCMs (as described in Chapter 6, subsection 6.2.2) and zombie green tagged SCFi55 (ZGiPSCs) were used to generate iMacs (as described in Chapter 5, subsection 5.2.2). The response of iMacs to a cardiac environment was assessed using two approaches - treating iMacs with iCM conditioned media and by

performing co-cultures of iCMs and iMacs (Figure 7.1). For iCM conditioned media studies, pre-macs were collected and plated at the desired density (described in section 7.2.2), with 1:1 ratio of iMac media and iCM conditioned media supplemented with 100 ng/ml M-CSF. iMacs treated with iCM conditioned media (iMacs_CM) were kept in culture for 7 days with one media change on day 3 of culture. For co-culture studies, iCMs were replated (described in section 7.2.3) and iMacs were added to previously attached iCM cultures. Co-cultures were treated with RPMI+i supplemented with 100 ng/ml M-CSF and kept in culture for 7 days (iMacs_co-culture).

iMacs_CM were assessed for their expression of CRM markers such as CD14, HLA-DR, CCR2 and CX3CR1 using flow cytometry. The functional ability of iMacs_CM was analysed by performing a phagocytosis assay where iMacs_CM were treated with zymosan particles and the particle uptake was quantified using a flow cytometer (detailed protocol in section 5.2.5). Additionally, the polarisation potential of iMacs_CM was also evaluated by treating iMacs_CM with LPS, a known pro-inflammatory factor (detailed protocol in section 5.2.4). Activation of iMacs_CM to a pro-inflammatory state was confirmed by performing ELISA on the secretome, for cytokines such as TNFα, IL6 and IL10. Finally, the expression of other CRM-specific markers such as connexin43 and CRR2 were assessed using immunofluorescence imaging (Figure 7.1).

Co-cultures of iMacs and iCMs were first assessed to confirm successful incorporation of iMacs into iCM cultures. Subsequently, to verify no potential pro-inflammatory effect in iMacs with conditioned media treatment or co-culture with iCMs, ELISAs were performed on secretome from iMacs_CM and iMacs_co-culture, to quantify the presence of cytokines such as TNFα, IL6 and IL10. iMacs_CM and iMacs_co-culture were assessed for the expression of a set of pro-regenerative (TGFB1, MRC1, IL10), pro-inflammatory (TNF, IFNG, NOS2) and functional (MMP9, CCR2, VEGFA, TRPV4, AREG and GJA1) genes, in addition to a set of CRM-specific (TIMD4, TBPL1, FOLR2, LYVE1 and MERTK) and cardiac developmental (GATA4, TBX18 and TBX5) genes (Figure 7.1). As deemed suitable, untreated iMacs or BDMs were used as control in all the studies.

The response of iCMs to the presence of iMacs, was another significant point of interest. Phenotypic changes in iCMs when co-cultured with iMacs was characterised by performing immunofluorescence imaging for cardiac troponin T (cTnT), which stains the

thin filaments of striated muscles. Immunofluorescence imaging was also performed for Sarcomeric actinin and the distance between the sarcomeres were measured as a readout for iCM maturity. Human atrial and ventricular tissue samples were used as controls for sarcomere length measurements. The expression of genes such as TNNT2, MYH6, MYH7 and SERCA2 were also used to evaluate improvement of iCM maturity in co-culture with iMacs. Finally, the beating rate as well as the response of iCMs and iCMs in co-culture with iMacs to drugs such as carbachol, isoproterenol and caffeine was quantified using calcium imaging (Figure 7.1).

7.3.2. iMacs treated with iCM conditioned media

For regular iMac culture, pre-macs (non-adherent cells released by EBs from day 14 of the initiation of haematopoiesis) were collected and plated at a density of 500,000 cells per well of a 6-well plate and cultured in X-VIVO media, supplemented with 100 ng/ml M-CSF, 1% Glutamax and 2% penicillin/streptomycin (iMac media) for 7 days. Conditioned media was collected from iCMs between day 20 and 30 of culture and centrifuged at 650 G, to remove dead cells and debris, before storing at -80 °C. For iCM conditioned media studies, pre-macs were collected and plated at a density of 500,000 cells per well of a 6-well plate or 100,000 cells per well of a 24-well plate, and cultured with 1:1 ratio of iMac media and iCM conditioned media supplemented with 100 ng/ml M-CSF. Media change was performed at day 3 of the culture and iMacs_CM were used for experiments at day 7 of culture. For immunofluorescence imaging with iCM conditioned media treatment, pre-macs were plated at a density of 500,000 cells per well of a 35mm μ-dish (IBIDI®) and cultured with 1:1 ratio of iMac media and iCM conditioned media supplemented with 100 ng/ml M-CSF. BDMs or untreated iMacs were used as controls and were cultured at the same cell density as iMacs_CM. BDMs were cultured in RPMI media with 50 ng/ml M-CSF, 10% FBS and 2% pen/strep (BDM media).

7.3.3. Co-culture of iMacs and iCMs

For performing co-cultures of iMacs and iCMs, iCMs were differentiated and cultured for up to 20 days before replating them at a density of 200,000 cells/cm^2, on Matrigel™ coated plates. Replated iCMs were allowed to attach for 48 hours before adding pre-macs to the cultures, at a 5:1 ratio of iCMs to iMacs. Co-cultures of iCMs and iMacs were cultured in RPMI+i (RPMI media with 2% B27™ and 2% pen/strep) supplemented with 100 ng/ml M-CSF. Cells were kept in culture for 7 days before performing experiments and a complete media change was performed at day 3. On day 7 of co-culture, cells were lifted from the plates by incubating them with 0.25% Trypsin-EDTA solution (Thermo Fisher Scientific) at 37 °C for 9 minutes. The lifted cell suspension was centrifuged at 300 G for 5 minutes, followed by resuspension in FACS sorting buffer (Ca/Mg^{2+} free PBS with 2.5 mM EDTA, 25 mM HEPES, 1% heat inactivated FBS and 1% pen/strep). Since iMacs were generated using ZGiPSCs and iCMs were generated using SFCi55 iPSCs, the resuspended cells were FACS sorted. Positive sorting was done for cells expressing zombie green (iMacs) and the flow through cells collected as iCMs. FACS sorted iMacs and iCMs were lysed using Trizol™, to perform RT-qPCR.

For calcium handling studies, iCMs were differentiated and cultured for up to 25 or 65 days. On day 25 or day 65, pre-macs were added to the iCM cultures at 5:1 ratio of iCMs to iMacs and cultured in RPMI+i media supplemented with 100 ng/ml M-CSF. Calcium imaging was performed by loading the samples with Cal-520® AM (detailed protocol in Chapter 3, subsection 3.8). Measurements were made using an epifluorescent microscope with a stage top live imaging chamber (Olympus Life Science).

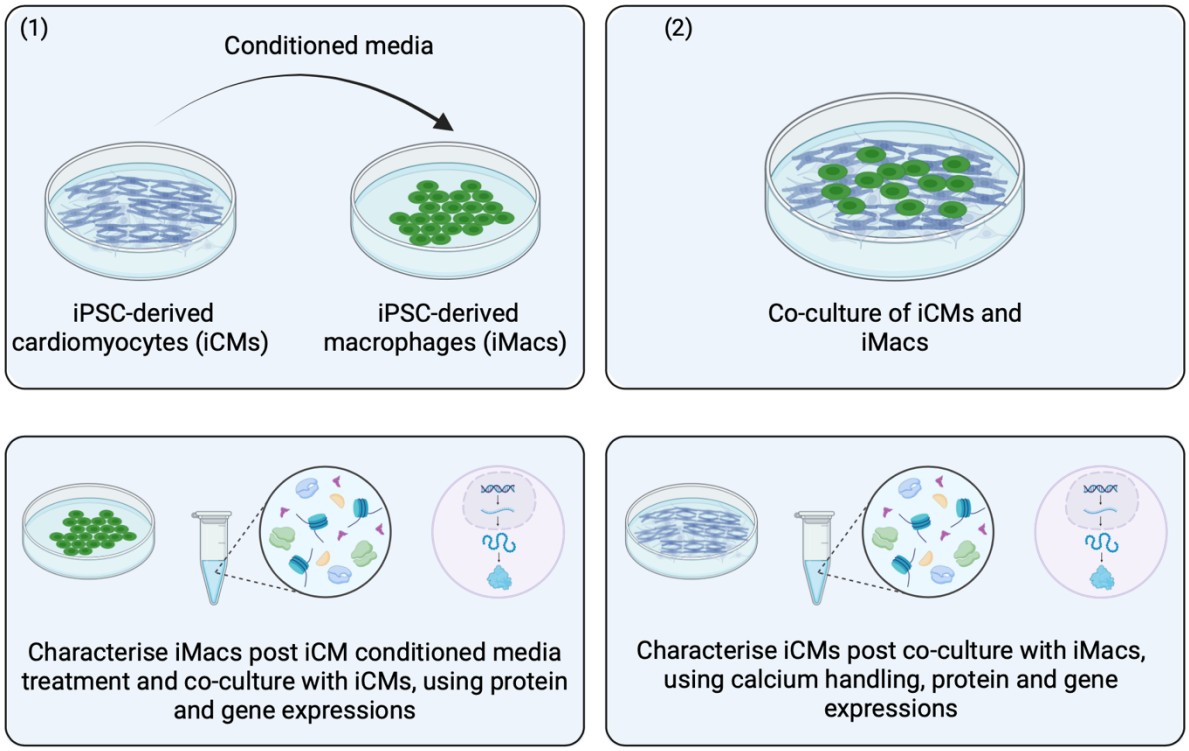

Figure 7.1: Graphical abstract. iPSCs were expanded and differentiated to obtain iCMs and iMacs. In order to provide iMacs with cardiac cues, two approaches were used. In approach (1), iMacs were cultured for 7 days in conditioned media and in approach (2), a co-culture of iCMs and iMacs were performed. The gene and protein expressions of both iMacs and iCMs were individually characterised, using techniques such as RT-qPCR, flow cytometry, immunofluorescence imaging and calcium imaging.

7.4. Results and discussion

7.4.1. iMacs are functionally active, with a differential protein expression profile upon culture with iCM conditioned media

The first form of cardiac cue provided to iMacs, was conditioned media from iCMs (Figure 7.2 (a)). Using BDMs and untreated iMacs as control, the expression of a number of macrophage cell surface markers was assessed, in iCM conditioned media treated iMacs (iMacs_CM). CD14 is a glycosylphosphatidylinositol-anchored TLR4 co-receptor, which is preferentially expressed on human monocytes and macrophages [360].

Reportedly, all cardiac macrophages abundantly express CD14 [106], and hence, the flow cytometry analysis performed in this study followed a similar gating strategy to previous work by Bajpai *et al.* [106], primarily gating for cell populations expressing CD14. In comparison to BDMs, iMacs and iMacs_CM expressed almost 41% more CD14 (Figure 7.2 (b)), highlighting a phenotype more akin to TRMs [361]. On examining the $CD14^{high}$ population of cells, 0% of the BDMs were negative for CCR2 (100% positive for CCR2), while almost 68% iMacs were negative (Figure 7.2 (c)), as reported in Chapter 5, subsection 5.5. Interestingly, iCM conditioned media treatment was found to increase the $CD14^{high}CCR2^{high}$ population by 67%, compared to iMacs (Figure 7.2 (c, d)). CCR2 upregulation is typically linked to chemotactic and migratory responses in macrophages [362]. Since CRMs are known to be $CCR2^{-}$ with high CD14 expression [106], further evaluation of iMacs_CM was performed on the $CD14^{high}CCR2^{low}$ cell populations. The expression of CX3CR1 was found to be significantly upregulated in $CD14^{high}CCR2^{low}$ iMacs_CM by almost 60% in comparison to iMacs (Figure 7.2 (e)). This finding is of particular interest, as Pinto *et al.* previously demonstrated the abundance of CX3CR1 expression in murine CRMs, using a $CX3CR1^{GFP/+}$ knock-in mouse model [363]. Additionally, Molawi *et al.* has also reported an abundance of CX3CR1 expression in CRMs found in murine heart, which eventually differentiated into $MHCII^{+}$ and $MHCII^{-}$ cells [364]. Through fate mapping studies, Molawi *et al.* identified that almost the entirety of the CRM population in new-born mice were $CX3CR1^{+}MHCII^{-}$, which over the span of 30 weeks, significantly drops down to 20% of the cardiac macrophage population [364]. Interestingly, their findings suggest that all adult cardiac macrophage populations must have developed from a $CX3CR1^{+}$ stage. Additionally, the expression of HLA-DR, the human equivalent to MHCII, was found to be 25% downregulated in iMacs_CM in comparison to iMacs (Figure 7.2 (f)).

The functional activity of iMacs_CM was validated by performing a phagocytosis assay. In comparison to iMacs, iMacs_CM showed comparable phagocytic potential (61%, compared to 62% by iMacs) (Figure 7.2 (g)). Similarly, iMacs_CM were also stimulated with LPS, to demonstrate their ability to be classically activated. Quantification of cytokine release revealed that untreated iMacs and iMacs_CM produced comparable amounts of TNFα, IL6 and IL10 (Figure 7.2 (h, i and j)). Notably, the response of

iMacs_CM to LPS treatment was found to highly supressed in comparison to LPS treated iMacs, with a 97% downregulation in IL6 release, 91% downregulation in TNFα release and 95% downregulation in IL10 release (Figure 7.2 (h, i and j)).

Further functional assessment was performed on iMacs_CM (Figure 7.3 (a)) using immunofluorescence imaging. Both iMacs and iMacs_CM expressed Cx43, with iMacs_CM displaying a 35% upregulation in the expression (Figure 7.3 (b, c)). The upregulation in the CCR2 expression in iMacs_CM that was revealed through flow cytometry (Figure 7.2 (c, d)) was further confirmed using immunofluorescence imaging. In line with earlier observations, iMacs stained negative for CCR2, while BDMs and iMacs_CM were found to express comparable levels (Figure 7.3 (d, e)).

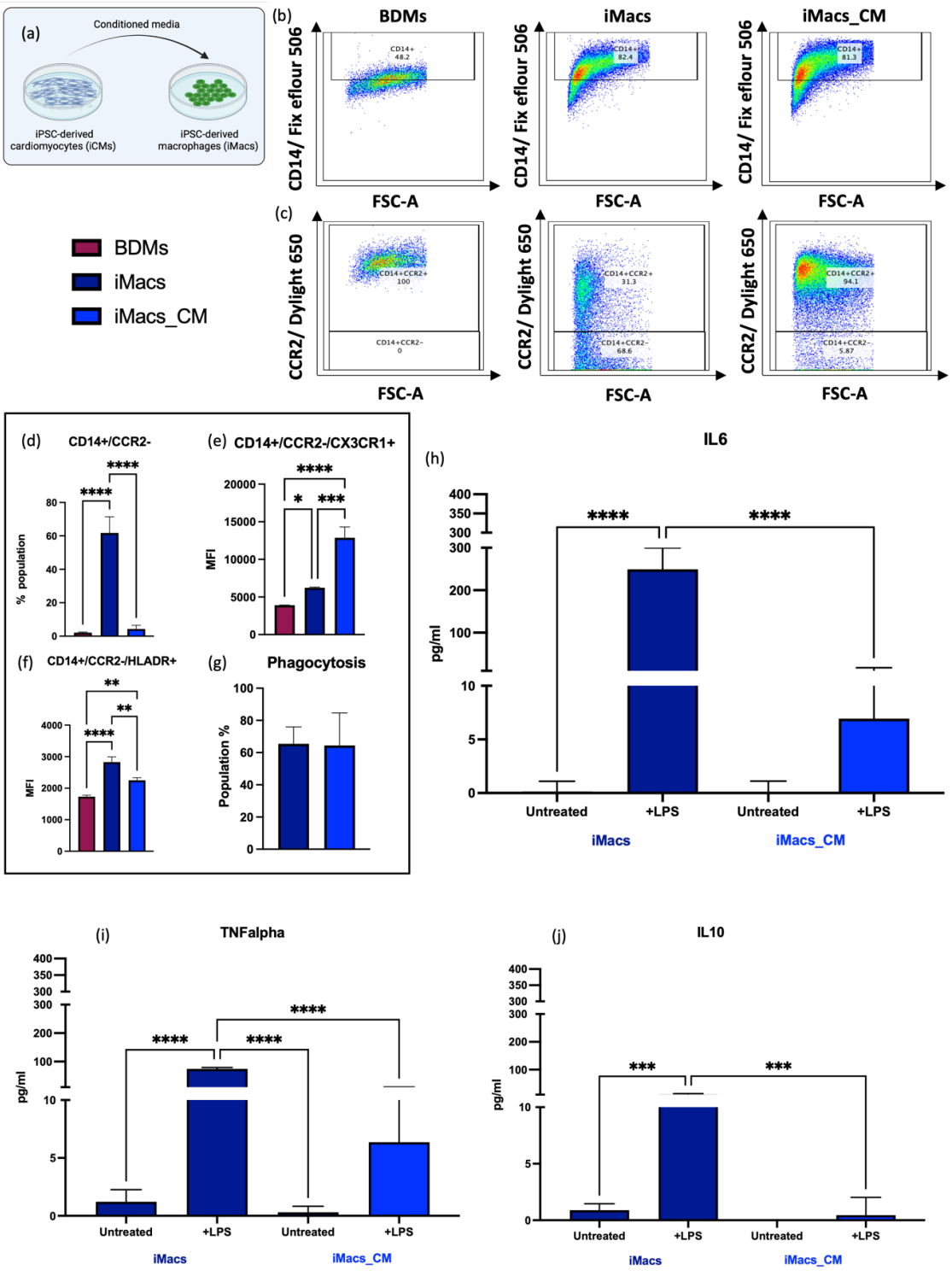

Figure 7.2: Characterisation of iCM conditioned media treated iMacs (iMacs_CM). (a) Schematic representation of the experimental set up. (b) Representative flow cytometry plots showing CD14 expression in BDMs, iMacs and iMacs_CM. (c) Representative flow cytometry plots showing CCR2 expression in $CD14^{high}$ BDMs, iMacs and iMacs_CM. (d) Quantification of $CD14^{high}CCR2^{low}$ populations of BDMs, iMacs and iMacs_CM. (e) Quantification of

$CD14^{high}CCR2^{low}CX3CR1^{high}$ populations of BDMs, iMacs and iMacs_CM. (f) Quantification of $CD14^{high}CCR2^{low}HLA\text{-}DR^{high}$ populations of BDMs, iMacs and iMacs_CM. (g) Quantification of phagocytic cell populations in iMacs and iMacs_CM. (h) Quantification of IL6 release by iMacs and iMacs_CM, post-LPS stimulation. (i) Quantification of TNFα release by iMacs and iMacs_CM, post-LPS stimulation. (j) Quantification of IL10 release by iMacs and iMacs_CM, post-LPS stimulation. Flow cytometry analysis performed using FlowJo. Statistical analysis used: one-way ANOVA with Tukey's comparison test for d, e, f, h, i and j; Student T test with Welch's correction for g. * represents P<0.05, ** represents P<0.01, *** represents P<0.001 and **** represents P<0.0001. N = 3 biological replicates for BDMs and 6 biological replicates for iMacs and iMacs_CM, with each point signifying the average of 3 technical replicates.

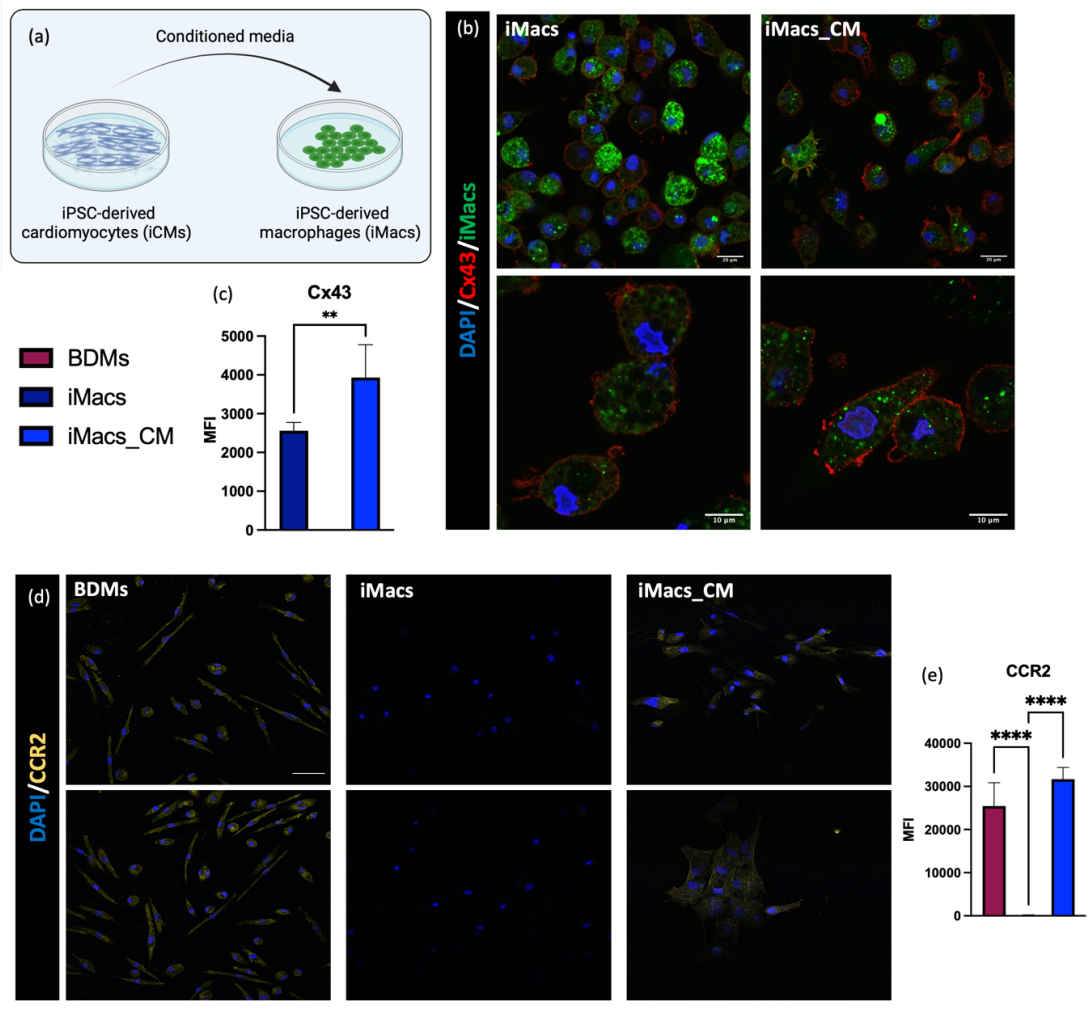

Figure 7.3: Characterisation of iCM conditioned media treated iMacs (iMacs_CM) using immunofluorescence imaging. (a) Schematic representation of the experimental set up. (b)

Representative images of iMacs and iMacs_CM stained with DAPI and connexin43. Scale bar – 20 µm, magnified image scale bar – 10 µm. (c) Mean fluorescence intensity (normalised to cell number) of connexin43 expression, quantified using ImageJ. (d) Representative images of BDMs, iMacs and iMacs_CM stained with DAPI and CCR2. Scale bar – 100 µm (e) Mean fluorescence intensity (normalised to cell number) of CCR2 expression, quantified using ImageJ. Statistical analysis - one-way ANOVA with Tukey's comparison test for e; Student T test with Welch's correction for c. ** represents $P<0.01$ and **** represents $P<0.0001$. N = 3 biological replicates for BDMs and 6 biological replicates for iMacs and iMacs_CM, with each point signifying the average of 3 technical replicates.

7.4.2. iMacs integrate well with iCM cultures and exhibit functional improvement

Having observed interesting responses in iMacs following treatment with iCM-conditioned media, the subsequent goal was to investigate how iMacs interact with iCMs in a co-culture setting. In murine hearts, the ratio of cardiomyocytes to CRMs have been reported to be 1:5 [22]. However, using state-of-the-art techniques such as single-cell and single-nucleus RNA sequencing and multiplex single-molecule fluorescence in situ hybridisation single cell RNA sequencing, Litviňuková *et al.* demonstrated that in adult human heart, the number of cardiac cell populations vary across different regions of the heart [42]. Litviňuková *et al.* reported an approximate 3:1 split of cardiomyocytes to immune cells in atrial tissues, whereas an approximate 9:1 split of the same, in ventricular tissue regions [42]. Calculating these ratios in bulk, across atrial and ventricular tissues, there appears to be a 5:1 split of cardiomyocytes and immune cells. Using these numbers, in this study, a 5:1 ratio of iCMs to iMacs was used when performing co-cultures (Figure 7.4 (a)). Despite iCMs being plated at high cell densities (200,000 cells/cm^2), iMacs were found to integrate well into iCM cultures (Figure 7.4 (b)), and in particular, into beating patches of iCMs. As previously demonstrated, both iCMs and iMacs express Cx43. In the myocardium, cardiomyocytes and CRMs communicate with each other through Cx43 gap junctions [21], and hence, the expression of Cx43 was assessed. Although shared Cx43 gap junctions could not be

isolated in iCM/iMac co-cultures, both the cell types abundantly expressed Cx43 (Figure 7.4 (c)).

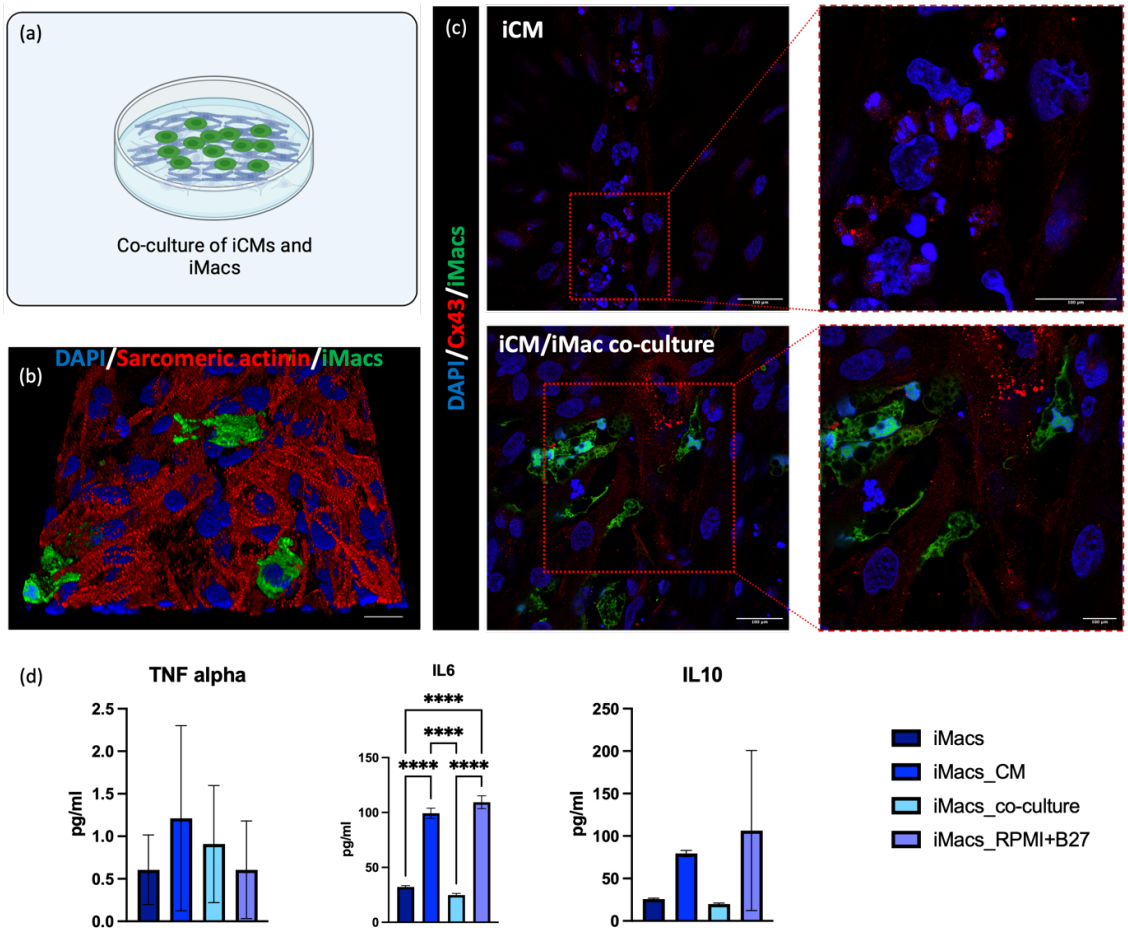

Figure 7.4: Characterisation of iMacs in co-culture with iCMs (iMacs_co-culture). (a) Schematic representation of the experimental set up. (b) Representative 3D reconstructed image of iCMs stained with Sarcomeric actinin, highlighting the integration of iMacs into iCM cultures. Scale bar – 50 µm (c) Representative images of iCMs and co-cultures of iMacs and iCMs stained with DAPI and connexin43. Scale bar – 100 µm. (d) Quantification of TNFα, IL6 and IL10 release by iMacs, iMacs_CM, iMacs_co-culture and iMacs cultured in RPMI with B27™. Statistical analysis - one-way ANOVA with Tukey's comparison test. **** represents P<0.0001. N = 4 technical replicates.

Previous work from the lab using BDMs showed a pro-inflammatory response in BDMs on treatment with iCM conditioned media, and the pro-inflammatory response was associated with B27™ supplement [365]. Therefore, secretome was collected from iMacs_CM and iMacs in co-culture with iCMs (iMacs_co-culture), and subjected to ELISA tests to verify the presence of pro-inflammatory cytokines. Untreated iMacs and iMacs cultured in RPMI+i (supplemented with 100 ng/ml M-CSF; iMacs_RPMI+B27) were used as controls. TNFα and IL10 productions were found to be minimal in all culture conditions (Figure 7.4 (d)). However, over 60% more IL6 was found to be present in iMacs_CM and iMacs_RPMI+B27 secretome, potentially indicating mild activation (Figure 7.4 (d)). Notably, iMacs displayed quiescence when in co-culture with iCMs, with strong suppression in their IL6 release (Figure 7.4 (d)).

Cardiomyocytes are specialised cells that deal with the intense mechanical and metabolic demands of the heart [22]. Potentially due to space restrictions, it is common to find dead or floating cells in iCM cultures. One of the first and the most stark differences to be noted in iCM/iMac co-cultures was the drop in the number of floating cells and debris, most likely due to iMacs performing phagocytosis (Figure 7.5 (b)). However, since the iCM cultures were not purified and had actively proliferating undifferentiated cells in the mix, it was not possible to quantify the reduction in cell debris for iCM/iMac co-cultures. Previous studies using RAW246.7 macrophages have shown their ability to phagocytose necrotic or apoptotic cells *in vitro* [366], supporting the findings reported in this study.

In attempt to further characterise iMacs_CM and iMacs_co-culture, their expression of a vast panel of genes was assessed, using untreated iMacs as control (Figure 7.5 (a)). While iMacs_CM displayed a highly upregulated pro-regenerative response, with a three-fold increase in TGFB1 and a two-fold increase in MRC1 expressions, iMacs_co-culture maintained quiescence, with no difference in their expression of TGFB1, MRC1 and IL10 in comparison to iMacs (Figure 7.5 (c)). On the other hand, the expression of pro-inflammatory genes such as TNF, IFNG and NOS2 were comparable between iMacs and iMacs_CM, while iMacs_co-culture exhibited a 90% downregulation of TNF and 80% downregulation of NOS2 (Figure 7.5 (d)). Although notably high levels of IL6 was

detected in iMacs_CM secretome (Figure 7.4 (d)), their gene expressions revealed a strong pro-regenerative response (Figure 7.5 (c, d)). Notably, previous work by Li *et al.* to study the interaction between cardiomyocytes and macrophages *in vitro* (using HL-1 and RAW264.7 cell lines), show a downregulation in pro-inflammatory markers when macrophages are exposed to cardiomyocyte conditioned media [367]. Using a murine model, Pinto *et al.* reported resemblance of CRMs to alternatively activated macrophages, with an upregulation in the expressions of markers such as Mrc1, CD163, and Lyve-1 [363]. In this study, although no notable alternative activation was found in iMacs_co-culture, a steady downregulation of pro-inflammatory genes was documented. Taken together, these results highlight the differences in the activation states of iMacs_CM and iMacs_co-culture, with iMacs_co-culture displaying a quiescent and anti-inflammatory phenotype (Figure 7.5 (c, d)).

In addition to the activation states, the functional ability of macrophages is also of great importance. Matrix metalloproteinase-9 (MMP9) plays a direct role in ECM degradation and activation of cytokines and chemokines, for the regulation of tissue remodeling [368]. Furthermore, in a number of pathological conditions such as arthritis, diabetes and cancer, high MMP9 production is highlighted as a biomarker for inflammation [369]. In the context of cardiovascular diseases, the deletion of MMP9 has been proven to be beneficial, to facilitate effective tissue remodelling post-MI [370]. In this study, the expression of MMP9 was found to be 99% lower in iMacs_co-culture than iMacs (Figure 7.5 (e)), indicating homeostasis and a potential for robust matrix production [368]. Additionally, in a study involving indirect cultures of cardiomyocytes and polarised macrophages, Wrona *et al.* demonstrated no difference in exogenous MMP9 production when macrophages were classically or alternatively activated [237]. The expressions of CCR2, VEGFA and TRPV4 further highlighted the quiescence of iMacs_co-culture (Figure 7.5 (e)). The $CCR2^{low}$ phenotype of iMacs has been previously demonstrated through gene (Figure 5.7 (c)) and protein (Figure 7.2 (c, d) and 7.3 (d, e)) expressions. Consistent with protein expression findings (Figure.7.3 (d, e)), iMacs_CM expressed 85% more CCR2 than iMacs (Figure 7.5 (e)). Remarkably, iMacs_co-culture maintained the $CCR2^{low}$ phenotype, which is of high significance, since CRMs are known

to be $CCR2^-$ [21, 22, 64, 90, 102, 104, 106, 125, 344, 363, 371]. In the myocardium, $CCR2^+$ and $CCR2^-$ macrophages express TRPV4 in abundance [372]. Wong *et al.*, demonstrated that macrophages respond to mechanical cues through TRPV4 channels, and that the inhibition of TRPV4 is detrimental to angiogenesis in murine hearts [372]. While TRPV4 and the angiogenesis marker VEGFA were significantly upregulated (84% and 48% respectively) in iMacs_CM, the expression of these genes were comparable between iMacs_co-culture and iMacs (Figure 7.5 (e)). Although the quiescence of iMacs_co-culture was evident in majority of the genes assessed, their functional potential was highlighted with the expressions of AREG and GJA1 (Figure 7.5 (e)). As previously mentioned, CRMs couple with cardiomyocytes *in vivo* through Cx43 gap junctions [21]. Dephosphorylation of Cx43 has been shown to affect cardiac function, by damaging the electrical coupling [373]. Additionally, more recent studies have demonstrated the role of amphiregulin (AREG), a growth factor produced by CRMs, in carrying out efficient Cx43 phosphorylation [374]. A 58% upregulation in AREG and 84% upregulation in GJA1 (Cx43) was found in iMacs_co-culture in comparison to iMacs (Figure 7.5 (e)). This upregulation demonstrates good interaction between iMacs and iCMs. Moreover, recent studies also emphasise the exceptionally strong ECM-binding motif possessed by AREG, for binding to multiple ubiquitous ECM proteins [375]. Collectively, these findings highlight the quiescent state of iMacs_co-culture, with a steady downregulation in CCR2 expression and upregulation in AREG and GJA1 expressions.

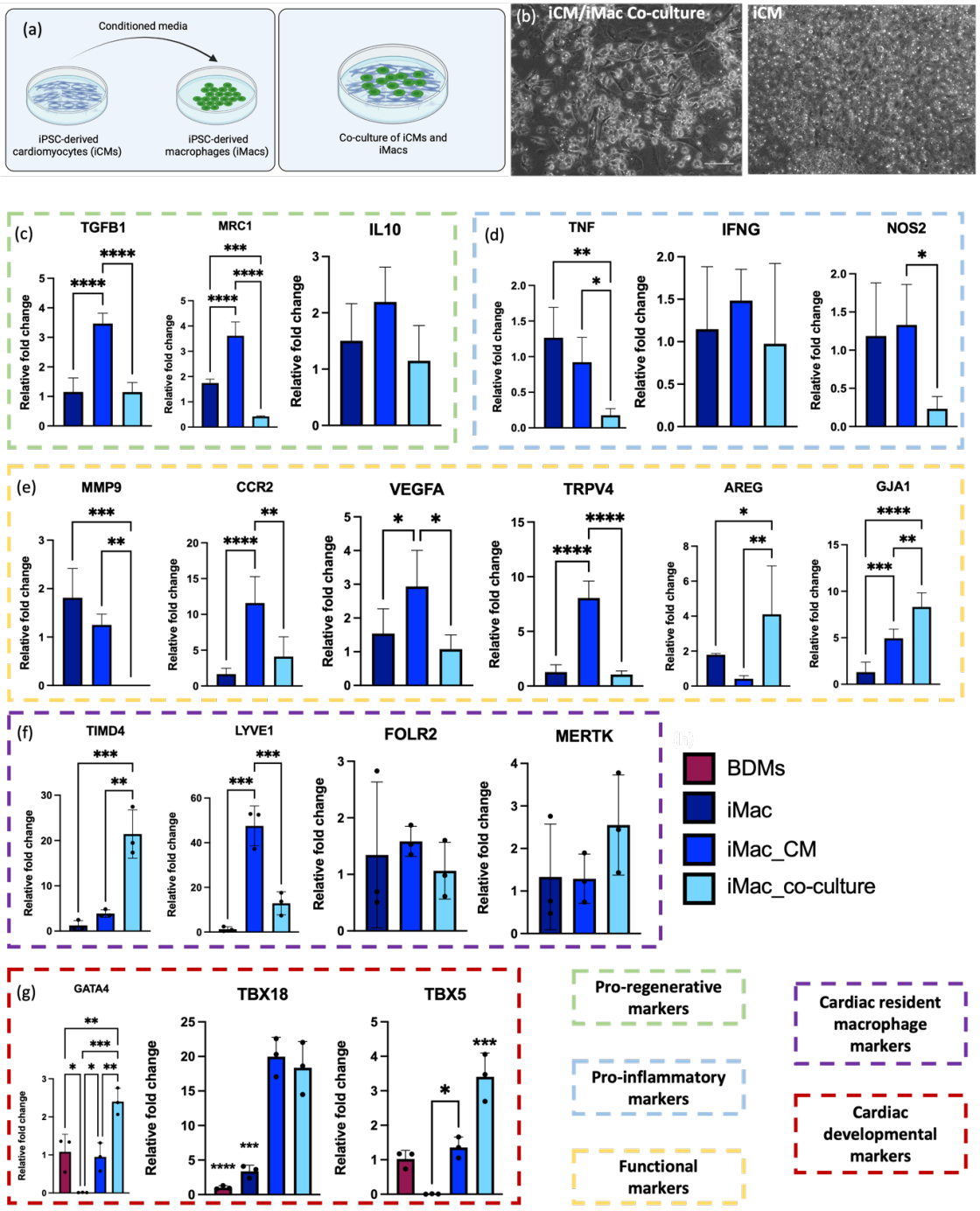

Figure 7.5: Gene expression analysis of iCM conditioned media treated iMacs (iMacs_CM) and iMacs in co-culture with iCMs (iMacs_co-culture). (a) Schematic representation of the experimental set up. (b) Representative images of iCMs and iCM/iMac co-cultures, highlighting the reduction in dead cells and debris. Scale bar – 100 µm (c) Expression of a set of pro-regenerative genes. (d) Expression of a set of pro-inflammatory genes. (e) Expression of a set of functional genes. (f) Expression of a set of cardiac resident macrophage-specific genes. (g)

Expression of a set of cardiac developmental genes. Statistical analysis - one-way ANOVA with Tukey's comparison test. * represents P<0.05, ** represents P<0.01, *** represents P<0.001 and **** represents P<0.0001. N = 3 biological replicates, with each point signifying the average of 3 technical replicates. Fold change of mRNA relative to iMacs for (c, d, e and f) and to BDMs for (g).

7.4.3. iMacs express CRM-specific as well as cardiac developmental genes when in co-culture with iCMs

As previously mentioned, through parabiotic and gene fate mapping studies, Dick *et al.* demonstrated that three distinct macrophage populations exist across multiple tissues, including the heart [64]. The macrophage populations according to Dick *et al.* include TLF^{+} macrophages that are maintained through self-renewal with minimal monocyte input (expressing TIMD4 and/or LYVE1 and/or FOLR2), $CCR2^{+}$ macrophages that are almost entirely replaced by monocytes ($TIMD4^{-}LYVE1^{-}FOLR2^{-}$), and MHC-$II^{hi}$ macrophages that are partially replaced by circulating monocytes ($TIMD4^{-}LYVE1^{-}FOLR2^{-}CCR2^{-}$) [64]. Observing pronounced differences in the expression of CCR2 between iMacs_CM and iMacs_co-culture (iMacs_CM being $CR2^{high}$ and iMacs_co-culture being $CCR2^{low}$), the expressions of other known CRM markers such as TIMD4, LYVE1 and FOLR2 were analysed. While iMacs_co-culture expressed a 94% upregulation in TIMD4 expression, iMacs_CM expressed a 97.2% upregulation in LYVE1 expression, in comparison to iMacs (Figure 7.5 (f)). In comparison to iMacs, iMacs_co-culture also exhibited a 89% upregulation of LYVE1 expression (Figure 7.5 (f)). FOLR2 was also detected in all three groups, however, the expressions were not found to be significantly different (Figure 7.5 (f)). The expression of MERTK was also found to be comparable across the three groups, with a subtle trend of upregulation (48%; although not significant) in iMacs_co-culture (Figure 7.5 (f)).

In the iMac differentiation protocol used, pre-macs are collected and matured for 7 days in order to get functional iMacs. Pre-macs generated using this protocol are considered

ideal precursors for the generation of macrophages resembling key features of TRMs such as alveolar macrophages or microglia cells [193, 201, 204, 376]. Bearing this in mind, iMacs_CM and iMacs_co-culture were assessed for the expression of cardiac developmental markers, to understand the impact of cardiac cues on iMacs. To make unbiased comparisons, BDMs were used as control, since iMacs do not come from cardiac lineage. Remarkably, iMacs_co-culture expressed a 99.2% upregulation of GATA4, 71% upregulation of TBX18 and 99.9% upregulation of TBX5, in comparison to iMacs (Figure 7.5 (g)). Additionally, the GATA4 and TBX5 expression in iMacs_co-culture were 43.4% and 51% (respectively) more than iMacs_CM (Figure 7.5 (g)). In the context of cardiac health, the contributions of GATA4 from cardiac fibroblasts and cardiomyocytes have been well studied. However, the impact of macrophage-derived GATA4 remains unexplored. Previous studies note that cardiomyocyte-derived GATA4 is essential in promoting intrauterine cardiac development, by driving the proliferation of foetal cardiomyocytes [377]. Similarly, cardiac fibroblast-derived GATA4 has been demonstrated to be essential for steady angiogenic response *in vitro* [378]. Interestingly, increased GATA4 levels have been shown to significantly reduce myocardial scar size after cryoinfarction injury in mice [377]. Taken together, the expression of all genes analysed shows that iMacs respond differently to being exposed to iCM conditioned media and to being in physical contact with iCMs. In particular, the responses of iMacs in co-culture with iCMs demonstrate a profile that resembles CRMs, with a downregulation in the expressions of MMP9 and CCR2; and an upregulation in the expressions of AREG, GJA1, TIMD4, LYVE1, GATA4, TBX18 and TBX5.

7.4.4. iCMs demonstrate phenotypic changes and express cardiac maturation genes when in co-culture with iMacs

After thoroughly analysing the phenotypic and genotypic characteristics of iMacs in co-culture with iCMs, it was of interest to comprehend the response of iCMs to the presence of iMacs in co-culture (Figure 7.6 (a)). In adult hearts, cardiomyocytes exhibit an elongated and rod-shaped morphology, with approximately 65% of them being mononucleated—a percentage that remains relatively constant throughout life [379,

380]. Despite the current advancements in differentiation efficiency, iCMs continue to display a smaller size and a rounder shape, indicating an immature or foetal phenotype [381]. On performing immunofluorescence imaging for cTnT on iCM/iMac co-cultures (Figure 7.6 (a)), a clear difference could be noted in the phenotype of iCMs in co-culture with iMacs, with an elongated morphology, much like adult cardiomyocytes (Figure 7.6 (b, c)). On quantifying the elongation using aspect ratio (ratio between the long axis to the short axis of a cell; perfect circle has an aspect ratio of 1 and elongated cells have an aspect ratio greater than 1), iCMs in co-culture with iMacs displayed a clear and significant 58.7% upregulation in the aspect ratio (Figure 7.6 (b)). A similar elongated morphology was also observed with Sarcomeric actinin staining (Figure 7.6 (d)). However, it is worth noting here that the aspect ratio measurements was made on cTnT stained iCMs, which stains the cytoplasm. Cell elongation can be better assessed by using a cell membrane stain, such as wheat germ agglutinin.

To investigate improvement in iCM maturity, the expression of a number of genes was assessed. The gene encoding cTnT, TNNT2, was found to be similarly expressed between iCMs and iCMs in co-culture with iMacs (2D co-culture) (Figure 7.6 (e)), indicating no dedifferentiation of iCMs. Previous work by Zhang *et al.* reported that depending on the method used for the reprogramming of iPSCs, iCMs can have residual expression of pluripotency transgenes OCT4 and NANOG, which may cause undesired effects such as teratoma formation and dedifferentiation [152]. Other common markers for cardiomyocyte maturation are MYH6 and MYH7. The gene MYH7 is responsible for encoding β-myosin heavy chain (MHC), the predominant MHC in the left ventricle of the adult human heart [382]. On the other hand, MYH6 encodes α-MHC and serves as the primary MHC in the adult atrium [382, 383]. In humans, the ratio of MYH7/MYH6 has been shown to increase with age [384], as the levels of MYH6 decreases [385]. This trend is also reported in extended culture conditions of iCMs [386] as well as in engineered heart tissues [16]. In comparison to iCMs, iCMs in co-culture with iMacs expressed comparable levels of MYH7 and 70% less MYH6 (Figure 7.6 (e)). Interestingly, the MYH7/MYH6 ratio was found to 62.5% upregulated in iCMs that were in co-culture with iMacs, demonstrating more maturation (Figure 7.6 (f)). Another key function of

cardiomyocytes, is their ability to efficiently handle calcium. The initiation of mechanical contraction in cardiomyocytes occur due to calcium-induced calcium release [387]. Sarcoplasmic/endoplasmic reticulum calcium ATPase (SERCA) is a key buffer responsible for calcium uptake preceding diastole [388]. Remarkably, a nine-fold (88.8%) upregulation was noted in the SERCA2 expression in iCMs in co-culture with iMacs, further highlighting genotypic maturation in iCMs (Figure 7.6 (g)). Although calcium uptake and release mediate contraction of cardiomyocytes, the structural integrity and the length between the sarcomeres of cardiomyocytes is considered an important read-out for cardiomyocyte maturity [389]. Human atrial and ventricular tissue samples were sectioned and stained with Sarcomeric actinin and used as a positive control (Figure 7.6 (h) to compare the sarcomere lengths of iCMs and iCMs in co-culture with iMacs. The number of different sarcomere lengths have been reported for iCMs in resting state, such as 1.31 µm [386], 1.65 µm [167], 1.84 µm [390], 1.7 µm [391], ~1.8 µm [392] etc. In agreement with this range, iCMs displayed an average sarcomere length of 1.76 µm and iCMs in co-culture with iMacs had an average sarcomere length of 1.52 µm (not significantly different) (Figure 7.6 (i)). However, these lengths were significantly shorter than human atrial and ventricular sarcomere lengths (2.01 µm and 2.77 µm respectively) (Figure 7.6 (i)). Previously reported sarcomere lengths for adult murine cardiomyocytes are ~1.91 µm [390, 391] and within the range of 1.9 µm to 2.2 µm for human cardiomyocytes [393]. Collectively, these findings highlight phenotypic (elongation) and genotypic (MYH7/MYH6 ratio and SERCA2 expression) maturation of iCMs when in co-culture with iMacs. However, there still remains room for improvement in iCM maturation, as demonstrated by significantly low sarcomere lengths in iCMs compared to primary human samples. However, it is important to note that, in the literature, sarcomere length measurements typically rely on TEM imaging [394], while immunofluorescence imaging is utilised in this work, potentially explaining some discrepancies.

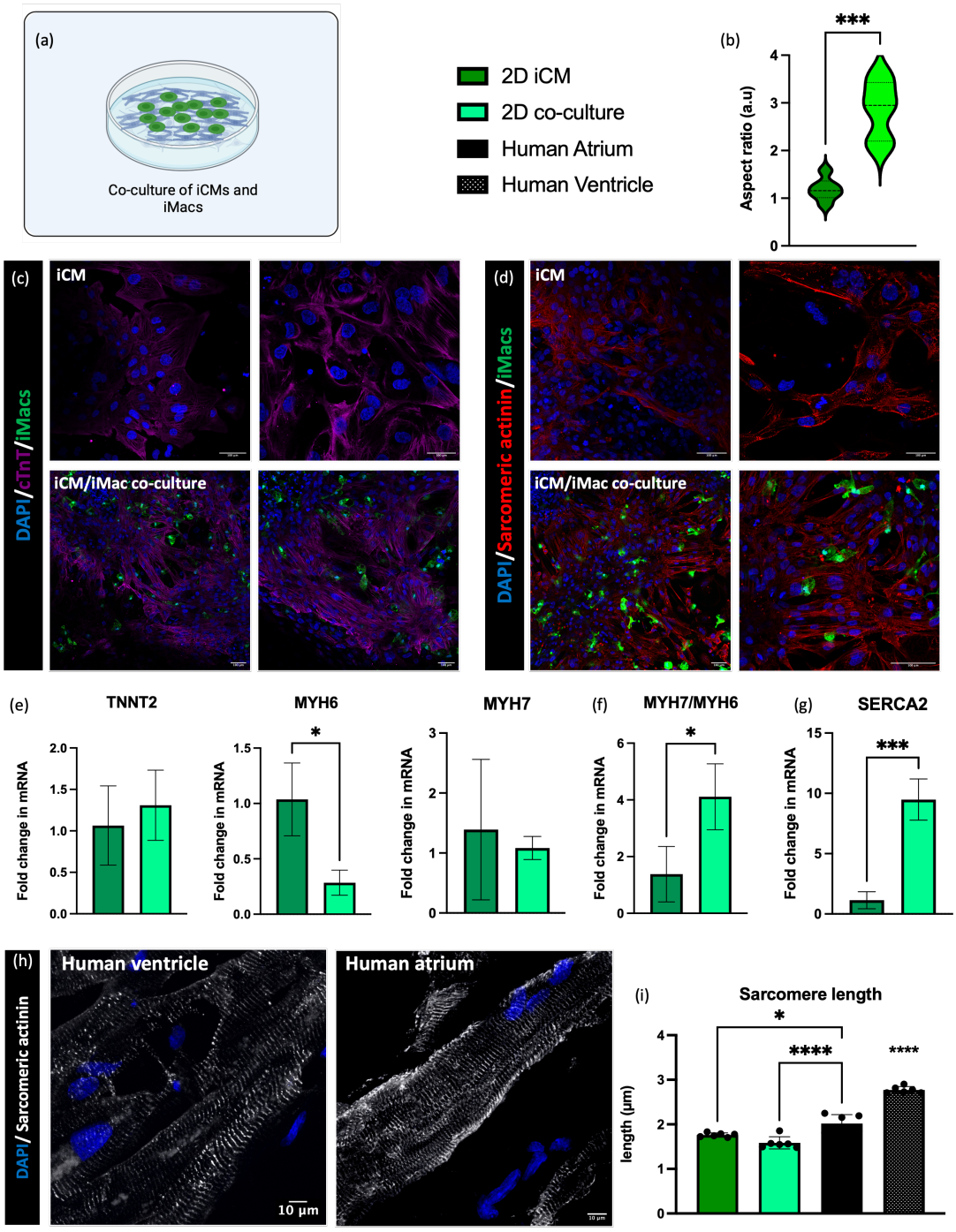

Figure 7.6: Characterisation of iCMs in co-culture with iMacs. (a) Schematic representation of the experimental set up. (b) Aspect ratio measurement of iCMs and iCMs in co-culture with iMacs. (c) Representative images of iCMs and iCM/iMac co-cultures stained with cardiac troponin T (cTnT). Scale bar – 100 µm (d) Representative images of iCMs and iCM/iMac co-cultures stained with Sarcomeric actinin. Scale bar – 100 µm (e) Expression of a set of cardiomyocyte-specific genes. (f) Ratio of the expression of MYH7/MHY6. (g) Expression of SERCA2. (h) Representative images of primary human atrial and ventricular tissue samples,

stained with Sarcomeric actinin. Scale bar – 10 µm. (i) Quantification of sarcomere lengths obtained from analysis using ImageJ. Statistical analysis - Student T test with Welch's correction for (b, e, f and g); one-way ANOVA with Tukey's comparison test for (i). * represents P<0.05, *** represents P<0.001 and **** represents P<0.0001. N = 3 biological replicates, with each point signifying the average of 3 technical replicates, for (e, f and g). Fold change of mRNA relative to iCMs in monolayer culture. N = 3 biological replicates, with each point signifying the average of sarcomere lengths determined from 3 separate images, for (i).

7.4.5. iCMs in co-culture with iMacs display improved calcium handling

In order to further characterise the functional aspects of iCM maturation, their intracellular calcium handling properties was evaluated using Cal520® AM dye. Asynchronous and heterogeneous spontaneous beating rates is one of the well-documented shortcomings of iCMs [395, 396]. Recent preclinical studies have indicated that transient, nonlethal ventricular tachycardia was increased after implantation of iPSC- or ESC- derived cardiomyocytes, which dramatically decreased after 2 weeks, when the engrafted CMs showed contractile synchronisation with the host heart [397, 398]. On assessing nine different regions of interest within a well of iCMs, there was no notable synchrony in the beating of iCMs in the nine regions (Figure 7.7 (b)). However, on performing similar assessment on iCM/iMac co-cultures, all the nine regions were found to beat in synchrony, with peaks corresponding to iCM contractions (Figure 7.7 (b); synchrony highlighted using red lines). In attempt to synchronise the beating of iCMs, previous studies have used a number of different approaches. One of the most common approaches used, is electrical stimulation [399]. For example, using a 5 Hz electrical stimulation, Ma *et al.* demonstrated synchronous beating in iCMs [400]. Other approaches used include fabrication of 3D tissue constructs, such as the Biowire platform, where synchronous beating was noted within two to three days [190]. Ribeiro *et al.* micropatterned single iCMs on deformable polyacrylamide substrates and improved their beating synchrony [401]. Using a similar mechanical stimulation approach, Nitsan *et al.* used an oscillatory mechanical probe that mimics the

deformations generated by neighbouring beating cardiac cells, to achieve synchrony [395]. Although these findings emphasise a major limitation of using iCMs with no additional priming or specialised culture surfaces, the addition of iMacs into iCM cultures could be an excellent solution to facilitating synchronous beating.

Following this, calcium transient read-outs were used to quantify the beat rate of iCMs and iCMs in co-culture with iMacs. Using the exact same approach as before, different regions of interest were chosen in individual wells of iCM cultures. On day 25 of differentiation, distinct patches of iCMs beat at vastly different paces ranging from 33 beats per minute (bpm) to 72 bpm, with an average of 49.92 ± 15.87 bpm (Figure 7.7 (c)). Some studies report a beating rate of 38 bpm [386] for iCMs, while some report 45 bpm [402], at similar time points during the differentiation process. Other published ranges for iCM beat rate include 20 – 35 bpm [403] and 50 – 70 bpm [152]. Additionally, commercially available, highly purified (near 100%) iCell™ cardiomyocytes (Cellular Dynamics International, Madison, WI) reportedly beat at 25 bpm [404]. Interestingly, iCMs in co-culture with iMacs were found to beat at paces ranging from 28 bpm to 38 bpm (Figure 7.7 (c)), with an average of 33.12 ± 2.72 bpm. The average beat rates reported in this study are much slower than human embryonic heart rate, which is 80 – 196 bpm [405], and adult heart rate, which is 60 – 100 bpm [403]. Correlating beating rate to *in vitro* iCM maturation has been controversial [386], with some studies claiming an increase in beat rate [406], while some others claiming a reduction [403]. This highlights the need for improving iCM culture conditions to obtain physiologically-relevant beating rates, potentially using electrical stimulation [149]. However, it is worth noting that iCMs in co-culture with iMacs exhibited remarkably low variability in terms of their rate of spontaneous beating.

Several compounds can also alter the beat rate of cardiomyocytes, and this effect can be induced by targeting different ion channels and processes. The response of iCMs to the exposure of such compounds or drugs has been well documented [407]. Subsequently, it was intriguing to investigate whether iCMs in co-culture with iMacs also respond to known drugs such as carbamylcholine (carbachol), isoproterenol and caffeine. Carbachol is a muscarinic acetylcholine receptor agonist that is known to reduce the beat rate of nodal tissue (sino-atrial and atrio-ventricular) and iCMs [408].

Previous studies report a dose dependant reduction in the beat rate of iCMs on treatment with carbachol [409]. Carbachol treatment was found to bring down the beat rate in iCMs (30.4 ± 7.3 bpm), although with large variability (Figure 7.7 (d)). The next drug assessed was isoproterenol, β-adrenergic agonist, which can at low doses, increases the beat rate of iCMs [410, 411]. Furthermore, comprehensive response to β-adrenergic agonists are an indicator of phenotypic maturation of iCMs [412]. Both iCMs and iCMs in co-culture with iMacs responded to isoproterenol treatment displaying beat rates of 53.6 ± 7.1 bpm (for iCMs) and 72 ± 2.6 bpm (for co-cultures) (Figure 7.7 (d)). However, similar to previous responses, beat rates of iCM/iMac co-cultures were highly robust, with very little variability, compared to iCMs (Figure 7.7 (d)). Interestingly, Huebsch *et al.* also report high variability in the beat rate of iCMs, with beat rate increasing from ~38 bpm to ~62 bpm with isoproterenol treatment [412], consistent with the findings of this study. Similarly, caffeine is also a commonly used drug that increases the beat rate of iCMs [413] and improve their active calcium transients [414]. Although iCMs did not show a significant increase in beat rate on exposure to caffeine (47.6 ± 10.2 bpm), iCM/iMac co-cultures were highly sensitive and displayed a steady beat rate of 56 ± 0 bpm (Figure 7.7 (d)). Despite iCMs being known to exhibit poor calcium handling (in comparison to ESC-derived cardiomyocytes) [415], the addition of iMacs show great potential in improving calcium handling and iCM maturity.

As previously mentioned, prolonged time in culture (>50 days) has been shown to improve iCM maturity, facilitating elongation of cells [166] and causing reduced beat rate [167, 416]. In agreement to these finding, iCMs kept in culture for 65 days showed a highly reduced beat rate of 20 ± 2.6 bpm, with very little variability (Figure 7.7 (e)). Remarkably, iCMs in co-culture with iMacs displayed a beat rate of 73.6 ± 6 bpm (Figure 7.7 (e)), within the physiological range of beating for adult human hearts [403]. Taken together, these findings strongly emphasise the functional maturity displayed by iCMs in co-culture with iMacs, with highly synchronous beating, robust response to drug treatments and physiologically accurate beat rates.

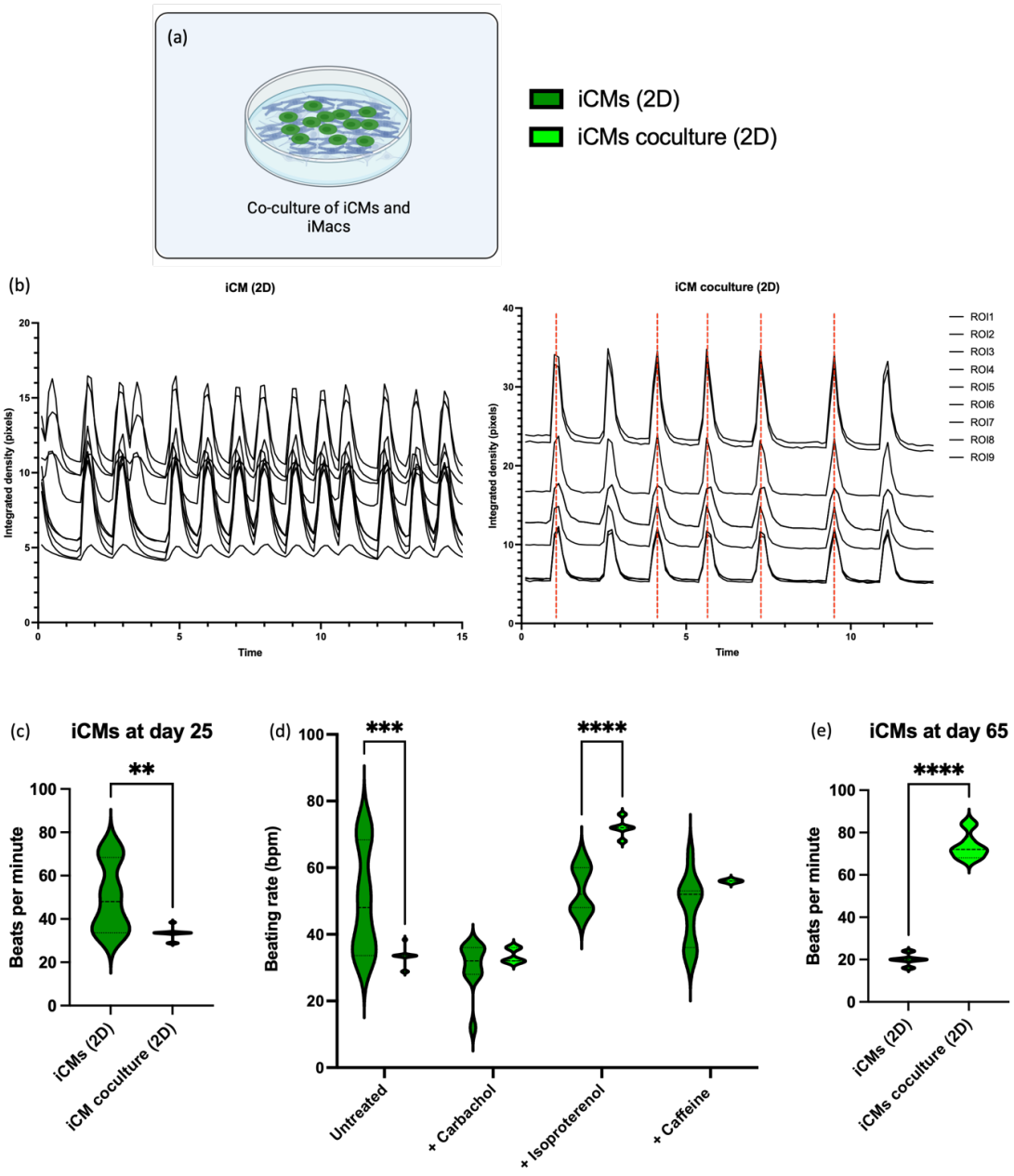

Figure 7.7: Characterisation of calcium handling and beat rate in iCMs and iCMs in co-culture with iMacs. (a) Schematic representation of the experimental set up. (b) Representative plots of the calcium transients in iCMs and iCMs in co-culture with iMacs. Nine regions of interest are assessed and the peaks denote individual spontaneous beat of the cells. Red lines highlight the synchronous beating of iCMs in co-culture with iMacs. (c) Quantified beat rate of iCMs and iCMs in co-culture with iMacs at day 25. (d) Quantified beat rate of iCMs and iCMs in co-culture with iMacs in response to treatment with carbachol, isoproterenol and caffeine. (e) Quantified beat

rate of iCMs and iCMs in co-culture with iMacs at day 65. Statistical analysis - Student T test with Welch's correction for (c and e), Two-way ANOVA with Tukey's multiple comparison for (d). ** represents P<0.01, *** represents P<0.001 and **** represents P<0.0001. N = 6 technical replicates, with each point signifying the average beat rates from 9 different regions within 1 well.

7.5. Conclusion

The field of cardiac immunology has gained more interest in the recent past, owing to the discovery of key interactions between cardiomyocytes and macrophages, and the role of macrophages (in particular, CRMs) in maintaining homeostasis within the myocardium. Most of the reported functions of CRMs are using murine models, leaving very little known about CRMs in humans. In order to deepen our understanding of human CRM biology, *in vitro* cultures can be used as an effective tool. The primary objective of this chapter was to understand how cardiomyocytes and macrophages interact with each other *in vitro*, using iCMs and iMacs from the same iPSC parent line (SFCi55). To efficiently simulate a cardiac environment *in vitro*, two approaches were chosen - providing iMacs with iCM conditioned media (iMacs_CM) and performing co-cultures of iMacs and iCMs (iMac_co-culture).

First, the functional activity of iMacs_CM was investigated, which revealed a unique protein expression profile, different to untreated iMacs. The analysis revealed that iCM-conditioned media treatment induced significant changes in iMacs, particularly in the expression of macrophage cell surface markers. Notably, CD14 expression increased, aligning iMacs more closely with TRMs [361] as well as CRMs [106]. The study further delved into specific subsets of $CD14^{high}CCR2^{low}$ iMacs_CM, revealing an upregulation of CX3CR1, a marker associated with CRMs [363, 364]. This finding was consistent with previous studies in murine models, emphasising the relevance of CX3CR1 in cardiac macrophage development. However, the study also noted a downregulation of HLA-DR, the human equivalent of MHC-II, in iMacs_CM compared to iMacs. This observation

suggests a potential modulation of immune response, and further functional assays, such as phagocytosis and response to LPS, indicated that iMacs_CM retained their phagocytic potential while exhibiting a suppressed response to classical activation. The downregulation of cytokine release in response to LPS treatment paralleled previous findings with lactate treatment, suggesting a potential link between metabolic cues and macrophage activation. The functional assessment of iMacs_CM extended to immunofluorescence imaging, confirming the upregulation of Cx43 in iMacs_CM, reinforcing the notion that iCM-conditioned media induces changes in iMacs mirroring features of CRMs. These findings laid the groundwork for exploring the interaction between iMacs and iCMs in co-culture settings. This approach aimed to mimic the physiological cardiac microenvironment, considering the heterogeneity of macrophage populations in the human heart, characterised by both $CCR2^{+}$ and $CCR2^{-}$ subsets.

In the co-culture experiments, a 5:1 ratio of iCMs to iMacs was established based on previous reports of the cell composition in different regions of the adult human heart [42]. Surprisingly, despite high cell densities of iCMs, iMacs integrated well into iCM cultures, particularly in beating patches. The expression of Cx43 in both cell types further emphasised potential communication through gap junctions, crucial for myocardial function. Comparative analysis of secretome from iMacs_CM and iMacs_co-culture revealed intriguing differences. iMacs_co-culture displayed quiescence, with suppressed IL6 release, in contrast to the pro-inflammatory response observed in iMacs_CM. Additionally, the reduction in floating cells and debris in co-cultures suggested a potential phagocytic role of iMacs in clearing dead or floating cells, enhancing the overall culture environment. To that end, although different media formulations for performing iCM/iMac co-cultures was not investigated, the suppression of IL6 in iMacs_co-culture and the reduction in cell debris acted as good indicators of homeostasis within the co-cultures.

Gene expression analysis further characterised iMacs_CM and iMacs_co-culture, highlighting differences in their phenotype. Notably, iMacs_co-culture displayed a steady downregulation of pro-inflammatory genes (TNF and NOS2), emphasising a

quiescent and anti-inflammatory phenotype, distinct from iMacs_CM. The assessment of MMP9 expression in iMacs_co-culture indicated a potential for robust matrix production and tissue remodeling [369, 370]. Additionally, the maintenance of the $CCR2^{low}$ phenotype, along with upregulation of AREG and GJA1 (Cx43), underscored the functional potential of iMacs in co-culture with iCMs, aligning them with much more closely with $CCR2^{-}$ CRMs [106, 374]. Further exploration into the expression of CRM-specific and cardiac developmental genes in iMacs_co-culture revealed upregulation of TIMD4, LYVE1, and GATA4, TBX18, TBX5, respectively. These findings suggested a profile resembling CRMs, hinting at the influence of cardiac cues on iMacs, with distinct differences when iMacs are in physical contact with iCMs.

Conclusively, the study showcased the differential responses of iMacs to conditioned media and co-culture with iCMs. While iCM conditioned media treatment induced some known CRM-specific responses in iMacs, such as a highly anti-inflammatory response (upregulation of TGB1, MRC1) and expression of CRM-specific gene LYVE1, there was a notably high CCR2 expression. On the other hand, iMacs_co-culture not only expressed anti-inflammatory genes (downregulation of TNF and NOS2), CRM-specific genes (TIMD4, LYVE1 and FOLR2) and cardiac developmental genes (GATA4, TBX18 and TBX5), an overall quiescence was also noted, which is key to TRMs. Due to these remarkable responses in iMacs_co-culture, this approach was chosen for future 3D studies.

In addition to the characterising the response of iMacs, the phenotypic and functional changes in iCMs was also investigated. In co-culture with iMacs, iCMs displayed elongation, which is a signature of mature cardiomyocytes. Additionally, maturation markers such as the ratio of MHY7/MHY6 and SERCA2 was also found to be highly upregulated in iCMs in co-culture with iMacs. Furthermore, one of the most significant drawbacks of iCM cultures, which is asynchronous beating of the cells, was found to be significantly improved upon adding iMacs to the cultures. The addition of iMacs also showed robust responses to drug treatments (carbachol, isoproterenol and caffeine), indicating improved calcium handling and enhanced maturity. Finally, on adding iMacs

to 65 day old iCM cultures, physiologically relevant, adult human heart beat rates was achieved.

In conclusion, the findings support the notion that iMacs in co-culture with iCMs exhibit a more CRM-like phenotype and iCMs display improved maturation and calcium handling. This suggests that for future research, a co-culture of iMacs holds promise for enhancing the maturation and functionality of both iMacs and iCMs. This study is first of its kind and contributes valuable insights into the complex interplay between iMacs and iCMs, providing a foundation for further investigations in cardiac regenerative medicine and tissue engineering. However, in order to further refine the maturity of iCMs to reach a state comparable to adult human cardiomyocytes, other methods such as electrical stimulation or the use of metabolic maturation media is required.

Chapter 8 Electrical Stimulation to improve the maturation of iCMs, iMacs and co-cultures

8.1. Abstract

Poor maturation of iPSC-derived cardiomyocytes (iCMs) has been a long standing challenge, limiting their representation of adult human cardiomyocytes. Multiple approaches exist to improve iCM maturation *in vitro*, out of which, electrical stimulation (ES) was chosen as a means to enhance iCM maturity in this chapter, drawing on decades of research supporting its efficacy. Unique to this study is its investigation into the effects of ES on iPSC-derived macrophages (iMacs), and co-cultures of iMacs and iCMs. The impact of periodic and continuous ES on iCMs was explored, revealing significant upregulation in maturation markers (including TNNT2, MYH6, MYH7, and SERCA2), when iCMs were subjected to continuous ES. Subsequent investigations into the pro-regenerative and functional responses of iMacs to continuous ES demonstrated a highly pro-regenerative phenotype and upregulation of functional activation markers (TRPV4 and GJA1). Co-cultures of iCMs and iMacs subjected to continuous ES showed that electrically stimulated iMacs remained quiescent yet functionally activated, expressing high levels of VEGFA, AREG and GJA1. Furthermore, continuous ES on iCMs/iMac co-cultures yielded enhanced iCM beat rates, maturation gene expressions, and robust cell elongation, indicating accelerated maturation. Importantly, co-cultures demonstrated superior calcium handling responses and reduced drug response variability, highlighting the synergistic effect of iMacs and ES on iCM maturation. In summary, this study comprehensively elucidates the impact of ES on iCMs and iMacs, both individually and in co-culture. The findings underscore the efficacy of ES in enhancing iCM maturity and the additive effect of iMacs in co-culture, providing insights into the development of an advanced *in vitro* model of the myocardium for regenerative medicine and tissue engineering applications.

8.2. Introduction

Cardiovascular disease remain the leading cause of death worldwide [1], with myocardial infarction (MI) being the most common cause of acute damage to the myocardium [2]. Given the limited regenerative capacity of the myocardium, over time, a dense collagenous scar replaces the contractile tissue, electrically isolating the affected portion of the myocardium [4], culminating in heart failure [5]. While numerous classes of pharmacologic drugs are routinely employed to address heart failure, and an increasing array of new molecules and signalling pathways are under investigation [8, 9], a subset of patients with heart failure do not achieve satisfactory responses to optimal pharmacologic therapy [8]. However, the scarcity of donor organs [10] and complications arising from the continuous immunosuppression required for these patients considerably limit this therapeutic avenue, prompting the exploration of alternative treatments. Therefore, cell-based therapies have emerged as a potential treatment. Cell-based therapies for cardiac repair range from dynamic cardiomyoplasty [417] to the generation of functional cells [418, 419] or grafts [420] for implantation onto or into the heart. Dynamic cardiomyoplasty involves the use of the latissimus dorsi muscle as a flap to wrap around the heart [417, 421]. The skeletal muscle undergoes transformation to acquire characteristics akin to the myocardium, rendering it fatigue-resistant. Through synchronised stimulation with the heart, it is hypothesised that the skeletal muscle will aid in myocardial contraction [421]. Although cardiomyoplasty has been performed on numerous patients, there has been varying degrees of success, making this process not entirely reliable [422]. Cell-based therapies involving direct delivery of cells into the myocardium, has also shown potential. Initially proposed based on the assumption that the injected cell types could substitute or regenerate the lost cardiomyocytes, Menasché *et al.*, carried out a pioneering attempt on one patient using autologous skeletal myoblasts and found functional improvement with evidence of contraction and viability in the grafted scar, 5 months post-transplant [423]. Seeing the safety and efficacy of such cell-based therapies, more studies were performed by injecting autologous bone marrow-derived mononuclear cells, with success [424, 425]. Although these small preliminary studies showed favourable outcomes, larger clinical trials using bone marrow-derived mononuclear cells did not yield better outcomes than

standard clinical therapy, and in some cases, were highly inconsistent [426, 427]. A number of other cell types have also been explored for cardiac repair, such as mesenchymal stromal cells (MSCs) [418], amniotic-fluid stem cell bodies [428], a combination of MSCs and cardiac stem cells [429], cardiosphere derived cells [430] etc. Although a number of non-marrow derived cell types reached clinical studies, they did not pass the safety trials due to reasons including the debate disputing the existence of cardiac stem cells [431-433]. Embryonic stem cells (ESCs) and induced pluripotent stem cells (iPSCs) are excellent candidates to generate new cardiomyocytes for cardiac repair, although pre-clinical safety studies are pending. Both ESC- and iPSC-derived cardiomyocytes have shown potential to regenerate non-human primate as well as pig hearts [397, 398, 419, 434]. However, since reprogramming somatic cells to obtain iPSCs do not involve ethical complications as with ESCs [435], iPSC-derived cardiomyocytes (iCMs) have become highly popular in this regard.

iCMs have been increasingly used in tissue engineering, regenerative medicine, and the development of organ-on-a-chip systems. Yet, iCMs display a highly immature phenotype, functionally closer to foetal cardiomyocytes rather than adult [163]. While adult human cardiomyocytes are large, binucleated cells, iCMs are often small, rounded and mononucleated [164]. Other differences between iCMs and their primary human counterpart include, more positive maximum diastolic potential and a slower upstroke velocity in adult human cardiomyocytes, in comparison to iCMs [163]. Moreover, iCMs display spontaneous beating, unlike mature ventricular cardiomyocytes that only beat upon excitation [152, 165]. In order to address these dissimilarities, multiple approaches have been used in literature, and are detailed in Chapter 2, subsection 2.6.1.1. Briefly, one of the first approach tested was performing long term culture of iCMs [164]. Early experiments using EB-based differentiation to obtain iCMs, where EBs were kept in culture for up to 60 days, showed structural alterations in the cells, such as changes in sarcomere organisation, increase in cell size, and a notable reduction in proliferation [166]. Similarly, monolayer differentiation approaches with long term cultures (3 to 4 months) also yielded additional maturation features such as increased cell size, myofibril alignment, elongation and improved contractile performance, calcium

handling and action potential amplitudes [167]. Furthermore, longer term studies (1 year) with iCMs have reported gradual increases in the ratio of MLC2V (ventricular cardiomyocyte marker) to MLV2A (atrial cardiomyocyte marker), in addition to increased sarcomere organisation [168]. However, the time required for iCMs to reach maturation comparable to adult cardiomyocytes is too long, with often only a small subset of cells expressing the maturation [169]. Co-culture with support cell types have also shown positive impact on iCM maturation. Some reported cell types include fibroblasts [178], MSCs [436], a combination of fibroblasts and endothelial cells [313] etc.

Some other commonly used strategies of improving iCM maturation also include the use of metabolic and hormonal cues. After birth, the levels of thyroid hormone tri-iodothyronine (T_3) is known to rise sharply, and this hormonal axis is essential for the normal functioning of the heart [170]. Yang *et al.* demonstrated strongly improvement in iCM maturation on treatment with T_3, with an increase in cell size, sarcomere length, contractile force, calcium-transient kinetics, mitochondrial biogenesis and mitochondrial respiration capacity [171]. Additionally, glucocorticoids [172], a combination of glucocorticoids and T_3 [173], as well as angiotensin II [174] have been used by several studies to demonstrate improved structural and functional maturation in iCMs. Furthermore, in terms of metabolic maturation, fatty-acid rich media [175, 176] and glucose deprivation [177] have shown notable improvement in metabolic and structural properties of iCMs. In addition to metabolic and hormonal cues, electrical coupling is also a critical approach used to improve iCM maturation. In the myocardium, effective cell-to-cell electrical coupling via gap junctions is crucial for electrical propagation. In immature cardiomyocytes (such as iCMs), the components of the intercalated disc complex, including connexin 43 (Cx43; encoded by GJA1) are distributed circumferentially [437]. However, Cx43 gradually polarises to the ends of the cardiomyocyte during *in vivo* cell maturation. Although this polarisation phenomenon is not observed in traditional 2D culture of iCMs, it can be induced by spatially restricting the cells, for example, with patterned adhesive substrates [438], cyclic uniaxial mechanical stretching [179] or with the use of micro gradient or micro grooved patterned surfaces [180, 181]. Another interesting avenue within the realm of

mechanical maturation of iCMs include the use of biomaterials with stiffness properties comparable to native human myocardium (~10 kPa) [182]. Using substrates of over 1 GPa and 1 MPa stiffness, Herron *et al.* showed that the softer substrates induced an upregulation in the expression of ion-channel genes (SCN5A and KCNJ2) and in the levels of associated sodium currents and cellular hypertrophy [183]. However, while mechanical stimulation contributes to increased iCM maturation and contraction through hypertrophic pathways, achievement of cell-cell coupling and improved calcium handling requires electrical stimulation (ES).

In recent years, ES has emerged as one of the most effective techniques for inducing maturation of cardiomyocytes *in vitro*. Typically, ES setups are straightforward in design, employing two electrodes to deliver bulk field stimulation to the culture container, with electrical impulses directed through the culture media [184]. Electrodes commonly consist of either carbon rods or platinum wires, and optimising parameters such as stimulation duration, voltage, and frequency has been shown to enhance cell response within a specific biomaterial system [184]. Over two decades ago, Radisic *et al.* demonstrated that ES significantly improved cell alignment and enhanced sarcomere structure in 2D culture of rat neonatal cardiomyocytes [185], by employing pulsatile rectangular 5 V/cm waves, at 2 ms pulse width and 1 Hz frequency, which are characteristic to the native myocardium [185, 186]. Since, numerous 2D studies have employed ES on cardiomyocytes, to show improved expression of cardiac transcriptional factors such as GATA4, NFAT3 and NRF-1 [187], robust calcium handling [187, 188] and increased Cx43 expression [189]. An ES regimen involving gradual ramping up of the frequency has been reported by Nunes et al. [14] and Ronaldson-Bouchard *et al.* [16] (referred to as 'intensity training') reportedly demonstrating remarkable structural maturity in iCMs [16]. More recent studies using the ramped ES scheme have also achieved chamber-specific (atrial and ventricular) differentiation of iCMs [191]. For ventricular differentiation, the frequency was increased by 1 Hz every week and for atrial differentiation, the frequency was increased by 0.4 Hz daily (from 2 Hz to 6 Hz) [191]. To that end, ES remains at the forefront of efficient techniques to

facilitate iCM maturation, showing great potential towards disease modelling, drug testing, and critically sized construct formation.

After characterising iCMs in Chapter 6 and observing significant improvement in the structural and functional properties of iCMs in Chapter 7 (when in co-culture with iMacs), in this Chapter, further improvement of iCM maturity is explored. iCMs are subjected to ES and improvement in their maturation is assessed. Since iMacs also undergo the same ES scheme in a co-culture setting, iMacs as well as iCM/iMac co-cultures were subjected to the optimised ES regime to evaluate phenotypic and functional changes. Finally, ES was employed on co-cultures of iCMs and iMacs to analyse calcium handling properties of iCMs.

8.3. Materials and Methods

8.3.1. Experimental design

Two iPSC lines – SFCi55 and zombie green tagged SFCi55 (ZGiPSCs) – were expanded. SFCi55 iPSCs were used to generate iCMs and ZGiPSCs were used to generate iMacs. A carbon electrode-based custom built bioreactor was used to generate the ES. Briefly, the bioreactor comprises of carbon electrodes attached to the lid of a 6-well plate, which is also attached to a waveform generator and an oscilloscope (detailed description in section 8.2.2). Delivering ES with physiologically relevant parameters has been well explored; and studies suggest that iCMs return back to their original beating frequency, as soon as the ES stops [395]. Hence, we employed two different ES regimes. Both the ES regimes used were biphasic pulsatile waves, with ±2.5 V voltage, 2 Hz frequency, 2 ms pulse width and the first pacing regime (iCM_PR1) was delivered for 1 hour every day for 5 days, while the second pacing regime (iCM_PR2) was delivered continuously for 5 full days. After assessing the differences between periodic and continuous pacing regimes on iCM maturity (by expression of genes such as TNNT2, ratio between MYH7 and MYH6 and SERCA2), the optimal pacing regime selected was used to stimulate iMacs. Electrically stimulated iMacs were examined for their

expression of phenotypic (TGB1, MRC1, IL10, NOS2 and TNF) and functional genes (MMP9, CCR2, VEGFA, TRPV4, AREG and GJA1). Finally, co-cultures of iCMs and iMacs were also subjected to the optimal ES scheme and the cells were assessed individually for their phenotype, genotypic profile and calcium handling functions. Co-cultures were also treated with the drugs carbachol, isoproterenol and caffeine, to assess the robustness of their response (Figure 8.1).

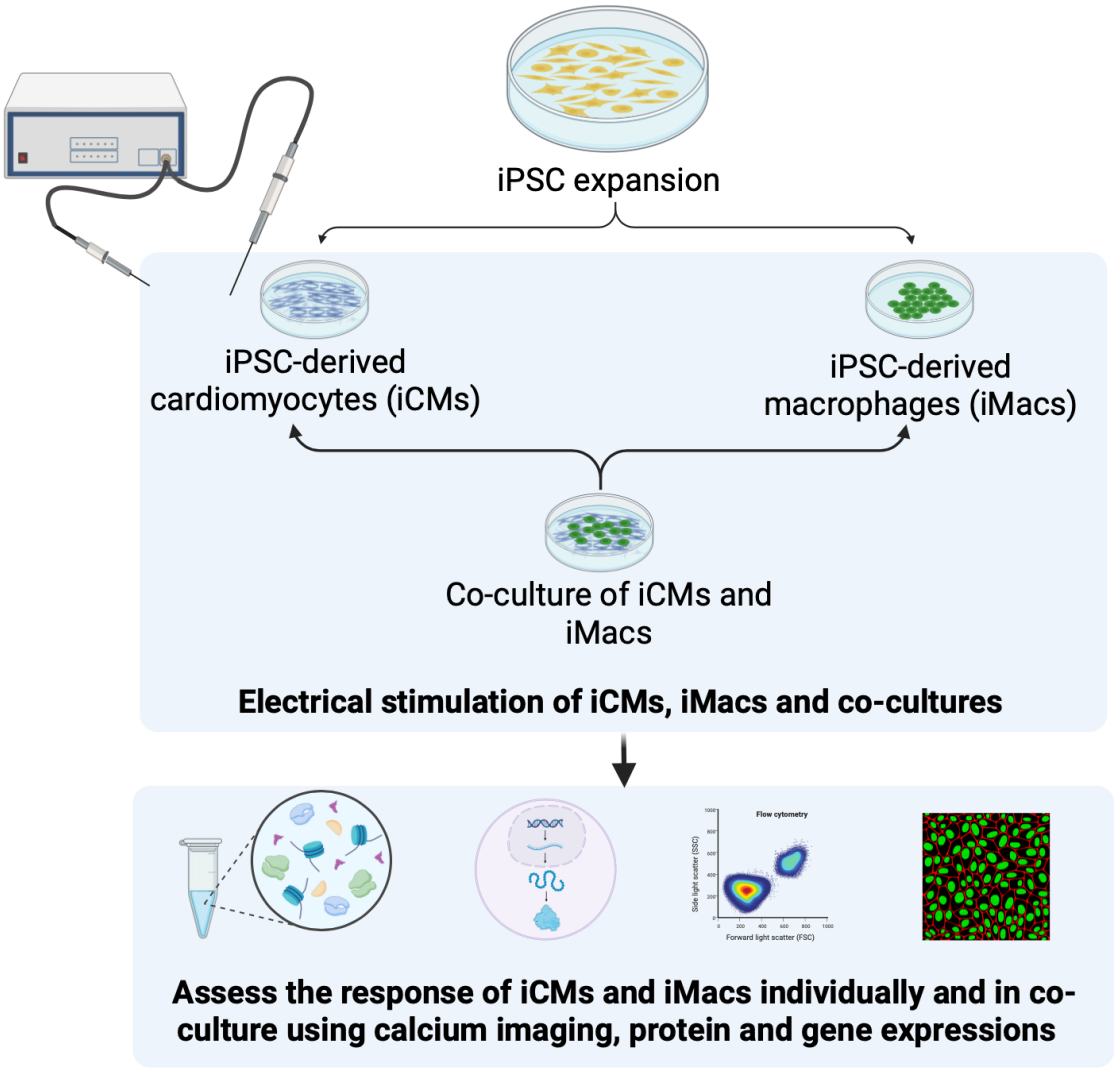

Figure 8.1: Graphical abstract. iPSCs were expanded and differentiated to obtain iCMs and iMacs. iCMs, iMacs and co-cultures of iCMs and iMacs were subjected to electrical stimulation. The cells were characterised using gene and protein expressions, using techniques such as RT-qPCR, ELISA, immunofluorescence imaging and calcium imaging.

8.3.2. Electrical Stimulation bioreactor setup

The bioreactor set up to generate ES was custom-built for previous studies in the lab [439]. Schematic representation of the bioreactor set up in Figure 8.2. Briefly, a 1 mm hole was drilled one end of each of the twelve 22 mm long cylindrical carbon electrode, to secure a platinum-iridium wire (Figure. 8.2 (a)). The platinum wires and carbon electrodes were kept in place by immobilising them using PDMS Sylgard^{TM} 184, using a 3D printed mould (Figure 8.2 (a i - vi)). A lid adaptor that fits into the lid of a 6-well plate was 3D printed (Figure 8.2 (b i, ii)). The lid adaptor allowed the attachment of platinum-iridium wires and carbon electrodes, through PDMS fillers (Figure 8.2 (b i, ii)). The carbon rod electrodes were kept at 15 mm distance between each other and facilitated the generation of ES to a 6-well plate (Figure 8.2 (b iii, c)). The lid adaptor attached to the lid of the 6-well plate through six screws, and also had spaces in between the electrodes for optical accessibility with both upright and inverted microscopes. A 5 mm gap between the adaptor and the lid was accounted for holding the wiring. The source ground and positive wires connected externally to a bread board where a waveform generator (RSDG2000X, Radionics) and an oscilloscope (RSDS 1052 DL +, Radionics) were also connected. (Figure 8.2 (d)). To perform live imaging of samples, a plate stand was 3D printed to mount the 6-well plate and a Dino-lite digital microscope (RS Pro) was used (Figure 8.2 (b iii)).

8.3.3. Electrical stimulation on iCMs, iMacs and iCM/iMac co-cultures

As previously mentioned (Chapter 7), iCMs were generated using SFCi55 iPSCs and iMacs were generated using ZGiPSCs. For providing ES to iCMs, iCMs were differentiated and kept in culture for 20 to 25 days in 6-well plates, before subjecting them to two different pacing regimes (as mentioned in 8.2.1). Using their expression of maturation genes as a readout, the optimal ES regime was chosen. Next, to stimulate iMacs, pre-macs (non-adherent macrophage precursors collected from 14 days of the differentiation) were plated on 6-well plates and allowed to attach for 48 hours, after which, iMacs were subjected to the optimised ES regime. Similarly, for iCM/iMac co-cultures, iMacs were added to iCM cultures at a 1:5 ratio of iMacs to iCMs. After 48

hours of iMac addition, the co-cultures were treated with the optimised ES regime. For pacing regime 1 (PR1; 1 hour of pacing every day), fresh media was added every day before the stimulation and for pacing regime 2 (PR2; 5 full days of pacing), fresh media was added on day 3 of stimulation. For immunofluorescence imaging iCMs were differentiated on 12 mm glass cover slips. On the day of the ES, the glass cover slips were attached to the bottom of the 6-well plates by using 2% agarose to keep the coverslips in place. Co-cultures were also performed on glass cover slips to perform immunofluorescence imaging.

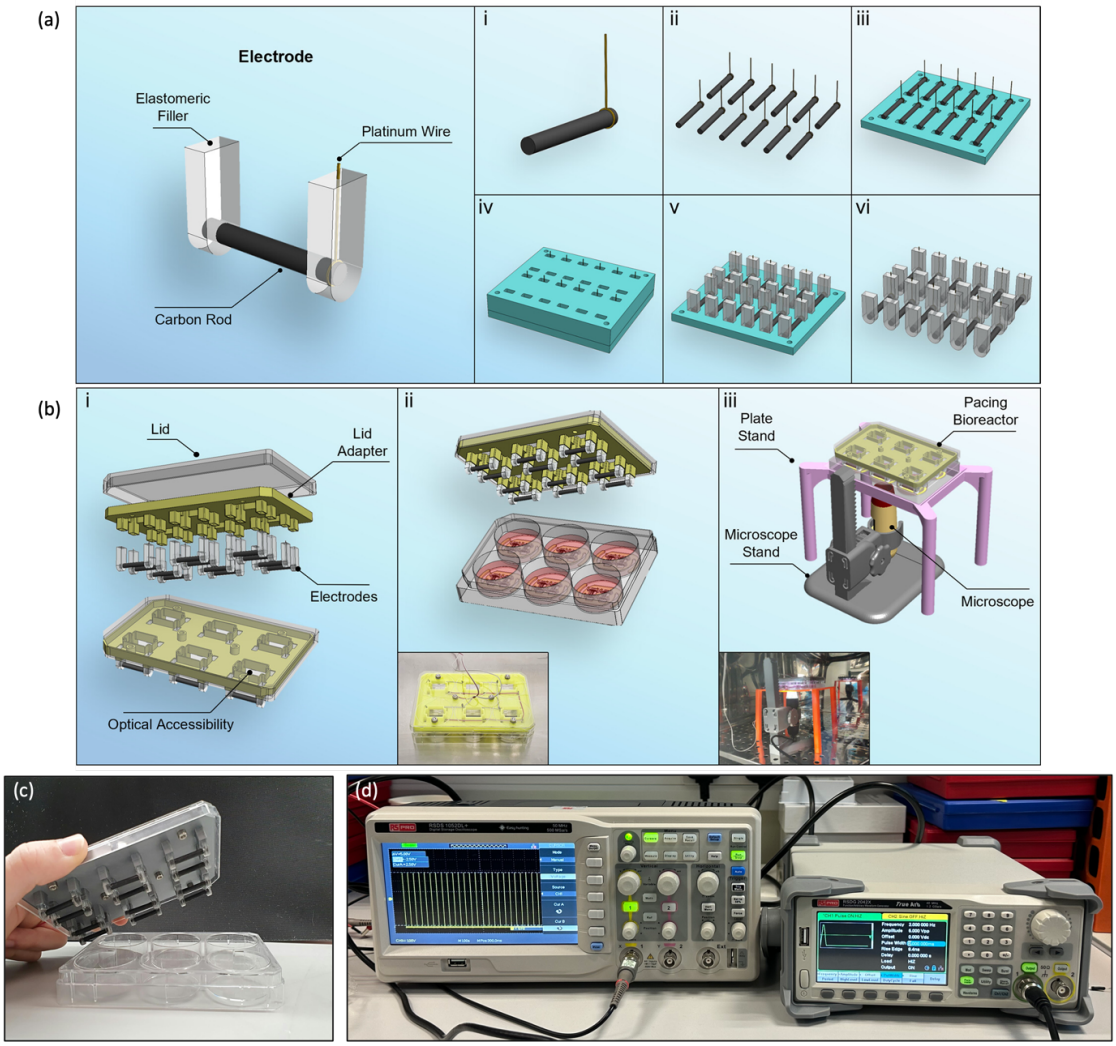

Figure 8.2: Representation of the electrical stimulation set up, modified from Solazzo *et al*. [439]. (a) Schematic representation of the carbon electrode, attached to platinum wires, kept in place using PDMS Sylgard^{TM} 184. (a i to vi) Schematic representation of the fabrication of the attached carbon electrode and platinum wire system (b i) Schematic representation of the lid of a 6-well

plate, the 3D printed lid adaptor and the electrodes. The 3D printed lid adaptor also facilitates live imaging, by virtue of the empty spaces built into the adaptor. (b ii, iii) Schematic representation of the entire ES set up, with the plate stand and the digital microscope. (c) Image of the 6-well plate with the ES bioreactor lid. (d) Image of the oscilloscope (left) and waveform generator (right).

8.4. Results and discussion

8.4.1. The gene expression profile of iCMs indicate maturation when subjected to 5 days of electrical stimulation

Achieving improved maturation of iCMs has been a challenge in the field of cardiac regenerative medicine for decades. Out of a multitude of approaches used to improve iCM maturation, in this study, the effect of periodic and continuous electrical stimulation was explored. Using a commercially available ES set up, Nitsan *et al.* reported that iCMs revert back to their original beat rate as soon as the stimulation stops [395]. The duration of the ES reported by Nitsan *et al.* was only seconds long (30 seconds maximum), which led the research question in this Chapter, concerning whether continuous electrical stimulation could yield more favourable outcomes when compared to periodic stimulation. Although the most common practise for maturing iCMs includes the use of a ramped ES regimen [14], more physiologically accurate ES was explored in this chapter. Similar to the characteristics of native myocardium [185, 186], biphasic pulsatile waveforms of 2 ms pulse width, ± 2.5 V and 2 Hz frequency was used. Previous studies also suggest that for 2D cultures, delivery of ES for 5 days is sufficient to achieve cardiomyocyte maturation [440]. Hence, for periodic stimulation, iCMs were exposed to ES for 1 hour for 5 days (iCM_PR1) and for continuous stimulation, iCMs were exposed to ES for 5 full days (iCM_PR2) (Figure 8.3 (a)). On assessing the gene expression profiles, iCMs undergoing continuous stimulation, iCM_PR2, were found to express 95.4% more TNNT2 than iCMs (Figure 8.3 (b)). A similar increase in the expression of cTnT (encoded by TNNT2) has been reported by Yoshida *et al.* on ES of iCMs, using pulsatile waves of 1 Hz, 1 V and 20 ms pulse width [441]. Notable upregulations were also seen in the expressions of MYH6 (89.4% higher) and MYH7

(97.5% higher) in iCMs_PR2 (Figure 8.3 (b)). The gene MYH6 encodes α-myosin heavy chain (MHC) and serves as the primary MHC in the adult atrium, while MYH7 is responsible for encoding β-MHC, the predominant MHC in the left ventricle of the adult human heart [382, 383]. Although iCM_PR2 showed a strong upregulation in the expressions of MYH6 and MYH7, iCM_PR1 highly expressed MYH6 (92.3% more than iCMs) and not MYH7. Previous studies report the ratio of MYH7/MYH6 increase with age in humans [384], as the levels of MYH6 decreases [385]. This trend is also reported in extended culture conditions of iCMs [386] as well as in engineered heart tissues [16]. Notably, the MYH7/MYH6 ratio was 62.7% upregulated in iCM_PR2 compared to iCMs (Figure 8.3 (c)), highlighting improved iCM maturity. Additionally, it is well-reported that the initiation of mechanical contraction in cardiomyocytes occur due to calcium-induced calcium release [387]. Sarcoplasmic/endoplasmic reticulum calcium ATPase (SERCA) is a key buffer responsible for calcium uptake preceding diastole [388]. The expression of SERCA2 was 97% upregulated in iCM_PR2, compared to iCMs, further highlighting the improvement in calcium handling in iCMs undergoing continuous ES (Figure 8.3 (c)). The expression of GJA1 was found to be comparable between all the groups (Figure 8.3 (c)). Collectively, these findings demonstrate a high upregulation of key genes indicating iCM maturation, when electrically stimulated non-stop for 5 days.

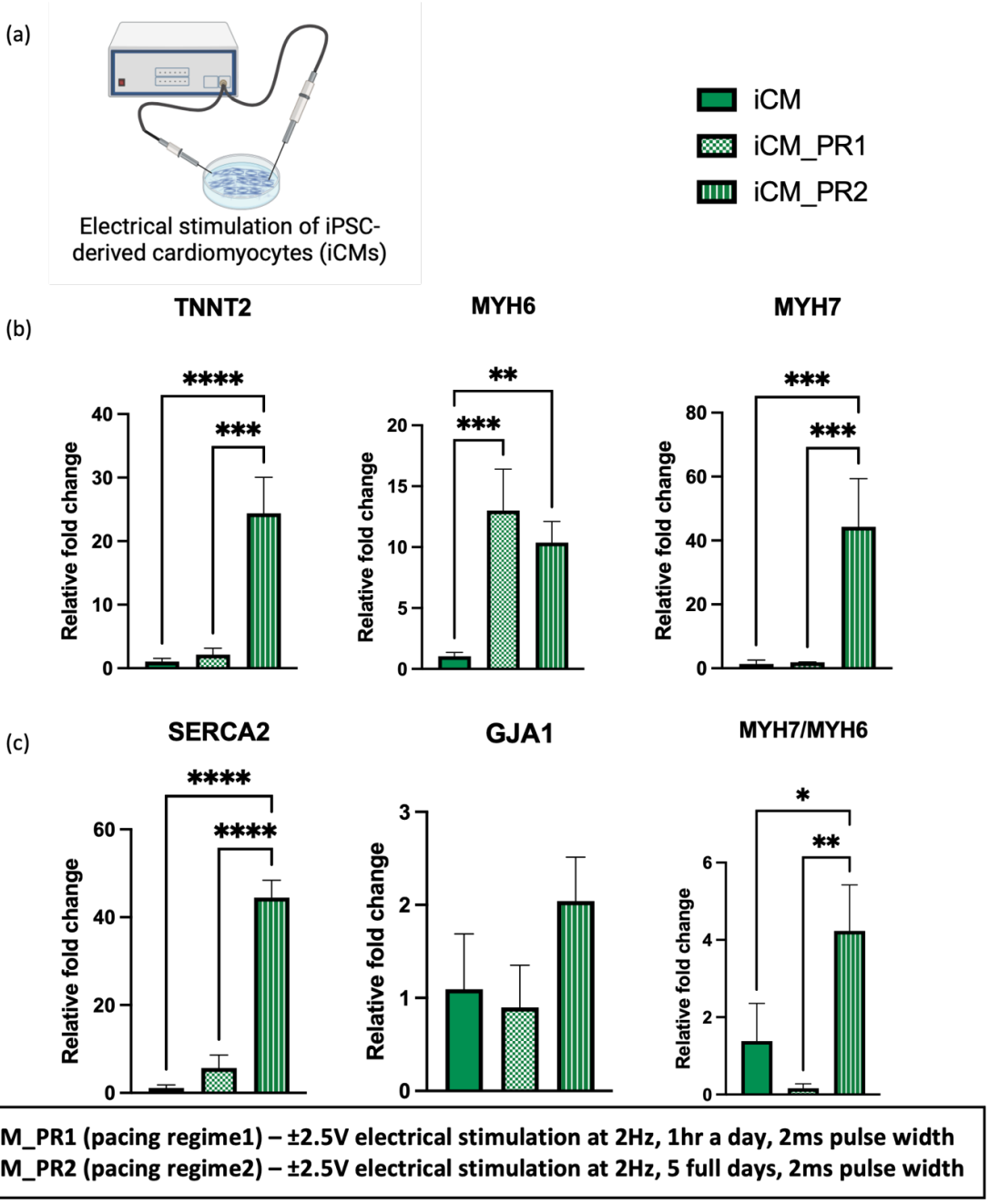

Figure 8.3: Characterisation of electrically stimulated iCMs. (a) Schematic representation of the experimental set up. (b) Expression of the genes TNNT2, MYH6 and MYH7, normalised to unstimulated iCMs. (c) Expression of the genes SERCA2, GJA1 and ratio between MYH7/MHY6, normalised to unstimulated iCMs. Statistical analysis – One-way ANOVA with Tukey's multiple comparison test. * represents P<0.05, ** represents P<0.01, *** represents P<0.001 and **** represents P<0.0001. N = 3 biological replicates for iCMs and 2 biological replicates for iCM_PR1 and iCM_PR2, with each point signifying the average of 3 technical replicates. Fold change of mRNA relative to iCMs in monolayer culture with no electrical stimulation.

8.4.2. iMacs are highly pro-regenerative and functionally active when subjected to 5 days of electrical stimulation

ES of a number of different cell types have been explored, mostly in the context of wound healing and cell migration [442, 443]. An example of cells used in ES studies in the past include dermal fibroblasts which have shown robust expression of pro-healing factors [442, 444]. Additionally, ES has been reported to perform a plethora of functions including increase osteogenic differentiation and cell proliferation [445], increase neurite outgrowth [446] and, in a much broader context, alleviate pain, promote blood circulation and reduce skeletal muscle tension [447]. A range of ES voltage intensities from 0.1 V/cm to 12 V/cm have been tested in various studies to show efficient cell migration, with no significant damage to cells [448-450]. Although ES is recognised as an invaluable tool in regenerative medicine [443], the effect of ES on macrophages is not fully explored. Furthermore, despite the abundance of studies concentrating on ES of iCMs, there is a notable lack of research addressing non-myocytes, such as cardiac fibroblasts and CRMs.

Following the findings reported in section 8.3.1, the ES regime of 5 days of non-stop stimulation was used for further studies, due to the strong expression of maturation genes by iCMs. Since iMacs are also expected to experience the same stimulation in a co-culture setting, the next objective was to assess the response of iMacs to 5 days of ES (iMacs_5d ES) (Figure 8.4 (b)). Notably, upon 5 days of ES, iMacs expressed 82.7% more TGFB1, 84.5% more MRC1 and 79.6% more IL10, in comparison to unstimulated iMacs, displaying a highly pro-regenerative response (Figure 8.4 (a)). The anti-inflammatory response was also highlighted by the downregulation in NOS2 (92%, compared to iMacs) and no significant difference in TNF gene expression (Figure 8.4 (d)). Mccann *et al.* in a pioneering study delivering ES to macrophages (in 1983) reported that, using a conventional DC source for 2 hours (12.7 to 30.5 V/s electric fields), macrophages could be polarised to a pro-regenerative and anti-inflammatory

phenotype [451]. With newer studies moving towards AC sources, Jia *et al.* developed an ES system that delivers 10, 60 and 100 Hz of electric field to THP-1 cells [452]. They reported that 10 and 60 Hz frequencies facilitated an anti-inflammatory phenotype in THP-1 cells, with upregulation of CD206 [452]. ES-induced anti-inflammatory response in THP-1 cells has also been reported by Xu *et al.* [453].

Additionally, genes associated with functional activation of iMacs were also assessed. MMP9 is a key regulator of ECM degradation and regulation of tissue remodeling [368]. In cardiovascular diseases, the deletion of MMP9 has been proven to be beneficial, to facilitate effective tissue remodelling post-MI [370]. In this study, the expression of MMP9 was found to be 91% lower in iMacs undergoing 5 days of ES (Figure 8.4 (c)), indicating homeostasis and a potential for robust matrix production [368]. Although the direct impact of electrically stimulated macrophage-derived MMP9 has not been reported, a combinatorial delivery of ES together with a self-assembled tannic acid–siRNA–PVA hydrogel matrix has shown to cause a remarkable decrease in MMP-9 levels and other pro-inflammatory cytokines, thereby promoting macrophage polarisation and helping repair chronic diabetic wounds in rats [454]. Furthermore, iMacs_5d ES also exhibited 83.3% upregulation of CCR2, 36% upregulation of TRPV4 and 72.8% upregulation of GJA1 (Figure 8.4 (c)), demonstrating potential activation of gap junctions. These findings are particularly interesting in the context of the myocardium, as both the $CCR2^{+}$ and $CCR2^{-}$ macrophages express TRPV4 and GJA1 in abundance [21, 372]. No significant difference was noted in the expressions of VEGFA and AREG, between iMacs_5d ES and untreated iMacs (Figure 8.4 (c)). Overall, this study is first of its kind, examining the effects of providing macrophages (iMacs) with cardiac-specific ES. These results not only reiterate the highly anti-inflammatory phenotype of iMacs under ES, but also underline the safety of delivering ES to iMacs.

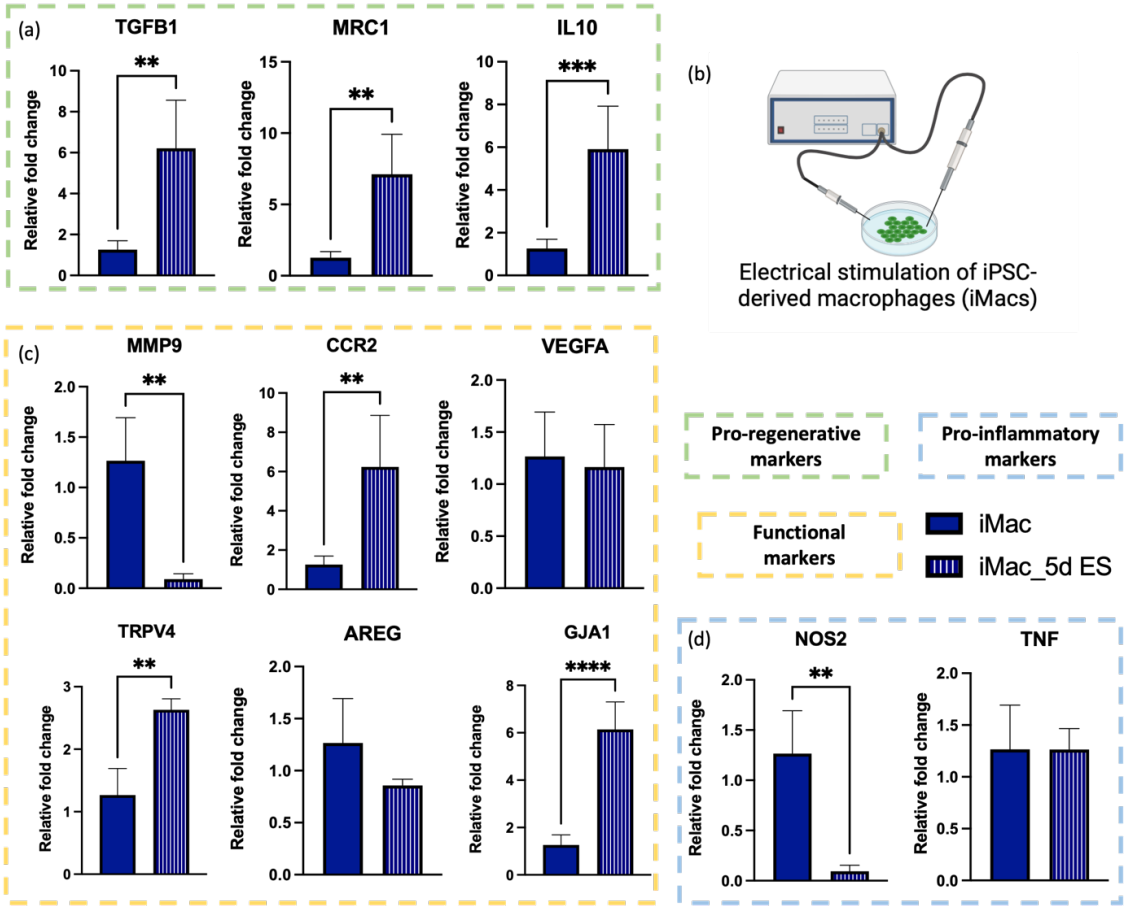

Figure 8.4: Characterisation of electrically stimulated iMacs. (a) Expression of a set of pro-regenerative genes. (b) Schematic representation of the experimental set up. (c) Expression of a set of macrophage functional genes. (d) Expression of a set of pro-inflammatory genes. Statistical analysis - Student T test with Welch's correction. ** represents P<0.01, *** represents P<0.001 and **** represents P<0.0001. N = 3 biological replicates, with each point signifying the average of 3 technical replicates. Fold change of mRNA relative to iMacs with no electrical stimulation.

8.4.3. iMacs separated from electrically stimulated iCM/iMac co-cultures remain highly quiescent, with notable functional activation.

After individually characterising electrically stimulated iCMs and iMacs, co-cultures of iCMs and iMacs were subjected to 5 days of ES (Figure 8.5 (a, e)). The first set of

assessment was performed on iMacs in co-culture with iCMs, to evaluate the improvement in functional ability of iMacs. While non-stop ES for 5 days caused an upregulation in the expression of pro-regenerative genes (Figure 8.4 (a)), iMacs were found to be highly quiescent when in co-culture with iCMs and exposed to the same ES (Figure 8.5 (b)). Quiescence is a key feature of TRMs, in order to maintain tissue homeostasis [299]. Additionally, Li *et al.* demonstrated that macrophage remain quiescent when exposed to cardiomyocyte-derived secreted factors, using cardiomyocyte and macrophage cell lines [367], consistent with the findings reported in this chapter. The quiescence of iMacs could also be seen in their expression of pro-inflammatory genes such as NOS2 and TNF (91.6% downregulation in comparison to iMacs) (Figure 8.5 (c)). Although ES of iMacs in co-culture with iCMs yielded a quiescent phenotype in iMacs, strong functional activation was also noted. Compared to untreated iMacs, a 77% upregulation was found in VEGFA expression, 97.5 % upregulation in AREG expression, and a 92.8% upregulation was found in GJA1 (Figure 8.5 (d)), all genes of critical importance in CRMs [21, 142, 372, 374] . As mentioned previously, both the $CCR2^{+}$ and $CCR2^{-}$ macrophages express AREG and GJA1 in abundance [21, 372, 374]. Additionally, Revelo *et al.* demonstrated the highly angiogenic ability of CRMs (with upregulation of VEGFA) and also highlighted the same angiogenic potential *in vitro*, by culture CRMs derived from rat myocardium with HUVEC cells [142]. It is worth noting that, phenotypically and functionally, iMacs and electrically stimulated iMacs_co-culture were similar, except for the highly upregulated expressions of VEGFA and AREG in stimulated iMacs_co-culture. Moreover, on examining electrically stimulated iMacs for their expression of CRM-specific and cardiac developmental genes, the expressions were either lower than unstimulated iMacs_co-culture, or not significantly different from unstimulated iMacs_co-culture (Appendix. Figure. 1). Hence, electrically stimulated iMacs_co-culture were not examined for their expression of cardiac developmental and CRM-specific genes.

Furthermore, the secretome from iMacs in co-culture with iCMs, with and without ES were collected and assessed for the presence of pro-inflammatory cytokines. While negligible amount of TNFα was found in the secretome of both the test conditions, a

94.1% downregulation of IL6 and 97.1% downregulation of IL10 was found in electrically stimulated iMac_co-culture compared to unstimulated co-cultures. Interestingly, using an ES scheme of 150 mV/mm for 2 hours, Hoare *et al.* reported an upregulation in TNFα in the secretome of BDMs [455]. Regardless, in this chapter, no inflammatory response was found, which in part can be associated with the synergistic effect of iMacs being in physical contact with iCMs, as well as the potential anti-inflammatory factors released by iCMs. Taken together, these findings further highlight the phenotypic quiescence of electrically stimulated iMacs in co-culture with iCMs, with remarkable functional activation, exhibiting high VEGFA, AREG and GJA1 expressions. These findings underline the benefits of ES in conjunction with iCM culture for functional improvement of iMacs.

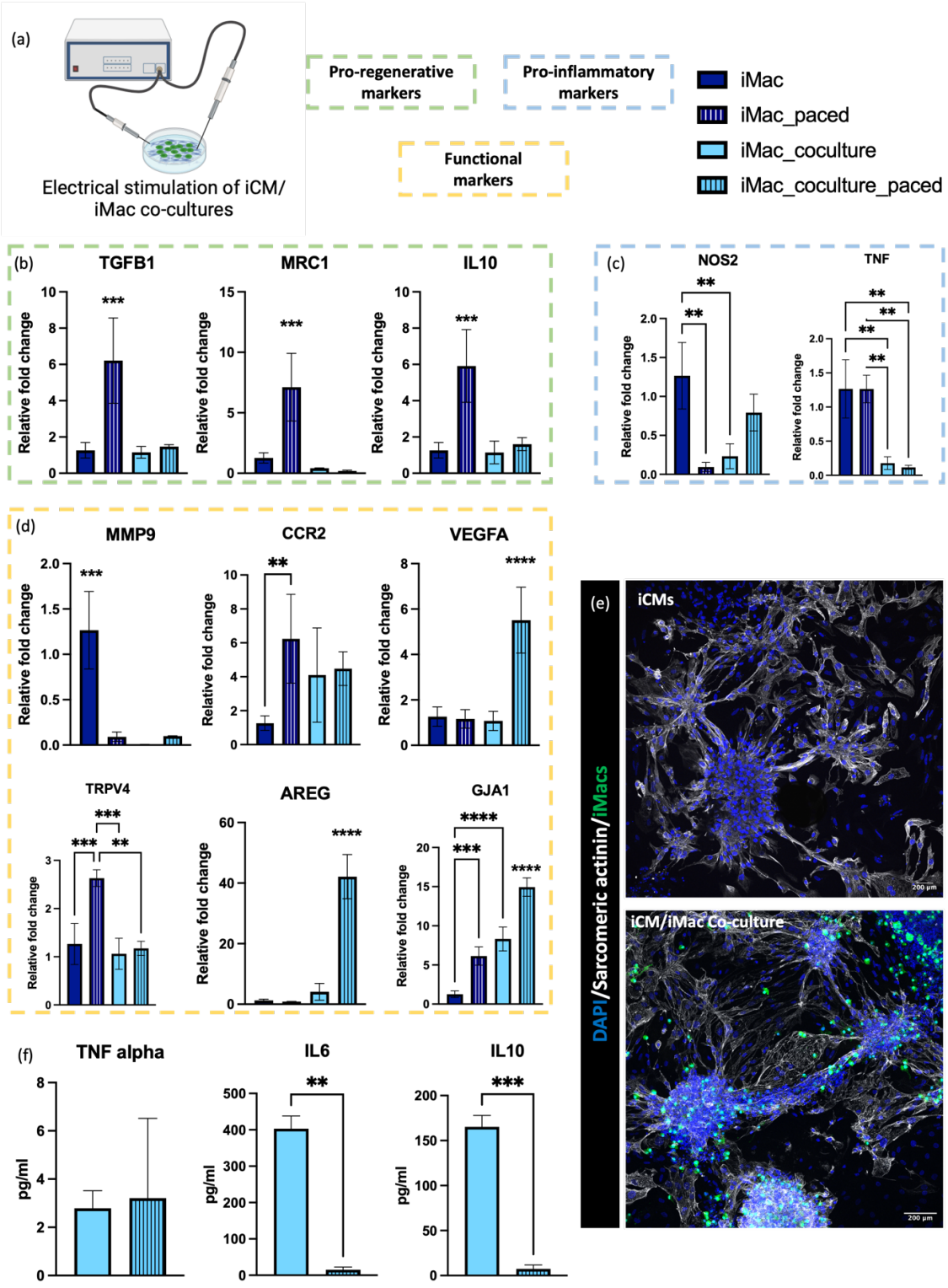

Figure 8.5: Characterisation of electrically stimulated iMacs in co-culture with iCMs, compared to of electrically stimulated iMacs and unstimulated iMacs as well as unstimulated iMacs in co-culture with iCMs. (a) Schematic representation of the experimental set up. (b) Expression of a set of pro-regenerative genes. (c) Expression of a set of pro-inflammatory genes. (d) Expression

of a set of macrophage functional genes. (e) Representative images of iCMs and iCM/iMac co-culture stained with sarcomeric actinin. Scale bar – 200 µm. iCMs generated using SFCi55 iPSCs and iMacs generated using Zombie green tagged SFCi55 iPSCs. Statistical analysis - Student T test with Welch's correction. * represents P<0.05, ** represents P<0.01 and *** represents P<0.001 and **** represents P<0.0001. N = 6 biological replicates for iMacs and 3 biological replicates for other groups, with each point signifying the average of 3 technical replicates. Fold change of mRNA relative to iMacs with no electrical stimulation.

8.4.4. iCMs FACS sorted from electrically stimulated iCM/iMac co-cultures show an elongated morphology and functional maturity with improved beat rate and calcium handling.

Following the observation of excellent functional activation in electrically stimulated iMacs_co-culture, the next focus was on analysing the maturation of electrically stimulated iCMs in co-culture with iMacs (Figure 8.6 (a)). After 5 days of ES, iCMs and iCM in co-culture with iMacs showed improved beat rates, with very little variance (Figure 8.6 (b)). Notably, paced iCMs displayed a 27.5% upregulation in the beat rate (87 ± 6 bpm) compared to paced co-cultures (63 ± 6 bpm) (Figure 8.6 (b)). Additionally, the beating of the electrically stimulated cells was highly synchronous. Regardless, both paced iCMs and paced co-cultures exhibited physiologically relevant beat rates for adult human hearts, which is 60 – 100 bpm [403]. Next, the expressions of cardiomyocyte maturation genes were assessed. As previously shown (Figure 8.3 (b, c)), 5 days of ES resulted in a notable increase in the iCM maturation genes of evaluated. In comparison, paced iCMs in co-culture exhibited comparable levels of TNNT2 (94.5% more than unstimulated iCMs) (Figure 8.6 (c)). Similarly, the ratio of MYH7/MYH6 was also comparable between paced iCMs and paced iCMs in co-culture, with 71.7% upregulation compared to iCMs (Figure 8.6 (c)). However, the expression of SERCA2 was 79.6% higher in paced iCMs than paced iCMs in co-culture (Figure 8.6 (c)). SERCA2t expression as comparable between electrically stimulated iCMs in co-culture and unstimulated iCMs in co-culture (Figure 8.6 (c)).

In Chapter 7, significant elongation was observed in iCMs when in co-culture with iMacs (refer to Figure 7.6 (b, c)). With the aim of evaluating whether electrically stimulated iCMs and co-cultures displayed elongation in the cell morphology, they were stained for Sarcomeric actinin (Figure 8.5 (e)) and the aspect ratio of the cells were calculated. Aspect ratio is the ratio between the major and minor axis of a cell; the aspect ratio of a circle would be 1 and that of elongated cells would be more than 1. Electrically stimulated iCMs and co-cultures exhibited a similar aspect ratio as unstimulated iCMs in co-culture with iMacs (Figure 8.6 (d)), indicating robust cell elongation. On assessing the morphology of iCMs, the aspect ratio evidently increased by 52.6% upon ES (increase from 1.18 ± 0.24 to 2.39 ± 0.46) (Figure 8.6 (d)). Interestingly, iCMs in co-culture with iMacs did not show statistically significant upregulation in the aspect ratio upon ES (2.86 ± 0.61 for unstimulated co-cultures; 3.15 ± 0.75 for stimulated co-cultures) (Figure 8.6 (d)).

Continuous ES evidently yields excellent responses in iCM maturation gene expressions, morphology (elongation) and beat rate. However, it was of interest to assess whether iCM/iMac co-cultures need the entire 5 days of ES to exhibit robust calcium handling responses. Hence, iCM/iMac co-cultures were electrically stimulated for 2 days and the beat rate and calcium handling functions of iCMs were evaluated. After 2 days of ES, iCMs displayed a beat rate of 53 ± 7 bpm while paced iCM/iMac co-cultures displayed a robust 72 ± 2 bpm, with very little variability, reiterating the exceptional ability of iMacs to facilitate synchronous beating of iCMs (Figure 8.6 (e)). Beat rate of 2 day paced co-cultures were not only in the range of adult human heart [403], but also significantly higher (54.1% more) than unstimulated co-cultures on the same time point (Figure 8.6 (f)). Furthermore, the intensity of calcium signals (F/F0) transmitted within iCMs and iCM/iMac co-cultures was examined. This quantification involved finding the ratio between the highest fluorescence intensity and the bassline intensity. On day 25 of the culture, iCMs displayed 18.75% higher intensity in calcium signalling than co-cultures (Figure 8.6 (g)). However, after 2 days of ES, the intensity of calcium signalling between iCMs and co-cultures were found to be comparable, and 83% higher than unstimulated co-cultures (Figure 8.6 (g)).

Finally, the response of electrically stimulated (for 2 days) iCMs to the exposure of known drugs, was explored. iCMs are known to respond to several compounds or drugs [407] and previous studies have documented a reduction in beat rate of iCMs on treatment with carbamylcholine (carbachol) [409], and an increase in beat rate with isoproterenol [412] and caffeine [413] treatments. On treating electrically stimulated samples with carbachol, the beat rate was found to be 48 ± 27 bpm for iCMs and 43 ± 6 bpm for iCMs in co-culture with iMacs (Figure 8.6 (h)). Next, isoproterenol treatment increased the beat rate to 50 ± 21 bpm for iCMs and 68 ± 3 bpm for co-cultures (Figure 8.6 (h)). Furthermore, caffeine treatment was found to increase the beat rate to 61 ± 22 bpm for iCMs and 87 ± 3 bpm for co-cultures, yielding a 30.1% increase in co-cultures (Figure 8.6 (h)). Nevertheless, it was worth noting that 2 days of ES was found to yield robust responses in iCMs in co-culture with iMacs, with notably low variability on treatment with carbachol, isoproterenol and caffeine, while iCMs showed high variability in the beat rate (Figure 8.6 (h)).

These observations emphasise that while iCMs remain fairly immature even with 2 days of ES, iCMs in co-culture with iMacs show improved maturation, comparable to the maturation achieved after 5 days of ES, in terms of their gene expression profile and elongated morphology. Moreover, with 2 days of ES, iCMs in co-culture with iMacs also carry out robust calcium handling functions. Taken together, these results highlight the potential of using iMacs as an excellent support cell type to improve iCM maturation and function, by enhancing synchronous beating, increasing structural maturation (by facilitating elongation), improving calcium handling and upregulating the expression of maturation genes.

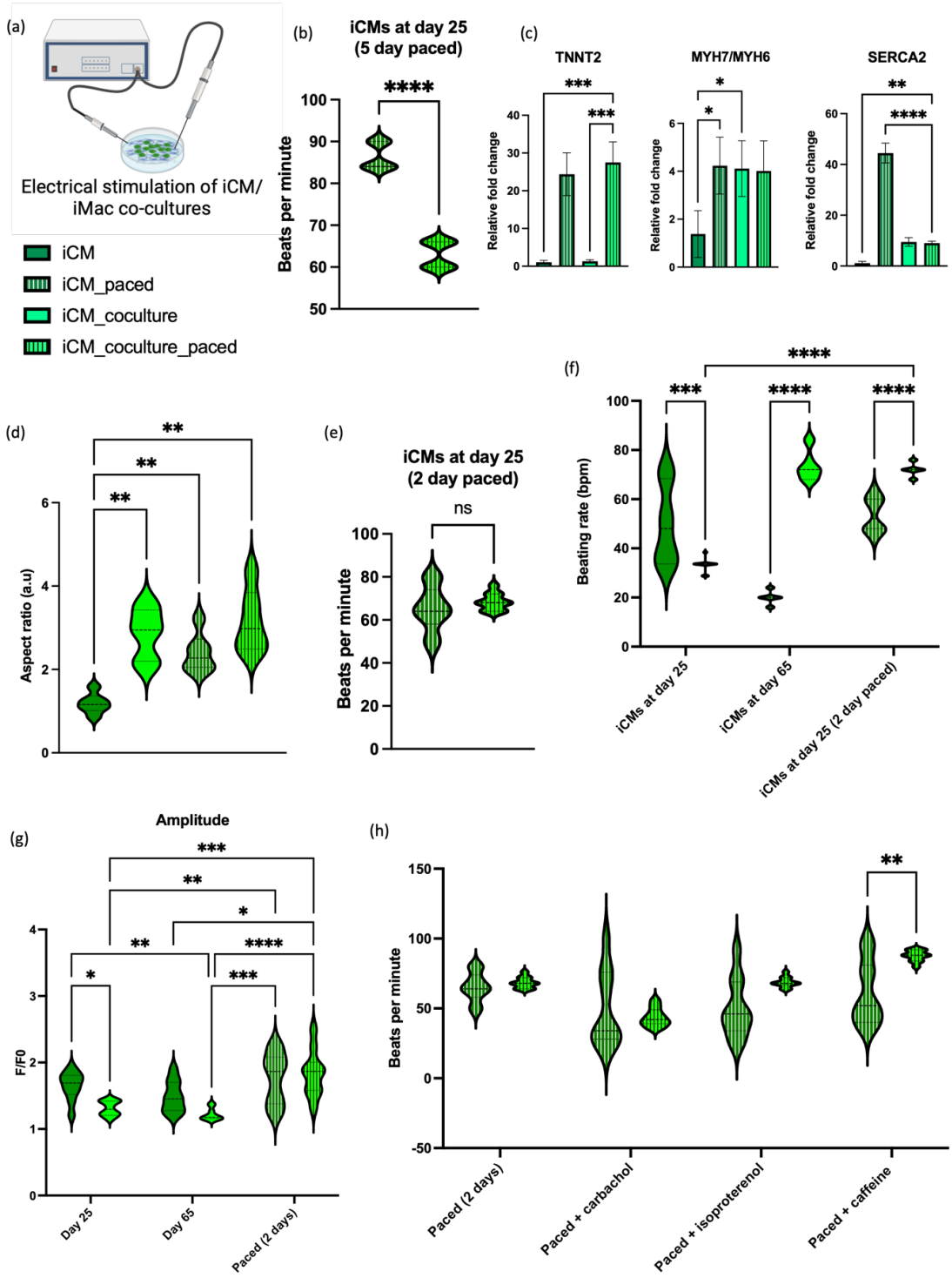

Figure 8.6: Characterisation of electrically stimulated iCMs in co-culture with iMacs, compared to of electrically stimulated iCMs and unstimulated iCMs as well as unstimulated iCMs in co-culture with iMacs. (a) Schematic representation of the experimental set up. (b) Quantified beat rate of iCMs and co-cultures after 5 days of ES. (c) Expression of a set of cardiomyocyte maturation genes. (d) Aspect ratio of iCMs and co-cultures, with and without 5 days of ES. (e) Quantified beat rate of iCMs and co-cultures after 2 days of ES. (f) Quantified beat rate of iCMs

and co-cultures at day 25, day 65 and after 2 days of ES. (g) Intensity (F/F0) of calcium signalling by iCMs and co-cultures at day 25, day 65 and after 2 days of ES. (h) Quantified beat rate of iCMs and co-cultures in response to treatment with carbachol, isoproterenol and caffeine, after 2 days of ES. Statistical analysis - Students T test with Welch's correction for (b and e); One-Way ANOVA with Tukey's multiple comparison for (c and d); Two-way ANOVA with Tukey's multiple comparison for (f, g and h). * represents $P<0.05$, ** represents $P<0.01$ and *** represents $P<0.001$ and **** represents $P<0.0001$. N = 3 biological replicates, with each point signifying the average of 3 technical replicates, for (c). Fold change of mRNA relative to iCMs in monolayer culture. N = 8 technical replicates, with each point signifying the average of 9 different regions of a well, for (b, e, d, f and h).

8.5. Conclusion

The primary objective of this study was to address the limitation of poor iCM maturity in *in vitro* cultures, rendering them inept to represent adult human cardiomyocytes [163]. In order to achieve improvement in iCM maturity, electrical stimulation (ES) was chosen, as over 2 decades of research backs the efficacy of this approach [185]. With the interest in this study predominantly coming from the idea of fabricating an *in vitro* model of the myocardium, the effect of ES on iCMs, iMacs and iCM/iMac co-cultures were thoroughly investigated, making this study unique and novel.

First, the impact of periodic and continuous ES on iCMs was explored. The study adopted a physiologically accurate ES regimen resembling native myocardium characteristics. Periodic stimulation involved exposure to ES for 1 hour daily for 5 days, while continuous stimulation encompassed continuous ES for 5 full days. The gene expression profiles revealed a remarkable 95.4% increase in TNNT2 expression in iCM_PR2, along with significant upregulation in MYH6, MYH7, and SERCA2, demonstrating enhanced maturation and improved potential for calcium handling. After having optimised the ES regime for further experiments, the study delved into the pro-regenerative and functional responses of iMacs to 5 days of ES. In a pioneering exploration, iMacs exhibited an high upregulation in the expressions of TGFB1, MRC1 and IL10, indicating a highly pro-regenerative response. Furthermore, functional activation markers,

including MMP9, CCR2, TRPV4, and GJA1, were notably upregulated, demonstrating the multifaceted impact of ES on iMacs. These findings not only reiterated the anti-inflammatory phenotype of iMacs under ES but also highlighted the safety of delivering ES to iMacs.

Subsequent investigations involved co-cultures of iCMs and iMacs subjected to 5 days of ES. The examination of iMacs from electrically stimulated co-cultures revealed that they remained highly quiescent, expressing pro-inflammatory genes at significantly reduced levels. However, these iMacs demonstrated exceptional functional activation, emphasising high VEGFA, AREG, and GJA1 expressions. The secretome analysis further validated the phenotypic quiescence of electrically stimulated iMacs in co-culture, reinforcing the benefits of ES in conjunction with iCM culture for functional improvement of iMacs.

The focus then shifted to the evaluation of maturation of electrically stimulated iCMs in co-culture with iMacs. After 5 days of ES, iCMs exhibited improved beat rates, comparable maturation gene expressions to paced iCMs, and robust cell elongation. Interestingly, iCMs in co-culture with iMacs achieved significant elongation in cell morphology without the requirement of ES, highlighting the effect of iMacs on facilitating iCM elongation. Importantly, the study demonstrated that iCM/iMac co-cultures exhibited robust calcium handling responses even after 2 days of ES, showcasing the potential for accelerated maturation. The study concluded with drug response assessments, revealing that iCMs in co-culture with iMacs displayed exceptional maturation and reduced variability in response to known drugs, even after 2 days of ES. This highlighted the superior maturation achieved in iCMs in co-culture compared to standalone iCMs. In summary, the study provides a comprehensive understanding of the impact of ES on iCMs and iMacs individually and in co-culture. The results underline that 5 days of ES remarkably improves iCM maturity, while the addition of iMacs into iCM cultures brings about a comparable maturation state.

Chapter 9 Fabrication of engineered heart tissues to model healthy and diseased myocardium

9.1. Abstract

Engineered heart tissue (EHT) models have significantly improved our understanding of how cardiac tissue responds to various drugs, in a human-specific context. Although most of the EHT models in existence only focus on cardiomyocytes, or a combination of cardiomyocytes and cardiac fibroblasts, newer studies have also started focusing on other non-myocytes, such as cardiac endothelial cells. Having recognised the importance of macrophages in the myocardium, together with excellent *in vitro* interactions between cardiomyocytes and macrophages reported in Chapters 7 and 8, in this chapter, EHTs with isogenic iPSC-derived cell types - cardiomyocytes (iCMs), cardiac fibroblasts (iCFs), and macrophages (iMacs) were generated. For the first time, CRM-like cells were introduced into EHTs, creating both healthy and early stage activated myofibroblast-mediated models of the myocardium. First, the compatibility of iMacs within a collagen/Matrigel^{TM} hydrogel was confirmed, ensuring their non-activation and suitability for use in tissue models. Next, an EHT bioreactor was designed and fabricated, and its efficacy in improving tissue alignment and beat rate was evaluated, showing enhanced cell alignment and synchronous beat rates compared to free-floating EHTs. Isogenic iCM/iMac EHTs were fabricated and compared with iCM EHTs, revealing reduced variability in beat rate, improved cell alignment, elongation, and increased tissue compaction with the addition of iMacs. Investigations into tri-culture EHTs containing iMacs, iCMs, and activated iCFs revealed strikingly high tissue compaction. While similar beat rates were observed between iCM/iCF and iCM/iCF/iMac EHTs, iCF activation was found to be further accelerated in the presence of iMacs, mediated by IL6 rather than TGFβ-1. These findings suggest alternative pathways in iMac-mediated iCF activation, warranting further exploration. Taken together, this study comprehensively explores isogenic macrophage integration into

EHTs, highlighting their positive impact on tissue function and structure. The findings offer insights into complex interactions between macrophages and fibroblasts, paving the way for true multicellular healthy and fibrotic models of the myocardium.

9.2. Introduction

Animal testing has long stood as the gold standard for pre-clinical evaluation of new therapeutic strategies [456]. Although pre-clinical evaluations include *in vitro*, *ex vivo* and *in silico* tests, *in vivo* studies using animals are a regulatory requirement in most parts of the world [456]. The use of *in vivo* models still prevail, predominantly because of their highly complex nature, involving immune responses, vasculature and a multicellular and multi-organ response to tested therapeutics. Thousands of animals are sacrificed annually to elucidate the mechanistic responses and potential impacts of pharmaceutical interventions. For example, in 2017, 850,000 animals were used for *in vivo* toxicity and regulatory studies in the EU [457]. While animal studies have played a crucial role in advancing our understanding of drug effects, there exists limitations. About 90% of the drugs that enter clinical trials (after passing pre-clinical assessment) tend to be rejected by the regulatory authorities, highlighting the lack of translatability between animal and human systems [458]. Additionally, a number of ethical concerns surround animal use, including genetic manipulation of the animals (which arguably adds to poor translation into human systems), as well as high costs of experiments [459]. The 3Rs—Replacement, Reduction, and Refinement—have become rallying principles in order to address these ethical and scientific shortcomings, and to drive a paradigm shift towards more humane and predictive approaches [460].

With a surge of interest in alternative methods to animal models, *in vitro* and *in silico* modelling have gained significant traction, offering promising avenues for more ethical, efficient, and human-relevant drug discovery processes. *In silico* or computational modelling uses advanced software technologies with unlimited parameters to predict the outcomes of physiologic and pharmacologic processes [461]. Although there have been numerous successful *in silico* models, finding the right parameters for the model,

still remains a big challenge [462]. Additionally, understanding and finding reasonable interpretations for the results from these models are also considered difficult [462]. Such challenges often lead to models that are mathematically sophisticated, but biologically unrealistic [462]. The lack of pre-clinical model selection in biomedical research became even more evident during the COVID-19 pandemic [463]. In the initial stages, there was uncertainty about the species susceptible to SARS-CoV-2, and there was a lack of readily accessible models to investigate the disease progression and identify potential drug targets against this novel pathogen [463, 464]. The presence of suitable and easily accessible disease models could have significantly accelerated our understanding of virus-host interactions and facilitated the rapid identification of effective drugs through repurposing studies [463]. Together with the FDA Modernisation Act 2.0 expanding the range of accepted preclinical models, scientists are now being urged to prioritise testing drug efficacy and safety using *in vitro* models whenever feasible [465]. *In vitro* modelling involves experiments conducted outside living organisms, and has emerged as a key player in reshaping drug discovery. Together with tissue engineering strategies, researchers have successfully generated disease models and healthy tissue constructs in controlled laboratory environments, providing a platform for testing drug responses in a more human-like context [466].

In vitro tissue models range from self-organised 3D structures such as organoids, tissue engineered scaffolds containing cells, and miniaturised organ-on-a-chip systems [465]. Multiple protocols are available for the generation of iPSC derived organoids for a number of human organs such as gut [467], liver [468],pancreas [469], lung [470], kidney [471] etc. However, these protocols can be highly cell line and method dependant, resulting in poor reproducibility [472]. While organoids self-assemble and help researchers gain insight into the development of tissues, organ-on-a-chip models can facilitate cross-tissue interactions [473, 474]. Such cross tissue interactions are of great interest and importance, particularly in regards to the gut brain axis, with bidirectional interactions mediating homeostatic and physiological functions in the body, including immune regulation and sleep [475]. Crosstalk between multiple organs have been achieved *in vitro* using organ-on-a-chip technology [476], and it is hypothesised that

human-on-a-chip models can also be fabricated using the same principle [477]. Nevertheless, since iPSCs are heavily relied upon for the fabrication of these *in vitro* models, failure to achieve tissue maturation comparable to their human counterparts is a limitation. In comparison, tissue engineered models with cells, scaffolds and stimulating factors provide a platform with multiple tuneable avenues, in terms of the scaffold architecture, stiffness and physical properties [465, 478]. Promising tissue engineered disease models have been developed for organs such as the liver [479], lungs [480], central nervous system [481], musculoskeletal system [482], heart [16] etc. Although majority of the *in vitro* models that are on clinical trials at the moment focus on cancer [465], this opens up a new avenue of improving existing *in vitro* models to achieve better physiological relevance.

In order to fabricate humanised tissue engineered *in vitro* models, there are a number of things to consider. The *in vitro* model and the target tissue should have morphological, geometric, metabolic and functional similarities, in addition to potential for scalability. One notable area in tissue engineering where the limitations of traditional *in vitro* models are evident, is in cardiac research. Over the past two decades, scientists have dedicated considerable efforts to developing cardiac models that can serve as reliable tools for drug screening and disease modelling [13, 17, 190, 483]. Tissue engineered cardiac models or engineered heart tissues (EHTs) have been fabricated using different architectures, materials and with varying levels of cellular complexities. In terms of the design of the EHT setup, the most common approach involves the attachment of the EHT to two anchoring points – this could be two Velcro coated glass tubes as reported by Eschenhagen *et al*. [13], two polymer wires as reported by Zhao *et al.* [191] or two pillars (posts or cantilevers) as reported by Turnbull *et al.* [254] or Hansen *et al.* [252]. Other geometries that have been explored also include ring-shaped EHTs [17, 251], cylindrical shaped EHTs [257] and EHTs formed around a suture [14]. Similarly, a number of different supporting biomaterials have also been explored with EHTs. The most commonly used materials include Matrigel®, collagen and fibrin, with some studies using a combination of these three materials [13, 17, 190, 252, 254, 483-485]. While earlier EHT models used chick embryonic cardiomyocytes [13] and rat

cardiomyocytes [251], later models saw the use of embryonic stem cell (ESC)-derived cardiomyocytes and later, iPSC-derived cardiomyocytes (iCMs) [14]. Regardless, the use of EHTs has not only facilitated in generating more mature cardiac tissue *in vitro* using iCMs, it has also significantly improved our understanding of the response of human heart tissues to different drugs.

As discussed in detail in Chapter 8, iCMs exhibit a highly immature phenotype, resembling foetal cells. One of the ways to improve iCM maturation is by culturing them in 3D, in the form of EHTs. EHT models, particularly the ones that allow the tissue to anchor to two points, provide a uniaxial mechanical strain field to the EHTs and hence can be utilised as a platform for delivering uniaxial stretch to the tissues to enhance iCM maturation. In addition to the added mechanical stress, more recent studies also explore the use of support cells to improve tissue maturity and function. In 2011, using EHTs fabricated with ESC-derived cardiomyocytes supplemented with different combinations of human umbilical vein endothelial cells (HUVECs), MSCs or cardiac fibroblasts, Tulloch *et al.* reported that cardiomyocytes showed increased proliferative capacity when cultured with HUVECs and improved vessel formation ability when supplemented with stromal cells [486]. Building on this finding, multiple EHT models have been fabricated using iCMs and MSCs [436, 485], iCMs and fibroblasts (iCFs [487] or primary human cardiac fibroblasts [191, 488]), iCMs and endothelial cells [486] and a combination of iCMs, iCFs and iPSC-derived cardiac endothelial cells [28, 313]. While these models have contributed significantly to our knowledge, a critical gap persists—the absence of innate immune cell components, in particular macrophages. Cardiac macrophages (resident and circulating) play crucial roles in the maintenance of homeostasis and in disease progression [21, 22, 125] and hence is a vital element that needs to be introduced to EHT models, to create more comprehensive and physiologically relevant systems. Notably, Bailey *et al.* studied the effects of SARS-CoV-2 on EHTs fabricated with iCMs, iCFs and cardiac macrophages derived from human patient samples [260]. Although, this served as a model to study myocarditis due to SARS-CoV-2 infection [260], the intricacies of cardiomyocyte-macrophage interactions

or the structural and functional abilities of the EHTs without SARS-CoV-2 were not assessed.

In the previous chapters, the derivatisation and characterisation of iMacs, iCMs and iCFs have been demonstrated. Specifically, the TRM-like phenotype exhibited by iMacs, their expression of CRM-specific markers when in co-culture with iCMs as well as their exceptional ability to improve iCM structure and function, make iMacs an ideal support cell type for addition into EHTs. From literature, some of the key components of efficient EHT fabrication, such as effective design strategies, choosing the right biomaterial for support, adding physiologically relevant ratios of cardiac cells (particularly for multicellular models) and additional maturation strategies, were taken as the main points to focus in this chapter. Here, the fabrication of a unique EHT model with iCMs, iCFs and iMacs (of isogenic origin) is demonstrated. The support hydrogel used was a mixture of bovine Type I collagen and Matrigel®, with the fabrication set up yielding 3 EHTs per well of a six-well plate. First, EHTs are fabricated without any confinement (free-floating hydrogel with cells, without using the EHT bioreactor) and with confinement, such that the tissues attach to two anchoring points (using the EHT bioreactor); comparisons between these two EHT fabrication techniques were used to identify the benefits of the added mechanical stress provided by confining the EHTs to the posts. Next, EHTs were generated with a combination of iCMs and iMacs to assess the impact of iMacs on beat rate, cell elongation and tissue compaction. Finally, activated iCFs were then added to iCM/iMac EHTs and were subjected to electrical stimulation (ES) to achieve a diseased model of the myocardium, mediated by myofibroblasts.

9.3. Materials and Methods

9.3.1. Experimental design

In this chapter, iCMs and iCFs were differentiated using SFCi55 iPSCs and iMacs were differentiated using zombie green tagged SFCi55 iPSCs. The hydrogel combination used was a mixture of bovine Type I collagen and Matrigel®, as this combination has been

previously used successfully for EHT fabrication [17, 254, 485] (details of hydrogel fabrication in subsection 9.2.2). Similarly, the EHT bioreactor was modified from previously published work from Prof. Kevin Costa's group in Icahn School of Medicine at Mount Sinai [254, 489]. The modified design was made simple and was scaled down to fit into 6-well plates, as opposed to the EHT bioreactor from Costa group, which was designed to be used in 60 mm x 15 mm or 100 mm x 20 mm petri dishes [254]. The final EHT bioreactor design (detailed description in subsection 9.2.3) yielded 3 EHTs per well of a 6-well plate and could also be integrated with the electrical stimulation (ES) bioreactor described in Chapter 8.

The initial phase involved validating the significance of utilising the EHT bioreactor. This involved fabrication of a set of EHTs with and without the bioreactor (tissue formation details outlined in subsection 9.2.4). EHTs formed using the bioreactor were securely anchored to posts, while those without the bioreactor remained free. Following a comparative analysis of the two types of EHTs and assessing the role of mechanical stress (provided by the anchorage of the tissues to the posts), additional EHTs were engineered either using only iCMs, or a combination of iCMs and iMacs (Figure 9.1). These tissues were meticulously evaluated for alignment, elongation, beat rate, and tissue compaction. Subsequently, additional EHTs were further populated with iCMs and iCFs (iCM/iCF EHT), as well as with the addition of iMacs (iCM/iCF/iMac EHT), focusing on beat rate and tissue compaction. Finally, iCM/iCF and iCM/iCF/iMac EHTs were subjected to a 5-day period of ES (Figure 9.1). Post-stimulation, the tissues were stained for alpha smooth muscle actin (alpha SMA) to analyse fibroblast activation and to demonstrate the fabrication of a diseased model of the myocardium by manipulating iMac-iCF interactions.

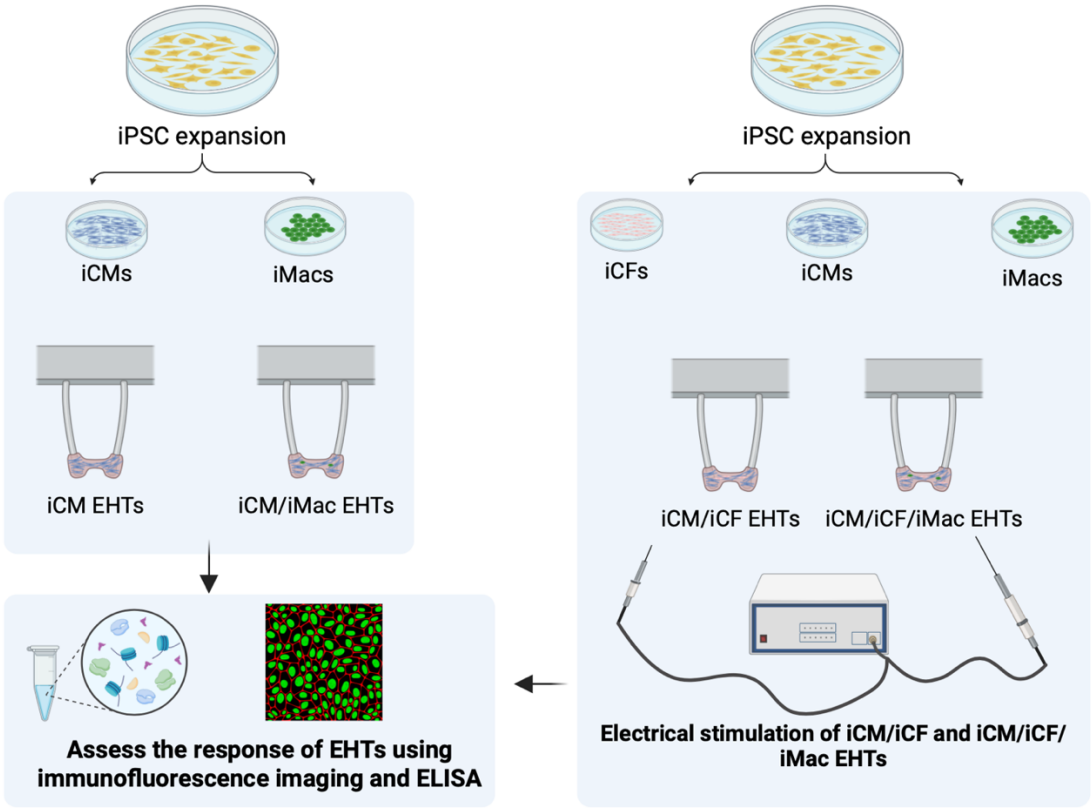

Figure 9.1: Graphical abstract. iPSCs were expanded and differentiated to obtain iCMs, iCFs and iMacs. Initially, engineered heart tissues (EHTs) were developed either using only iCMs, or a combination of iCMs and iMacs, to perform preliminary evaluation of the performance of the tissues. Subsequently, EHTs were fabricated using iCMs and iCFs, as well as iCMs, iCFs and iMacs. These tissues were also subjected to electrical stimulation Techniques such as ELISA and immunofluorescence imaging was performed to assess tissue maturation and performance.

9.3.2. Collagen/Matrigel® hydrogel fabrication

The hydrogel combination used in this study was a mixture of bovine Type I collagen and Matrigel®. The hydrogels were fabricated by modifying previously published data [254, 489], to obtain a final solution containing 2 mg/ml concentration of bovine Type I collagen (Telocol®-6, Advanced Biomatrix) and 0.9 mg/ml Matrigel® (Corning). Other components in the hydrogel mixture include 10x Minimum Essential Media (MEM), 10x PBS, sterile water and the cell/media mixture. Optimised hydrogel formation volumes in Table 10.

Table 10: Collagen-Matrigel® hydrogel composition

Component	Volume (in %)
Collagen	33.33
10 x MEM	4.17
10 x PBS	8.67
Sterile water	25.5
Matrigel® (varies depending on the lot)	10 (for the lot used in this study)
Media (with cells)	18.33

Hydrogels were fabricated using the volume percentages in Table 10 and collagen neutralisation was confirmed using pH strips (range 6 to 7.7, Sigma Aldrich). Once successfully neutralised, the hydrogel was allowed to self-assemble at 37°C for 2 hours.

9.3.3. Engineered heart tissue bioreactor fabrication

The EHT bioreactor was fabricated by modifying a previously established model [254, 489]. First, this model was scaled down to fit into a well of a 6-well plate, in order for the bioreactor to integrate with the ES set up. Different iterations of designs were trialled by 3D printing using a 3D printer (Formlabs 2), until the optimal dimensions and design was achieved (Appendix Figure 2). The optimal design comprised of a two-part mould (Figure 9.2 (a 1, 2)) which attached to each other (Figure 9.2 (b)). Sylgard 184 Elastomer (PDMS; VWR International) was casted onto this mould and allowed to cure at 80°C for 1 hour, to obtain the EHT bioreactor with posts (Figure 9.2 (c)). A frame (Figure 9.2 (a 3)) was also developed to allow the attachment of the EHT device, for structural support (Figure 9.2 (d)). Finally, the hydrogel mixture was casted on to the three cylindrical slots of the baseplate (Figure 9.2 (a 4)) and the EHT device with the frame was attached to the baseplate (Figure 9.2 (e)) to allow the hydrogel to form around the posts of the EHT bioreactor. The moulds on which PDMS was casted (Figure 9.2 (a 1 and 2) were machined from aluminium, whereas the frame (Figure 9.2 (a 3)) and the baseplate (Figure 9.2 (a 4)) were machined from polysulfone and polytetrafluoroethylene (PTFE), respectively. All the parts required for the EHT bioreactor (Figure 9.2 (e)) were thoroughly cleaned and sterilised before cell culture

experiments by treating them with 70% ethanol for 20 minutes, followed by 20 minutes of UV irradiation on either sides of the parts.

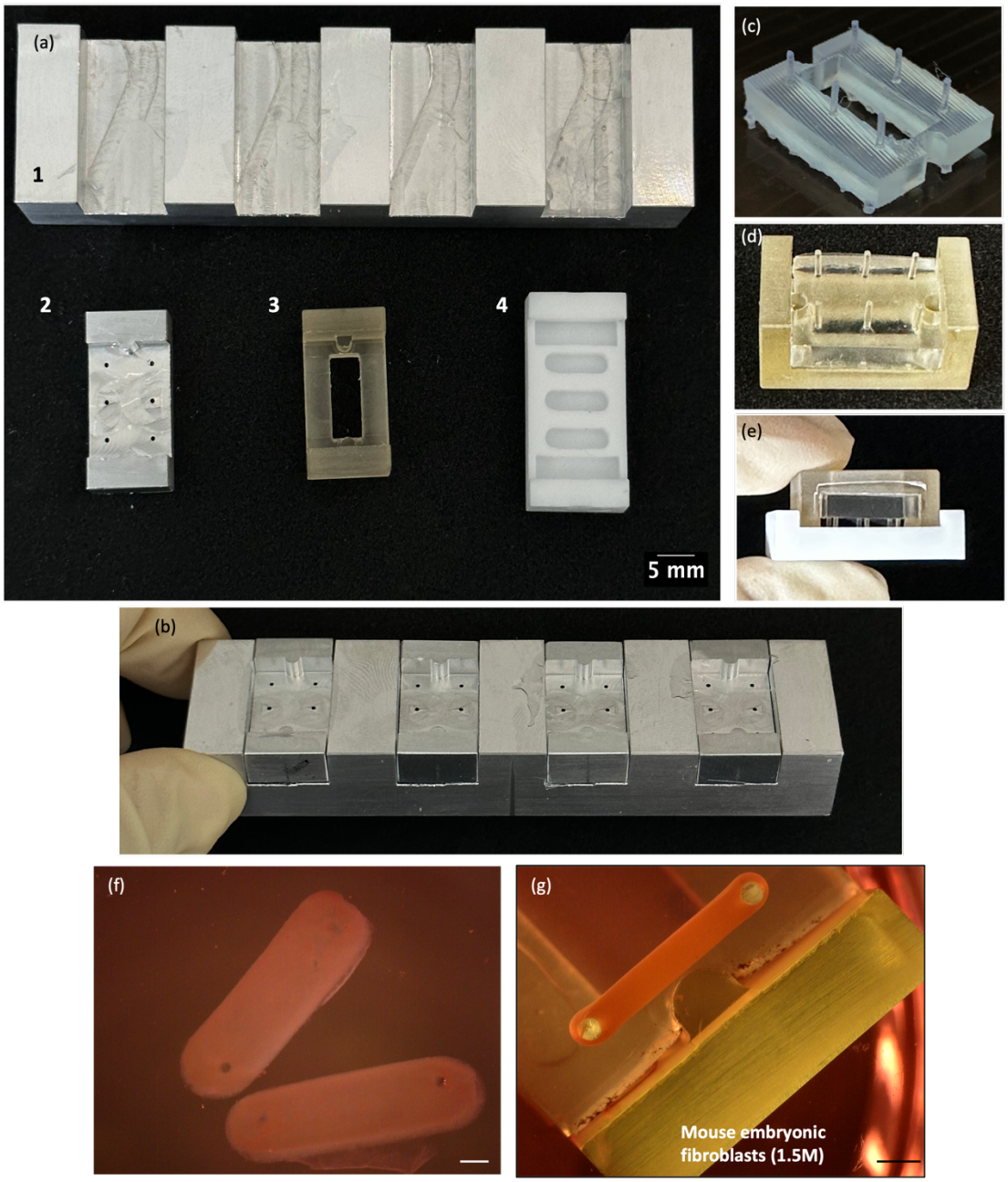

Figure 9.2: Engineered heart tissue bioreactor fabrication. (a) The four components required for the fabrication of EHTs. 1 and 2 are made with aluminium and are attached with each other; 3 is the frame and 4 is the baseplate. (b) Parts 1 and 2 attached to each other. (c) EHT bioreactor with posts, obtained by casting PDMS on to the aluminium moulds in (b). (d) EHT bioreactor attached to the frame. (e) Final EHT bioreactor set up with the baseplate. (f) Sample image of hydrogels made with the EHT bioreactor (without cells). Scale bar – 1mm. (g) Sample image of

a tissue made with 1.5 million mouse embryonic fibroblasts, attached to the EHT bioreactor posts. Scale bar – 1mm.

9.3.4. Engineered heart tissue fabrication

As described above, the EHT bioreactor was constructed, cleaned and sterilised before cell culture experiments. On the day of EHT fabrication, first the Collagen-Matrigel® hydrogel mixture was prepared without the cell and media component, and left on ice inside the biosafety cabinet. iCMs and iCFs were detached from cell culture plates by incubating them at 37°C for 9 minutes with 0.25% Trypsin. Similarly, pre-macs (non-adherent macrophage progenitors) were collected and centrifuged at 350 G for 5 minutes. All the cell types were resuspended in RPMI media with B27® (RPMI+i) and depending on the cell composition of the EHTs being fabricated, cells were added to the hydrogel to obtain a final total volume of 18.33%. The cell-hydrogel mix was casted on to the baseplate and the EHT bioreactor was attached to the baseplate. Once casted and attached, individual ETH bioreactors were placed per well of a 6-well plate and allowed to solidify in a 37°C incubator (5% CO_2 and 20% O_2) for 2 hours. After two hours, 4 ml media was added per well and the EHTs were allowed to form around the posts of the bioreactor for 48 hours at 37°C. iCM and iCM/iCF EHTs were cultured in RPMI+i while EHTs containing iMacs were cultured in RPMI+i supplemented with M-CSF. After 48 hours, the EHT bioreactor was separated from the baseplate (Figure 9.2 (g)) and kept in culture with half media changes performed every other day for up to 14 days.

For experiments involving ES, the EHTs were allowed to assemble for 48 hours as mentioned above and the ES bioreactor lid was attached to the 6-well plates. This allowed the EHTs to stay between the carbon electrodes and experience 5 days of ES. A complete media change was performed on day 3 of ES.

9.4. Results and discussion

9.4.1. Collagen-Matrigel® hydrogel does not trigger pro-inflammatory response in iMacs

Since the aim of this study was to fabricate EHTs with iMacs in them, it was pertinent to confirm that iMacs do not polarise in Collagen-Matrigel® hydrogels. Hence, the hydrogel mixture was prepared with 500,000 iMacs per gel, using a PDMS mould with cylindrical slots embedded in them (2.56 mm x 3 mm) to allow hydrogel formation (Figure 9.3 (a)). The hydrogels containing iMacs were allowed to form in a 37°C incubator for 2 hours (Figure 9.3 (b)), before adding X-VIVO media supplemented with 2% Pen/Strep and 100 ng/ml M-CSF. On day 7 of the experiment, the hydrogels were treated with either 260 U/ml or 900 U/ml collagenase for 30 minutes. The hydrogels subjected to collagenase degradation were checked every 10-15 minutes to ensure complete digestion. Once successfully digested, iMacs were retrieved from the hydrogels to perform flow cytometry analysis. iMacs were also cultured in 2D and treated with 260 U/ml or 900 U/ml collagenase for 30 minutes, to use as controls. Previous studies have used 275 U/ml of collagenase for 45-90 minutes to digest human heart samples [490]. Additionally, it was also of interest to evaluate the effect of a higher concentration (which might yield a shorter incubation time) of collagenase on hydrogels seeded with iMacs. It was found that while hydrogels treated with 900 U/ml collagenase dissociated within 20 minutes, 260 U/ml collagenase treatment took 30 minutes. On staining the retrieved cells for CD80, CD86, CD163 and CD206, no significant difference was found in the intensity of any of the markers (Figure 9.3 (c)), indicating no polarisation.

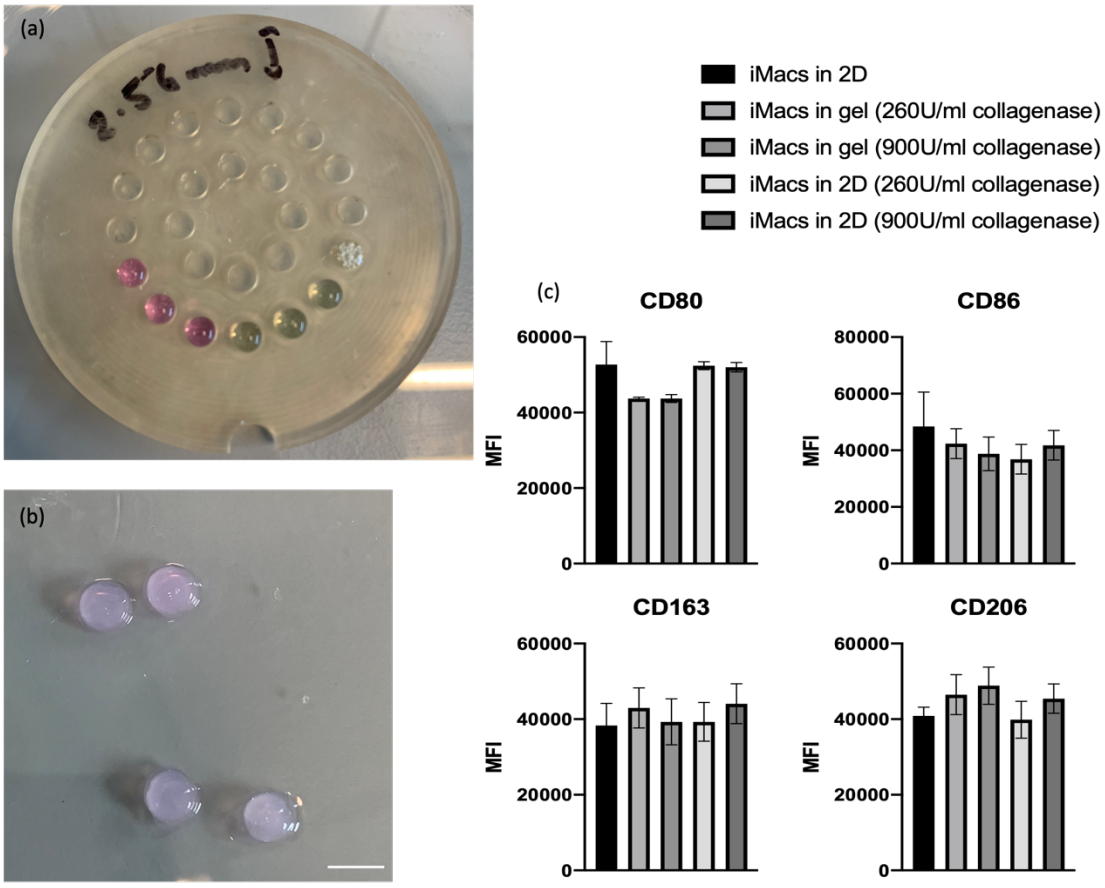

Figure 9.3: Characterisation of the hydrogel. (a) Collagen-Matrigel® hydrogels with iMacs were casted on PDMS mould of 2.56 mm x 3 mm dimension. (b) Representative images of hydrogels after 2 hours of incubation at 37°C. Scale bar – 3 mm. (c) Quantification of the mean fluorescence intensity (MFI) of CD80, CD86, CD163 and CD206 stains on iMacs cultured in Collagen-Matrigel® hydrogels for 7 days. Flow cytometry analysis performed using FlowJo. Statistical analysis - One Way ANOVA. N = 3 biological replicates, with each point signifying the average of 3 technical replicates.

9.4.2. EHTs fabricated using the custom-built bioreactor shows improved alignment and beat rate

After confirming that iMacs do not polarise in the hydrogels, the efficacy of the EHT bioreactor was evaluated. In order to perform this, EHTs were fabricated by casting the hydrogel-iCM mixture on the baseplate and allowing the hydrogel to form for 48 hours at 37°C. Following this, the hydrogels were peeled off from the baseplate and allowed

to freely float in the 6-well plate (iCM EHT free) (Figure 9.4 (a)). On the contrary, EHTs were also fabricated using the bioreactor, where the tissues were anchored to the posts (iCM EHT anchored) (Figure 9.4 (a)). At day 7 of the culture, immunofluorescence imaging was performed on both free and anchored EHTs (Figure 9.4 (b)). On staining the EHTs with cardiac troponin T (cTnT), the alignment of iCMs was evident. While the EHTs that were allowed to form outside of the bioreactor (iCM EHT free) formed a ball-like shape due to constant contraction of iCMs, the EHTs formed using the bioreactor maintained an elongated shape. Quantification of the cell alignment (using the OrientationJ plugin on FIJI) clearly indicated one directional peak for anchored EHTs, denoting preferential alignment of the cells along one direction (Figure 9.4 (c)). However, free EHTs displayed multiple peaks, indicating no preferential alignment (Figure 9.4 (c)). This finding is in agreement with Thavandiran *et al.*, who also demonstrated that having EHTs with uniaxial tension, resulted in highly aligned tissues [491]. Furthermore, the beat rate of free and anchored EHTs revealed no significant difference (Figure 9.4 (d)), however free EHTs displayed a beat rate of 87 ± 42 bpm with high variability, while anchored EHTs beat at 68 ± 10 bpm (Figure 9.4 (d)). Collectively, these results underline the improvement in tissue function when the EHTs were fabricated using the bioreactor, with preferential alignment of the cells along the axis of anchorage as well as more synchronous beat rates.

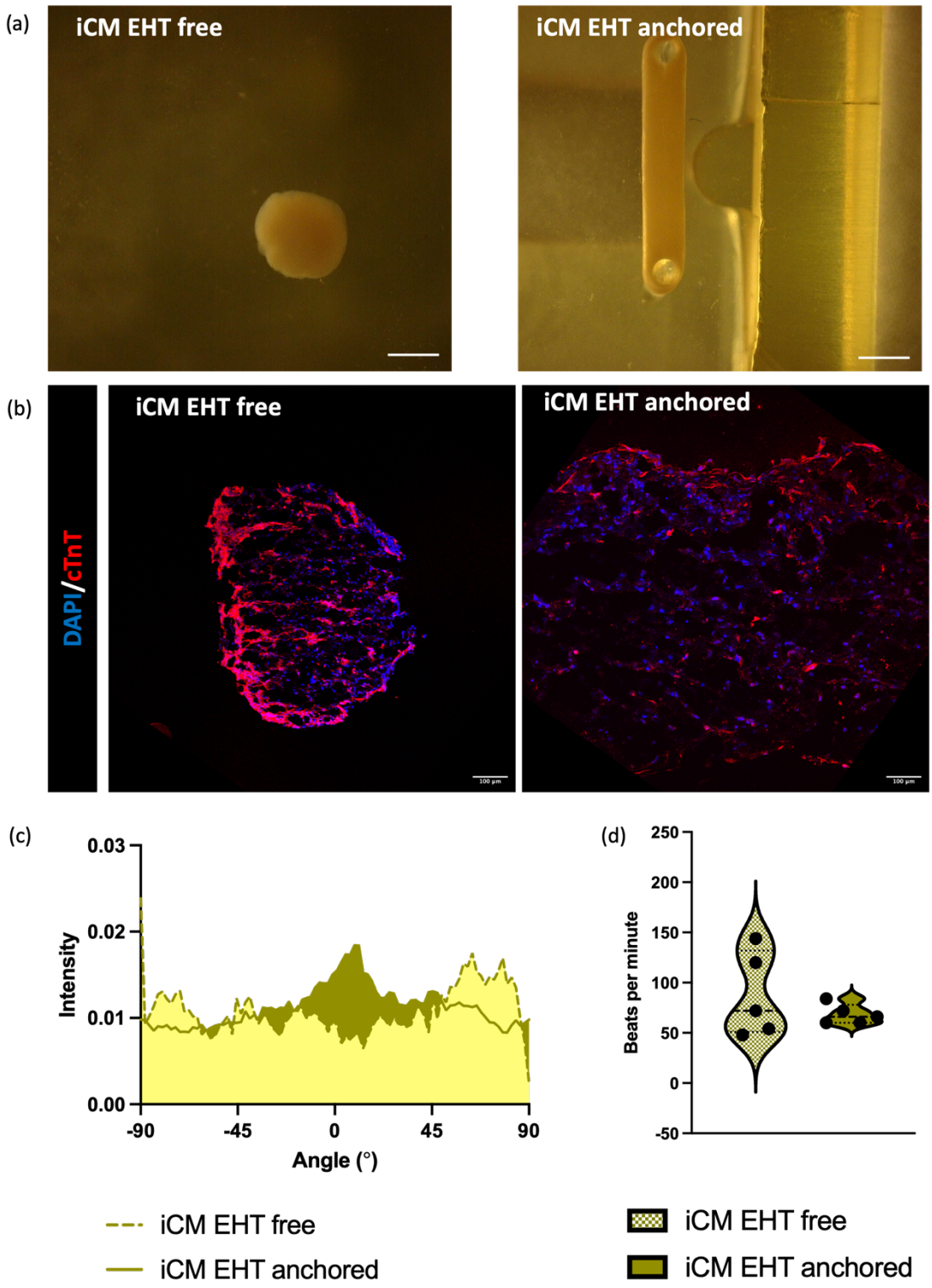

Figure 9.4: Comparison between free and anchored EHTs. (a) Representative images of EHTs that are free and EHTs that are fabricated using the bioreactor (anchored). Scale bar – 1 mm (b) Representative images of free and anchored EHTs stained with cardiac troponin T (cTnT). Scale bar – 100 µm. (c) Quantification of the alignment of free and anchored EHTs. Yellow area with dotted lines indicate the alignment of free EHTs; green area with solid line indicates the

alignment of anchored EHTs. (d) Quantification of beat rate of free and anchored EHTs. Statistical analysis - Student T test with Welch's correction. N = 6 technical replicates, with each point signifying the average of 3 different points in a tissue, for (d).

9.4.3. EHTs containing iMacs display improved iCM elongation, beat rate and tissue compaction

Using isogenic iCMs and iMacs, two groups of EHTs were fabricated – one containing only iCMs and the other containing both iCMs and iMacs (Figure 9.5 (a, c)). iCM/iMac EHTs contained 1 million cells in total, split at a ratio of 800,000 iCMs to 200,000 iMacs. Similarly, iCM EHTs contained 1 million iCMs. While both iCM and iCM/iMac EHTs showed alignment to the axis of anchorage, more cells (greater intensity) displayed preferential alignment in iCM/iMac EHTs (Figure 9.5 (b)). On assessing the elongation of iCMs in the EHTs, iCMs were found to be more elongated in the iCM/iMac EHTs, with a 36.7% increase in the aspect ratio (Figure 9.6 (c)). However, in comparison to iCMs in monolayer (aspect ratio of 1.1; the aspect ratio of a circle is 1), iCMs in EHTs displayed significantly greater elongation (aspect ratio of 3.18), highlighting structural maturation. Similar elongation of iCMs in EHTs has been shown in previous work, although not quantified [252, 486]. Both iCM EHTs and iCM/iMac EHTs displayed physiologic beat rates (Figure 9.6 (d); range highlighted in light green) that were comparable to each other. While iCM EHTs beat at 68 ± 10 bpm, iCM/iMac EHTs beat at 72 ± 4 bpm, distinctly demonstrating improved synchrony and reduced variability in the beat rate. Unsurprisingly, the reported beat rates for EHTs vary vastly, owing to the large degree of variability across iPSC lines. While Hansen *et al.* reported a range of beat rates from 20 to 162 bpm [252], other reports include 42 bpm [486], 50 bpm [408] and 49 bpm [492]. However, Mannhardt *et al*. reported a baseline beat rate of 61 ± 2 bpm (close to the value reported in this study), for fibrin-based EHTs [483]. Finally, the degree of compaction of the tissues, which is a hallmark of tissue remodelling, matrix deposition and contractile performance [493-495], was also assessed. As early as day 3 of the culture, EHTs containing iMacs showed improved compaction, which was found to be

further accelerated by day 7 (Figure 9.6 (e)). Notably, iCM EHTs did not compact over the period of 7 days (Figure 9.6 (e)). Compaction has been reported in EHTs in the past [14, 191], and has also been associated with increased stiffness, cell density and force production [496]. Zhao *et al.* reported a compaction of about 50% in EHTs (fabricated with collagen and Matrigel®) over a course of 7 days [191], much higher than the compaction reported in this study, in iCM/iMac EHTs. Another important observation made by Rivera-Arbeláez *et al.* suggested that EHTs with higher compaction also translated to higher contractile forces [495]. Taken together, these results illuminate the advantages of adding iMacs to EHTs, to improve the beat rate and compaction of the tissues, in addition to facilitating iCM elongation.

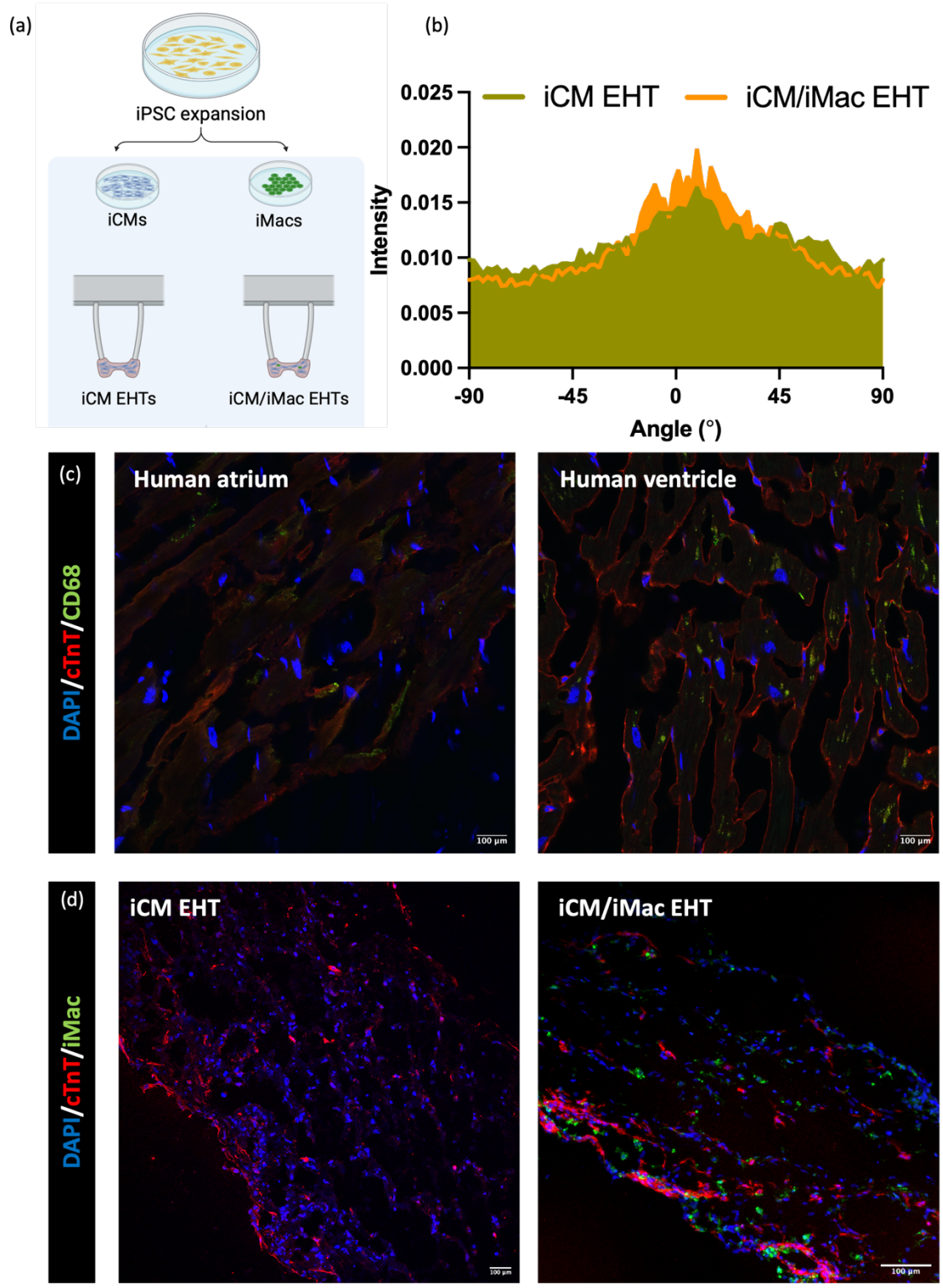

Figure 9.5: Structural comparison between iCM EHTs and iCM/iMac EHTs. (a) Schematic representation of the experimental set up (b) Quantification of the alignment of iCM and iCM/iMac EHTs. Green area with indicates the alignment of iCM EHTs; orange area indicates the alignment of iCM/iMac EHTs. (c) Representative images of human atrial and ventricular tissue samples stained with cardiac troponin T (staining iCMs) and CD68 (staining macrophages). Scale

bar – 100 µm (d) Representative images of iCM and iCM/iMac EHTs stained with cardiac troponin T. Scale bar – 100 µm.

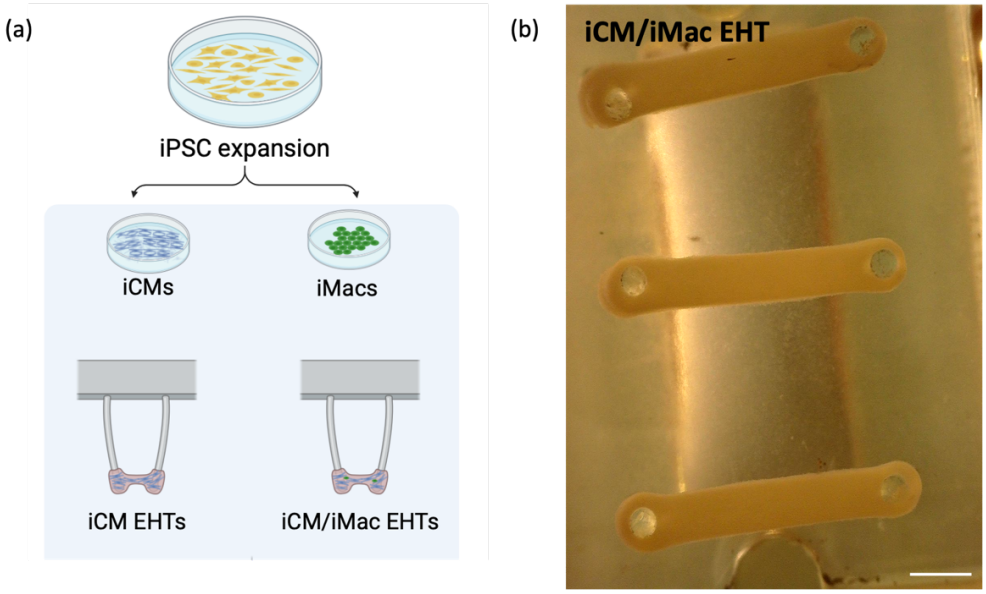
(a)
iPSC expansion
iCMs
iMacs
iCM EHTs
iCM/iMac EHTs
(b)
iCM/iMac EHT

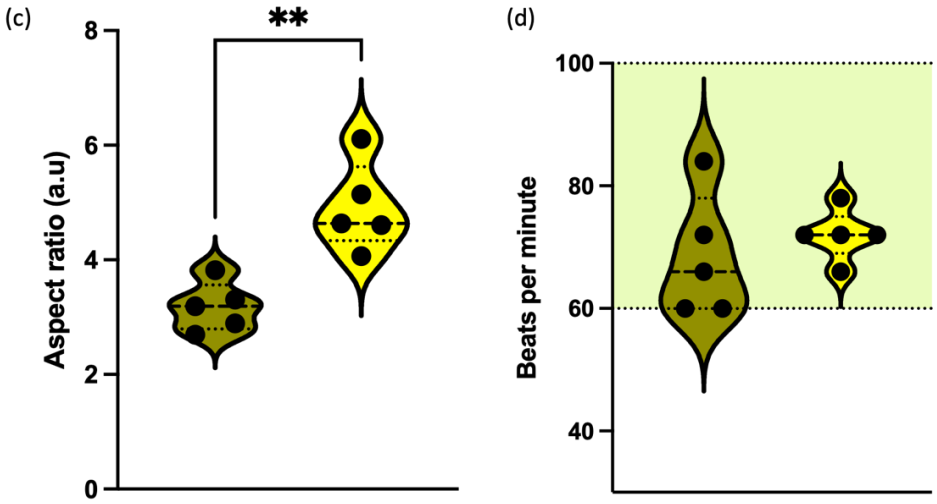
(c)
**
Aspect ratio (a.u)
8
6
4
2
0
(d)
Beats per minute
100
80
60
40

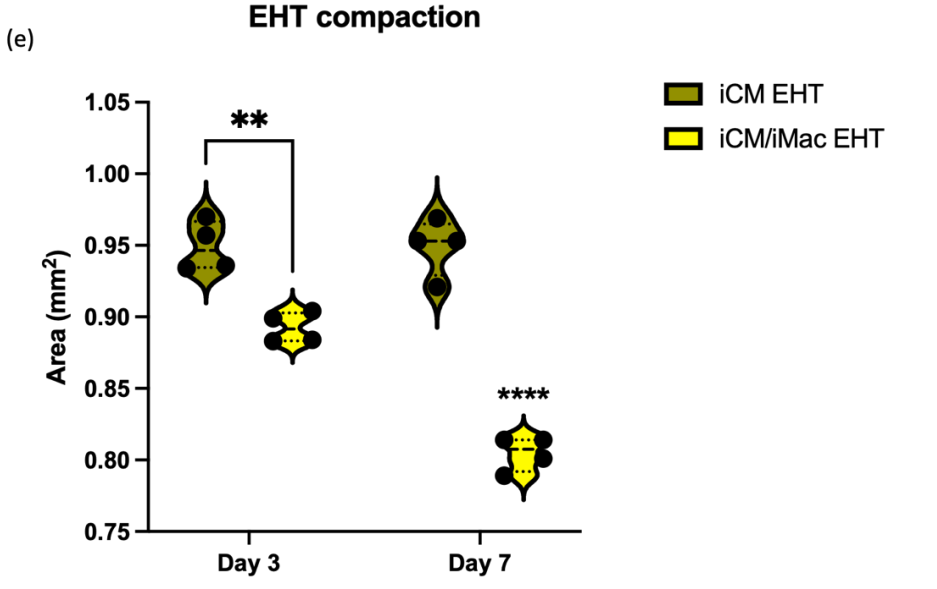
EHT compaction
(e)
iCM EHT
iCM/iMac EHT
Area (mm²)
1.05
1.00
0.95
0.90
0.85
0.80
0.75
**
****
Day 3
Day 7

Figure 9.6: Functional comparison between iCM EHTs and iCM/iMac EHTs. (a) Schematic representation of the experimental set up (b) Representative images of iCM/iMac EHTs in culture. Scale bar – 1 mm (c) Quantified aspect ratio of iCMs in iCM EHTs and in iCM/iMac EHTs. (d) Quantified beat rate (in bpm) of iCM and iCM/iMac EHTs. Light green area highlights range of human heart beat rate. (e) Compaction of EHTs over a period of 7 days. Statistical analysis - Student T test with Welch's correction for c and d; Two-way ANOVA with Tukey's multiple comparison for e. ** represents $P<0.01$ and **** represents $P<0.0001$. N = 3 biological replicates, with each point signifying the average of different points in a tissue, for (c and d); each point signify the area of a tissue, for (e).

9.4.4. Addition of iCFs into EHTs containing iMacs indicate increased myofibroblast activation

Numerous previous studies focusing on macrophage-fibroblast interaction *in vitro*, report fibroblast activation when in co-culture with macrophages [497-501]. Leveraging this phenomenon and increasing the level of complexity of the EHTs, the next objective was to introduce the second most common cell type of the myocardium – cardiac fibroblasts [42] – into the EHTs to demonstrate the potential of fabricating a diseased model of the myocardium, mediated by myofibroblasts. Hence, isogenic cultures of iCMs, iCFs and iMacs were used to fabricate EHTs with either iCMs and iCFs (iCM/iCF EHT) or with iCMs, iCFs and iMacs (iCM/iCF/iMac EHTs) (Figure 9.7 (a)). In particular, the iCFs used in this study were not treated with SD208 (TGF-β1 blocker), to ensure potential fibrotic response. Furthermore, to keep the number of contractile cells constant across all EHTs, iCM/iCF EHTs were fabricated at a ratio of 700,000 iCMs to 300,000 iCFs, whereas iCM/iCF/iMac EHTs were fabricated at a ratio of 700,000 iCMs, 200,000 iMacs and 100,000 iCFs. One of the most striking differences to be noted in iCM/iCF/iMac EHTs as opposed to iCM/iCF EHTs, was the strong compaction spotted early in the culture (Figure 9.7 (b, c)). Consistent with previous findings, the addition of cardiac fibroblasts facilitated tissue compaction [191, 495] (Figure 9.7 (b)), highlighting the importance of cardiac fibroblasts in remodelling kinetics of the ECM [502]. However, tissues with iMacs displayed a highly pronounced 35.1% greater compaction on day 7 and 55.2% greater compaction on day 14, in comparison to iCM/iCF EHTs on the

respective time points (Figure 9.7 (b)). Remarkably, in comparison to iCM/iCF EHTs, iCM/iCF/iMac EHTs displayed a highly robust 74 ± 3 bpm beat rate, while iCF/iCF EHTs beat at 64 ± 11 bpm (Figure 9.7 (d)). Nevertheless, both EHT types beat within the range of human heart beat [503]. However, as early as 2 days after EHT formation, iMacs were found to leave the tissues and attach at the bottom of the plate (Figure 9.7 (e)).

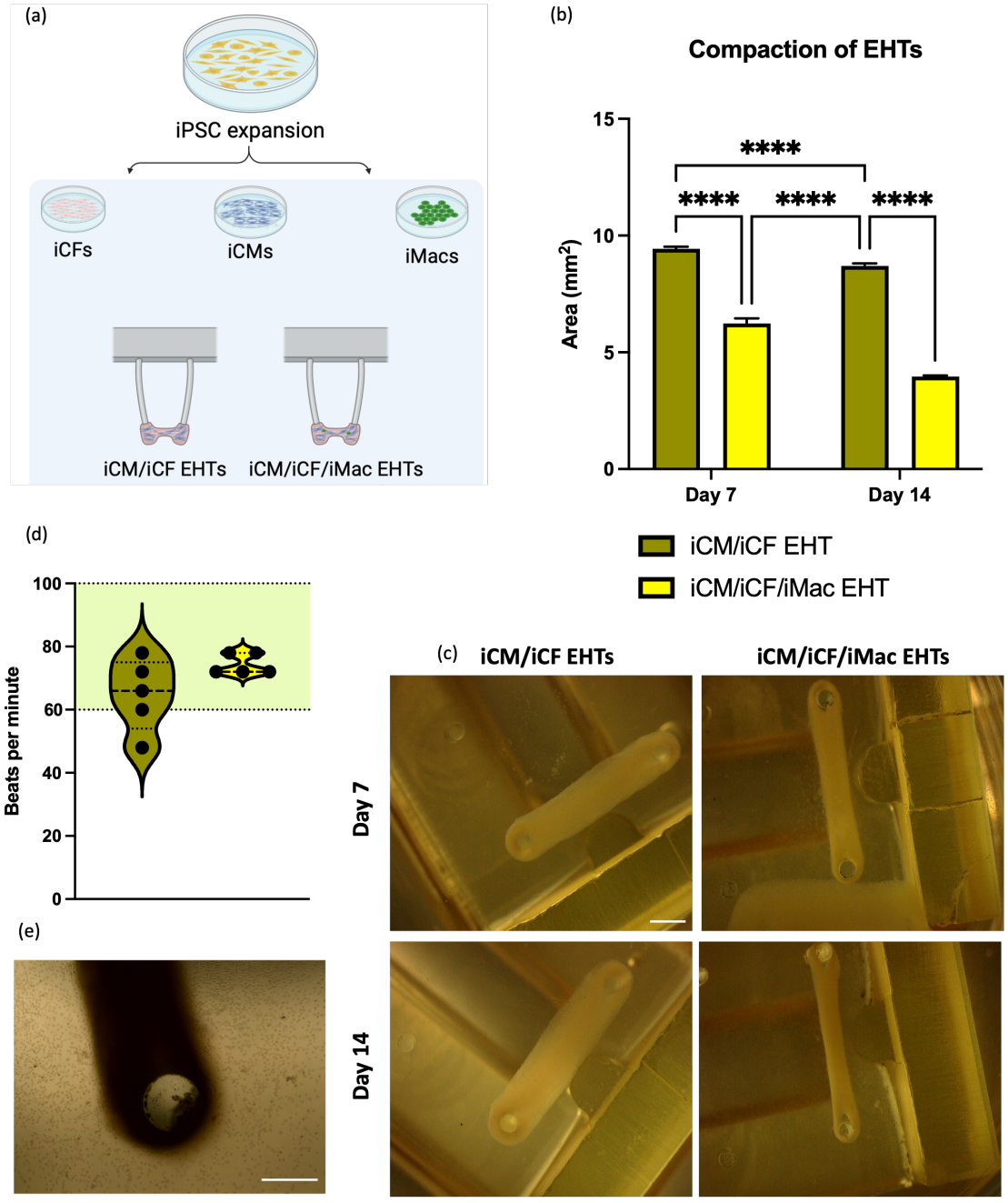

Figure 9.7: Comparison between iCM/iCF and iCM/iCF/iMac EHTs (a) Schematic representation of the experimental set up. (b) Compaction of EHTs over a period of 14 days (c) Representative images of iCM/iCF and iCM/iCF/iMac EHTs in culture, undergoing compaction. Scale bar – 1 mm (d) Quantified beat rate (in bpm) of iCM/iCF and iCM/iCF/iMac EHTs. Light green area highlights range of human heart beat rate. (e) Representative image of iCM/iCF/iMac EHT with macrophages coming out of the tissues. Scale bar – 0.5 mm. Statistical analysis - Two-way ANOVA with Tukey's multiple comparison for b; Student T test with Welch's correction for d. **** represents P<0.0001. N = 6 technical replicates, with each point signifying the average of different points in a tissue, for (d); each point signify the area of a tissue, for (b).

This observation led to the hypothesis that iCFs were getting activated in the presence of iMacs, squeezing iMacs out of the tissues. Hence, to conclusively determine the activation of iCFs and to assess the impact of ES on iMac-iCF interaction, iCM/iCF and iCM/iCF/iMac EHTs were fabricated and electrically stimulated (Figure 9.8 (a)). Alpha smooth muscle actin (alpha SMA) staining of the EHTs revealed that iCFs in iCM/iCF/iMac EHTs (with and without ES) were significantly more activated, indicating a the early stage of a myofibroblast mediated fibrotic response (Figure 9.8 (b, c)). Moreover, while iCM/iCF EHTs did not exhibit significant differences in alpha SMA expression when electrically stimulated, ES caused a 29.6% upregulation in the intensity of alpha SMA expression in iCM/iCF/iMac EHTs (Figure 9.8 (b, c)). It is important to note that findings from previous chapters underline the quiescence of iMacs in co-culture with iCMs, even while being electrically stimulated. However, activation of iCFs in the EHTs in the presence of iMacs was evident. Literature highlights the interplay between alternatively activated macrophages and fibroblasts, and the crucial role played by macrophages in tissue repair. Transforming growth factor β1 (TGF-β1) produced by macrophages governs the proliferation, differentiation, migration, and various physiological activities of fibroblasts [499]. Macrophage-mediated activation of fibroblasts is well documented [499, 501], and in return, fibroblasts indirectly modulate macrophages through the release of cytokines [501]. For example, in a co-culture study

using THP-1 cells and dermal fibroblasts, Wu *et al.* reported activation of fibroblasts (into myofibroblasts) through M-CSF mediated TGFβ-1 [500]. TGFβ-1 is one among multiple factors that can trigger fibroblast activation, including MMPs and TIMPs [499, 501]. Although based on findings from previous chapters, iMacs in co-culture with iCMs minimally express TGFB1 gene, it was interest to determine if iCF activation was mediated through TGFβ-1. ELISAs were performed first to assess macrophage activation and then to assess TGFβ-1 production. Notably, an upregulation (87.5%) of IL6 was found in electrically stimulated EHTs, in comparison to the unstimulated controls (Figure 9.9 (a)). Macrophages and fibroblasts are known to produce IL6, and IL6 induces fibroblast activation through TGFβ-1 [497]. Additionally, Roy *et al.* reported an upregulation in IL6 production on culturing BDMs on cardiac fibroblast-derived matrix [504]. No other pro-inflammatory response was noted between paced and non-paced iCM/iCF/iMac EHTs, with no significant difference in TNFα production (Figure 9.8 (b)). However, alternative activation of iMacs was confirmed with 63.2% upregulation in IL10 production (Figure 9.8 (c)). Nevertheless, no significant difference was noted in TGFβ-1 production in EHTs containing iMacs, indicating that iCF activation was not directly TGFβ-1 mediated (Figure 9.8 (d, e)). With a growing body of work evidencing fibrosis and fibroblast activation independent of TGFβ-1 [505-508], other pathways need to be investigated to determine the cause of iMac-mediated iCF activation. Out of the wide spectrum of alternatively activated macrophages, the M2a subtype characteristically expresses high amounts of IL10 [509]. Additionally, M2a macrophages are key players in enhancing cell growth and tissue repair [509]. In a recent study, using THP-1 cells and dermal fibroblasts, Sapudom *et al.* demonstrated activation of fibroblasts with high alpha SMA expression upon co-culture with M2a macrophages [498]. Taken together, these findings emphasise the need to focus on iMac-iCF interactions further, in order to improve advanced EHT models. However, an isogenic tri-culture model of the myocardium with iCMs, iCFs and iMacs could serve as a fibrotic model by virtue of iMac-iCF interactions.

(a)

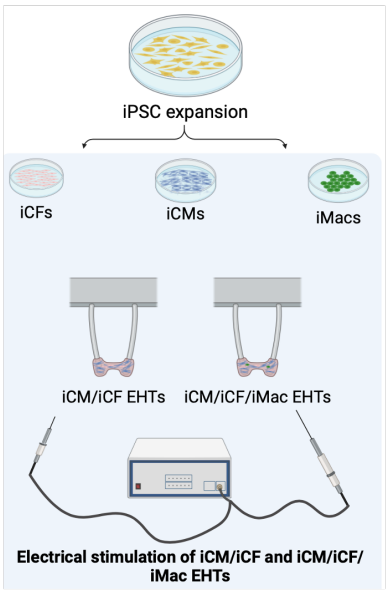

(c)

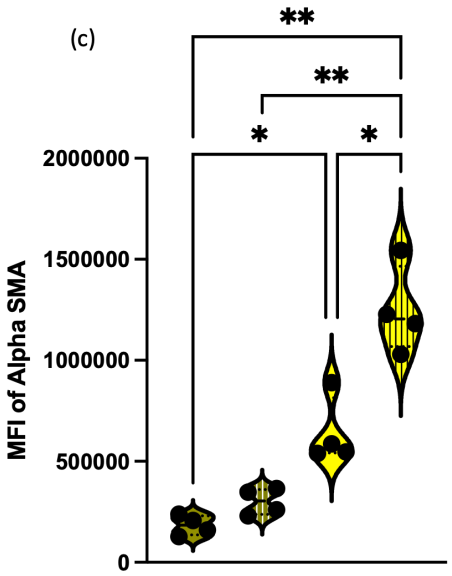

(b)

iCM/iCF EHT
iCM/iCF EHT paced
iCM/iCF/iMac EHT
iCM/iCF/iMac EHT paced

(b)

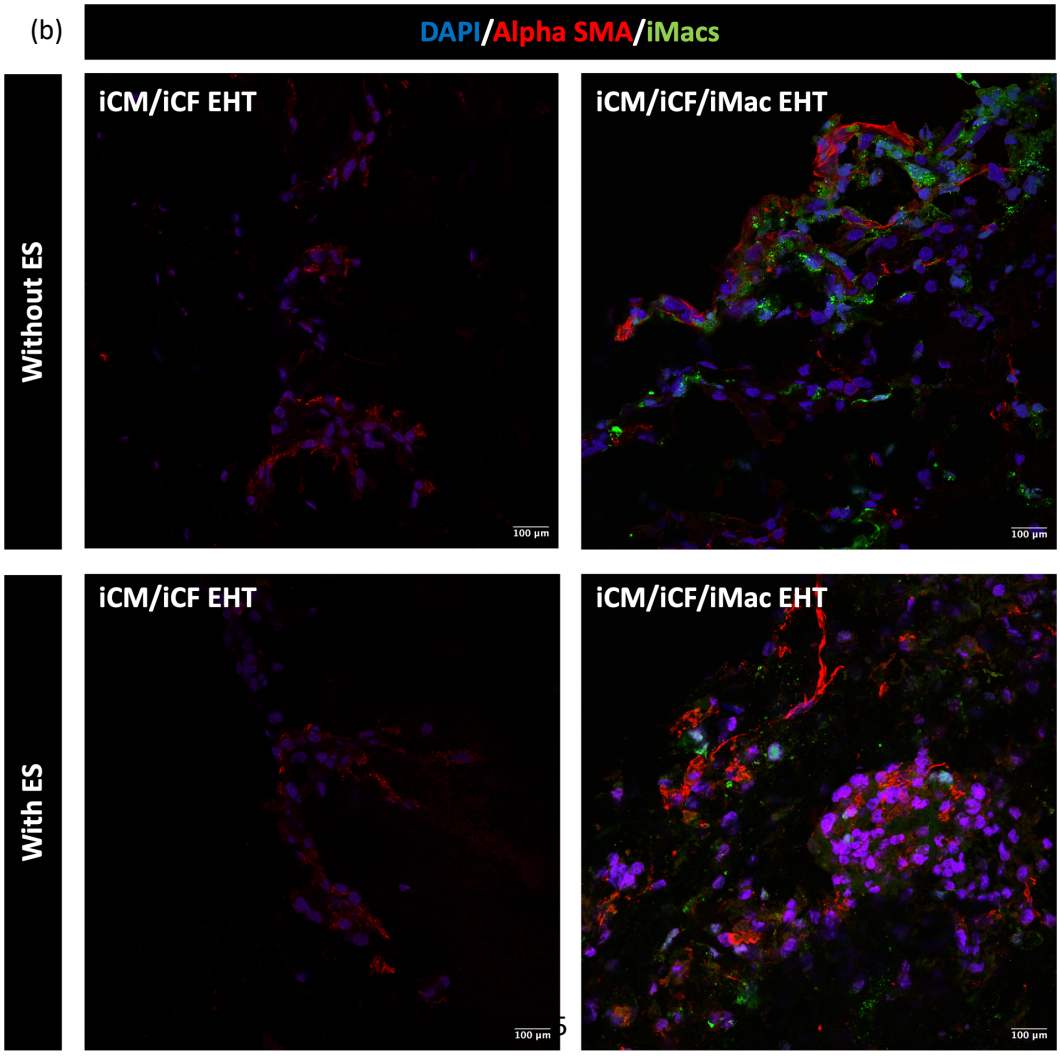

Figure 9.8: Comparison between iCM/iCF and iCM/iCF/iMac EHTs with and without electrical stimulation (a) Schematic representation of the experimental set up. (b) Representative images of iCM/iCF and iCM/iCF/iMac EHTs stained with alpha SMA, highlighting fibrosis. Scale bar – 100 µm (c) Mean fluorescence intensity of alpha SMA staining (normalised to cell number). Statistical analysis - One-way ANOVA with Tukey's multiple comparison. * represents P<0.05 and ** represents P<0.01. N = 6 technical replicates, with each point signifying the average alpha SMA intensity from 3 images.

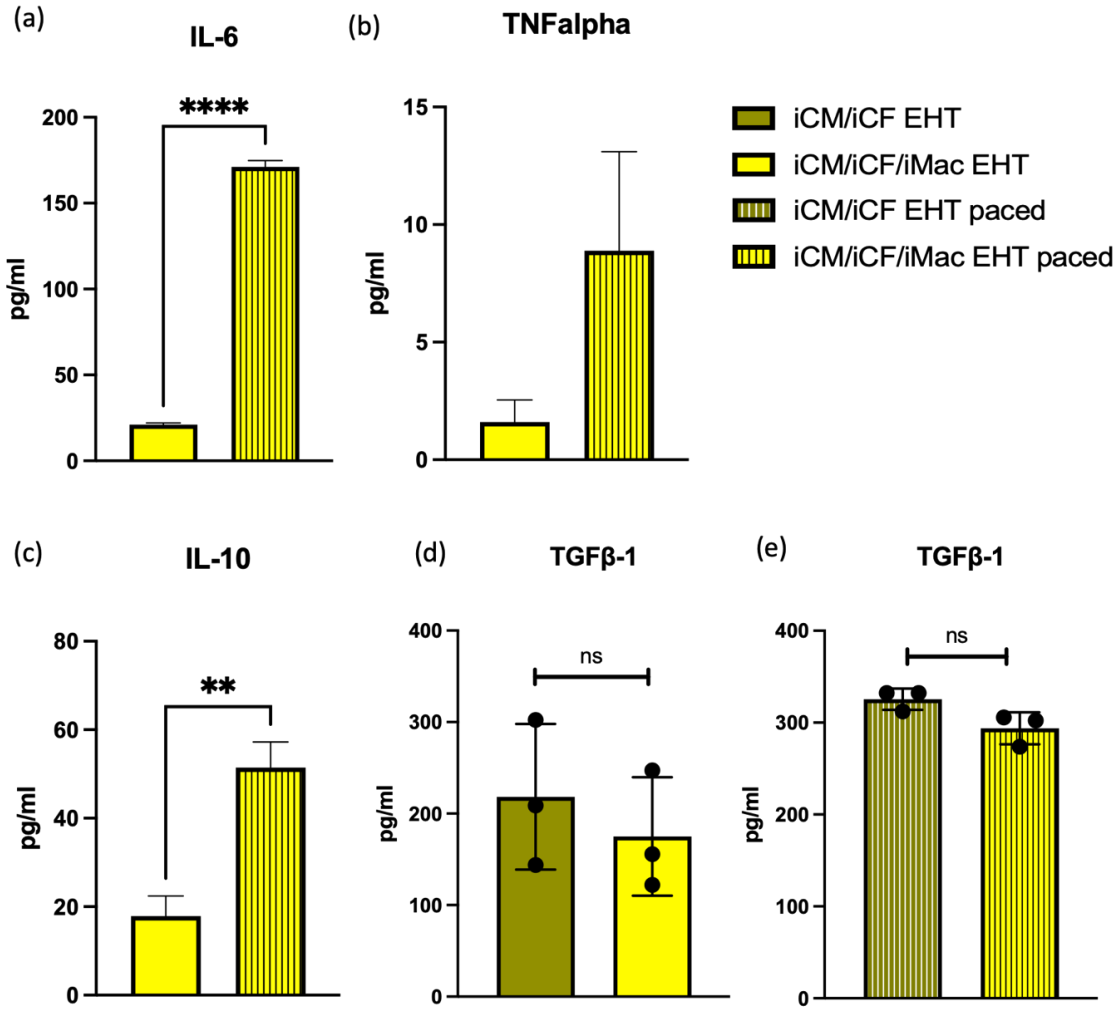

Figure 9.9: ELISAs assessing iMac and iCF activation. Quantification of endogenous (a) IL6, (b) TNFα and (c) IL10 in electrically stimulated and non-stimulated iCM/iCF/iMac EHTs. (d) Endogenous TGFβ-1 in iCM/iCF and iCM/iCF/iMac EHTs. (e) Endogenous TGFβ-1 in electrically stimulated iCM/iCF and iCM/iCF/iMac EHTs. Statistical analysis - Student T test with Welch's

correction. * represents P<0.05, ** represents P<0.01 and **** represents P<0.0001. N = 6 technical replicates.

9.5. Conclusion

The majority of EHT models in existence either only include cardiomyocytes, or a combination of cardiomyocytes and cardiac fibroblasts [14, 16, 191]. This pioneering study aimed to fabricate EHTs with isogenic cell types – iCMs, iCFs and iMacs and investigate their impact on tissue function and complexity. This study is unique in that CRM-like cells were introduced into EHTs for the first time, in the context of a healthy and an early stage activated myofibroblast-mediated model of the myocardium. Using the well documented combination of hydrogel used for EHT fabrication, the initial focus was on confirming that iMacs do not trigger a pro-inflammatory response in the collagen-Matrigel® hydrogel—a crucial step in ensuring their compatibility for use in EHTs. iMacs encapsulated within the hydrogel showed no significant polarisation, as confirmed by flow cytometry analysis of CD markers (CD80 and CD86 for pro-inflammatory activation and CD163 and CD206 for anti-inflammatory activation), indicating that iMacs remain non-activated in this environment.

Building on this confirmation, the study then evaluated the efficacy of an EHT bioreactor in improving tissue alignment and beat rate. The bioreactor-fabricated EHTs exhibited enhanced cell alignment and more synchronous beat rates compared to free-floating EHTs, highlighting the positive impact of the bioreactor on tissue function. After verifying the advantages of the EHT bioreactor, isogenic iCM/iMac EHTs were fabricated and compared with iCM EHTs. Addition of iMacs significantly reduced the variability in the beat rate of the tissues, improved cell alignment and elongation, as well as remarkably increased tissue compaction. While these initial results indicate that in comparison to traditional EHTs, EHTs with iMacs might be more enhanced and physiologically relevant, further characterisations, such as electrical and metabolic measurements need to be done.

Expanding the complexity of EHTs, the study investigated the inclusion of iMacs in EHTs containing isogenic iCMs and iCFs. Leveraging on numerous previous studies reporting fibroblast activation when in co-culture with alternatively activated macrophages, EHTs containing both iMacs and activated iCFs were expected to be fibrotic. This tri-culture model demonstrated similar beat rate, but strikingly high tissue compaction compared to EHTs with just iCMs and iCFs. Interestingly, iMacs were observed leaving the tissues and attaching to the plate, prompting a deeper investigation into iCF activation in the presence of iMacs. As expected, the activation of iCFs, as evidenced by alpha SMA staining, was more pronounced in the presence of iMacs, with iCM/iCF/iMac EHTs expressing significantly higher levels of alpha SMA. Furthermore, electrical stimulation experiments revealed accelerated cardiac fibroblast activation in EHTs containing iMacs. It was of interest to determine the pathway through which iMacs trigger iCF activation, in order to manipulate this pathway to fabricate tri-culture EHT models without an activated response or even a more pronounced activation towards fibrosis. However, the study found that the observed fibrotic response was not mediated through TGFβ-1, a well-known fibrosis-inducing factor. Instead, IL6, a pro-inflammatory cytokine associated with fibroblast activation, was dramatically upregulated in electrically stimulated EHTs. This suggests that alternative pathways, beyond TGFβ-1, might be involved in iMac-mediated iCF activation.

In conclusion, the study presents a comprehensive exploration of isogenic macrophage integration into EHTs, demonstrating their positive impact on tissue function and structure. The findings open avenues for further research, particularly in understanding the complex interactions between macrophages and fibroblasts to develop true multicellular healthy and fibrotic models. Future perspectives include unravelling the molecular mechanisms underlying iMac-iCF interactions, exploring additional pathways involved in fibrosis, and refining the integration of immune components for more accurate representation of *in vivo* conditions. It was also of great interest to assess the response of SD208 treated iCFs in multicellular EHT models. Moreover, the study highlights the potential of iMacs as excellent support cells in EHTs, contributing to

improved tissue function and providing a foundation for advancing cardiac tissue engineering.

Chapter 10 Discussion and future perspectives

The journey of this thesis has taken a significant step in immunoengineering human myocardium. Although the prominence of macrophages in the myocardium has recently been realised and appreciated, most of the reports available are based on animal models, which often fail to recapitulate human systems. Hence, in this study, iPSCs were used to derive isogenic populations of cardiomyocytes, cardiac fibroblasts and macrophages. The derivatisation of these cell types from iPSCs have been performed numerous times in literature, however, in this work, the differentiation and characterisation of SFCi55 iPSCs into these cell types is demonstrated for the first time. This is of particular significance, as iPSC-based differentiation protocols tend to vary depending on the cell line [510]. This study delves deep into the characterisation of the effect of cardiac cues (in the form of iCM conditioned media and co-culture with iCMs) on iMacs, and how it impacts the phenotype and function of iMacs. Subsequently, one of the major findings of this study draws attention to the remarkable improvement in maturation shown by iCMs when in co-culture with iMacs. Furthermore, this study explores the use of ES to improve iCM maturation. Impressively, this study also reports comparable levels of structural and functional improvement in iCMs when subjected to 5 days of ES and when in co-culture with iMacs. While initial work focuses on characterising the interactions between iMacs and iCMs in 2D cultures, this foundational work has culminated in the development of a unique 3D model of the healthy myocardium— first of its kind—that incorporates iMacs into EHTs. This novel 3D model has showcased substantial improvement in tissue function, with improved beat rate and tissue compaction, in addition to cell alignment and elongation. Moreover, adding activated iCFs into the EHTs has resulted in a diseased model of the myocardium, mediated by myofibroblasts, owing to the inherent interactions between macrophages and fibroblasts. However, it is important to point out that many of the conclusions made are based on gene expression analysis, and protein expression (western blots, for example) needs to be assessed to have more robust conclusions. Additionally, validating the current findings using different iPSC lines would also be

beneficial to highlight the reproducibility of these results. Another avenue of improvement includes routine karyotyping of the iPSCs to ensure good cell hygiene. Regardless, the findings of this study opens up new avenues in the field of cardiac tissue engineering and regenerative medicine, to help fabricate drug screening models for healthy and fibrotic myocardium. However, as with any pioneering work, there are areas that can be further explored and enhanced to maximise the potential of this ground-breaking approach.

Keeping the EHT model as it is, one key aspect that requires further exploration is the need for comprehensive electrical and metabolic measurements to conclusively characterise iCM-iMac interactions. This would involve assessing parameters such as action potential propagation and force measurements, and metabolic activity within the 3D tissue constructs as well as in 2D cultures. These measurements are crucial for understanding the functional impact of macrophages on cardiomyocytes and providing a more comprehensive view of the tissue dynamics. Electrical measurements of iCMs can be performed using patch clamps and multi-electrode arrays, and gives a comprehensive understanding of the action potential durations, resting membrane potential etc. [14]. Similarly, the metabolic activity of iCMs (and iMacs) would be of great interest to assess. Oxidative phosphorylation (OXPHOS) is the physiological means of ATP production in the heart [511]. Embryonic and foetal hearts on the other hand, rely on glycolysis, as their natural environment in hypoxic [512]. iCMs, being highly immature and foetal-like, have been shown to improve maturation when in glucose and glutamine depleted, lactate containing media conditions [513, 514]. Similarly, fatty acid containing media has also shown the ability to facilitate iCM maturation [515]. However, having observed structural and functional changes in iCMs when cultured with isogenic iMacs, it is important to also assess potential metabolic differences, to conclusively determine improvement in iCM function. Other key readouts to determine iCM maturation also include mitochondrial numbers, mitochondrial fidelity, placement of mitochondria (closer to the sarcomeres indicate enhanced maturation) etc. [512]. Although the key highlight of this study is the addition of iMacs as a support cell in EHTs, the EHTs experience electrical and mechanical stimulations, which also contribute to

advanced maturation of iCMs. Another avenue to explore here includes the fabrication of EHTs with iMacs and ES, together with metabolic maturation media, to further enhance the maturity and functionality of the engineered tissues. This multifaceted approach acknowledges the synergistic effects of different stimuli on tissue development, aiming for a more comprehensive representation of *in vivo* conditions.

Understanding the paracrine effects of iMacs in tissues is another exciting avenue for future investigation. In this study, the EHT bioreactor is designed such that three EHTs are cultured per well of a 6-well plate. This approach could be used to answer more complex questions regarding the effect of molecular signals and cytokines released by iMacs within the EHTs. By setting up the EHT bioreactor such that one well hosts EHTs containing iMacs as well as fibrotic or 'injured' EHTs, the paracrine effects of iMacs on injured tissues could be elucidated, providing insights into the broader regulatory mechanisms influencing tissue behaviour and function. The paracrine effects of iMacs in enhancing cell proliferation, migration, rescue of the injury condition etc. could provide priceless insights into potentially using iMacs as a therapeutic for cardiac diseases. Interestingly, iMacs have been proven beneficial in treating pulmonary alveolar proteinosis [516, 517], as well as liver fibrosis [518]. Furthermore, in the phase 2 trial titled "Use of Ixmyelocel-T Treatment in Patients with Heart Failure Due to Dilated Cardiomyopathy," Ixmyelocel-T, which is a multicellular therapy including bone-marrow derived myeloid and lymphoid cells that express CD45, was administered to patients via intramyocardial injection [519]. Alternatively activated (M2) macrophages were a part of this multicellular treatment. Positive outcomes including symptom improvement, were observed in patients with ischemic dilated cardiomyopathy, whereas similar benefits were not observed in the nonischaemic population. Moreover, the treatment group of ischemic patients experienced a significant decrease in major adverse cardiovascular events, suggesting the favourable efficacy of Ixmyelocel-T [519]. These findings further illuminate the potential of alternatively activated macrophages, such as iMacs, as a therapeutic for cardiac diseases.

Building on the foundation laid by this study, future research could focus on inducing injury within the EHTs to model specific cardiac diseases. Comparing the responses of the *in vitro* disease model with established animal injury models would provide valuable insights into the accuracy and reliability of the engineered tissue as a disease model. This could be particularly relevant for acute cardiac events, such as MI, where macrophages play a crucial role in the disease progression [20, 125]. Furthermore, cardiac inflammatory diseases such as myocarditis [260] can also be studied using the EHT model developed in this work. More nuanced and genetic cardiac conditions can be modelled using EHTs through iPSCs derived from patients. For example, patient-derived iPSCs have been used to study long QT syndrome [262, 263], dilated cardiomyopathy [266], hypertrophic cardiomyopathy [267] etc. By deriving iCMs, iCFs, iMacs and other cardiac cell types from patient-derived iPSCs, highly clinically relevant EHTs can be fabricated for rescue and drug discovery studies.

Moving towards more clinically relevant conditions require transitioning from B27®-supplemented media to chemically defined, Good Manufacturing Practice (GMP)-compliant media, for standardisation and scalability [316]. In this study, EHTs were cultured in RPMI 1640 media, which is chemically defined [520], supplemented with B27®, which is a complex mixture of 21 components mostly of animal origin, originally designed for the culture of hippocampal neurons [521]. Chemically defined media has been previously developed and could serve as a reliable alternative to commercially available, undefined media components [316, 522]. Similarly, exploring alternative ECM sources beyond Matrigel®, such as fibrin [15, 252, 408] or decellularised ECM, aligns with the goal of creating a fully biomimetic environment for cardiac tissue development. Although decellularised myocardial matrices are animal derived [523], EHTs fabricated with decellularised myocardial matrix would still be more physiologically relevant than EHTs fabricated with Matrigel®. Moreover, complete GMP-compliance could also be achieved by using cell-derived matrices [524] or by using commercially available human collagen (for example, VitroCol® from Advanced Biomatrix) or human Vitronectin (Gibco) solutions, which can be used as alternatives to Matrigel® coating for iPSC culture.

To mimic the complexity of the native myocardium, future studies could incorporate additional cell types such as cardiac endothelial cells and smooth muscle cells into the EHTs. This shift towards a multi-cellular approach acknowledges the importance of interactions not only between cardiomyocytes and macrophages but also with other cardiac cell types. Previous work from Giacomelli *et al.* and Campostrini *et al.* utilising endothelial cells in the fabrication of 3D cardiac models have shown promising results with improved tissue function [28, 146, 165, 381]. In this study, high upregulation of VEGF was noted when iCMs and iMacs were electrically stimulated in co-culture. This finding further supports the addition of endothelial cells into EHTs, as positive interactions can be expected between iMacs and endothelial cells, potentially facilitating organised channel formations. Moreover, creating nutrient channels with endothelial cells could be a significant step towards scaling up the size of EHTs. Additionally, exploring the incorporation of extracellular vesicles (EVs) into EHTs could enhance the regenerative potential of the engineered tissues. EVs, known for their role in intercellular communication, could be isolated from iMacs or other cell types and introduced to the EHTs to assess their impact on tissue maturation and function, in addition to the therapeutic potential of the EVs. In a recent study, male mice with MI were treated with endothelial progenitor cell-derived EVs to find improved angiogenesis and revascularisation [525]. Similarly, vascular endothelial cell-derived EVs have shown cardioprotective effects in a human heart-on-a-chip model with ischemia-reperfusion injury [526]. Having seen great functional improvement in iCMs when in co-culture with iMacs, assessment of iMac-derived EVs would be of great interest, in improving EHT function.

With the rise in interest to generate patient-specific disease models, sex-related disparities often tend to get overlooked. Clinical and pre-clinical trials have traditionally been dominated by male patients, resulting in the belief that sex-based differences are only relevant in reproductive diseases [478]. However, sex differences are now being actively researched, particularly in the context of CVDs [527]. Sex-related differences in the immune system is well recognised, with females showing an increased baseline level

of inflammatory markers [528]. However, more recent studies delving deeper into sex-differences in CVDs highlight key disparities. Hartman *et al.* studied atherosclerotic tissue samples from age-matched female and male patients to show that pro-atherosclerotic genes that were more active in females were associated with endothelial cells and mesenchymal cells, whereas the same in males were associated with immune cells [529]. Another interesting study published in 2021 demonstrated that sex-specific differences exist in cardiomyocytes well before the gonads are activated in the embryo, independent of the influence of sex hormones or environment [530]. Through these studies, we now know that just relying on male and female cell types is not enough to fabricate a truly sex-specific EHT model. Potential preliminary improvements to achieve sex-specific models could be using iPSCs derived from male (XY) and females (XX) differentiated to the cardiac cell types of interest, cultured sex-specific decellularised ECM or inert polymers (unlike PDMS, which absorbs hydrophobic molecules), with hormone-free basal media supplemented with testosterone (for male cultures) and oestrogen/progesterone (for female cultures) [478]. Furthermore, new studies draw attention to increased risk of MI and ischaemic stroke in transgender women receiving exogenous oestrogen as part of their treatment, compared with cisgender women [531, 532]. Although no such complications have been reported with transgender men receiving testosterone treatment, in general, transgender population is associated with a larger cardiac health risk than cisgender individuals [531, 532]. Similarly, anabolic androgenic steroids (commonly taken by bodybuilders), which contain supraphysiological levels of testosterone, has been associated with increased cardiovascular risk [533]. Moreover, hormone replacement therapy is very common amongst post-menopausal women, and the cardioprotective nature of oestrogen is well documented [534]. The increased occurrence of heart diseases in post-menopausal women has been shown to reduce with oestrogen treatment [535]. However, the exact mode of delivery (oral or transdermal), timing of the delivery (when to initiate the treatment and for how long) as well as the dose of the hormone has been controversial [534, 535]. With a plethora of useful framework available in literature, the strong need for true sex-specific EHT models can be achieved, to not only make existing EHT models

more physiologically relevant, but also to progress the outcomes related to cardiac health for individuals undergoing hormone treatments.

In summary, the future perspectives of this study revolve around refining and expanding the EHT model. This includes optimising culture conditions, introducing additional cell types, exploring diverse stimuli, and embracing advanced technologies to create more sophisticated and clinically relevant cardiac tissue models. The potential applications extend beyond tissue engineering, encompassing disease modelling, drug screening, and serving as a platform for deeper understanding of the intricate interplay between different cell types within the myocardium.

References

[1] C. W. Tsao *et al.*, "Heart Disease and Stroke Statistics-2023 Update: A Report From the American Heart Association," *Circulation,* vol. 147, no. 8, pp. e93-e621, Feb 21 2023

[2] K. Thygesen *et al.*, "Universal definition of myocardial infarction," *Circulation,* vol. 116, no. 22, pp. 2634-53, Nov 27 2007

[3] N. G. Frangogiannis, "Pathophysiology of Myocardial Infarction," *Compr Physiol,* vol. 5, no. 4, pp. 1841-75, Sep 20 2015

[4] W. J. Richardson, S. A. Clarke, T. A. Quinn, and J. W. Holmes, "Physiological Implications of Myocardial Scar Structure," *Compr Physiol,* vol. 5, no. 4, pp. 1877-909, Sep 20 2015

[5] K. M. Talha, A. Pandey, M. Fudim, J. Butler, S. D. Anker, and M. S. Khan, "Frailty and heart failure: State-of-the-art review," *J Cachexia Sarcopenia Muscle,* vol. 14, no. 5, pp. 1959-1972, Oct 2023

[6] D. Masarone, M. Kittleson, A. Petraio, and G. Pacileo, "Advanced heart failure: state of the art and future directions," *RCM,* vol. 23, no. 2, 2022-02-24 2022

[7] S. Frantz, J. Bauersachs, and G. Ertl, "Post-infarct remodelling: contribution of wound healing and inflammation," *Cardiovasc Res,* vol. 81, no. 3, pp. 474-81, Feb 15 2009

[8] C. W. Yancy *et al.*, "2016 ACC/AHA/HFSA Focused Update on New Pharmacological Therapy for Heart Failure: An Update of the 2013 ACCF/AHA Guideline for the Management of Heart Failure: A Report of the American College of Cardiology/American Heart Association Task Force on Clinical Practice Guidelines and the Heart Failure Society of America," *J Am Coll Cardiol,* vol. 68, no. 13, pp. 1476-1488, Sep 27 2016

[9] S. Cresci *et al.*, "Heart Failure in the Era of Precision Medicine: A Scientific Statement From the American Heart Association," *Circ Genom Precis Med,* vol. 12, no. 10, pp. 458-485, Oct 2019

[10] S. A. Hunt *et al.*, "2009 focused update incorporated into the ACC/AHA 2005 Guidelines for the Diagnosis and Management of Heart Failure in Adults: a report of the American College of Cardiology Foundation/American Heart Association Task Force on Practice Guidelines: developed in collaboration with the International Society for Heart and Lung Transplantation," *Circulation,* vol. 119, no. 14, pp. e391-479, Apr 14 2009

[11] E. M. Blalock *et al.*, "Harnessing the power of gene microarrays for the study of brain aging and Alzheimer's disease: statistical reliability and functional correlation," *Ageing Res Rev,* vol. 4, no. 4, pp. 481-512, Nov 2005

[12] D. Rajamohan *et al.*, "Current status of drug screening and disease modelling in human pluripotent stem cells," *Bioessays,* vol. 35, no. 3, pp. 281-98, Mar 2013

[13] T. Eschenhagen *et al.*, "Three-dimensional reconstitution of embryonic cardiomyocytes in a collagen matrix: a new heart muscle model system," *The FASEB Journal,* vol. 11, no. 8, pp. 683-694, 1997/07/01 1997

[14] S. S. Nunes *et al.*, "Biowire: a platform for maturation of human pluripotent stem cell-derived cardiomyocytes," *Nat Methods,* vol. 10, no. 8, pp. 781-787, 2013

[15] E. Querdel *et al.*, "Human Engineered Heart Tissue Patches Remuscularize the Injured Heart in a Dose-Dependent Manner," *Circulation,* vol. 143, no. 20, pp. 1991-2006, May 18 2021

[16] K. Ronaldson-Bouchard *et al.*, "Advanced maturation of human cardiac tissue grown from pluripotent stem cells," *Nature,* vol. 556, no. 7700, pp. 239-243, Apr 2018

[17] W. H. Zimmermann *et al.*, "Tissue engineering of a differentiated cardiac muscle construct," *Circ Res,* vol. 90, no. 2, pp. 223-30, Feb 8 2002
[18] J. W. Williams, C. Giannarelli, A. Rahman, G. J. Randolph, and J. C. Kovacic, "Macrophage Biology, Classification, and Phenotype in Cardiovascular Disease: JACC Macrophage in CVD Series (Part 1)," *Journal of the American College of Cardiology,* vol. 72, no. 18, pp. 2166-2180, 2018
[19] S. Gordon and A. Plüddemann, "Tissue macrophages: heterogeneity and functions," *BMC Biology,* vol. 15, no. 1, p. 53, 2017/06/29 2017
[20] K. J. Lavine *et al.*, "The Macrophage in Cardiac Homeostasis and Disease: JACC Macrophage in CVD Series (Part 4)," *Journal of the American College of Cardiology,* vol. 72, no. 18, pp. 2213-2230, 2018
[21] M. Hulsmans *et al.*, "Macrophages Facilitate Electrical Conduction in the Heart," *Cell,* vol. 169, no. 3, pp. 510-522.e20, Apr 20 2017
[22] J. A. Nicolás-Ávila *et al.*, "A Network of Macrophages Supports Mitochondrial Homeostasis in the Heart," *Cell,* Sep 9 2020
[23] A. Shigeta *et al.*, "Endocardially Derived Macrophages Are Essential for Valvular Remodeling," *Dev Cell,* vol. 48, no. 5, pp. 617-630.e3, Mar 11 2019
[24] G. de Couto, "Macrophages in cardiac repair: Environmental cues and therapeutic strategies," *Exp Mol Med,* vol. 51, no. 12, pp. 1-10, Dec 19 2019
[25] J. W. Godwin, R. Debuque, E. Salimova, and N. A. Rosenthal, "Heart regeneration in the salamander relies on macrophage-mediated control of fibroblast activation and the extracellular landscape," *NPJ Regen Med,* vol. 2, 2017
[26] S. L. Lai *et al.*, "Reciprocal analyses in zebrafish and medaka reveal that harnessing the immune response promotes cardiac regeneration," *Elife,* vol. 6, Jun 20 2017
[27] S. Steffens, M. Nahrendorf, and R. Madonna, "Immune cells in cardiac homeostasis and disease: emerging insights from novel technologies," *Eur Heart J,* vol. 43, no. 16, pp. 1533-1541, Apr 19 2022
[28] G. Campostrini *et al.*, "Generation, functional analysis and applications of isogenic three-dimensional self-aggregating cardiac microtissues from human pluripotent stem cells," *Nat Protoc,* vol. 16, no. 4, pp. 2213-2256, Apr 2021
[29] J. F. Murphy *et al.*, "Adult human cardiac stem cell supplementation effectively increases contractile function and maturation in human engineered cardiac tissues," *Stem Cell Research & Therapy,* vol. 10, no. 1, p. 373, 2019/12/04 2019
[30] A. P. Voorhees and H. C. Han, "Biomechanics of Cardiac Function," *Compr Physiol,* vol. 5, no. 4, pp. 1623-44, Sep 20 2015
[31] F. Saremi *et al.*, "Fibrous Skeleton of the Heart: Anatomic Overview and Evaluation of Pathologic Conditions with CT and MR Imaging," *Radiographics,* vol. 37, no. 5, pp. 1330-1351, Sep-Oct 2017
[32] K. A. Anita Arackal, Ed. *Histology, Heart*. Treasure Island (FL): StatPearls, Updated 2023 Jan 2. [Online]. Available: https://www.ncbi.nlm.nih.gov/books/NBK545143/.
[33] S. Virani Salim *et al.*, "Heart Disease and Stroke Statistics—2020 Update: A Report From the American Heart Association," *Circulation,* vol. 141, no. 9, pp. e139-e596, 2020/03/03 2020
[34] T. A. Gaziano, "Cardiovascular disease in the developing world and its cost-effective management," *Circulation,* vol. 112, no. 23, pp. 3547-53, Dec 6 2005
[35] G. A. Roth *et al.*, "Global Burden of Cardiovascular Diseases and Risk Factors, 1990-2019: Update From the GBD 2019 Study," *J Am Coll Cardiol,* vol. 76, no. 25, pp. 2982-3021, Dec 22 2020
[36] E. Olvera Lopez, B. D. Ballard, and A. Jan, "Cardiovascular Disease," in *StatPearls*. Treasure Island (FL) with ineligible companies. Disclosure: Brian Ballard declares no

relevant financial relationships with ineligible companies. Disclosure: Arif Jan declares no relevant financial relationships with ineligible companies.: StatPearls Publishing
Copyright © 2024, StatPearls Publishing LLC., 2024.
[37] K. Thygesen, J. S. Alpert, A. S. Jaffe, M. L. Simoons, B. R. Chaitman, and H. D. White, "Third Universal Definition of Myocardial Infarction," *Circulation,* vol. 126, no. 16, pp. 2020-2035, 2012

[38] J. A. Kirk and D. A. Kass, "Electromechanical Dyssynchrony and Resynchronization of the Failing Heart," *Circulation Research,* vol. 113, no. 6, pp. 765-776, 2013

[39] C. S. Fox, M. J. Pencina, P. W. Wilson, N. P. Paynter, R. S. Vasan, and R. B. D'Agostino, Sr., "Lifetime risk of cardiovascular disease among individuals with and without diabetes stratified by obesity status in the Framingham heart study," *Diabetes Care,* vol. 31, no. 8, pp. 1582-4, Aug 2008

[40] D. M. Lloyd-Jones, M. G. Larson, A. Beiser, and D. Levy, "Lifetime risk of developing coronary heart disease," *Lancet,* vol. 353, no. 9147, pp. 89-92, Jan 9 1999

[41] E. J. Benjamin *et al.*, "Heart Disease and Stroke Statistics-2018 Update: A Report From the American Heart Association," *Circulation,* vol. 137, no. 12, pp. e67-e492, Mar 20 2018

[42] M. Litviňuková *et al.*, "Cells of the adult human heart," *Nature,* pp. 1-7, Sep 24 2020

[43] P. Zhou and W. T. Pu, "Recounting Cardiac Cellular Composition," *Circulation research,* vol. 118, no. 3, pp. 368-370, 2016

[44] K. Fountoulaki, N. Dagres, and E. K. Iliodromitis, "Cellular Communications in the Heart," *Card Fail Rev,* vol. 1, no. 2, pp. 64-68, 2015

[45] L. He *et al.*, "Preexisting endothelial cells mediate cardiac neovascularization after injury," *J Clin Invest,* vol. 127, no. 8, pp. 2968-2981, Aug 1 2017

[46] A. K. Olsson, A. Dimberg, J. Kreuger, and L. Claesson-Welsh, "VEGF receptor signalling - in control of vascular function," *Nat Rev Mol Cell Biol,* vol. 7, no. 5, pp. 359-71, May 2006

[47] Y. R. Jiang, J. Y. Du, D. D. Wang, and X. Yang, "miRNA-130a improves cardiac function by down-regulating TNF-α expression in a rat model of heart failure," *Eur Rev Med Pharmacol Sci,* vol. 22, no. 23, pp. 8454-8461, Dec 2018

[48] O. A. Segiet, A. Piecuch, L. Mielanczyk, M. Michalski, and E. Nowalany-Kozielska, "Role of interleukins in heart failure with reduced ejection fraction," *Anatol J Cardiol,* vol. 22, no. 6, pp. 287-299, 2019

[49] S. A. Doppler *et al.*, "Cardiac fibroblasts: more than mechanical support," *J Thorac Dis,* vol. 9, no. Suppl 1, pp. S36-S51, 2017

[50] M. J. Ivey and M. D. Tallquist, "Defining the Cardiac Fibroblast," *Circ J,* vol. 80, no. 11, pp. 2269-2276, 2016

[51] P. Libby, P. M. Ridker, and G. K. Hansson, "Progress and challenges in translating the biology of atherosclerosis," *Nature,* vol. 473, no. 7347, pp. 317-25, May 19 2011

[52] K. Ley, A. B. Pramod, M. Croft, K. S. Ravichandran, and J. P. Ting, "How Mouse Macrophages Sense What Is Going On," *Front Immunol,* vol. 7, p. 204, 2016

[53] A. M. Lundberg and G. K. Hansson, "Innate immune signals in atherosclerosis," *Clin Immunol,* vol. 134, no. 1, pp. 5-24, Jan 2010

[54] D. Wolf, A. Zirlik, and K. Ley, "Beyond vascular inflammation--recent advances in understanding atherosclerosis," *Cell Mol Life Sci,* vol. 72, no. 20, pp. 3853-69, Oct 2015

[55] M. N. Amin *et al.*, "Inflammatory cytokines in the pathogenesis of cardiovascular disease and cancer," *SAGE Open Med,* vol. 8, p. 2050312120965752, 2020

[56] N. Lasrado, B. Yalaka, and J. Reddy, "Triggers of Inflammatory Heart Disease," *Frontiers in Cell and Developmental Biology,* Mini Review vol. 8, 2020-March-24 2020

[57] P. M. Ridker *et al.*, "Antiinflammatory Therapy with Canakinumab for Atherosclerotic Disease," *N Engl J Med,* vol. 377, no. 12, pp. 1119-1131, Sep 21 2017

[58] E. De Angelis, M. Pecoraro, M. R. Rusciano, M. Ciccarelli, and A. Popolo, "Cross-Talk between Neurohormonal Pathways and the Immune System in Heart Failure: A Review of the Literature," *Int J Mol Sci,* vol. 20, no. 7, Apr 5 2019
[59] P. Yang, Z. Chen, W. Huang, J. Zhang, L. Zou, and H. Wang, "Communications between macrophages and cardiomyocytes," *Cell Communication and Signaling,* vol. 21, no. 1, p. 206, 2023/08/16 2023
[60] C. M. Weyand, H. Fujii, L. Shao, and J. J. Goronzy, "Rejuvenating the immune system in rheumatoid arthritis," *Nat Rev Rheumatol,* vol. 5, no. 10, pp. 583-8, Oct 2009
[61] K. Shirakawa and M. Sano, "T Cell Immunosenescence in Aging, Obesity, and Cardiovascular Disease," *Cells,* vol. 10, no. 9, Sep 15 2021
[62] L. Adamo *et al.*, "Myocardial B cells are a subset of circulating lymphocytes with delayed transit through the heart," *JCI Insight,* vol. 5, no. 3, Feb 13 2020
[63] J. Grune *et al.*, "Neutrophils incite and macrophages avert electrical storm after myocardial infarction," *Nature Cardiovascular Research,* vol. 1, no. 7, pp. 649-664, 2022/07/01 2022
[64] S. A. Dick *et al.*, "Three tissue resident macrophage subsets coexist across organs with conserved origins and life cycles," *Science Immunology,* vol. 7, no. 67, p. eabf7777, 2022
[65] L. C. Davies, S. J. Jenkins, J. E. Allen, and P. R. Taylor, "Tissue-resident macrophages," *Nature Immunology,* vol. 14, no. 10, pp. 986-995, 2013/10/01 2013
[66] A. I. Tauber, "Metchnikoff and the phagocytosis theory," *Nat Rev Mol Cell Biol,* vol. 4, no. 11, pp. 897-901, Nov 2003
[67] S. Yona and S. Gordon, "From the Reticuloendothelial to Mononuclear Phagocyte System - The Unaccounted Years," *Front Immunol,* vol. 6, pp. 328-328, 2015
[68] M. M. Wintrobe, "Blood, Pure and Eloquent," *Journal of Pediatric Hematology/Oncology,* vol. 3, no. 3, p. 334, 1981
[69] R. van Furth, Z. A. Cohn, J. G. Hirsch, J. H. Humphrey, W. G. Spector, and H. L. Langevoort, "The mononuclear phagocyte system: a new classification of macrophages, monocytes, and their precursor cells," *Bull World Health Organ,* vol. 46, no. 6, pp. 845-52, 1972
[70] R. M. Steinman and Z. A. Cohn, "Identification of a novel cell type in peripheral lymphoid organs of mice. I. Morphology, quantitation, tissue distribution," *J Exp Med,* vol. 137, no. 5, pp. 1142-62, May 1 1973
[71] D. A. Hume, "The mononuclear phagocyte system," *Curr Opin Immunol,* vol. 18, no. 1, pp. 49-53, Feb 2006
[72] R. van Furth and Z. A. Cohn, "The origin and kinetics of mononuclear phagocytes," *J Exp Med,* vol. 128, no. 3, pp. 415-35, Sep 1 1968
[73] D. R. Barreda, H. R. Neely, and M. F. Flajnik, "Evolution of Myeloid Cells," *Microbiol Spectr,* vol. 4, no. 3, Jun 2016
[74] M. D. Cooper and M. N. Alder, "The evolution of adaptive immune systems," *Cell,* vol. 124, no. 4, pp. 815-22, Feb 24 2006
[75] S. Gordon and P. R. Taylor, "Monocyte and macrophage heterogeneity," *Nat Rev Immunol,* vol. 5, no. 12, pp. 953-64, Dec 2005
[76] A. M. Lichanska and D. A. Hume, "Origins and functions of phagocytes in the embryo," *Exp Hematol,* vol. 28, no. 6, pp. 601-11, Jun 2000
[77] G. Hoeffel and F. Ginhoux, "Ontogeny of Tissue-Resident Macrophages," *Front Immunol,* vol. 6, p. 486, 2015
[78] I. M. Samokhvalov, "Deconvoluting the ontogeny of hematopoietic stem cells," *Cell Mol Life Sci,* vol. 71, no. 6, pp. 957-78, Mar 2014
[79] B. Kasaai *et al.*, "Erythro-myeloid progenitors can differentiate from endothelial cells and modulate embryonic vascular remodeling," *Sci Rep,* vol. 7, p. 43817, Mar 8 2017

[80] S. H. Orkin and L. I. Zon, "Hematopoiesis: an evolving paradigm for stem cell biology," *Cell,* vol. 132, no. 4, pp. 631-44, Feb 22 2008
[81] E. Mass *et al.*, "Specification of tissue-resident macrophages during organogenesis," *Science,* vol. 353, no. 6304, Sep 9 2016
[82] F. Ginhoux *et al.*, "Fate mapping analysis reveals that adult microglia derive from primitive macrophages," *Science,* vol. 330, no. 6005, pp. 841-5, Nov 5 2010
[83] G. Hoeffel *et al.*, "Adult Langerhans cells derive predominantly from embryonic fetal liver monocytes with a minor contribution of yolk sac-derived macrophages," *J Exp Med,* vol. 209, no. 6, pp. 1167-81, Jun 4 2012
[84] Y. Wang *et al.*, "IL-34 is a tissue-restricted ligand of CSF1R required for the development of Langerhans cells and microglia," *Nat Immunol,* vol. 13, no. 8, pp. 753-60, Jun 24 2012
[85] A. T. Satpathy, X. Wu, J. C. Albring, and K. M. Murphy, "Re(de)fining the dendritic cell lineage," *Nature immunology,* vol. 13, no. 12, pp. 1145-1154, 2012
[86] C. Schulz *et al.*, "A lineage of myeloid cells independent of Myb and hematopoietic stem cells," *Science,* vol. 336, no. 6077, pp. 86-90, Apr 6 2012
[87] C. Auffray *et al.*, "Monitoring of blood vessels and tissues by a population of monocytes with patrolling behavior," *Science,* vol. 317, no. 5838, pp. 666-70, Aug 3 2007
[88] C. Jakubzick *et al.*, "Minimal differentiation of classical monocytes as they survey steady-state tissues and transport antigen to lymph nodes," *Immunity,* vol. 39, no. 3, pp. 599-610, Sep 19 2013
[89] D. Hashimoto *et al.*, "Tissue-resident macrophages self-maintain locally throughout adult life with minimal contribution from circulating monocytes," *Immunity,* vol. 38, no. 4, pp. 792-804, Apr 18 2013
[90] S. Epelman *et al.*, "Embryonic and adult-derived resident cardiac macrophages are maintained through distinct mechanisms at steady state and during inflammation," *Immunity,* vol. 40, no. 1, pp. 91-104, Jan 16 2014
[91] S. Yona *et al.*, "Fate mapping reveals origins and dynamics of monocytes and tissue macrophages under homeostasis," *Immunity,* vol. 38, no. 1, pp. 79-91, Jan 24 2013
[92] M. Haldar *et al.*, "Heme-mediated SPI-C induction promotes monocyte differentiation into iron-recycling macrophages," *Cell,* vol. 156, no. 6, pp. 1223-1234, Mar 13 2014
[93] M. Kohyama *et al.*, "Role for Spi-C in the development of red pulp macrophages and splenic iron homeostasis," *Nature,* vol. 457, no. 7227, pp. 318-21, Jan 15 2009
[94] A. G. N *et al.*, "The nuclear receptor LXRalpha controls the functional specialization of splenic macrophages," *Nat Immunol,* vol. 14, no. 8, pp. 831-9, Aug 2013
[95] S. Abutbul *et al.*, "TGF-beta signaling through SMAD2/3 induces the quiescent microglial phenotype within the CNS environment," *Glia,* vol. 60, no. 7, pp. 1160-71, Jul 2012
[96] O. Butovsky *et al.*, "Identification of a unique TGF-beta-dependent molecular and functional signature in microglia," *Nat Neurosci,* vol. 17, no. 1, pp. 131-43, Jan 2014
[97] Y. Okabe and R. Medzhitov, "Tissue-specific signals control reversible program of localization and functional polarization of macrophages," *Cell,* vol. 157, no. 4, pp. 832-44, May 8 2014
[98] O. Fainaru *et al.*, "Runx3 regulates mouse TGF-beta-mediated dendritic cell function and its absence results in airway inflammation," *Embo j,* vol. 23, no. 4, pp. 969-79, Feb 25 2004
[99] C. Hacker *et al.*, "Transcriptional profiling identifies Id2 function in dendritic cell development," *Nat Immunol,* vol. 4, no. 4, pp. 380-6, Apr 2003
[100] E. L. Gautier *et al.*, "Systemic analysis of PPARgamma in mouse macrophage populations reveals marked diversity in expression with critical roles in resolution of inflammation and airway immunity," *J Immunol,* vol. 189, no. 5, pp. 2614-24, Sep 1 2012

[101] Y. Lavin *et al.*, "Tissue-resident macrophage enhancer landscapes are shaped by the local microenvironment," *Cell,* vol. 159, no. 6, pp. 1312-26, Dec 4 2014
[102] S. A. Dick *et al.*, "Self-renewing resident cardiac macrophages limit adverse remodeling following myocardial infarction," *Nat Immunol,* vol. 20, no. 1, pp. 29-39, Jan 2019
[103] H. B. Sager *et al.*, "Proliferation and Recruitment Contribute to Myocardial Macrophage Expansion in Chronic Heart Failure," *Circulation research,* vol. 119, no. 7, pp. 853-864, 2016
[104] G. Bajpai *et al.*, "Tissue Resident CCR2- and CCR2+ Cardiac Macrophages Differentially Orchestrate Monocyte Recruitment and Fate Specification Following Myocardial Injury," *Circ Res,* vol. 124, no. 2, pp. 263-278, Jan 18 2019
[105] T. Heidt *et al.*, "Differential contribution of monocytes to heart macrophages in steady-state and after myocardial infarction," *Circ Res,* vol. 115, no. 2, pp. 284-95, Jul 7 2014
[106] G. Bajpai *et al.*, "The human heart contains distinct macrophage subsets with divergent origins and functions," *Nat Med,* vol. 24, no. 8, pp. 1234-1245, Aug 2018
[107] N. R. Tucker *et al.*, "Transcriptional and Cellular Diversity of the Human Heart," *Circulation,* May 14 2020
[108] L. Honold and M. Nahrendorf, "Resident and Monocyte-Derived Macrophages in Cardiovascular Disease," *Circ Res,* vol. 122, no. 1, pp. 113-127, Jan 5 2018
[109] J. Leid, J. Carrelha, H. Boukarabila, S. Epelman, S. E. Jacobsen, and K. J. Lavine, "Primitive Embryonic Macrophages are Required for Coronary Development and Maturation," *Circ Res,* vol. 118, no. 10, pp. 1498-511, May 13 2016
[110] A. R. Pinto, J. W. Godwin, and N. A. Rosenthal, "Macrophages in cardiac homeostasis, injury responses and progenitor cell mobilisation," *Stem Cell Res,* vol. 13, no. 3 Pt B, pp. 705-14, Nov 2014
[111] Y. Li, Q. Li, and G. C. Fan, "Macrophage Efferocytosis in Cardiac Pathophysiology and Repair," *Shock,* Jul 15 2020
[112] M. DeBerge *et al.*, "MerTK Cleavage on Resident Cardiac Macrophages Compromises Repair After Myocardial Ischemia Reperfusion Injury," *Circ Res,* vol. 121, no. 8, pp. 930-940, Sep 29 2017
[113] I. Melentijevic *et al.*, "C. elegans neurons jettison protein aggregates and mitochondria under neurotoxic stress," *Nature,* vol. 542, no. 7641, pp. 367-371, 2017
[114] M. Suku, L. Forrester, M. Biggs, and M. G. Monaghan, "Resident Macrophages and Their Potential in Cardiac Tissue Engineering," *Tissue Eng Part B Rev,* vol. 28, no. 3, pp. 579-591, Jun 2022
[115] K. A. Reimer, R. B. Jennings, and A. H. Tatum, "Pathobiology of acute myocardial ischemia: metabolic, functional and ultrastructural studies," *Am J Cardiol,* vol. 52, no. 2, pp. 72a-81a, Jul 20 1983
[116] M. Nahrendorf *et al.*, "The healing myocardium sequentially mobilizes two monocyte subsets with divergent and complementary functions," *J Exp Med,* vol. 204, no. 12, pp. 3037-47, Nov 26 2007
[117] W. Li *et al.*, "Heart-resident CCR2(+) macrophages promote neutrophil extravasation through TLR9/MyD88/CXCL5 signaling," *JCI Insight,* vol. 1, no. 12, p. e87315, 2016
[118] I. Hilgendorf *et al.*, "Ly-6Chigh monocytes depend on Nr4a1 to balance both inflammatory and reparative phases in the infarcted myocardium," *Circ Res,* vol. 114, no. 10, pp. 1611-22, May 9 2014
[119] W. W. Lee *et al.*, "PET/MRI of inflammation in myocardial infarction," *J Am Coll Cardiol,* vol. 59, no. 2, pp. 153-63, Jan 10 2012
[120] F. Leuschner *et al.*, "Rapid monocyte kinetics in acute myocardial infarction are sustained by extramedullary monocytopoiesis," *J Exp Med,* vol. 209, no. 1, pp. 123-37, Jan 16 2012

[121] S. Frantz and M. Nahrendorf, "Cardiac macrophages and their role in ischaemic heart disease," *Cardiovasc Res,* vol. 102, no. 2, pp. 240-8, May 1 2014
[122] N. G. Frangogiannis, "Inflammation in cardiac injury, repair and regeneration," *Curr Opin Cardiol,* vol. 30, no. 3, pp. 240-5, May 2015
[123] S. M. Dunlay, S. A. Weston, M. M. Redfield, J. M. Killian, and V. L. Roger, "Tumor necrosis factor-alpha and mortality in heart failure: a community study," *Circulation,* vol. 118, no. 6, pp. 625-31, Aug 5 2008
[124] N. G. Frangogiannis, "The inflammatory response in myocardial injury, repair, and remodelling," *Nat Rev Cardiol,* vol. 11, no. 5, pp. 255-65, May 2014
[125] K. J. Lavine *et al.*, "Distinct macrophage lineages contribute to disparate patterns of cardiac recovery and remodeling in the neonatal and adult heart," *Proc Natl Acad Sci U S A,* vol. 111, no. 45, pp. 16029-34, Nov 11 2014
[126] B. Chen and N. G. Frangogiannis, "Macrophages in the Remodeling Failing Heart," *Circulation research,* vol. 119, no. 7, pp. 776-778, 2016
[127] M. J. van Amerongen, M. C. Harmsen, N. van Rooijen, A. H. Petersen, and M. J. A. van Luyn, "Macrophage depletion impairs wound healing and increases left ventricular remodeling after myocardial injury in mice," *Am J Pathol,* vol. 170, no. 3, pp. 818-829, 2007
[128] M. Shiraishi *et al.*, "Alternatively activated macrophages determine repair of the infarcted adult murine heart," *J Clin Invest,* vol. 126, no. 6, pp. 2151-66, Jun 1 2016
[129] F. Leuschner *et al.*, "Therapeutic siRNA silencing in inflammatory monocytes in mice," *Nat Biotechnol,* vol. 29, no. 11, pp. 1005-1010, 2011
[130] R. J. Vagnozzi *et al.*, "An acute immune response underlies the benefit of cardiac stem cell therapy," *Nature,* vol. 577, no. 7790, pp. 405-409, Jan 2020
[131] Y. Zouggari *et al.*, "B lymphocytes trigger monocyte mobilization and impair heart function after acute myocardial infarction," *Nat Med,* vol. 19, no. 10, pp. 1273-80, Oct 2013
[132] M. Hulsmans, F. Sam, and M. Nahrendorf, "Monocyte and macrophage contributions to cardiac remodeling," *J Mol Cell Cardiol,* vol. 93, pp. 149-55, Apr 2016
[133] H. B. Sager, T. Kessler, and H. Schunkert, "Monocytes and macrophages in cardiac injury and repair," *J Thorac Dis,* vol. 9, no. Suppl 1, pp. S30-S35, 2017
[134] A. Leask, "Getting to the heart of the matter: new insights into cardiac fibrosis," *Circ Res,* vol. 116, no. 7, pp. 1269-76, Mar 27 2015
[135] M. A. Ismahil, T. Hamid, S. S. Bansal, B. Patel, J. R. Kingery, and S. D. Prabhu, "Remodeling of the mononuclear phagocyte network underlies chronic inflammation and disease progression in heart failure: critical importance of the cardiosplenic axis," *Circ Res,* vol. 114, no. 2, pp. 266-82, Jan 17 2014
[136] A. J. Whitehead and A. J. Engler, "Regenerative Crosstalk between Cardiac Cells and Macrophages," *American Journal of Physiology-Heart and Circulatory Physiology,* vol. 0, no. 0, p. null,
[137] L. T. Cooper, Jr., "Myocarditis," *N Engl J Med,* vol. 360, no. 15, pp. 1526-38, Apr 9 2009
[138] A. Anzai *et al.*, "Self-reactive CD4(+) IL-3(+) T cells amplify autoimmune inflammation in myocarditis by inciting monocyte chemotaxis," *J Exp Med,* vol. 216, no. 2, pp. 369-383, Feb 4 2019
[139] X. Liao *et al.*, "Cardiac macrophages regulate isoproterenol-induced Takotsubo-like cardiomyopathy," *JCI Insight,* vol. 7, no. 3, Feb 8 2022
[140] H. Zhang *et al.*, "Self-Maintenance of Cardiac Resident Reparative Macrophages Attenuates Doxorubicin-Induced Cardiomyopathy Through the SR-A1-c-Myc Axis," *Circ Res,* vol. 127, no. 5, pp. 610-627, Aug 14 2020

[141] K. Zhang *et al.*, "TREM2(hi) resident macrophages protect the septic heart by maintaining cardiomyocyte homeostasis," *Nat Metab,* vol. 5, no. 1, pp. 129-146, Jan 2023
[142] X. S. Revelo *et al.*, "Cardiac Resident Macrophages Prevent Fibrosis and Stimulate Angiogenesis," *Circulation Research,* vol. 129, no. 12, pp. 1086-1101, 2021
[143] S. Cho, C. Lee, M. A. Skylar-Scott, S. C. Heilshorn, and J. C. Wu, "Reconstructing the heart using iPSCs: Engineering strategies and applications," *J Mol Cell Cardiol,* vol. 157, pp. 56-65, Aug 2021
[144] Y. Shi, H. Inoue, J. C. Wu, and S. Yamanaka, "Induced pluripotent stem cell technology: a decade of progress," *Nature Reviews Drug Discovery,* vol. 16, no. 2, pp. 115-130, 2017/02/01 2017
[145] X. Lian *et al.*, "Directed cardiomyocyte differentiation from human pluripotent stem cells by modulating Wnt/β-catenin signaling under fully defined conditions," *Nat Protoc,* vol. 8, no. 1, pp. 162-75, Jan 2013
[146] E. Giacomelli, M. Bellin, V. V. Orlova, and C. L. Mummery, "Co-Differentiation of Human Pluripotent Stem Cells-Derived Cardiomyocytes and Endothelial Cells from Cardiac Mesoderm Provides a Three-Dimensional Model of Cardiac Microtissue," *Curr Protoc Hum Genet,* vol. 95, pp. 21.9.1-21.9.22, Oct 18 2017
[147] J. Zhang *et al.*, "Functional cardiac fibroblasts derived from human pluripotent stem cells via second heart field progenitors," *Nature Communications,* vol. 10, no. 1, p. 2238, 2019/05/20 2019
[148] I. Kehat *et al.*, "Human embryonic stem cells can differentiate into myocytes with structural and functional properties of cardiomyocytes," *J Clin Invest,* vol. 108, no. 3, pp. 407-14, Aug 2001
[149] J. Q. He, Y. Ma, Y. Lee, J. A. Thomson, and T. J. Kamp, "Human embryonic stem cells develop into multiple types of cardiac myocytes: action potential characterization," *Circ Res,* vol. 93, no. 1, pp. 32-9, Jul 11 2003
[150] M. A. Laflamme *et al.*, "Cardiomyocytes derived from human embryonic stem cells in pro-survival factors enhance function of infarcted rat hearts," *Nat Biotechnol,* vol. 25, no. 9, pp. 1015-24, Sep 2007
[151] L. Yang *et al.*, "Human cardiovascular progenitor cells develop from a KDR+ embryonic-stem-cell-derived population," *Nature,* vol. 453, no. 7194, pp. 524-8, May 22 2008
[152] J. Zhang *et al.*, "Functional cardiomyocytes derived from human induced pluripotent stem cells," *Circ Res,* vol. 104, no. 4, pp. e30-41, Feb 27 2009
[153] I. Banerjee, J. W. Fuseler, R. L. Price, T. K. Borg, and T. A. Baudino, "Determination of cell types and numbers during cardiac development in the neonatal and adult rat and mouse," *Am J Physiol Heart Circ Physiol,* vol. 293, no. 3, pp. H1883-91, Sep 2007
[154] A. C. Nag, "Study of non-muscle cells of the adult mammalian heart: a fine structural analysis and distribution," *Cytobios,* vol. 28, no. 109, pp. 41-61, 1980
[155] C. Vasquez, P. Mohandas, K. L. Louie, N. Benamer, A. C. Bapat, and G. E. Morley, "Enhanced fibroblast-myocyte interactions in response to cardiac injury," *Circ Res,* vol. 107, no. 8, pp. 1011-20, Oct 15 2010
[156] H. Naito *et al.*, "Optimizing engineered heart tissue for therapeutic applications as surrogate heart muscle," *Circulation,* vol. 114, no. 1 Suppl, pp. I72-8, Jul 4 2006
[157] J. Zhang *et al.*, "Extracellular matrix promotes highly efficient cardiac differentiation of human pluripotent stem cells: the matrix sandwich method," *Circ Res,* vol. 111, no. 9, pp. 1125-36, Oct 12 2012
[158] S. J. Kattman *et al.*, "Stage-specific optimization of activin/nodal and BMP signaling promotes cardiac differentiation of mouse and human pluripotent stem cell lines," *Cell Stem Cell,* vol. 8, no. 2, pp. 228-40, Feb 4 2011

[159] A. D. Witty *et al.*, "Generation of the epicardial lineage from human pluripotent stem cells," *Nat Biotechnol,* vol. 32, no. 10, pp. 1026-35, Oct 2014
[160] D. Iyer *et al.*, "Robust derivation of epicardium and its differentiated smooth muscle cell progeny from human pluripotent stem cells," *Development,* vol. 142, no. 8, pp. 1528-41, Apr 15 2015
[161] X. Bao *et al.*, "Long-term self-renewing human epicardial cells generated from pluripotent stem cells under defined xeno-free conditions," *Nat Biomed Eng,* vol. 1, 2016
[162] H. Zhang *et al.*, "Generation of Quiescent Cardiac Fibroblasts From Human Induced Pluripotent Stem Cells for In Vitro Modeling of Cardiac Fibrosis," *Circ Res,* vol. 125, no. 5, pp. 552-566, Aug 16 2019
[163] D. Sinnecker, A. Goedel, K.-L. Laugwitz, and A. Moretti, "Induced Pluripotent Stem Cell-Derived Cardiomyocytes," *Circulation Research,* vol. 112, no. 6, pp. 961-968, 2013
[164] E. Karbassi *et al.*, "Cardiomyocyte maturation: advances in knowledge and implications for regenerative medicine," *Nat Rev Cardiol,* vol. 17, no. 6, pp. 341-359, Jun 2020
[165] M. Hoekstra, C. Mummery, A. Wilde, C. Bezzina, and A. Verkerk, "Induced pluripotent stem cell derived cardiomyocytes as models for cardiac arrhythmias," *Frontiers in Physiology,* Review vol. 3, 2012-August-31 2012
[166] M. Snir *et al.*, "Assessment of the ultrastructural and proliferative properties of human embryonic stem cell-derived cardiomyocytes," *Am J Physiol Heart Circ Physiol,* vol. 285, no. 6, pp. H2355-63, Dec 2003
[167] S. D. Lundy, W. Z. Zhu, M. Regnier, and M. A. Laflamme, "Structural and functional maturation of cardiomyocytes derived from human pluripotent stem cells," *Stem Cells Dev,* vol. 22, no. 14, pp. 1991-2002, Jul 15 2013
[168] T. Kamakura *et al.*, "Ultrastructural maturation of human-induced pluripotent stem cell-derived cardiomyocytes in a long-term culture," *Circ J,* vol. 77, no. 5, pp. 1307-14, 2013
[169] J. M. Churko *et al.*, "Defining human cardiac transcription factor hierarchies using integrated single-cell heterogeneity analysis," *Nat Commun,* vol. 9, no. 1, p. 4906, Nov 21 2018
[170] M. Li, S. E. Iismaa, N. Naqvi, A. Nicks, A. Husain, and R. M. Graham, "Thyroid hormone action in postnatal heart development," *Stem Cell Res,* vol. 13, no. 3 Pt B, pp. 582-91, Nov 2014
[171] X. Yang *et al.*, "Tri-iodo-l-thyronine promotes the maturation of human cardiomyocytes-derived from induced pluripotent stem cells," *J Mol Cell Cardiol,* vol. 72, pp. 296-304, Jul 2014
[172] E. A. Rog-Zielinska *et al.*, "Glucocorticoids promote structural and functional maturation of foetal cardiomyocytes: a role for PGC-1α," *Cell Death Differ,* vol. 22, no. 7, pp. 1106-16, Jul 2015
[173] S. S. Parikh *et al.*, "Thyroid and Glucocorticoid Hormones Promote Functional T-Tubule Development in Human-Induced Pluripotent Stem Cell-Derived Cardiomyocytes," *Circ Res,* vol. 121, no. 12, pp. 1323-1330, Dec 8 2017
[174] L. Wu *et al.*, "Angiotensin II promotes cardiac differentiation of embryonic stem cells via angiotensin type 1 receptor," *Differentiation,* vol. 86, no. 1-2, pp. 23-9, Jul-Sep 2013
[175] X. Yang *et al.*, "Fatty Acids Enhance the Maturation of Cardiomyocytes Derived from Human Pluripotent Stem Cells," *Stem Cell Reports,* vol. 13, no. 4, pp. 657-668, Oct 8 2019
[176] C. Correia *et al.*, "Distinct carbon sources affect structural and functional maturation of cardiomyocytes derived from human pluripotent stem cells," *Sci Rep,* vol. 7, no. 1, p. 8590, Aug 17 2017

[177] H. Nakano *et al.*, "Glucose inhibits cardiac muscle maturation through nucleotide biosynthesis," *Elife,* vol. 6, Dec 12 2017
[178] C. Tu, B. S. Chao, and J. C. Wu, "Strategies for Improving the Maturity of Human Induced Pluripotent Stem Cell-Derived Cardiomyocytes," *Circ Res,* vol. 123, no. 5, pp. 512-514, Aug 17 2018
[179] A. Salameh *et al.*, "Cyclic mechanical stretch induces cardiomyocyte orientation and polarization of the gap junction protein connexin43," *Circ Res,* vol. 106, no. 10, pp. 1592-602, May 28 2010
[180] E. Huethorst *et al.*, "Enhanced Human-Induced Pluripotent Stem Cell Derived Cardiomyocyte Maturation Using a Dual Microgradient Substrate," *ACS Biomater Sci Eng,* vol. 2, no. 12, pp. 2231-2239, Dec 12 2016
[181] C. Rao *et al.*, "The effect of microgrooved culture substrates on calcium cycling of cardiac myocytes derived from human induced pluripotent stem cells," *Biomaterials,* vol. 34, no. 10, pp. 2399-411, Mar 2013
[182] A. J. Engler *et al.*, "Embryonic cardiomyocytes beat best on a matrix with heart-like elasticity: scar-like rigidity inhibits beating," *J Cell Sci,* vol. 121, no. Pt 22, pp. 3794-802, Nov 15 2008
[183] T. J. Herron *et al.*, "Extracellular Matrix-Mediated Maturation of Human Pluripotent Stem Cell-Derived Cardiac Monolayer Structure and Electrophysiological Function," *Circ Arrhythm Electrophysiol,* vol. 9, no. 4, p. e003638, Apr 2016
[184] N. Tandon, A. Marsano, R. Maidhof, L. Wan, H. Park, and G. Vunjak-Novakovic, "Optimization of electrical stimulation parameters for cardiac tissue engineering," *J Tissue Eng Regen Med,* vol. 5, no. 6, pp. e115-25, Jun 2011
[185] M. Radisic *et al.*, "Functional assembly of engineered myocardium by electrical stimulation of cardiac myocytes cultured on scaffolds," *Proc Natl Acad Sci U S A,* vol. 101, no. 52, pp. 18129-34, Dec 28 2004
[186] R. Nuccitelli, "Endogenous ionic currents and DC electric fields in multicellular animal tissues," *Bioelectromagnetics,* vol. Suppl 1, pp. 147-57, 1992
[187] Y. Xia *et al.*, "Electrical stimulation of neonatal cardiac myocytes activates the NFAT3 and GATA4 pathways and up-regulates the adenylosuccinate synthetase 1 gene," *J Biol Chem,* vol. 275, no. 3, pp. 1855-63, Jan 21 2000
[188] R. Passier *et al.*, "CaM kinase signaling induces cardiac hypertrophy and activates the MEF2 transcription factor in vivo," *J Clin Invest,* vol. 105, no. 10, pp. 1395-406, May 2000
[189] S. Baumgartner *et al.*, "Electrophysiological and morphological maturation of murine fetal cardiomyocytes during electrical stimulation in vitro," *J Cardiovasc Pharmacol Ther,* vol. 20, no. 1, pp. 104-12, Jan 2015
[190] S. S. Nunes *et al.*, "Biowire: a platform for maturation of human pluripotent stem cell-derived cardiomyocytes," *Nat Methods,* vol. 10, no. 8, pp. 781-7, Aug 2013
[191] Y. Zhao *et al.*, "A Platform for Generation of Chamber-Specific Cardiac Tissues and Disease Modeling," *Cell,* vol. 176, no. 4, pp. 913-927.e18, Feb 7 2019
[192] N. Hagemeyer *et al.*, "Transcriptome-based profiling of yolk sac-derived macrophages reveals a role for Irf8 in macrophage maturation," *Embo j,* vol. 35, no. 16, pp. 1730-44, Aug 15 2016
[193] W. Haenseler *et al.*, "A Highly Efficient Human Pluripotent Stem Cell Microglia Model Displays a Neuronal-Co-culture-Specific Expression Profile and Inflammatory Response," *Stem Cell Reports,* vol. 8, no. 6, pp. 1727-1742, Jun 6 2017
[194] S. Gutbier *et al.*, "Large-Scale Production of Human iPSC-Derived Macrophages for Drug Screening," *Int J Mol Sci,* vol. 21, no. 13, Jul 7 2020
[195] X. Cao, G. K. Yakala, F. E. van den Hil, A. Cochrane, C. L. Mummery, and V. V. Orlova, "Differentiation and Functional Comparison of Monocytes and Macrophages from

hiPSCs with Peripheral Blood Derivatives," *Stem Cell Reports,* vol. 12, no. 6, pp. 1282-1297, Jun 11 2019

[196] T. Nenasheva *et al.*, "Macrophages Derived From Human Induced Pluripotent Stem Cells Are Low-Activated "Naïve-Like" Cells Capable of Restricting Mycobacteria Growth," *Front Immunol,* vol. 11, p. 1016, 2020

[197] J. Shi, C. Xue, W. Liu, and H. Zhang, "Differentiation of Human-Induced Pluripotent Stem Cells to Macrophages for Disease Modeling and Functional Genomics," *Curr Protoc Stem Cell Biol,* vol. 48, no. 1, p. e74, Feb 2019

[198] S. S. Haideri *et al.*, "Injection of embryonic stem cell derived macrophages ameliorates fibrosis in a murine model of liver injury," *NPJ Regen Med,* vol. 2, p. 14, 2017

[199] M. L. Litvack *et al.*, "Alveolar-like Stem Cell-derived Myb(-) Macrophages Promote Recovery and Survival in Airway Disease," *Am J Respir Crit Care Med,* vol. 193, no. 11, pp. 1219-29, Jun 1 2016

[200] F. Moroni *et al.*, "Safety profile of autologous macrophage therapy for liver cirrhosis," *Nat Med,* vol. 25, no. 10, pp. 1560-1565, Oct 2019

[201] J. Buchrieser, W. James, and M. D. Moore, "Human Induced Pluripotent Stem Cell-Derived Macrophages Share Ontogeny with MYB-Independent Tissue-Resident Macrophages," *Stem Cell Reports,* vol. 8, no. 2, pp. 334-345, Feb 14 2017

[202] F. Tasnim *et al.*, "Generation of mature kupffer cells from human induced pluripotent stem cells," *Biomaterials,* vol. 192, pp. 377-391, Feb 2019

[203] C. Z. W. Lee, T. Kozaki, and F. Ginhoux, "Studying tissue macrophages in vitro: are iPSC-derived cells the answer?," *Nat Rev Immunol,* vol. 18, no. 11, pp. 716-725, Nov 2018

[204] K. Takata *et al.*, "Induced-Pluripotent-Stem-Cell-Derived Primitive Macrophages Provide a Platform for Modeling Tissue-Resident Macrophage Differentiation and Function," *Immunity,* vol. 47, no. 1, pp. 183-198.e6, Jul 18 2017

[205] A. Quarta *et al.*, "Murine iPSC-derived microglia and macrophage cell culture models recapitulate distinct phenotypical and functional properties of classical and alternative neuro-immune polarisation," *Brain Behav Immun,* vol. 82, pp. 406-421, Nov 2019

[206] W. T'Jonck, M. Guilliams, and J. Bonnardel, "Niche signals and transcription factors involved in tissue-resident macrophage development," *Cell Immunol,* vol. 330, pp. 43-53, 2018

[207] A. Buttgereit *et al.*, "Sall1 is a transcriptional regulator defining microglia identity and function," *Nat Immunol,* vol. 17, no. 12, pp. 1397-1406, Dec 2016

[208] M. Lopez-Yrigoyen *et al.*, "Genetic programming of macrophages generates an in vitro model for the human erythroid island niche," *Nature Communications,* vol. 10, no. 1, p. 881, 2019/02/20 2019

[209] H. Zhang *et al.*, "Functional analysis and transcriptomic profiling of iPSC-derived macrophages and their application in modeling Mendelian disease," *Circ Res,* vol. 117, no. 1, pp. 17-28, Jun 19 2015

[210] B. van Wilgenburg, C. Browne, J. Vowles, and S. A. Cowley, "Efficient, long term production of monocyte-derived macrophages from human pluripotent stem cells under partly-defined and fully-defined conditions," *PLoS One,* vol. 8, no. 8, p. e71098, 2013

[211] N. Lachmann *et al.*, "Large-scale hematopoietic differentiation of human induced pluripotent stem cells provides granulocytes or macrophages for cell replacement therapies," *Stem Cell Reports,* vol. 4, no. 2, pp. 282-96, Feb 10 2015

[212] P. Douvaras *et al.*, "Directed Differentiation of Human Pluripotent Stem Cells to Microglia," *Stem cell reports,* vol. 8, no. 6, pp. 1516-1524, 2017

[213] J. Muffat *et al.*, "Efficient derivation of microglia-like cells from human pluripotent stem cells," *Nat Med,* vol. 22, no. 11, pp. 1358-1367, Nov 2016

[214] C. Dollinger *et al.*, "Incorporation of resident macrophages in engineered tissues: Multiple cell type response to microenvironment controlled macrophage-laden gelatine hydrogels," *J Tissue Eng Regen Med,* vol. 12, no. 2, pp. 330-340, Feb 2018
[215] M. Juhas *et al.*, "Incorporation of macrophages into engineered skeletal muscle enables enhanced muscle regeneration," *Nat Biomed Eng,* vol. 2, no. 12, pp. 942-954, Dec 2018
[216] L. S. Saleh and S. J. Bryant, "The Host Response in Tissue Engineering: Crosstalk Between Immune cells and Cell-laden Scaffolds," *Curr Opin Biomed Eng,* vol. 6, pp. 58-65, Jun 2018
[217] M. D. Costantino, A. Schuster, H. Helmholz, A. Meyer-Rachner, R. Willumeit-Römer, and B. J. C. Luthringer-Feyerabend, "Inflammatory response to magnesium-based biodegradable implant materials," *Acta Biomater,* vol. 101, pp. 598-608, Jan 1 2020
[218] K. M. Hotchkiss, N. M. Clark, and R. Olivares-Navarrete, "Macrophage response to hydrophilic biomaterials regulates MSC recruitment and T-helper cell populations," *Biomaterials,* vol. 182, pp. 202-215, Nov 2018
[219] R. Sridharan, B. Cavanagh, A. R. Cameron, D. J. Kelly, and F. J. O'Brien, "Material stiffness influences the polarization state, function and migration mode of macrophages," *Acta Biomater,* vol. 89, pp. 47-59, Apr 15 2019
[220] R. Sridharan, E. J. Ryan, C. J. Kearney, D. J. Kelly, and F. J. O'Brien, "Macrophage Polarization in Response to Collagen Scaffold Stiffness Is Dependent on Cross-Linking Agent Used To Modulate the Stiffness," *ACS Biomaterials Science & Engineering,* vol. 5, no. 2, pp. 544-552, 2019/02/11 2019
[221] K. L. Spiller *et al.*, "Sequential delivery of immunomodulatory cytokines to facilitate the M1-to-M2 transition of macrophages and enhance vascularization of bone scaffolds," *Biomaterials,* vol. 37, pp. 194-207, 2015
[222] N. Jetten, S. Verbruggen, M. J. Gijbels, M. J. Post, M. P. De Winther, and M. M. Donners, "Anti-inflammatory M2, but not pro-inflammatory M1 macrophages promote angiogenesis in vivo," *Angiogenesis,* vol. 17, no. 1, pp. 109-18, Jan 2014
[223] E. M. Moore, G. Ying, and J. L. West, "Macrophages Influence Vessel Formation in 3D Bioactive Hydrogels," *Advanced Biosystems,* vol. 1, no. 3, p. 1600021, 2017/03/01 2017
[224] O. R. Mahon *et al.*, "Nano-particle mediated M2 macrophage polarization enhances bone formation and MSC osteogenesis in an IL-10 dependent manner," *Biomaterials,* vol. 239, p. 119833, May 2020
[225] M. Romero-López *et al.*, "Macrophage Effects on Mesenchymal Stem Cell Osteogenesis in a Three-Dimensional In Vitro Bone Model," *Tissue Eng Part A,* Jun 2 2020
[226] K. A. Rose, N. S. Holman, A. M. Green, M. E. Andersen, and E. L. LeCluyse, "Co-culture of Hepatocytes and Kupffer Cells as an In Vitro Model of Inflammation and Drug-Induced Hepatotoxicity," *J Pharm Sci,* vol. 105, no. 2, pp. 950-964, Feb 2016
[227] T. V. Nguyen *et al.*, "Establishment of a hepatocyte-kupffer cell coculture model for assessment of proinflammatory cytokine effects on metabolizing enzymes and drug transporters," *Drug Metab Dispos,* vol. 43, no. 5, pp. 774-85, May 2015
[228] L. R. Pires, D. N. Rocha, L. Ambrosio, and A. P. Pêgo, "The role of the surface on microglia function: implications for central nervous system tissue engineering," *J R Soc Interface,* vol. 12, no. 103, p. 20141224, 2015
[229] N. Goshi, R. K. Morgan, P. J. Lein, and E. Seker, "A primary neural cell culture model to study neuron, astrocyte, and microglia interactions in neuroinflammation," *Journal of Neuroinflammation,* vol. 17, no. 1, p. 155, 2020/05/11 2020
[230] H. Ishii *et al.*, "Alveolar macrophage-epithelial cell interaction following exposure to atmospheric particles induces the release of mediators involved in monocyte mobilization and recruitment," *Respir Res,* vol. 6, no. 1, pp. 87-87, 2005

[231] M. Hittinger, N. A. Mell, H. Huwer, B. Loretz, N. Schneider-Daum, and C. M. Lehr, "Autologous co-culture of primary human alveolar macrophages and epithelial cells for investigating aerosol medicines. Part II: evaluation of IL-10-loaded microparticles for the treatment of lung inflammation," *Altern Lab Anim,* vol. 44, no. 4, pp. 349-360, Sep 2016
[232] S. Kletting *et al.*, "Co-culture of human alveolar epithelial (hAELVi) and macrophage (THP-1) cell lines," *Altex,* vol. 35, no. 2, pp. 211-222, 2018
[233] F. Weinberger, I. Mannhardt, and T. Eschenhagen, "Engineering Cardiac Muscle Tissue: A Maturating Field of Research," *Circ Res,* vol. 120, no. 9, pp. 1487-1500, Apr 28 2017
[234] I. C. P. Rodrigues, A. Kaasi, R. Maciel Filho, A. L. Jardini, and L. P. Gabriel, "Cardiac tissue engineering: current state-of-the-art materials, cells and tissue formation," *Einstein (Sao Paulo),* vol. 16, no. 3, pp. eRB4538-eRB4538, 2018
[235] I. Pallotta, B. Sun, E. A. Wrona, and D. O. Freytes, "BMP protein-mediated crosstalk between inflammatory cells and human pluripotent stem cell-derived cardiomyocytes," *J Tissue Eng Regen Med,* vol. 11, no. 5, pp. 1466-1478, May 2017
[236] C. Wang *et al.*, "Cardiomyocyte dedifferentiation and remodeling in 3D scaffolds to generate the cellular diversity of engineering cardiac tissues," *Biomater Sci,* vol. 7, no. 11, pp. 4636-4650, Nov 1 2019
[237] E. A. Wrona, B. Sun, S. Romero-Torres, and D. O. Freytes, "Effects of polarized macrophages on the in vitro gene expression after Co-Culture of human pluripotent stem cell-derived cardiomyocytes," *Journal of Immunology and Regenerative Medicine,* vol. 4, p. 100018, 2019/06/01/ 2019
[238] P. G. Hitscherich, L.-H. Xie, D. Del Re, and E. J. Lee, "The effects of macrophages on cardiomyocyte calcium-handling function using in vitro culture models," *Physiol Rep,* vol. 7, no. 13, pp. e14137-e14137, 2019
[239] P. R. Lawler *et al.*, "Targeting cardiovascular inflammation: next steps in clinical translation," *Eur Heart J,* vol. 42, no. 1, pp. 113-131, Jan 1 2021
[240] S. Huang and N. G. Frangogiannis, "Anti-inflammatory therapies in myocardial infarction: failures, hopes and challenges," *Br J Pharmacol,* vol. 175, no. 9, pp. 1377-1400, 2018
[241] P. M. Ridker *et al.*, "Antiinflammatory Therapy with Canakinumab for Atherosclerotic Disease," *New England Journal of Medicine,* vol. 377, no. 12, pp. 1119-1131, 2017
[242] P. M. Ridker *et al.*, "Low-Dose Methotrexate for the Prevention of Atherosclerotic Events," *New England Journal of Medicine,* vol. 380, no. 8, pp. 752-762, 2018
[243] P. M. Ridker, "From CANTOS to CIRT to COLCOT to Clinic," *Circulation,* vol. 141, no. 10, pp. 787-789, 2020
[244] J.-C. Tardif *et al.*, "Efficacy and Safety of Low-Dose Colchicine after Myocardial Infarction," *New England Journal of Medicine,* vol. 381, no. 26, pp. 2497-2505, 2019
[245] S. M. Nidorf *et al.*, "Colchicine in Patients with Chronic Coronary Disease," *New England Journal of Medicine,* vol. 383, no. 19, pp. 1838-1847, 2020
[246] A. Acun, D. C. Vural, and P. Zorlutuna, "A Tissue Engineered Model of Aging: Interdependence and Cooperative Effects in Failing Tissues," *Scientific Reports,* vol. 7, no. 1, p. 5051, 2017/07/11 2017
[247] P. W. Alford, A. W. Feinberg, S. P. Sheehy, and K. K. Parker, "Biohybrid thin films for measuring contractility in engineered cardiovascular muscle," *Biomaterials,* vol. 31, no. 13, pp. 3613-21, May 2010
[248] T. Boudou *et al.*, "A microfabricated platform to measure and manipulate the mechanics of engineered cardiac microtissues," *Tissue Eng Part A,* vol. 18, no. 9-10, pp. 910-9, May 2012
[249] M. Radisic *et al.*, "Biomimetic approach to cardiac tissue engineering: oxygen carriers and channeled scaffolds," *Tissue Eng,* vol. 12, no. 8, pp. 2077-91, Aug 2006

[250] O. Caspi *et al.*, "Tissue Engineering of Vascularized Cardiac Muscle From Human Embryonic Stem Cells," *Circulation Research,* vol. 100, no. 2, pp. 263-272, 2007/02/02 2007
[251] W. H. Zimmermann, C. Fink, D. Kralisch, U. Remmers, J. Weil, and T. Eschenhagen, "Three-dimensional engineered heart tissue from neonatal rat cardiac myocytes," *Biotechnology and Bioengineering,* <106::AID-BIT13>3.0.CO;2-3 vol. 68, no. 1, pp. 106-114, 2000/04/05 2000
[252] A. Hansen *et al.*, "Development of a Drug Screening Platform Based on Engineered Heart Tissue," *Circulation Research,* vol. 107, no. 1, pp. 35-44, 2010/07/09 2010
[253] T. Boudou *et al.*, "A microfabricated platform to measure and manipulate the mechanics of engineered cardiac microtissues," *Tissue engineering. Part A,* vol. 18, no. 9-10, pp. 910-919, 2012
[254] I. C. Turnbull *et al.*, "Advancing functional engineered cardiac tissues toward a preclinical model of human myocardium," *FASEB journal : official publication of the Federation of American Societies for Experimental Biology,* vol. 28, no. 2, pp. 644-654, 2014
[255] S. S. Nunes *et al.*, "Biowire: a platform for maturation of human pluripotent stem cell–derived cardiomyocytes," *Nat Methods,* vol. 10, no. 8, pp. 781-787, 2013/08/01 2013
[256] W. Bian, C. P. Jackman, and N. Bursac, "Controlling the structural and functional anisotropy of engineered cardiac tissues," *Biofabrication,* vol. 6, no. 2, pp. 024109-24109, 2014
[257] C. P. Jackman, A. L. Carlson, and N. Bursac, "Dynamic culture yields engineered myocardium with near-adult functional output," *Biomaterials,* vol. 111, pp. 66-79, 2016
[258] E. Querdel *et al.*, "Human Engineered Heart Tissue Patches Remuscularize the Injured Heart in a Dose-Dependent Manner," *Circulation,* vol. 0, no. 0,
[259] C. Zuppinger, "3D Cardiac Cell Culture: A Critical Review of Current Technologies and Applications," *Front Cardiovasc Med,* vol. 6, pp. 87-87, 2019
[260] A. L. Bailey *et al.*, "SARS-CoV-2 Infects Human Engineered Heart Tissues and Models COVID-19 Myocarditis," *JACC Basic Transl Sci,* vol. 6, no. 4, pp. 331-345, Apr 2021
[261] A. Moretti, K. L. Laugwitz, T. Dorn, D. Sinnecker, and C. Mummery, "Pluripotent stem cell models of human heart disease," *Cold Spring Harb Perspect Med,* vol. 3, no. 11, Nov 1 2013
[262] A. Moretti *et al.*, "Patient-specific induced pluripotent stem-cell models for long-QT syndrome," *N Engl J Med,* vol. 363, no. 15, pp. 1397-409, Oct 7 2010
[263] I. Itzhaki *et al.*, "Modelling the long QT syndrome with induced pluripotent stem cells," *Nature,* vol. 471, no. 7337, pp. 225-9, Mar 10 2011
[264] R. P. Davis *et al.*, "Cardiomyocytes derived from pluripotent stem cells recapitulate electrophysiological characteristics of an overlap syndrome of cardiac sodium channel disease," *Circulation,* vol. 125, no. 25, pp. 3079-91, Jun 26 2012
[265] M. Yazawa *et al.*, "Using induced pluripotent stem cells to investigate cardiac phenotypes in Timothy syndrome," *Nature,* vol. 471, no. 7337, pp. 230-4, Mar 10 2011
[266] N. Sun *et al.*, "Patient-specific induced pluripotent stem cells as a model for familial dilated cardiomyopathy," *Sci Transl Med,* vol. 4, no. 130, p. 130ra47, Apr 18 2012
[267] F. Lan *et al.*, "Abnormal calcium handling properties underlie familial hypertrophic cardiomyopathy pathology in patient-specific induced pluripotent stem cells," *Cell Stem Cell,* vol. 12, no. 1, pp. 101-13, Jan 3 2013
[268] P. Hofbauer *et al.*, "Cardioids reveal self-organizing principles of human cardiogenesis," *Cell,* vol. 184, no. 12, pp. 3299-3317.e22, 2021
[269] C. Schmidt *et al.*, "Multi-chamber cardioids unravel human heart development and cardiac defects," *Cell,* vol. 186, no. 25, pp. 5587-5605.e27, 2023

[270] Y. R. Lewis-Israeli *et al.*, "Self-assembling human heart organoids for the modeling of cardiac development and congenital heart disease," *Nat Commun,* vol. 12, no. 1, p. 5142, Aug 26 2021
[271] Y. R. Lewis-Israeli, M. Abdelhamid, I. Olomu, and A. Aguirre, "Modeling the Effects of Maternal Diabetes on the Developing Human Heart Using Pluripotent Stem Cell-Derived Heart Organoids," *Curr Protoc,* vol. 2, no. 6, p. e461, Jun 2022
[272] L. Drakhlis *et al.*, "Human heart-forming organoids recapitulate early heart and foregut development," *Nat Biotechnol,* vol. 39, no. 6, pp. 737-746, Jun 2021
[273] M. Filippo Buono, L. von Boehmer, J. Strang, S. P. Hoerstrup, M. Y. Emmert, and B. Nugraha, "Human Cardiac Organoids for Modeling Genetic Cardiomyopathy," *Cells,* vol. 9, no. 7, Jul 20 2020
[274] G. Kensah *et al.*, "Murine and human pluripotent stem cell-derived cardiac bodies form contractile myocardial tissue in vitro," *Eur Heart J,* vol. 34, no. 15, pp. 1134-46, Apr 2013
[275] M. Szepes *et al.*, "Dual Function of iPSC-Derived Pericyte-Like Cells in Vascularization and Fibrosis-Related Cardiac Tissue Remodeling In Vitro," *Int J Mol Sci,* vol. 21, no. 23, Nov 25 2020
[276] H. K. Voges, R. J. Mills, D. A. Elliott, R. G. Parton, E. R. Porrello, and J. E. Hudson, "Development of a human cardiac organoid injury model reveals innate regenerative potential," *Development,* vol. 144, no. 6, pp. 1118-1127, Mar 15 2017
[277] R. J. Mills *et al.*, "BET inhibition blocks inflammation-induced cardiac dysfunction and SARS-CoV-2 infection," *Cell,* vol. 184, no. 8, pp. 2167-2182.e22, Apr 15 2021
[278] R. X. Z. Lu *et al.*, "Heart-on-a-chip model of immune-induced cardiac dysfunction reveals the role of free mitochondrial DNA and therapeutic effects of endothelial exosomes," *bioRxiv,* p. 2023.08.09.552495, 2023
[279] J. M. Bliley *et al.*, "Dynamic loading of human engineered heart tissue enhances contractile function and drives a desmosome-linked disease phenotype," *Sci Transl Med,* vol. 13, no. 603, Jul 21 2021
[280] E. Y. Wang *et al.*, "Biowire Model of Interstitial and Focal Cardiac Fibrosis," *ACS Central Science,* vol. 5, no. 7, pp. 1146-1158, 2019/07/24 2019
[281] K. J. Livak and T. D. Schmittgen, "Analysis of relative gene expression data using real-time quantitative PCR and the 2(-Delta Delta C(T)) Method," *Methods,* vol. 25, no. 4, pp. 402-8, Dec 2001
[282] F. O. Martinez, A. Sica, A. Mantovani, and M. Locati, "Macrophage activation and polarization," *Front Biosci,* vol. 13, pp. 453-61, Jan 1 2008
[283] F. Porcheray *et al.*, "Macrophage activation switching: an asset for the resolution of inflammation," *Clin Exp Immunol,* vol. 142, no. 3, pp. 481-9, Dec 2005
[284] A. Shapouri-Moghaddam *et al.*, "Macrophage plasticity, polarization, and function in health and disease," *J Cell Physiol,* vol. 233, no. 9, pp. 6425-6440, Sep 2018
[285] A. Das *et al.*, "Monocyte and macrophage plasticity in tissue repair and regeneration," *Am J Pathol,* vol. 185, no. 10, pp. 2596-606, Oct 2015
[286] S. P. Nobs and M. Kopf, "Tissue-resident macrophages: guardians of organ homeostasis," *Trends Immunol,* vol. 42, no. 6, pp. 495-507, Jun 2021
[287] K. R. Karlsson, S. Cowley, F. O. Martinez, M. Shaw, S. L. Minger, and W. James, "Homogeneous monocytes and macrophages from human embryonic stem cells following coculture-free differentiation in M-CSF and IL-3," *Exp Hematol,* vol. 36, no. 9, pp. 1167-75, Sep 2008
[288] M. Lopez-Yrigoyen *et al.*, "A human iPSC line capable of differentiating into functional macrophages expressing ZsGreen: a tool for the study and in vivo tracking of therapeutic cells," *Philos Trans R Soc Lond B Biol Sci,* vol. 373, no. 1750, p. 20170219, 2018

[289] S. Arandjelovic and K. S. Ravichandran, "Phagocytosis of apoptotic cells in homeostasis," *Nat Immunol,* vol. 16, no. 9, pp. 907-17, Sep 2015
[290] J. M. Opalek, N. A. Ali, J. M. Lobb, M. G. Hunter, and C. B. Marsh, "Alveolar macrophages lack CCR2 expression and do not migrate to CCL2," *J Inflamm (Lond),* vol. 4, p. 19, Sep 22 2007
[291] K. Alasoo *et al.*, "Transcriptional profiling of macrophages derived from monocytes and iPS cells identifies a conserved response to LPS and novel alternative transcription," *Scientific Reports,* vol. 5, no. 1, p. 12524, 2015/07/30 2015
[292] D. Cui *et al.*, "High-Yield Human Induced Pluripotent Stem Cell-Derived Monocytes and Macrophages Are Functionally Comparable With Primary Cells," *Front Cell Dev Biol,* vol. 9, p. 656867, 2021
[293] G. L. Boulting *et al.*, "A functionally characterized test set of human induced pluripotent stem cells," *Nat Biotechnol,* vol. 29, no. 3, pp. 279-86, Mar 2011
[294] A. M. Vitale *et al.*, "Variability in the generation of induced pluripotent stem cells: importance for disease modeling," *Stem Cells Transl Med,* vol. 1, no. 9, pp. 641-50, Sep 2012
[295] D. Hirayama, T. Iida, and H. Nakase, "The Phagocytic Function of Macrophage-Enforcing Innate Immunity and Tissue Homeostasis," *Int J Mol Sci,* vol. 19, no. 1, Dec 29 2017
[296] M. Locati, G. Curtale, and A. Mantovani, "Diversity, Mechanisms, and Significance of Macrophage Plasticity," *Annu Rev Pathol,* vol. 15, pp. 123-147, Jan 24 2020
[297] Y. Liu *et al.*, "MicroRNA-98 negatively regulates IL-10 production and endotoxin tolerance in macrophages after LPS stimulation," *FEBS Lett,* vol. 585, no. 12, pp. 1963-8, Jun 23 2011
[298] S. S. Iyer, A. A. Ghaffari, and G. Cheng, "Lipopolysaccharide-mediated IL-10 transcriptional regulation requires sequential induction of type I IFNs and IL-27 in macrophages," *J Immunol,* vol. 185, no. 11, pp. 6599-607, Dec 1 2010
[299] Y. T. Wang *et al.*, "Select autophagy genes maintain quiescence of tissue-resident macrophages and increase susceptibility to Listeria monocytogenes," *Nat Microbiol,* vol. 5, no. 2, pp. 272-281, Feb 2020
[300] G. Zago, P. H. V. Saavedra, K. R. Keshari, and J. S. A. Perry, "Immunometabolism of Tissue-Resident Macrophages - An Appraisal of the Current Knowledge and Cutting-Edge Methods and Technologies," *Front Immunol,* vol. 12, p. 665782, 2021
[301] K. L. Spiller *et al.*, "Differential gene expression in human, murine, and cell line-derived macrophages upon polarization," *Exp Cell Res,* vol. 347, no. 1, pp. 1-13, Sep 10 2016
[302] E. J. Benjamin *et al.*, "Heart Disease and Stroke Statistics-2017 Update: A Report From the American Heart Association," *Circulation,* vol. 135, no. 10, pp. e146-e603, Mar 7 2017
[303] J. Benjamin Emelia *et al.*, "Heart Disease and Stroke Statistics—2017 Update: A Report From the American Heart Association," *Circulation,* vol. 135, no. 10, pp. e146-e603, 2017/03/07 2017
[304] "Tissue Engineering Techniques for Induced Pluripotent Stem Cell Derived Three-Dimensional Cardiac Constructs," *Tissue Engineering Part B: Reviews,* vol. 28, no. 4, pp. 891-911, 2022
[305] T. O'Hara and Y. Rudy, "Quantitative comparison of cardiac ventricular myocyte electrophysiology and response to drugs in human and nonhuman species," *Am J Physiol Heart Circ Physiol,* vol. 302, no. 5, pp. H1023-30, Mar 1 2012
[306] I. Batalov and A. W. Feinberg, "Differentiation of Cardiomyocytes from Human Pluripotent Stem Cells Using Monolayer Culture," *Biomark Insights,* vol. 10, no. Suppl 1, pp. 71-6, 2015

[307] M. J. Ivey, J. T. Kuwabara, J. T. Pai, R. E. Moore, Z. Sun, and M. D. Tallquist, "Resident fibroblast expansion during cardiac growth and remodeling," *J Mol Cell Cardiol,* vol. 114, pp. 161-174, Jan 2018
[308] L. Hortells, A. K. Z. Johansen, and K. E. Yutzey, "Cardiac Fibroblasts and the Extracellular Matrix in Regenerative and Nonregenerative Hearts," *J Cardiovasc Dev Dis,* vol. 6, no. 3, Aug 20 2019
[309] R. O. Hynes, "Stretching the boundaries of extracellular matrix research," *Nat Rev Mol Cell Biol,* vol. 15, no. 12, pp. 761-3, Dec 2014
[310] S. H. Kim, J. Turnbull, and S. Guimond, "Extracellular matrix and cell signalling: the dynamic cooperation of integrin, proteoglycan and growth factor receptor," *J Endocrinol,* vol. 209, no. 2, pp. 139-51, May 2011
[311] M. Rienks, A. P. Papageorgiou, N. G. Frangogiannis, and S. Heymans, "Myocardial extracellular matrix: an ever-changing and diverse entity," *Circ Res,* vol. 114, no. 5, pp. 872-88, Feb 28 2014
[312] M. Ieda *et al.*, "Cardiac fibroblasts regulate myocardial proliferation through beta1 integrin signaling," *Dev Cell,* vol. 16, no. 2, pp. 233-44, Feb 2009
[313] E. Giacomelli *et al.*, "Human-iPSC-Derived Cardiac Stromal Cells Enhance Maturation in 3D Cardiac Microtissues and Reveal Non-cardiomyocyte Contributions to Heart Disease," *Cell Stem Cell,* vol. 26, no. 6, pp. 862-879.e11, Jun 4 2020
[314] Q. C. Zeng *et al.*, "Cardiac fibroblast-derived extracellular matrix produced in vitro stimulates growth and metabolism of cultured ventricular cells," *Int Heart J,* vol. 54, no. 1, pp. 40-4, 2013
[315] F. Niro *et al.*, "An iPSC-derived bio-inspired scaffold modelling the structure and the effects of extracellular matrix in cardiac fibrosis," *bioRxiv,* p. 2024.02.07.578948, 2024
[316] P. W. Burridge *et al.*, "Chemically defined generation of human cardiomyocytes," *Nat Methods,* vol. 11, no. 8, pp. 855-60, Aug 2014
[317] S. Bhattacharya *et al.*, "High efficiency differentiation of human pluripotent stem cells to cardiomyocytes and characterization by flow cytometry," *J Vis Exp,* no. 91, p. 52010, Sep 23 2014
[318] S. Tohyama *et al.*, "Distinct metabolic flow enables large-scale purification of mouse and human pluripotent stem cell-derived cardiomyocytes," *Cell Stem Cell,* vol. 12, no. 1, pp. 127-37, Jan 3 2013
[319] A. R. Pinto *et al.*, "Revisiting Cardiac Cellular Composition," *Circ Res,* vol. 118, no. 3, pp. 400-9, Feb 5 2016
[320] C. Vasquez, N. Benamer, and G. E. Morley, "The cardiac fibroblast: functional and electrophysiological considerations in healthy and diseased hearts," *J Cardiovasc Pharmacol,* vol. 57, no. 4, pp. 380-8, Apr 2011
[321] B. A. Afouda, "Towards Understanding the Gene-Specific Roles of GATA Factors in Heart Development: Does GATA4 Lead the Way?," *Int J Mol Sci,* vol. 23, no. 9, May 9 2022
[322] Y. Liu *et al.*, "Sox17 is essential for the specification of cardiac mesoderm in embryonic stem cells," *Proc Natl Acad Sci U S A,* vol. 104, no. 10, pp. 3859-64, Mar 6 2007
[323] T. Moore-Morris, P. Cattaneo, M. Puceat, and S. M. Evans, "Origins of cardiac fibroblasts," *J Mol Cell Cardiol,* vol. 91, pp. 1-5, Feb 2016
[324] P. Snider, K. N. Standley, J. Wang, M. Azhar, T. Doetschman, and S. J. Conway, "Origin of cardiac fibroblasts and the role of periostin," *Circ Res,* vol. 105, no. 10, pp. 934-47, Nov 6 2009
[325] A. Holtzinger, G. E. Rosenfeld, and T. Evans, "Gata4 directs development of cardiac-inducing endoderm from ES cells," *Dev Biol,* vol. 337, no. 1, pp. 63-73, Jan 1 2010

[326] P. Tandon, Y. V. Miteva, L. M. Kuchenbrod, I. M. Cristea, and F. L. Conlon, "Tcf21 regulates the specification and maturation of proepicardial cells," *Development,* vol. 140, no. 11, pp. 2409-21, Jun 2013
[327] M. Milgrom-Hoffman, Z. Harrelson, N. Ferrara, E. Zelzer, S. M. Evans, and E. Tzahor, "The heart endocardium is derived from vascular endothelial progenitors," *Development,* vol. 138, no. 21, pp. 4777-87, Nov 2011
[328] H. Hu, S. Lin, S. Wang, and X. Chen, "The Role of Transcription Factor 21 in Epicardial Cell Differentiation and the Development of Coronary Heart Disease," *Front Cell Dev Biol,* vol. 8, p. 457, 2020
[329] F. Jinqi *et al.*, "Inhibition of Tgfβ signaling enables durable ventricular pacing by TBX18 gene transfer," *bioRxiv,* p. 2022.06.02.493572, 2022
[330] S. A. Doppler *et al.*, "Cardiac fibroblasts: more than mechanical support," *J Thorac Dis,* vol. 9, no. Suppl 1, pp. S36-s51, Mar 2017
[331] B. G. Bruneau *et al.*, "Chamber-specific cardiac expression of Tbx5 and heart defects in Holt-Oram syndrome," *Dev Biol,* vol. 211, no. 1, pp. 100-8, Jul 1 1999
[332] J. L. Steven, "Metchnikoff on the Comparative Pathology of Inflammation," *Glasgow Med J,* vol. 38, no. 3, pp. 195-205, Sep 1892
[333] L. Aschoff, "Das reticulo-endotheliale System," in *Ergebnisse der Inneren Medizin und Kinderheilkunde: Sechsundzwanzigster Band*, F. Kraus *et al.* Eds. Berlin, Heidelberg: Springer Berlin Heidelberg, 1924, pp. 1-118.
[334] A. Bajgar and G. Krejčová, "On the origin of the functional versatility of macrophages," *Front Physiol,* vol. 14, p. 1128984, 2023
[335] Y. Lavin and M. Merad, "Macrophages: gatekeepers of tissue integrity," *Cancer Immunol Res,* vol. 1, no. 4, pp. 201-9, Oct 2013
[336] S. Galván-Peña and L. A. O'Neill, "Metabolic reprograming in macrophage polarization," *Front Immunol,* vol. 5, p. 420, 2014
[337] A. Sródka, R. W. Gryglewski, and W. Szczepariski, "Browicz or Kupffer cells?," *Pol J Pathol,* vol. 57, no. 4, pp. 183-5, 2006
[338] P. Rous and J. W. Beard, "SELECTION WITH THE MAGNET AND CULTIVATION OF RETICULO-ENDOTHELIAL CELLS (KUPFFER CELLS)," *J Exp Med,* vol. 59, no. 5, pp. 577-91, Apr 30 1934
[339] P. Rio-Hortega, "THE MICROGLIA," *The Lancet,* vol. 233, no. 6036, pp. 1023-1026, 1939/05/06/ 1939
[340] R. van Furth and Z. A. Cohn "THE ORIGIN AND KINETICS OF MONONUCLEAR PHAGOCYTES," *Journal of Experimental Medicine,* vol. 128, no. 3, pp. 415-435, 1968
[341] F. Ginhoux, J. L. Schultze, P. J. Murray, J. Ochando, and S. K. Biswas, "New insights into the multidimensional concept of macrophage ontogeny, activation and function," *Nat Immunol,* vol. 17, no. 1, pp. 34-40, Jan 2016
[342] F. Ginhoux and M. Guilliams, "Tissue-Resident Macrophage Ontogeny and Homeostasis," *Immunity,* vol. 44, no. 3, pp. 439-449, Mar 15 2016
[343] F. Ginhoux and M. Merad, "Ontogeny and homeostasis of Langerhans cells," *Immunol Cell Biol,* vol. 88, no. 4, pp. 387-92, May-Jun 2010
[344] S. Epelman, P. P. Liu, and D. L. Mann, "Role of innate and adaptive immune mechanisms in cardiac injury and repair," *Nature reviews. Immunology,* vol. 15, no. 2, pp. 117-129, 2015
[345] G. Sreejit, A. J. Fleetwood, A. J. Murphy, and P. R. Nagareddy, "Origins and diversity of macrophages in health and disease," *Clin Transl Immunology,* vol. 9, no. 12, p. e1222, 2020
[346] R. C. Paolicelli *et al.*, "Synaptic pruning by microglia is necessary for normal brain development," *Science,* vol. 333, no. 6048, pp. 1456-8, Sep 9 2011

[347] I. Theurl *et al.*, "On-demand erythrocyte disposal and iron recycling requires transient macrophages in the liver," *Nat Med,* vol. 22, no. 8, pp. 945-51, Aug 2016
[348] J. A. Whitsett, S. E. Wert, and T. E. Weaver, "Alveolar surfactant homeostasis and the pathogenesis of pulmonary disease," *Annu Rev Med,* vol. 61, pp. 105-19, 2010
[349] A. B. Aurora *et al.*, "Macrophages are required for neonatal heart regeneration," *J Clin Invest,* vol. 124, no. 3, pp. 1382-92, Mar 2014
[350] P. Dutta *et al.*, "Myocardial Infarction Activates CCR2(+) Hematopoietic Stem and Progenitor Cells," *Cell Stem Cell,* vol. 16, no. 5, pp. 477-87, May 7 2015
[351] N. G. Frangogiannis, C. W. Smith, and M. L. Entman, "The inflammatory response in myocardial infarction," *Cardiovasc Res,* vol. 53, no. 1, pp. 31-47, Jan 2002
[352] P. Panizzi *et al.*, "Impaired infarct healing in atherosclerotic mice with Ly-6C(hi) monocytosis," *J Am Coll Cardiol,* vol. 55, no. 15, pp. 1629-38, Apr 13 2010
[353] M. J. van Amerongen, M. C. Harmsen, N. van Rooijen, A. H. Petersen, and M. J. van Luyn, "Macrophage depletion impairs wound healing and increases left ventricular remodeling after myocardial injury in mice," *Am J Pathol,* vol. 170, no. 3, pp. 818-29, Mar 2007
[354] J. D. Bailey *et al.*, "Isolation and culture of murine bone marrow-derived macrophages for nitric oxide and redox biology," *Nitric Oxide,* vol. 100-101, pp. 17-29, Aug 1 2020
[355] E. R. Stanley and P. M. Heard, "Factors regulating macrophage production and growth. Purification and some properties of the colony stimulating factor from medium conditioned by mouse L cells," *J Biol Chem,* vol. 252, no. 12, pp. 4305-12, Jun 25 1977
[356] U. Kreuzburg-Duffy and C. Macdonald, "Establishment of immortalized cell lines from mouse peritoneal macrophages following transformation with SV40 early region DNA deleted at the origin of replication," *Immunology,* vol. 72, no. 3, pp. 368-72, Mar 1991
[357] E. Blasi, R. Barluzzi, V. Bocchini, R. Mazzolla, and F. Bistoni, "Immortalization of murine microglial cells by a v-raf/v-myc carrying retrovirus," *J Neuroimmunol,* vol. 27, no. 2-3, pp. 229-37, May 1990
[358] V. Bocchini, R. Mazzolla, R. Barluzzi, E. Blasi, P. Sick, and H. Kettenmann, "An immortalized cell line expresses properties of activated microglial cells," *J Neurosci Res,* vol. 31, no. 4, pp. 616-21, Apr 1992
[359] H. Pandya *et al.*, "Differentiation of human and murine induced pluripotent stem cells to microglia-like cells," *Nature Neuroscience,* vol. 20, no. 5, pp. 753-759, 2017/05/01 2017
[360] J. Xue *et al.*, "Transcriptome-based network analysis reveals a spectrum model of human macrophage activation," *Immunity,* vol. 40, no. 2, pp. 274-88, Feb 20 2014
[361] F. Naeim, P. Nagesh Rao, S. X. Song, and R. T. Phan, "Chapter 2 - Principles of Immunophenotyping," in *Atlas of Hematopathology (Second Edition)*, F. Naeim, P. Nagesh Rao, S. X. Song, and R. T. Phan Eds.: Academic Press, 2018, pp. 29-56.
[362] C. C. Biguetti *et al.*, "CCR2 Contributes to F4/80+ Cells Migration Along Intramembranous Bone Healing in Maxilla, but Its Deficiency Does Not Critically Affect the Healing Outcome," *Front Immunol,* Original Research vol. 9, 2018-August-10 2018
[363] A. R. Pinto *et al.*, "An abundant tissue macrophage population in the adult murine heart with a distinct alternatively-activated macrophage profile," *PLoS One,* vol. 7, no. 5, p. e36814, 2012
[364] K. Molawi *et al.*, "Progressive replacement of embryo-derived cardiac macrophages with age," *J Exp Med,* vol. 211, no. 11, pp. 2151-8, Oct 20 2014
[365] S. O'Rourke, "Engineering innate immunology in cardiovascular disease models and regenerative medicine," PhD, Mechanical and Manufacturing Engineering, The University of Dublin, Dublin, 2023.

[366] J. J. Choi, C. F. Reich, 3rd, and D. S. Pisetsky, "The role of macrophages in the in vitro generation of extracellular DNA from apoptotic and necrotic cells," *Immunology,* vol. 115, no. 1, pp. 55-62, May 2005

[367] Z. Li, A. E. Bryant, T. Parimon, and D. L. Stevens, "Cardiac dysfunction in StrepTSS: Group A streptococcus disrupts the directional cardiomyocyte-to-macrophage crosstalk that maintains macrophage quiescence," *Cytokine,* vol. 59, no. 1, pp. 191-194, 2012/07/01/ 2012

[368] A. Yabluchanskiy, Y. Ma, R. P. Iyer, M. E. Hall, and M. L. Lindsey, "Matrix metalloproteinase-9: Many shades of function in cardiovascular disease," *Physiology (Bethesda),* vol. 28, no. 6, pp. 391-403, Nov 2013

[369] G. V. Halade, Y. F. Jin, and M. L. Lindsey, "Matrix metalloproteinase (MMP)-9: a proximal biomarker for cardiac remodeling and a distal biomarker for inflammation," *Pharmacol Ther,* vol. 139, no. 1, pp. 32-40, Jul 2013

[370] A. Ducharme *et al.*, "Targeted deletion of matrix metalloproteinase-9 attenuates left ventricular enlargement and collagen accumulation after experimental myocardial infarction," *J Clin Invest,* vol. 106, no. 1, pp. 55-62, Jul 2000

[371] X. Liao *et al.*, "Distinct roles of resident and nonresident macrophages in nonischemic cardiomyopathy," *Proc Natl Acad Sci U S A,* vol. 115, no. 20, pp. E4661-e4669, May 15 2018

[372] N. R. Wong *et al.*, "Resident cardiac macrophages mediate adaptive myocardial remodeling," *Immunity,* vol. 54, no. 9, pp. 2072-2088.e7, Sep 14 2021

[373] M. A. Beardslee *et al.*, "Dephosphorylation and intracellular redistribution of ventricular connexin43 during electrical uncoupling induced by ischemia," *Circ Res,* vol. 87, no. 8, pp. 656-62, Oct 13 2000

[374] J. Sugita *et al.*, "Cardiac macrophages prevent sudden death during heart stress," *Nat Commun,* vol. 12, no. 1, p. 1910, Mar 26 2021

[375] Y. K. Alshoubaki *et al.*, "A superior extracellular matrix binding motif to enhance the regenerative activity and safety of therapeutic proteins," *npj Regenerative Medicine,* vol. 8, no. 1, p. 25, 2023/05/22 2023

[376] M. Ackermann *et al.*, "Bioreactor-based mass production of human iPSC-derived macrophages enables immunotherapies against bacterial airway infections," *Nat Commun,* vol. 9, no. 1, p. 5088, Nov 30 2018

[377] M. Malek Mohammadi *et al.*, "The transcription factor GATA4 promotes myocardial regeneration in neonatal mice," *EMBO Mol Med,* vol. 9, no. 2, pp. 265-279, Feb 2017

[378] G. M. Dittrich *et al.*, "Fibroblast GATA-4 and GATA-6 promote myocardial adaptation to pressure overload by enhancing cardiac angiogenesis," *Basic Res Cardiol,* vol. 116, no. 1, p. 26, Apr 19 2021

[379] S. D. Bird *et al.*, "The human adult cardiomyocyte phenotype," *Cardiovasc Res,* vol. 58, no. 2, pp. 423-34, May 1 2003

[380] M. Mollova *et al.*, "Cardiomyocyte proliferation contributes to heart growth in young humans," *Proc Natl Acad Sci U S A,* vol. 110, no. 4, pp. 1446-51, Jan 22 2013

[381] E. Giacomelli, C. L. Mummery, and M. Bellin, "Human heart disease: lessons from human pluripotent stem cell-derived cardiomyocytes," *Cell Mol Life Sci,* vol. 74, no. 20, pp. 3711-3739, Oct 2017

[382] A. M. Gacita *et al.*, "Genetic Variation in Enhancers Modifies Cardiomyopathy Gene Expression and Progression," *Circulation,* vol. 143, no. 13, pp. 1302-1316, 2021

[383] B. D. Lowes *et al.*, "Changes in gene expression in the intact human heart. Downregulation of alpha-myosin heavy chain in hypertrophied, failing ventricular myocardium," *J Clin Invest,* vol. 100, no. 9, pp. 2315-24, Nov 1 1997

[384] L. Cyganek *et al.*, "Deep phenotyping of human induced pluripotent stem cell-derived atrial and ventricular cardiomyocytes," *JCI Insight,* vol. 3, no. 12, Jun 21 2018
[385] J. England and S. Loughna, "Heavy and light roles: myosin in the morphogenesis of the heart," *Cell Mol Life Sci,* vol. 70, no. 7, pp. 1221-39, Apr 2013
[386] J. Lewandowski *et al.*, "The impact of in vitro cell culture duration on the maturation of human cardiomyocytes derived from induced pluripotent stem cells of myogenic origin," *Cell Transplant,* vol. 27, no. 7, pp. 1047-1067, Jul 2018
[387] D. A. Eisner, J. L. Caldwell, K. Kistamás, and A. W. Trafford, "Calcium and Excitation-Contraction Coupling in the Heart," *Circulation Research,* vol. 121, no. 2, pp. 181-195, 2017
[388] D. M. Bers, "Cardiac excitation-contraction coupling," *Nature,* vol. 415, no. 6868, pp. 198-205, Jan 10 2002
[389] F. S. Korte and K. S. McDonald, "Sarcomere length dependence of rat skinned cardiac myocyte mechanical properties: dependence on myosin heavy chain," *J Physiol,* vol. 581, no. Pt 2, pp. 725-39, Jun 1 2007
[390] H. Lemcke, A. Skorska, C. I. Lang, L. Johann, and R. David, "Quantitative Evaluation of the Sarcomere Network of Human hiPSC-Derived Cardiomyocytes Using Single-Molecule Localization Microscopy," *Int J Mol Sci,* vol. 21, no. 8, Apr 17 2020
[391] C. Zuppinger, G. Gibbons, P. Dutta-Passecker, A. Segiser, H. Most, and T. M. Suter, "Characterization of cytoskeleton features and maturation status of cultured human iPSC-derived cardiomyocytes," *Eur J Histochem,* vol. 61, no. 2, p. 2763, Jun 21 2017
[392] D. Jeziorowska *et al.*, "Differential Sarcomere and Electrophysiological Maturation of Human iPSC-Derived Cardiac Myocytes in Monolayer vs. Aggregation-Based Differentiation Protocols," *Int J Mol Sci,* vol. 18, no. 6, Jun 1 2017
[393] N. Hamdani *et al.*, "Sarcomeric dysfunction in heart failure," *Cardiovascular Research,* vol. 77, no. 4, pp. 649-658, 2007
[394] L. Burbaum *et al.*, "Molecular-scale visualization of sarcomere contraction within native cardiomyocytes," *Nat Commun,* vol. 12, no. 1, p. 4086, Jul 2 2021
[395] I. Nitsan, S. Drori, Y. E. Lewis, S. Cohen, and S. Tzlil, "Mechanical communication in cardiac cell synchronized beating," *Nature Physics,* vol. 12, no. 5, pp. 472-477, 2016/05/01 2016
[396] J. K. Yu, J. A. Liang, S. H. Weinberg, and N. A. Trayanova, "Computational modeling of aberrant electrical activity following remuscularization with intramyocardially injected pluripotent stem cell-derived cardiomyocytes," *J Mol Cell Cardiol,* vol. 162, pp. 97-109, Jan 2022
[397] J. J. Chong *et al.*, "Human embryonic-stem-cell-derived cardiomyocytes regenerate non-human primate hearts," *Nature,* vol. 510, no. 7504, pp. 273-7, Jun 12 2014
[398] Y. Shiba *et al.*, "Allogeneic transplantation of iPS cell-derived cardiomyocytes regenerates primate hearts," *Nature,* vol. 538, no. 7625, pp. 388-391, Oct 20 2016
[399] A. Llucià-Valldeperas *et al.*, "Physiological conditioning by electric field stimulation promotes cardiomyogenic gene expression in human cardiomyocyte progenitor cells," *Stem Cell Res Ther,* vol. 5, no. 4, p. 93, Aug 4 2014
[400] R. Ma *et al.*, "Electrical Stimulation Enhances Cardiac Differentiation of Human Induced Pluripotent Stem Cells for Myocardial Infarction Therapy," *Antioxid Redox Signal,* vol. 28, no. 5, pp. 371-384, Feb 10 2018
[401] A. J. S. Ribeiro *et al.*, "Multi-Imaging Method to Assay the Contractile Mechanical Output of Micropatterned Human iPSC-Derived Cardiac Myocytes," *Circulation Research,* vol. 120, no. 10, pp. 1572-1583, 2017

[402] M. K. Jonsson, Q. D. Wang, and B. Becker, "Impedance-based detection of beating rhythm and proarrhythmic effects of compounds on stem cell-derived cardiomyocytes," *Assay Drug Dev Technol,* vol. 9, no. 6, pp. 589-99, Dec 2011
[403] L. B. Hazeltine *et al.*, "Effects of substrate mechanics on contractility of cardiomyocytes generated from human pluripotent stem cells," *Int J Cell Biol,* vol. 2012, p. 508294, 2012
[404] O. Sirenko, E. F. Cromwell, C. Crittenden, J. A. Wignall, F. A. Wright, and I. Rusyn, "Assessment of beating parameters in human induced pluripotent stem cells enables quantitative in vitro screening for cardiotoxicity," *Toxicol Appl Pharmacol,* vol. 273, no. 3, pp. 500-7, Dec 15 2013
[405] R. S. Howe, K. J. Isaacson, J. L. Albert, and C. B. Coutifaris, "Embryonic heart rate in human pregnancy," *J Ultrasound Med,* vol. 10, no. 7, pp. 367-71, Jul 1991
[406] G. Földes *et al.*, "Modulation of human embryonic stem cell-derived cardiomyocyte growth: a testbed for studying human cardiac hypertrophy?," *J Mol Cell Cardiol,* vol. 50, no. 2, pp. 367-76, Feb 2011
[407] M. Valls-Margarit *et al.*, "Engineered Macroscale Cardiac Constructs Elicit Human Myocardial Tissue-like Functionality," *Stem Cell Reports,* vol. 13, no. 1, pp. 207-220, 2019/07/09/ 2019
[408] M. D. Lemoine *et al.*, "Human Induced Pluripotent Stem Cell-Derived Engineered Heart Tissue as a Sensitive Test System for QT Prolongation and Arrhythmic Triggers," *Circ Arrhythm Electrophysiol,* vol. 11, no. 7, p. e006035, Jul 2018
[409] E. G. Navarrete *et al.*, "Screening Drug-Induced Arrhythmia Using Human Induced Pluripotent Stem Cell–Derived Cardiomyocytes and Low-Impedance Microelectrode Arrays," *Circulation,* vol. 128, no. 11_suppl_1, pp. S3-S13, 2013
[410] E. Forte *et al.*, "Type 2 MI induced by a single high dose of isoproterenol in C57BL/6J mice triggers a persistent adaptive immune response against the heart," *Journal of Cellular and Molecular Medicine,* vol. 25, no. 1, pp. 229-243, 2021
[411] F. Giannetti *et al.*, "A detailed characterization of the hyperpolarization-activated "funny" current (I(f)) in human-induced pluripotent stem cell (iPSC)-derived cardiomyocytes with pacemaker activity," *Pflugers Arch,* vol. 473, no. 7, pp. 1009-1021, Jul 2021
[412] N. Huebsch *et al.*, "Miniaturized iPS-Cell-Derived Cardiac Muscles for Physiologically Relevant Drug Response Analyses," *Sci Rep,* vol. 6, p. 24726, Apr 20 2016
[413] A. Novak *et al.*, "Functional abnormalities in iPSC-derived cardiomyocytes generated from CPVT1 and CPVT2 patients carrying ryanodine or calsequestrin mutations," *J Cell Mol Med,* vol. 19, no. 8, pp. 2006-18, Aug 2015
[414] H.-T. Yang *et al.*, "The ryanodine receptor modulates the spontaneous beating rate of cardiomyocytes during development," *Proceedings of the National Academy of Sciences,* vol. 99, no. 14, pp. 9225-9230, 2002
[415] Y. K. Lee *et al.*, "Calcium homeostasis in human induced pluripotent stem cell-derived cardiomyocytes," *Stem Cell Rev Rep,* vol. 7, no. 4, pp. 976-86, Nov 2011
[416] F. Seibertz *et al.*, "Electrophysiological and calcium-handling development during long-term culture of human-induced pluripotent stem cell-derived cardiomyocytes," *Basic Research in Cardiology,* vol. 118, no. 1, p. 14, 2023/04/05 2023
[417] A. B. Hill and R. C. Chiu, "Dynamic cardiomyoplasty for treatment of heart failure," *Clin Cardiol,* vol. 12, no. 12, pp. 681-8, Dec 1989
[418] H. C. Quevedo *et al.*, "Allogeneic mesenchymal stem cells restore cardiac function in chronic ischemic cardiomyopathy via trilineage differentiating capacity," *Proc Natl Acad Sci U S A,* vol. 106, no. 33, pp. 14022-7, Aug 18 2009
[419] C. Templin *et al.*, "Transplantation and tracking of human-induced pluripotent stem cells in a pig model of myocardial infarction: assessment of cell survival, engraftment, and

distribution by hybrid single photon emission computed tomography/computed tomography of sodium iodide symporter transgene expression," *Circulation,* vol. 126, no. 4, pp. 430-9, Jul 24 2012

[420] K. L. Christman, A. J. Vardanian, Q. Fang, R. E. Sievers, H. H. Fok, and R. J. Lee, "Injectable fibrin scaffold improves cell transplant survival, reduces infarct expansion, and induces neovasculature formation in ischemic myocardium," *J Am Coll Cardiol,* vol. 44, no. 3, pp. 654-60, Aug 4 2004

[421] G. Calsamiglia, F. Cobelli, M. Rinaldi, and M. Viganò, "[Cardiomyoplasty. Critical review of experimental and clinical results]," *G Ital Cardiol,* vol. 26, no. 12, pp. 1467-79, Dec 1996

[422] R. M. e. Oakley and J. C. Jarvis, "Cardiomyoplasty. A critical review of experimental and clinical results," *Circulation,* vol. 90, no. 4, pp. 2085-2090, 1994

[423] P. Menasché *et al.*, "Myoblast transplantation for heart failure," *Lancet,* vol. 357, no. 9252, pp. 279-80, Jan 27 2001

[424] B. Assmus *et al.*, "Transplantation of Progenitor Cells and Regeneration Enhancement in Acute Myocardial Infarction (TOPCARE-AMI)," *Circulation,* vol. 106, no. 24, pp. 3009-17, Dec 10 2002

[425] E. C. Perin *et al.*, "Transendocardial, autologous bone marrow cell transplantation for severe, chronic ischemic heart failure," *Circulation,* vol. 107, no. 18, pp. 2294-302, May 13 2003

[426] A. A. Quyyumi *et al.*, "PreSERVE-AMI: A Randomized, Double-Blind, Placebo-Controlled Clinical Trial of Intracoronary Administration of Autologous CD34+ Cells in Patients With Left Ventricular Dysfunction Post STEMI," *Circ Res,* vol. 120, no. 2, pp. 324-331, Jan 20 2017

[427] A. Mathur *et al.*, "The effect of intracoronary infusion of bone marrow-derived mononuclear cells on all-cause mortality in acute myocardial infarction: the BAMI trial," *Eur Heart J,* vol. 41, no. 38, pp. 3702-3710, Oct 7 2020

[428] W. Y. Lee *et al.*, "Enhancement of cell retention and functional benefits in myocardial infarction using human amniotic-fluid stem-cell bodies enriched with endogenous ECM," *Biomaterials,* vol. 32, no. 24, pp. 5558-67, Aug 2011

[429] A. R. Williams *et al.*, "Enhanced effect of combining human cardiac stem cells and bone marrow mesenchymal stem cells to reduce infarct size and to restore cardiac function after myocardial infarction," *Circulation,* vol. 127, no. 2, pp. 213-23, Jan 15 2013

[430] K. Cheng *et al.*, "Human cardiosphere-derived cells from advanced heart failure patients exhibit augmented functional potency in myocardial repair," *JACC Heart Fail,* vol. 2, no. 1, pp. 49-61, Feb 2014

[431] J. H. van Berlo and J. D. Molkentin, "An emerging consensus on cardiac regeneration," *Nat Med,* vol. 20, no. 12, pp. 1386-93, Dec 2014

[432] C. L. Cai and J. D. Molkentin, "The Elusive Progenitor Cell in Cardiac Regeneration: Slip Slidin' Away," *Circ Res,* vol. 120, no. 2, pp. 400-406, Jan 20 2017

[433] C. Vicinanza *et al.*, "Kit(cre) knock-in mice fail to fate-map cardiac stem cells," *Nature,* vol. 555, no. 7697, pp. E1-e5, Mar 21 2018

[434] Y. W. Liu *et al.*, "Human embryonic stem cell-derived cardiomyocytes restore function in infarcted hearts of non-human primates," *Nat Biotechnol,* vol. 36, no. 7, pp. 597-605, Aug 2018

[435] T. Halevy and A. Urbach, "Comparing ESC and iPSC-Based Models for Human Genetic Disorders," *J Clin Med,* vol. 3, no. 4, pp. 1146-62, Oct 24 2014

[436] S. Yoshida *et al.*, "Maturation of Human Induced Pluripotent Stem Cell-Derived Cardiomyocytes by Soluble Factors from Human Mesenchymal Stem Cells," *Mol Ther,* vol. 26, no. 11, pp. 2681-2695, Nov 7 2018

[437] G. J. Scuderi and J. Butcher, "Naturally Engineered Maturation of Cardiomyocytes," *Front Cell Dev Biol,* vol. 5, p. 50, 2017
[438] T. C. McDevitt *et al.*, "In vitro generation of differentiated cardiac myofibers on micropatterned laminin surfaces," *J Biomed Mater Res,* vol. 60, no. 3, pp. 472-9, Jun 5 2002
[439] M. Solazzo and M. G. Monaghan, "A Workflow to Produce a Low-Cost In Vitro Platform for the Electric-Field Pacing of Cellularised 3D Porous Scaffolds," *ACS Biomaterials Science & Engineering,* vol. 9, no. 8, pp. 4573-4582, 2023/08/14 2023
[440] N. Tandon *et al.*, "Electrical stimulation systems for cardiac tissue engineering," *Nature Protocols,* vol. 4, no. 2, pp. 155-173, 2009/02/01 2009
[441] S. Yoshida, K. Sumomozawa, K. Nagamine, and M. Nishizawa, "Hydrogel Microchambers Integrated with Organic Electrodes for Efficient Electrical Stimulation of Human iPSC-Derived Cardiomyocytes," *Macromol Biosci,* vol. 19, no. 6, p. e1900060, Jun 2019
[442] Y. Wang, M. Rouabhia, and Z. Zhang, "Pulsed electrical stimulation benefits wound healing by activating skin fibroblasts through the TGFβ1/ERK/NF-κB axis," *Biochim Biophys Acta,* vol. 1860, no. 7, pp. 1551-9, Jul 2016
[443] C. Chen, X. Bai, Y. Ding, and I. S. Lee, "Electrical stimulation as a novel tool for regulating cell behavior in tissue engineering," *Biomater Res,* vol. 23, p. 25, 2019
[444] H. J. Park, M. Rouabhia, D. Lavertu, and Z. Zhang, "Electrical Stimulation Modulates the Expression of Multiple Wound Healing Genes in Primary Human Dermal Fibroblasts," *Tissue Eng Part A,* vol. 21, no. 13-14, pp. 1982-90, Jul 2015
[445] A. Kumar, K. C. Nune, and R. Misra, "Understanding the response of pulsed electric field on osteoblast functions in three-dimensional mesh structures," *J Biomater Appl,* vol. 31, no. 4, pp. 594-605, Oct 2016
[446] M. P. Prabhakaran, L. Ghasemi-Mobarakeh, G. Jin, and S. Ramakrishna, "Electrospun conducting polymer nanofibers and electrical stimulation of nerve stem cells," *J Biosci Bioeng,* vol. 112, no. 5, pp. 501-7, Nov 2011
[447] M. L. Hernández-Bule, M. Trillo, and A. Úbeda, "Molecular mechanisms underlying antiproliferative and differentiating responses of hepatocarcinoma cells to subthermal electric stimulation," *PLoS One,* vol. 9, no. 1, p. e84636, 2014
[448] S. N. Iwasa, R. Babona-Pilipos, and C. M. Morshead, "Environmental Factors That Influence Stem Cell Migration: An "Electric Field"," *Stem Cells Int,* vol. 2017, p. 4276927, 2017
[449] J. Liu *et al.*, "Electric signals regulate directional migration of ventral midbrain derived dopaminergic neural progenitor cells via Wnt/GSK3β signaling," *Exp Neurol,* vol. 263, pp. 113-21, Jan 2015
[450] H. Zhao, A. Steiger, M. Nohner, and H. Ye, "Specific Intensity Direct Current (DC) Electric Field Improves Neural Stem Cell Migration and Enhances Differentiation towards βIII-Tubulin+ Neurons," *PLoS One,* vol. 10, no. 6, p. e0129625, 2015
[451] F. V. McCann, J. J. Cole, P. M. Guyre, and J. A. Russell, "Action potentials in macrophages derived from human monocytes," *Science,* vol. 219, no. 4587, pp. 991-3, Feb 25 1983
[452] Y. Jia *et al.*, "Study on the effects of alternating capacitive electric fields with different frequencies on promoting wound healing," *Medicine in Novel Technology and Devices,* vol. 16, p. 100142, 2022/12/01/ 2022
[453] J. Xu *et al.*, "Non-contact electrical stimulation as an effective means to promote wound healing," *Bioelectrochemistry,* vol. 146, p. 108108, Aug 2022
[454] H. Lei and D. Fan, "A Combination Therapy Using Electrical Stimulation and Adaptive, Conductive Hydrogels Loaded with Self-Assembled Nanogels Incorporating Short Interfering RNA Promotes the Repair of Diabetic Chronic Wounds," *Adv Sci (Weinh),* vol. 9, no. 30, p. e2201425, Oct 2022

[455] J. I. Hoare, A. M. Rajnicek, C. D. McCaig, R. N. Barker, and H. M. Wilson, "Electric fields are novel determinants of human macrophage functions," *J Leukoc Biol,* vol. 99, no. 6, pp. 1141-51, Jun 2016

[456] J.-Y. Goh, R. J. Weaver, L. Dixon, N. J. Platt, and R. A. Roberts, "Development and use of in vitro alternatives to animal testing by the pharmaceutical industry 1980–2013," *Toxicology Research,* 10.1039/C5TX00123D vol. 4, no. 5, pp. 1297-1307, 2015

[457] (30-31 October 2019). *Guidance on the Safety Assessment of Nanomaterials in Cosmetics*.

[458] M. Hay, D. W. Thomas, J. L. Craighead, C. Economides, and J. Rosenthal, "Clinical development success rates for investigational drugs," *Nat Biotechnol,* vol. 32, no. 1, pp. 40-51, Jan 2014

[459] M. Ghasemi and A. R. Dehpour, "Ethical considerations in animal studies," *J Med Ethics Hist Med,* vol. 2, p. 12, 2009

[460] C. A. Salkowski, K. F. Bartizal, M. J. Balish, and E. Balish, "Colonization and pathogenesis of Cryptococcus neoformans in gnotobiotic mice," *Infect Immun,* vol. 55, no. 9, pp. 2000-5, Sep 1987

[461] R. B. Colquitt, D. A. Colquhoun, and R. H. Thiele, "In silico modelling of physiologic systems," *Best Pract Res Clin Anaesthesiol,* vol. 25, no. 4, pp. 499-510, Dec 2011

[462] D. Barh *et al.*, "In Silico Models: From Simple Networks to Complex Diseases," *Animal Biotechnology,* pp. 385-404, 2014

[463] P. P. Adhikary, Q. Ul Ain, A. C. Hocke, and S. Hedtrich, "COVID-19 highlights the model dilemma in biomedical research," *Nature Reviews Materials,* vol. 6, no. 5, pp. 374-376, 2021/05/01 2021

[464] C. Muñoz-Fontela *et al.*, "Animal models for COVID-19," *Nature,* vol. 586, no. 7830, pp. 509-515, 2020/10/01 2020

[465] A. Loewa, J. J. Feng, and S. Hedtrich, "Human disease models in drug development," *Nature Reviews Bioengineering,* vol. 1, no. 8, pp. 545-559, 2023/08/01 2023

[466] M. Nikolic, T. Sustersic, and N. Filipovic, "In vitro Models and On-Chip Systems: Biomaterial Interaction Studies With Tissues Generated Using Lung Epithelial and Liver Metabolic Cell Lines," *Front Bioeng Biotechnol,* Review vol. 6, 2018-September-03 2018

[467] J. R. Spence *et al.*, "Directed differentiation of human pluripotent stem cells into intestinal tissue in vitro," *Nature,* vol. 470, no. 7332, pp. 105-109, 2011/02/01 2011

[468] T. Takebe *et al.*, "Vascularized and functional human liver from an iPSC-derived organ bud transplant," *Nature,* vol. 499, no. 7459, pp. 481-484, 2013/07/01 2013

[469] L. Huang *et al.*, "Ductal pancreatic cancer modeling and drug screening using human pluripotent stem cell– and patient-derived tumor organoids," *Nature Medicine,* vol. 21, no. 11, pp. 1364-1371, 2015/11/01 2015

[470] A. P. Wong *et al.*, "Directed differentiation of human pluripotent stem cells into mature airway epithelia expressing functional CFTR protein," *Nat Biotechnol,* vol. 30, no. 9, pp. 876-882, 2012/09/01 2012

[471] A. Taguchi *et al.*, "Redefining the in vivo origin of metanephric nephron progenitors enables generation of complex kidney structures from pluripotent stem cells," *Cell Stem Cell,* vol. 14, no. 1, pp. 53-67, Jan 2 2014

[472] V. Chichagova *et al.*, "Human iPSC differentiation to retinal organoids in response to IGF1 and BMP4 activation is line- and method-dependent," *Stem Cells,* vol. 38, no. 2, pp. 195-201, 2019

[473] L. Si *et al.*, "A human-airway-on-a-chip for the rapid identification of candidate antiviral therapeutics and prophylactics," *Nature Biomedical Engineering,* vol. 5, no. 8, pp. 815-829, 2021/08/01 2021

[474] B. F. L. Lai *et al.*, "Recapitulating Pancreatic Tumor Microenvironment through Synergistic Use of Patient Organoids and Organ-on-a-Chip Vasculature," *Advanced Functional Materials,* vol. 30, no. 48, p. 2000545, 2020

[475] E. A. Mayer, K. Nance, and S. Chen, "The Gut-Brain Axis," *Annu Rev Med,* vol. 73, pp. 439-453, Jan 27 2022

[476] I. Maschmeyer *et al.*, "A four-organ-chip for interconnected long-term co-culture of human intestine, liver, skin and kidney equivalents," *Lab on a Chip,* 10.1039/C5LC00392J vol. 15, no. 12, pp. 2688-2699, 2015

[477] R. Novak *et al.*, "Robotic fluidic coupling and interrogation of multiple vascularized organ chips," *Nature Biomedical Engineering,* vol. 4, no. 4, pp. 407-420, 2020/04/01 2020

[478] R. Lock *et al.*, "A framework for developing sex-specific engineered heart models," *Nature Reviews Materials,* vol. 7, no. 4, pp. 295-313, 2022/04/01 2022

[479] P. Sphabmixay *et al.*, "High resolution stereolithography fabrication of perfusable scaffolds to enable long-term meso-scale hepatic culture for disease modeling," *Biofabrication,* vol. 13, no. 4, p. 045024, 2021/09/21 2021

[480] S. Upadhyay and L. Palmberg, "Air-Liquid Interface: Relevant In Vitro Models for Investigating Air Pollutant-Induced Pulmonary Toxicity," *Toxicological Sciences,* vol. 164, no. 1, pp. 21-30, 2018

[481] W. L. Cantley *et al.*, "Functional and Sustainable 3D Human Neural Network Models from Pluripotent Stem Cells," *ACS Biomaterials Science & Engineering,* vol. 4, no. 12, pp. 4278-4288, 2018/12/10 2018

[482] O. F. Vila *et al.*, "Bioengineered optogenetic model of human neuromuscular junction," *Biomaterials,* vol. 276, p. 121033, 2021/09/01/ 2021

[483] I. Mannhardt *et al.*, "Human Engineered Heart Tissue: Analysis of Contractile Force," *Stem cell reports,* vol. 7, no. 1, pp. 29-42, 2016

[484] I. Goldfracht *et al.*, "Generating ring-shaped engineered heart tissues from ventricular and atrial human pluripotent stem cell-derived cardiomyocytes," *Nature Communications,* vol. 11, no. 1, p. 75, 2020/01/07 2020

[485] J. F. Murphy *et al.*, "Adult human cardiac stem cell supplementation effectively increases contractile function and maturation in human engineered cardiac tissues," *Stem Cell Res Ther,* vol. 10, no. 1, p. 373, Dec 4 2019

[486] N. L. Tulloch *et al.*, "Growth of engineered human myocardium with mechanical loading and vascular coculture," *Circ Res,* vol. 109, no. 1, pp. 47-59, Jun 24 2011

[487] W. J. de Lange *et al.*, "Human iPSC-engineered cardiac tissue platform faithfully models important cardiac physiology," *Am J Physiol Heart Circ Physiol,* vol. 320, no. 4, pp. H1670-h1686, Apr 1 2021

[488] D. J. Richards *et al.*, "Inspiration from heart development: Biomimetic development of functional human cardiac organoids," *Biomaterials,* vol. 142, pp. 112-123, Oct 2017

[489] T. J. Au - Cashman, R. Au - Josowitz, B. D. Au - Gelb, R. A. Au - Li, N. C. Au - Dubois, and K. D. Au - Costa, "Construction of Defined Human Engineered Cardiac Tissues to Study Mechanisms of Cardiac Cell Therapy," *JoVE,* no. 109, p. e53447, 2016/03/01/ 2016

[490] G.-r. Guo, L. Chen, M. Rao, K. Chen, J.-p. Song, and S.-s. Hu, "A modified method for isolation of human cardiomyocytes to model cardiac diseases," *Journal of Translational Medicine,* vol. 16, no. 1, p. 288, 2018/10/22 2018

[491] N. Thavandiran *et al.*, "Design and formulation of functional pluripotent stem cell-derived cardiac microtissues," *Proc Natl Acad Sci U S A,* vol. 110, no. 49, pp. E4698-707, Dec 3 2013

[492] B. Schwarzová *et al.*, "Modulating cardiac physiology in engineered heart tissue with the bidirectional optogenetic tool BiPOLES," *Pflügers Archiv - European Journal of Physiology,* vol. 475, no. 12, pp. 1463-1477, 2023/12/01 2023
[493] D. Fan, A. Takawale, J. Lee, and Z. Kassiri, "Cardiac fibroblasts, fibrosis and extracellular matrix remodeling in heart disease," *Fibrogenesis Tissue Repair,* vol. 5, no. 1, p. 15, Sep 3 2012
[494] M. L. Rodriguez, B. T. Graham, L. M. Pabon, S. J. Han, C. E. Murry, and N. J. Sniadecki, "Measuring the contractile forces of human induced pluripotent stem cell-derived cardiomyocytes with arrays of microposts," *J Biomech Eng,* vol. 136, no. 5, p. 051005, May 2014
[495] J. M. Rivera-Arbeláez *et al.*, "Contractility analysis of human engineered 3D heart tissues by an automatic tracking technique using a standalone application," *PLoS One,* vol. 17, no. 4, p. e0266834, 2022
[496] N. J. Kaiser, R. J. Kant, A. J. Minor, and K. L. K. Coulombe, "Optimizing Blended Collagen-Fibrin Hydrogels for Cardiac Tissue Engineering with Human iPSC-derived Cardiomyocytes," *ACS Biomater Sci Eng,* vol. 5, no. 2, pp. 887-899, Feb 11 2019
[497] F. Ma *et al.*, "Macrophage-stimulated cardiac fibroblast production of IL-6 is essential for TGF β/Smad activation and cardiac fibrosis induced by angiotensin II," *PLoS One,* vol. 7, no. 5, p. e35144, 2012
[498] J. Sapudom, S. Karaman, W. K. E. Mohamed, A. Garcia-Sabaté, B. C. Quartey, and J. C. M. Teo, "3D in vitro M2 macrophage model to mimic modulation of tissue repair," *npj Regenerative Medicine,* vol. 6, no. 1, p. 83, 2021/11/30 2021
[499] S. Van Linthout, K. Miteva, and C. Tschöpe, "Crosstalk between fibroblasts and inflammatory cells," *Cardiovasc Res,* vol. 102, no. 2, pp. 258-69, May 1 2014
[500] J.-J. Wu *et al.*, "The ASIC3-M-CSF-M2 macrophage-positive feedback loop modulates fibroblast-to-myofibroblast differentiation in skin fibrosis pathogenesis," *Cell Death & Disease,* vol. 13, no. 6, p. 527, 2022/06/06 2022
[501] T. A. Wynn and L. Barron, "Macrophages: master regulators of inflammation and fibrosis," *Semin Liver Dis,* vol. 30, no. 3, pp. 245-57, Aug 2010
[502] K. E. Porter and N. A. Turner, "Cardiac fibroblasts: at the heart of myocardial remodeling," *Pharmacol Ther,* vol. 123, no. 2, pp. 255-78, Aug 2009
[503] R. Avram *et al.*, "Real-world heart rate norms in the Health eHeart study," *NPJ Digit Med,* vol. 2, p. 58, 2019
[504] S. Roy, K. Spinali, E. G. Schmuck, J. A. Kink, P. Hematti, and A. N. Raval, "Cardiac fibroblast derived matrix-educated macrophages express VEGF and IL-6, and recruit mesenchymal stromal cells," *J Immunol Regen Med,* vol. 10, Dec 2020
[505] M. A. Olman, "Beyond TGF-beta: a prostaglandin promotes fibrosis," *Nat Med,* vol. 15, no. 12, pp. 1360-1, Dec 2009
[506] T. Oga *et al.*, "Prostaglandin F(2alpha) receptor signaling facilitates bleomycin-induced pulmonary fibrosis independently of transforming growth factor-beta," *Nat Med,* vol. 15, no. 12, pp. 1426-30, Dec 2009
[507] M. Kaviratne *et al.*, "IL-13 activates a mechanism of tissue fibrosis that is completely TGF-beta independent," *J Immunol,* vol. 173, no. 6, pp. 4020-9, Sep 15 2004
[508] P. Gasse *et al.*, "IL-1R1/MyD88 signaling and the inflammasome are essential in pulmonary inflammation and fibrosis in mice," *J Clin Invest,* vol. 117, no. 12, pp. 3786-99, Dec 2007
[509] Y. Yao, X. H. Xu, and L. Jin, "Macrophage Polarization in Physiological and Pathological Pregnancy," *Front Immunol,* vol. 10, p. 792, 2019

[510] V. Volpato and C. Webber, "Addressing variability in iPSC-derived models of human disease: guidelines to promote reproducibility," *Dis Model Mech,* vol. 13, no. 1, Jan 17 2020
[511] K. Ait-Aissa *et al.*, "Mitochondrial Oxidative Phosphorylation defect in the Heart of Subjects with Coronary Artery Disease," *Scientific Reports,* vol. 9, no. 1, p. 7623, 2019/05/20 2019
[512] Y. Morita and S. Tohyama, "Metabolic Regulation of Cardiac Differentiation and Maturation in Pluripotent Stem Cells: A Lesson from Heart Development," *Jma j,* vol. 3, no. 3, pp. 193-200, Jul 15 2020
[513] S. Tohyama and K. Fukuda, "Safe and Effective Cardiac Regenerative Therapy With Human-Induced Pluripotent Stem Cells: How Should We Prepare Pure Cardiac Myocytes?," *Circ Res,* vol. 120, no. 10, pp. 1558-1560, May 12 2017
[514] S. Tohyama *et al.*, "Glutamine Oxidation Is Indispensable for Survival of Human Pluripotent Stem Cells," *Cell Metab,* vol. 23, no. 4, pp. 663-74, Apr 12 2016
[515] D. Hu *et al.*, "Metabolic Maturation of Human Pluripotent Stem Cell-Derived Cardiomyocytes by Inhibition of HIF1α and LDHA," *Circ Res,* vol. 123, no. 9, pp. 1066-1079, Oct 12 2018
[516] A. Mucci *et al.*, "iPSC-Derived Macrophages Effectively Treat Pulmonary Alveolar Proteinosis in Csf2rb-Deficient Mice," *Stem Cell Reports,* vol. 11, no. 3, pp. 696-710, Sep 11 2018
[517] C. Happle *et al.*, "Pulmonary Transplantation of Human Induced Pluripotent Stem Cell-derived Macrophages Ameliorates Pulmonary Alveolar Proteinosis," *Am J Respir Crit Care Med,* vol. 198, no. 3, pp. 350-360, Aug 1 2018
[518] S. Pouyanfard *et al.*, "Human Induced Pluripotent Stem Cell-Derived Macrophages Ameliorate Liver Fibrosis," *Stem Cells,* vol. 39, no. 12, pp. 1701-1717, 2021
[519] T. D. Henry *et al.*, "Safety and efficacy of ixmyelocel-T: an expanded, autologous multi-cellular therapy, in dilated cardiomyopathy," *Circ Res,* vol. 115, no. 8, pp. 730-7, Sep 26 2014
[520] G. E. Moore, R. E. Gerner, and H. A. Franklin, "Culture of normal human leukocytes," *Jama,* vol. 199, no. 8, pp. 519-24, Feb 20 1967
[521] G. J. Brewer and C. W. Cotman, "Survival and growth of hippocampal neurons in defined medium at low density: advantages of a sandwich culture technique or low oxygen," *Brain Res,* vol. 494, no. 1, pp. 65-74, Aug 7 1989
[522] P. W. Burridge, A. Holmström, and J. C. Wu, "Chemically Defined Culture and Cardiomyocyte Differentiation of Human Pluripotent Stem Cells," *Curr Protoc Hum Genet,* vol. 87, pp. 21.3.1-21.3.15, Oct 6 2015
[523] R. M. Wang and K. L. Christman, "Decellularized myocardial matrix hydrogels: In basic research and preclinical studies," *Adv Drug Deliv Rev,* vol. 96, pp. 77-82, Jan 15 2016
[524] G. I. Barbulescu, F. M. Bojin, V. L. Ordodi, I. D. Goje, A. S. Barbulescu, and V. Paunescu, "Decellularized Extracellular Matrix Scaffolds for Cardiovascular Tissue Engineering: Current Techniques and Challenges," *Int J Mol Sci,* vol. 23, no. 21, Oct 27 2022
[525] B. Yu *et al.*, "Extracellular vesicles engineering by silicates-activated endothelial progenitor cells for myocardial infarction treatment in male mice," *Nature Communications,* vol. 14, no. 1, p. 2094, 2023/04/13 2023
[526] M. Yadid *et al.*, "Endothelial extracellular vesicles contain protective proteins and rescue ischemia-reperfusion injury in a human heart-on-chip," *Sci Transl Med,* vol. 12, no. 565, Oct 14 2020
[527] V. Regitz-Zagrosek and C. Gebhard, "Gender medicine: effects of sex and gender on cardiovascular disease manifestation and outcomes," *Nature Reviews Cardiology,* vol. 20, no. 4, pp. 236-247, 2023/04/01 2023

[528] A. Khera *et al.*, "Race and gender differences in C-reactive protein levels," *J Am Coll Cardiol,* vol. 46, no. 3, pp. 464-9, Aug 2 2005
[529] R. J. G. Hartman *et al.*, "Sex-Stratified Gene Regulatory Networks Reveal Female Key Driver Genes of Atherosclerosis Involved in Smooth Muscle Cell Phenotype Switching," *Circulation,* vol. 143, no. 7, pp. 713-726, Feb 16 2021
[530] W. Shi *et al.*, "Cardiac proteomics reveals sex chromosome-dependent differences between males and females that arise prior to gonad formation," *Dev Cell,* vol. 56, no. 21, pp. 3019-3034.e7, Nov 8 2021
[531] T. Alzahrani *et al.*, "Cardiovascular Disease Risk Factors and Myocardial Infarction in the Transgender Population," *Circulation: Cardiovascular Quality and Outcomes,* vol. 12, no. 4, p. e005597, 2019
[532] P. J. Connelly *et al.*, "Gender-Affirming Hormone Therapy, Vascular Health and Cardiovascular Disease in Transgender Adults," *Hypertension,* vol. 74, no. 6, pp. 1266-1274, 2019
[533] A. L. Baggish *et al.*, "Cardiovascular Toxicity of Illicit Anabolic-Androgenic Steroid Use," *Circulation,* vol. 135, no. 21, pp. 1991-2002, May 23 2017
[534] K. Ryczkowska, W. Adach, K. Janikowski, M. Banach, and A. Bielecka-Dabrowa, "Menopause and women's cardiovascular health: is it really an obvious relationship?," *Arch Med Sci,* vol. 19, no. 2, pp. 458-466, 2023
[535] H. N. Hodis and W. J. Mack, "Menopausal Hormone Replacement Therapy and Reduction of All-Cause Mortality and Cardiovascular Disease: It Is About Time and Timing," *Cancer J,* vol. 28, no. 3, pp. 208-223, May-Jun 01 2022

Appendices

A. Chapter 8

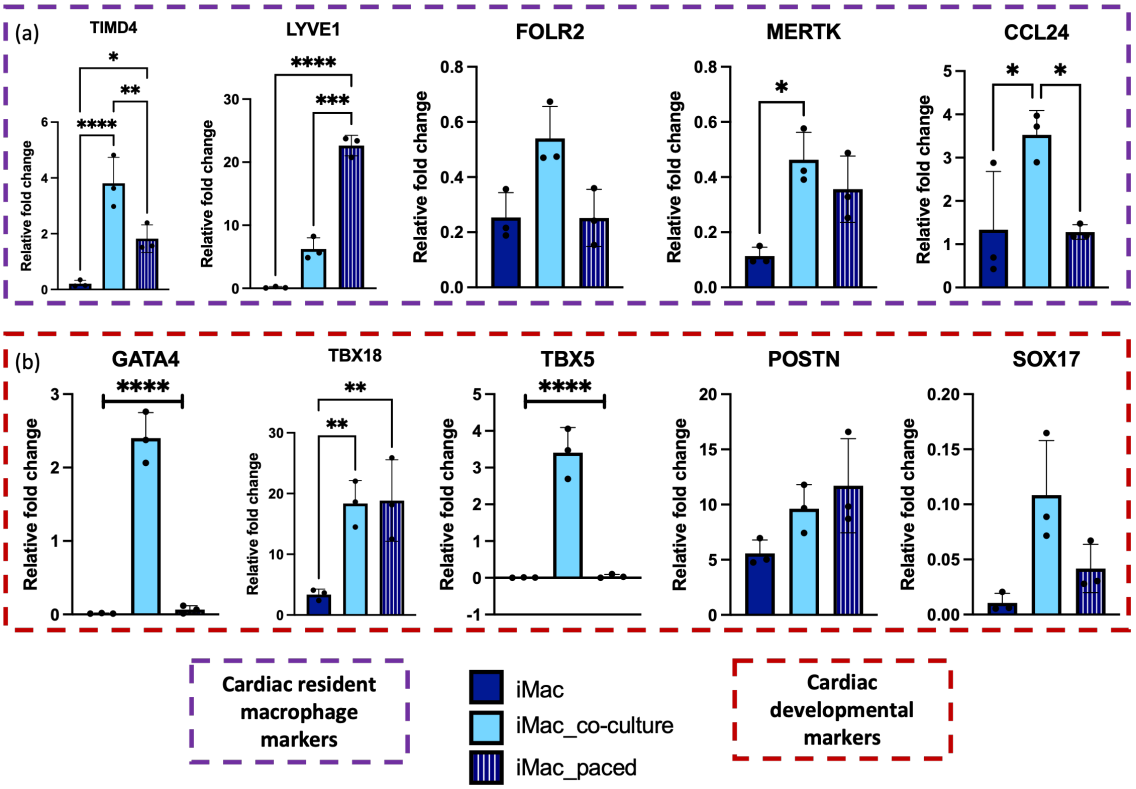

Appendix Figure 1: Comparison of electrically stimulated iMacs with unstimulated iMacs and iMacs in co-culture with iCMs. (a) Expression of a set of CRM-specific genes. (b) Expression of a set of cardiac developmental genes. Statistical analysis - One-way ANOVA with Tukey's multiple comparison test. * represents P<0.05, ** represents P<0.01, *** represents P<0.001 and **** represents P<0.0001.

B. Chapter 9

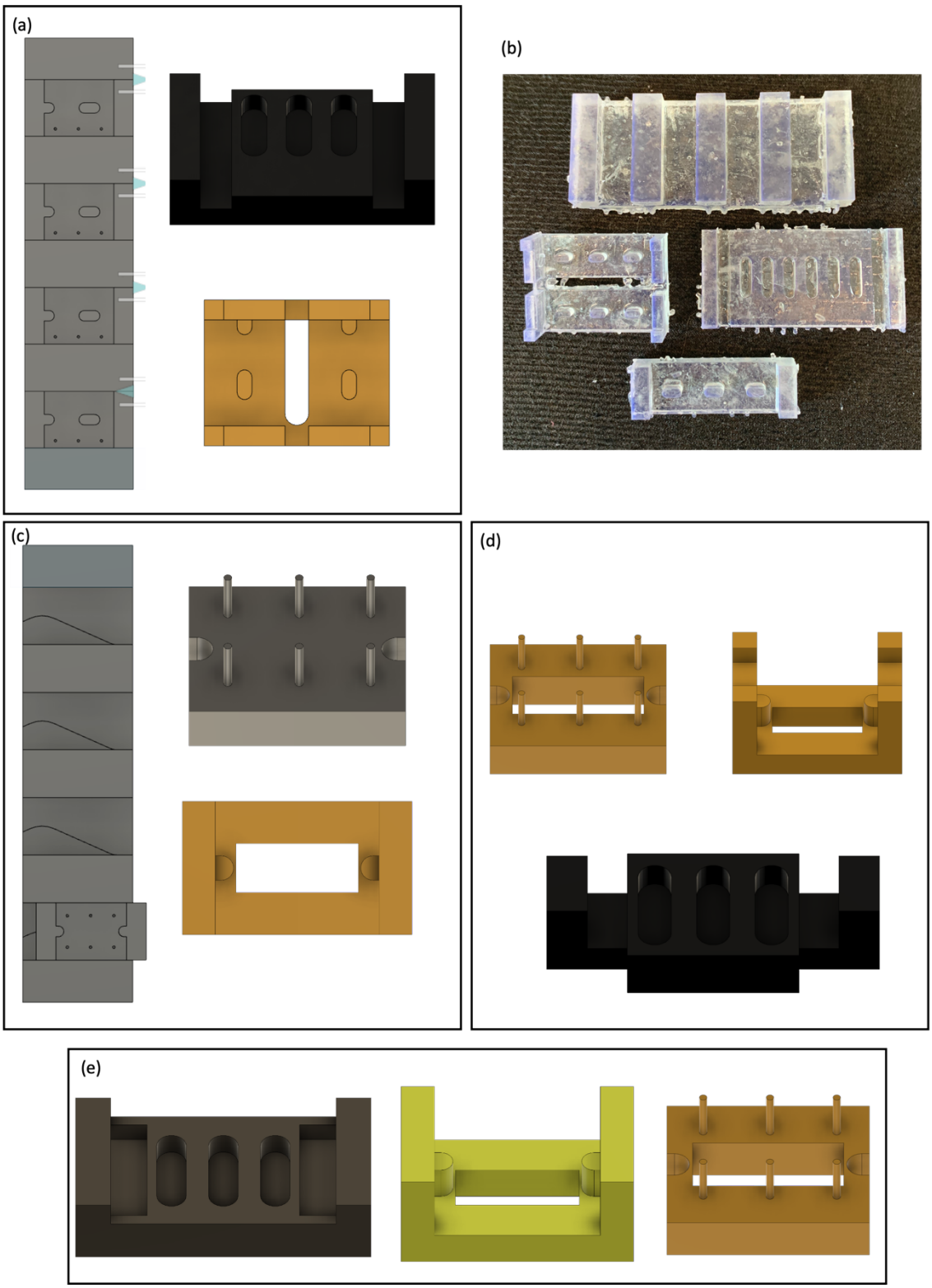

Appendix Figure 2: Iterations of EHT design. (a) First modified version of EHTs, designed to fit into a well of a 6 well plate (b) Representative image of 3D printed version of a larger EHT model.

(c) Modified design with a representative positive mould of the EHT bioreactor (d) Modified design with optical accessibility for live imaging of the EHTs. (e) Final version of the optimised EHT bioreactor.